SEISMIC PERFORMANCE ASSESSMENT OF REINFORCED CONCRETE OVERPASS BRIDGES WITH NONLINEAR ANALYSES

A THESIS SUBMITTED TO
THE GRADUATE SCHOOL OF NATURAL AND APPLIED SCIENCES
OF
MIDDLE EAST TECHNICAL UNIVERSITY

BY

TOLGA CANTÜRK

IN PARTIAL FULFILLMENT OF THE REQUIREMENTS
FOR
THE DEGREE OF MASTER OF SCIENCE
IN
CIVIL ENGINEERING

FEBRUARY 2022

Approval of the thesis:

SEISMIC PERFORMANCE ASSESSMENT OF REINFORCED CONCRETE OVERPASS BRIDGES WITH NONLINEAR ANALYSES

submitted by **TOLGA CANTÜRK** in partial fulfillment of the requirements for the degree of **Master of Science** i**n Civil Engineering, Middle East Technical University** by,

Prof. Dr. Halil Kalıpçılar
Dean, Graduate School of **Natural and Applied Sciences** _____

Prof. Dr. Erdem Canbay
Head of the Department, **Civil Engineering** _____

Prof. Dr. Eray Baran
Supervisor, **Civil Engineering, METU** _____

Examining Committee Members:

Prof. Dr. Ayşegül Askan Gündoğan
Civil Engineering Dept., METU _____

Prof. Dr. Eray Baran
Civil Engineering Dept., METU _____

Prof. Dr. Alp Caner
Civil Engineering Dept., METU _____

Assoc. Prof. Dr. Burcu Burak Bakır
Civil Engineering Dept., METU. _____

Assist. Prof. Dr. Halit Cenan Mertol
Civil Engineering Dept, Atılım University _____

Date: 08.02.2022

I hereby declare that all information in this document has been obtained and presented in accordance with academic rules and ethical conduct. I also declare that, as required by these rules and conduct, I have fully cited and referenced all material and results that are not original to this work.

Name Last name : Tolga Cantürk

Signature :

ABSTRACT

SEISMIC PERFORMANCE ASSESSMENT OF REINFORCED CONCRETE OVERPASS BRIDGES WITH NONLINEAR ANALYSES

Cantürk, Tolga
Master of Science, Civil Engineering
Supervisor: Prof. Dr. Eray Baran

February 2022, 298 pages

In this study, seismic performance assessment of reinforced concrete overpass bridges located along the currently under construction Kınalı-Tekirdağ-Çanakkale-Savaştepe Highway was conducted. Overpass bridges consisted of two-span precast concrete girders and reinforced concrete cast-in-place circular cross section columns. Because of proximity to active faults detailed seismic investigation of the region had already been conducted and site-specific seismic design spectrums had been developed. Structural design of these bridges is based on response spectrum analyses considering 2475 year return period seismic event. AASHTO (2017) iteration method was used to determine the internal plastic forces used in design of columns. To better understand and assess the performance levels of the overpass bridges accurately, nonlinear static pushover and time history analyses were conducted. In pushover analysis, lumped plastic hinge model was assumed for column hinges at possible hinge locations, while a distributed plastic hinge model was used with fiber section was employed in time-history analysis. In numerical analysis models special attention was paid to accurately reflect the effect of girder ends pounding against the cap beams and shear keys at pier and abutment locations. Performance levels of

overpass bridges were evaluated according to Turkish Bridge Earthquake Standard (2020) using the pushover and time history analysis results.

Keywords: Nonlinear pushover analysis, Nonlinear time history analysis, Lumped plastic hinge model, Distributed plastic hinge model, Fiber section, Performance level

ÖZ

DOĞRUSAL OLMAYAN ANALİZLER İLE BETONARME ÜST GEÇİT KÖPRÜLERİNİN SİSMİK PERFORMANS DEĞERLENDİRMESİ

Cantürk, Tolga
Yüksek Lisans, İnşaat Mühendisliği
Tez Yöneticisi: Prof. Dr. Eray Baran

Şubat 2022, 298 sayfa

Bu çalışmada, yapımı devam eden Kınalı-Tekirdağ-Çanakkale-Savaştepe Karayolu üzerinde bulunan betonarme üst geçit köprülerinin sismik performans değerlendirilmesi yapılmıştır. Üst geçit köprüleri, iki açıklıklı prekast beton kirişler ve dairesel kesitli yerinde dökme betonarme kolonlardan oluşmaktadır. Aktif faylara yakınlığı sebebiyle, bölgenin ayrıntılı sismik incelemesi yapılmış ve sahaya özel sismik tasarım spektrumları geliştirilmiştir. Bu köprülerin yapısal tasarımı, tekrarlanma periyodu 2475 yıl olan sismik hareketi dikkate alan tepki spektrumu analizlerine dayanmaktadır. Kolonların tasarımında kullanılan iç plastik kuvvetleri belirlemek için AASHTO (2017) iteratif yöntemi kullanılmıştır. Üstgeçit köprülerinin performans seviyelerini tam olarak daha iyi anlamak ve değerlendirmek için, doğrusal olmayan statik (itme) ve dinamik (zaman-tanım alanı) analizler yapılmıştır. İtme analizinde, olası mafsal bölgelerinde kolon mafsalları için yığılı plastik mafsal modeli varsayılırken, zaman tanım alanı analizinde lif kesit ile yayılı plastik mafsal modeli kullanılmıştır. Sayısal analiz modellerinde, orta ayak ve kenar ayak bölgelerinde kiriş uçlarının başlık kirişlerine ve deprem takozlarına çarpma etkisinin doğru bir şekilde yansıtılmasına özellikle dikkat edilmiştir. Üst geçit

köprülerinin performans seviyeleri, itme ve zaman tanım alanı analiz sonuçları kullanılarak Türkiye Köprü Deprem Yönetmeliğine (2020) göre değerlendirilmiştir.

Anahtar kelimeler: Doğrusal olmayan itme analizi, Doğrusal olmayan zaman tanım alanı analizi, Yığılı plastik mafsal modeli, Yayılı plastik mafsal modeli, Lif kesiti, Performans seviyesi

To my family

ACKNOWLEDGMENTS

This study was conducted under supervision of Prof. Dr. Eray Baran. I would like to express my sincere appreciation for the continuous guidance, constructive criticism he has provided throughout the study. Without his intelligent questions and directions, this thesis would have never been possible.

I am thankful to Mr. Zeki Harputoğlu who is the coordinator of the structural projects and Mr. Burak Kurtman who is the group manager of bridges department in Yüksel Proje for letting me use the documents related with overpass bridges in Çanakkale and their support.

My dear friend Ekin Özlü deserves thanks for her invaluable friendship and patience in proofreading.

I would like to thank to my best friend Burak Tuğrul Adalmış for letting me drink tea and chit-chat in his office when I need a break from the studies late in the evenings.

I am deeply grateful to my dearest mother and sister for their patience and constant support.

Finally, I would like to express my deepest appreciation to my dear friend Alper Öztürk who was always on my side all the way along the line, criticizing, helping, arguing, and utterly motivating me even in the frustrating days.

TABLE OF CONTENTS

LIST OF TABLES

TABLES

LIST OF FIGURES

FIGURES

CHAPTER 1

INTRODUCTION

Nonlinear analysis procedures are frequently used in order to assess the response of structural systems under seismic loading effects. This type of analysis provides valuable and detailed information on the progression of damage within the structural system when subjected to seismic loading. Results obtained form such analysis provide a powerful tool for evaluation of the structural system's performance. Two of the most popular analysis methods utilized in this type of performance assessment are nonlinear static pushover analysis and nonlinear dynamic time history analysis. Various seismic design codes (American Society of Civil Engineers (ASCE), 2017; EN 1998-3, 2005; ATC-40, 1996) recommend these analysis methods as part of performance assessement procedures. Nonlinear static pushover analysis is a practical tool for seismic performance assessment of structures. Nonlinear dynamic time history analysis, on the other hand, is usually more demanding in terms of computational effort.

Seismic design codes for steel or concrete buildings, bridges, and other structures allow the use of both elastic and inelastic analysis methods with some specific limitations. Elastic analysis represents the traditional method and uses the linear analysis results (i.e., member internal forcs) after applying a reduction to reflect the effect of inelastic actions that are expected to develop within the structural system. The reduction is usually done by applying a factor (i.e., q-factor in Eurocode, R-factor in AASHTO). These factors are determined by considering the expected overall ductility of the structural system. This analysis approach is also called as force method.

Inelastic analysis is usually conducted as part of a performance-based evaluation of structures. Inelastic forces and deformations of structural elements determined from this analysis reflecting the nonlinear material responses are then compared against the corresponding limits defining different performance levels. Performance criteria and damage limit states are given in seismic design codes for different types of structures considering several factros, such as life span of the structure, degree of importance, and cost of repairing.

Nonlinear analysis may be also used to determine minimum required reinforcement to provide lower limit of target performance level and may lead to a reduction in the required reinforcement amount compared to a linear analysis. However, in this study evaluation of existing overpass bridges was conducted with no attempt to reinforcement optimization.

Seismic behavior of existing reinforced concrete overpass bridges located on the currently under construction Kınalı-Tekirdağ-Çanakkale-Savaştepe Highway were investigated in the current study by using nonlinear analysis methods. Results from nonlinear pushover and time history analyses were used in performance evaluation of the bridges. Background information on performance criteria and the corresponding limits proposed for assessment of bridges by different sources is provided in the following section.

1.1 Seismic Performance Criteria for Bridges

A performance level is a measure of the expected damage in a structural system when subjected to a specific level of earthquake. Various qualitative measures of seismic performace levels have been presented for bridge structures in various sources. ATC 32 (1996) defines two performance levels, which are “Service Level” and “Damage Level”, according to ground motion on the location and importance category of bridge. Performance criteria of ATC 32 is tabulated in Table 1.1. Functional evaluation ground motion is probabilistically assessed ground motion and it has 40% probability of exceedance during bridge’s service life. However, safety evaluation ground motion represents a probabilistically assessed ground motion with a 1000-2000 year return period. For both functional and safety evaluation cases, performance levels of service and damage are considered. Immediate service level defines that traffic on the bridge must be open after an earthquake, whereas in the case of limited service level several days of restoration is expected and limited access is possible. Bridges are expected to behave elastically for minimal damage level. For repairable damage level, repairable damage is expected with the bridge remaining functional. Lastly, significant damage level corresponds to the case where repair will be needed with bridge out of service and there is a minimal risk of collapse.

Table 1.1 Performance criteria of ATC 32 (1996)

Ground Motion at Site		**Other Bridges**	**Important Bridges**
Functional Evaluation	Service Level	Immediate	Immediate
	Damage Level	Repairable	Minimal
Safety Evaluation	Service Level	Limited	Immediate
	Damage Level	Significant	Repairable

In Caltrans Seismic Design Code (1999), performance criteria of bridges are nearly the same with ATC 32 (1996) recommendations. According to Caltrans SDC, deterministic or probabilistic assessment may be done for the functional evaluation earthquake. It is noted that functional evaluation is not required for ordinary bridges, as long as the requirements explained in Caltrans-SDC are met. The requirements of ordinary bridges to provide performance target are given in terms of displacement ductility (Eq. (1.1)) and global displacement (Eq. (1.2)). The limiting displacement ductility values are given in Table 1.2. Ductile reinforced concrete members are expected to have a minimum local displacement ductility demand capacity of μ_c= 3 to provide rotational capacity in probable plastic hinge regions. The local displacement ductility capacity for structural members is defined in Eq. (1.3).

$$\mu_D = \frac{\Delta_D}{\Delta_Y} \qquad \text{Eq. (1.1)}$$

Where;

Δ_D: Estimated global displacement demand

Δ_Y : Global yield displacement

$$\Delta_C > \Delta_D \qquad \text{Eq. (1.2)}$$

Where;

Δ_C: Global displacement capacity

Δ_D: Global displacement demand

$$\mu_c = \frac{\Delta_c}{\Delta_Y^{col}} \qquad \text{Eq. (1.3)}$$

Where;

Δ_c: Displacement capacity measured from the point of maximum moment to the contra-flexure point

Δ_Y^{col}: Yield Displacement measured from the point of maximum moment to contra-flexure point

Table 1.2 Maximum displacement ductility demand requirements for bridges in Caltrans-SDC

Single column bents supported on fixed foundation	$\mu_D \leq 4$
Multi-column bents supported on fixed or pinned footings	$\mu_D \leq 5$
Pier walls supported on fixed or pinned footings in weak direction	$\mu_D \leq 5$
Pier walls supported on fixed or pinned footings in strong direction	$\mu_D \leq 1$

According to AASHTO-Seismic (2011), life safety performance level must be satisfied considering an earthquake with 1000 year return period (i.e., 7% probability of exceedance in 75 years) for all bridges. This performance level is expected to prevent collapse in a high-intensity earthquake and limit structural damage in a moderate-intensity earthquake. With this performance level, the bridge may sustain significant damage, repair of structural members may be required and traffic flow may be closed after the earthquake. Significant damage may consist of cracking of concrete elements, yielding in reinforcement, spalling of concrete, local buckling for steel columns, as well as deck slab cracking. Similar to Caltrans-SDC (2006), the limits for performance levels in AASHTO-Seismic (2011) are specified in terms of displacement ductility demand (Table 1.3). Displacement ductility demand is computed with Eq. (1.4).

Table 1.3 Displacement ductility demand for bridges with fixed foundation in AASHTO-Seismic

Single column bents	$\mu_D \leq 5$
Multi-column bents	$\mu_D \leq 6$
Pier walls in weak direction	$\mu_D \leq 5$
Pier walls in strong direction	$\mu_D \leq 1$

$$\mu_D = 1 + \frac{\Delta_{pd}}{\Delta_{yi}} \qquad \text{Eq. (1.4)}$$

Δ_{pd}: Plastic displacement demand

Δ_{yi}: Idealized yield displacement corresponding to idealized yield curvature

In FHWA Seismic Retrofitting Manual (2006), four performance levels shown in Table 1.4 are specified for concrete bridges. Performance Level 1 corresponds to significant damage consisting of yielding of reinforcement, as well as cracking and spalling of concrete. Bridge is expected to remanin closed during repair work. Performance Level 2 corresponds to minimal damage in the form of minor cracking in concrete elements with no plastic deformations. The required repair work is expected to be done with the bridge in service. Performance Level 3 corresponds to negligible damage condition, where only non-structural members are expected to sustain damage. A higher performance level than these can also be specified by the bridge owner for extremely important bridges.

Table 1.4 Performance criteria for four performance levels in FHWA (2006)

Performance Level 0 (PL0):	There is no level recommended.
Performance Level 1 (PL1):	Defined as life safety. It means there is significant damage under earthquake and service of bridge is disrupted but life safety is provided. Repairing of the bridge is likely necessary after an earthquake.
Performance Level 2 (PL2):	Defined as operational. Minimal damage is seen on the bridge and bridge is still open for emergency vehicles. Repairing must be done after an earthquake with opening traffic.
Performance Level 3 (PL3):	Defines as fully operational. It can be said that there is negligible damage. Furthermore, bridge is safely open for all vehicles after an earthquake, also if necessary, repairing can be done without closed bridge.

In Specifications for Highway Bridges in Japan (2002), three performance levels are defined considering the classification of bridges and ground motion level, as shown in Table 1.5. Two types of earthquakes, as inland and plate boundary, are specified for level 2 ground motion. The examples for the inland and plate boundary earthquakes are given respectively as Kobe Earthquake in 1994 and Kanto Earthquake in 1923. Performance level 1 represents the minimal damage and immediate service for ordinary and important bridges. Immediate service of bridge and repairable damage is expected for Performance level 2. Performance level 3 corresponds to limited service of the bridge and significant damage.

Table 1.5 Performance criteria of Japanese Specification

Ground Motion		Ordinary Bridges	Important Bridges
Level 1		Performance 1	
Level 2	Type 1	Performance 3	Performance 2
	Type 2		

In HAZUS (FEMA, 2003), five damage limit states given in Table 1.6 are defined for highway bridges. While detailed information of limit state description is given in Table 1.6, quantitative description of these damage limit state is not given. Functional and operational explanation are given for each damage limit state differently. Therefore, time needed for repairing for these damage limit states is also different. Additionally, necessary time increases for repairing while increasing the limit state.

Table 1.6 Limit state definition by HAZUS (FEMA, 2003)

Limit State	Description
None	There is no damage.
Slight	Minor cracking and spalling at column' face and plastic hinge locations.
Moderate	Plastic hinge formation, longitudinal reinforcement buckling, cracking of column core, damage in cap of pile
Extensive	Flexural or shear failure in columns, longitudinal reinforcement pulling, different settlement.
Complete	Collapsing of column, bearing failure and deck collapse, splice failure.

In Eurocode 8-Part 3, there are three damage limits indicated as Near Collapse (NC), Significant Damage (SD) and Damage Limitation (DL). These limit states are determined considering the return periods of the design earthquake as shown in Table 1.7. Near Collapse state represents a structure with severe damage and reduced stiffness. Load-bearing system can still resist the vertical loads safely, but there are large drifts on the structure, and structure would possibly not safe for another earthquake. Significant Damage state represents a structure with serious damage and some reduction in stiffness. The drift levels present in the structure are not large, and the structure is considered safe for after-shocks with moderate intensity. However, repairing of the structure is probably not economical. Damage Limitation state represents a slightly damaged structure with no yielding and stiffness reduction. There is negligible drift on the structure and no need for repair work. The limits for these damage states are defined in terms of chord rotation capacity. The chord rotation capacity for Near Collapse state is given by Eq. (1.5). The chord rotation capacity for Significant Damage state is equal to ¾ of the Near Collapse chord rotation capacity. Damage Limitation state chord rotation capacity is defined as the chord rotation at yielding, as given in Eq. (1.6).

Table 1.7 Limit states of designed earthquake return period in Eurocode 8-Part 3

Limit State	**Return Period**
Near Collapse (NC)	2475 years
Significant Damage (SD)	475 years
Damage Limitation (DL)	225 years

$$\theta_{um} = \frac{1}{\gamma_{el}}(\theta_y + (\phi_u - \phi_y)L_{pl}\left(1 - \frac{0.5\,L_{pl}}{L_V}\right)) \qquad \text{Eq. (1.5)}$$

Where:

θ_{um}: NC limit state chord rotation capacity

γ_{el}: 1.00 for secondary elements and 1.50 for primary seismic elements

θ_y: Yield chord rotation

ϕ_u: Ultimate curvature

ϕ_y: Yield curvature

L_{pl}: Plastic hinge length

L_V: Shear span length

$$\theta_y = \phi_y \frac{L_V + a_v z}{3} + 0.0014\left(1 + 1.5\frac{h}{L_V}\right) + \frac{\varepsilon_y}{d - d'}\frac{d_{bl} f_y}{6\sqrt{f_c}} \qquad \text{Eq. (1.6)}$$

Where:

θ_y: Chord rotation at yielding

$a_v z$: Tension shift in the moment diagram

f_y: Yield strength of reinforcement

f_c: Concrete strength

ε_y: Yield strain of element section

d: Depth to the tensile reinforcement

d': Depth to the compression reinforcement

d_{bl}: Average diameter of reinforcements

Hose *et al.* proposed five levels to describe seismic performance of bridge structures (2000). Damage assessment of the bridge is done by considering the repair and functional conditions, as shown Table 1.8, with the qualitative and quantitative performance definitions given in Table 1.9. Quantitative definition is given in terms of cracking width, angle of crack and concrete spalling locations.

Table 1.8 Damage classification and corresponding descriptions (Hose *et al.*, 2000)

Level	**Damage Classification**	**Damage Description**	**Repair Description**	**Socio-economic Description**
I	No	Barely visible cracking	No Repair	Fully Functional
II	Minor	Cracking	Possible Repair	Operational
III	Moderate	Open cracks Onset of spalling	Minimum Repair	Life Safety
IV	Major	Very wide cracks Extended concrete spalling	Repair	Near Collapse
V	Local Failure / Collapse	Visible permanent deformation Buckling/Rupture of reinforcement	Replacement	Collapse

Table 1.9 Seismic performance levels and corresponding descriptions (Hose *et al.*, 2000)

Level	**Performance Level**	**Qualitative Performance Description**	**Quantitative Performance Description**
I	Cracking	Onset of hairline cracks	Cracks barely visible
II	Yielding	Theoretical first yield of longitudinal reinforcement	Crack widths < 1mm
III	Initiation of Local Mechanism	Initiation of inelastic deformation Onset of concrete spalling Development of diagonal cracks	Crack widths 1-2 mm Length of spalled region > 1/10 cross-section depth
IV	Full Development of Local Mechanism	Wide crack widths/spalling over full local mechanism region	Crack widths > 2 mm Diagonal cracks extend over 2/3 cross section depth Length of spalled region > 1/2 cross-section depth
V	Strength Degradation	Buckling of main reinforcement Rupture of transverse reinforcement Crushing of core concrete	Crack widths > 2mm in concrete core Measurable dilation > 5% of original member dimension

Hwang *et al.* determined two approaches for assessment of damages observed on bridges (2001). Firstly, authors proposed the four damage states given in Table 1.10 considering the flexural capacity of bridge columns. First yielding in longitudinal reinforcement is represented as M_1 value, while M_y is defined as the yield moment obtained from the idealized moment-curvature diagram of the column cross section. Furthermore, θ_p is the plastic rotation at concrete strains of 0.002 and 0.004, respectively for columns with lap splices and without lap splices.

Table 1.10 Seismic damage assessment criteria for columns in flexure (Hwang *et al.*, 2001)

Criterion	**Description of Damage**	**Column Status**
$M_1 > M$	No reinforcing steel yielding, minor cracking in concrete	No Damage (OK)
$M_y > M \geq M_1$	Tensional reinforcement yielding and extensive cracking in concrete	Cracking (C)
$M \geq M_y$ $\theta < \theta_p$	Hinging in column, but no failure of column	Hinging (H)
$M \geq M_y$ $\theta > \theta_p$	Flexural failure of column	Flexural failure (F)

Secondly, damage states were determined for overall bridge seismic damage. Therefore, column status are specified in terms of displacement ductility ratio computed by Eq. (1.7). In this equation, Δ represents displacement at the column top and Δ_{cy1} represents column's relative displacement for first yielding of longitudinal reinforcement. The limiting conditions for displacement ductility ratio corresponding to the five damage states are given in Table 1.11. The value of μ_{cy1} is equal to 1.0. μ_{cy} is the displacement ductility ratio at initiation of yielding in

longitudinal reinforcement. μ_{c2} is the ductility ratio when concrete strain is equal to 0.002. Maximum ductility ratio (μ_{cmax}) is found by adding 3.0 to μ_{c2}.

Table 1.11 Damage states of bridges for displacement ductility ratios (Hwang *et al.*, 2001)

	Damage States	**Column Status**
N	No Damage	$\mu_{cy1} > \mu_d$
S	Slight/Minor Damage	$\mu_{cy} > \mu_d > \mu_{cy1}$
M	Moderate Damage	$\mu_{c2} > \mu_d > \mu_{cy}$
E	Extensive Damage	$\mu_{cmax} > \mu_d > \mu_{c2}$
C	Complete Damage	$\mu_d > \mu_{cmax}$

$$\mu_d = \frac{\Delta}{\Delta_{cy1}} \qquad \text{Eq. (1.7)}$$

Kowalsky proposed two damage states for RC bridge circular columns as "Serviceability" and "Damage Control" (2000). The serviceability state reflect the case where repairing of the column is not needed after the earthquake, while repairable damage is expected in "Damage Control" state. The concrete compressive strain limit and reinforcement tensile strain limit for these damage states are given in Table 1.12. The strain limits for Serviceability state correspond to initiation of concrete crushing and a residual crack width of approximately 1 mm. The strain limits for Damage Control state are given for columns with well detailed transversal reinforcement, so these cannot be used for columns with insufficient transverse reinforcement.

Table 1.12 Damage limit states and limiting strain values (Kowalsky, 2000)

Damage Limit State	Concrete Strain Limit	Reinforcement Strain Limit
Serviceability	0.004	0.015
Damage control	0.018	0.060

In Canadian Standard CAN/CSA-S6-19, performance levels are specified by considering the three bridge importance categories of lifeline, major-route, and other bridges. Performance levels are provided for these three bridge importance categories considering three return periods of 475, 975, and 2475 years, as shown in Table 1.13. Limits for Minimal Damage, Repairable Damage, and Extensive Damage performance levels are provided in Table 1.14 in terms of concrete compressive strain and longitudinal steel tensile strain. Minimal Damage performance level represents concrete cover spalling. Repairable Damage strain limit corresponds to hardening of the longitudinal reinforcement. The longitudinal reinforcement tensile strain limit for Extensive Damage performance level was set to avoid any reinforcement buckling. Furthermore, there is also another damage level called Probable Replacement, which represents severe damage with no crushing of the confined concrete. For this performance level, the steel tensile strain is limited to 0.075 in order to prevent fracture of reinforcement.

Table 1.13 Performance levels and damage requirements in CAN/CSA-S6-19

Return period of earthquake	**Lifeline bridges**		**Major-route bridges**		**Other bridges**	
	Service	**Damage**	**Service**	**Damage**	**Service**	**Damage**
475 years	-	-	Immediate	Minimal	Service Limited	Repairable
975 years	Immediate	Minimal	-	-	-	-
2475 years	Service Limited	Repairable	Service Disruption	Extensive	Life Safety	Probable Replacement

Table 1.14 Damage level strain limits in CAN/CSA-S6-S19

Damage Level	**Strain Limits**
Minimal Damage	$\varepsilon_c \leq 0.006$ $\varepsilon_s \leq 0.01$
Repairable Damage	$\varepsilon_s \leq 0.025$
Extensive Damage	$\varepsilon\_c \leq 0.80\varepsilon_{cu}$ $\varepsilon_s \leq 0.05$

Turkish Bridge Earthquake Standard (TBES) (2020) categorizes damage level into two classes for nonlinear analysis type. These classes are called Controlled Damage and Collapse Prevention. Furthermore, Limited Damage level is also considered for the first order analysis. Plastic rotation limits for these three performance levels can be found by using Eq. (1.8).

$$\theta_p^{(LD)} = (0.1875\phi_u - \phi_y)L_p$$
$$\theta_p^{(CD)} = (0.5\phi_u - \phi_y)L_p \quad \text{Eq. (1.8)}$$
$$\theta_p^{(CP)} = (0.67\phi_u - \phi_y)L_p$$

Where;

$\theta_p^{(LD)}$: Plastic rotation limit of limited damage level (rad)

$\theta_p^{(CD)}$: Plastic rotation limit of controlled damage level (rad)

$\theta_p^{(CP)}$: Plastic rotation limit of collapse prevention damage level (rad)

ϕ_u: Ultimate curvature (rad/m)

ϕ_y: Yield curvature (rad/m)

L_p: Plastic hinge length (m)

According to TBES (2020), the performance level is also determined by comparing the maximum strains in the reinforcement and in the confined concrete with the corresponding limit values for more detailed analysis. Strain limits for the reinforcement and confined concrete for three performance levels are given in Eq. (1.9).

$$\varepsilon_c^{(LD)} = 0.003 \;\&\; \varepsilon_s^{(LD)} = 0.015$$
$$\varepsilon_c^{(CD)} = 0.5\varepsilon_{cu} \leq 0.0135 \;\&\; \varepsilon_s^{(CD)} = 0.5\varepsilon_{su} = 0.040 \quad \text{Eq. (1.9)}$$
$$\varepsilon_c^{(CP)} = 0.67\varepsilon_{cu} \leq 0.018 \;\&\; \varepsilon_s^{(CP)} = 0.67\varepsilon_{su}$$

Where;

$\varepsilon_c^{(LD)}$: Confined concrete strain limit for limited damage level

$\varepsilon_s^{(LD)}$: Reinforcement strain limit for limited damage level

$\varepsilon_c^{(CD)}$: Confined concrete strain limit for controlled damage level

ε_{cu}: Ultimate strain for confined concrete

$\varepsilon_s^{(CD)}$: Reinforcement strain limit for controlled damage level

1.2 Aim and Scope of the Study

Main aims of this study are as follows:

- To understand the performance and behavior of reinforced concrete overpass bridges with gaps on each axis under seismic event.
- To assess performance level and behavior of each axis columns when column height is equal and not equal for each other. Especially, only one analysis model is created for elastic analysis, but bridges with gaps needs to consider all earthquake direction scenario because of the pounding effect.
- To understand difference in between nonlinear time history analysis and pushover analysis results by using distributed plastic hinge with fiber section and lumped plastic hinge respectively.

Following this introduction and literature review, all information's of bridges are explained in Chapter 2. In Chapter 3, nonlinear bridge modelling was mentioned in detail. Pushover analysis philosophy and how to create a lumped plastic hinge were mentioned in Chapter 4, after that pushover analysis results of six bridges considering in this study were given in Chapter 5. In Chapter 6, nonlinear time history analysis was introduced with fiber hinges. Nonlinear time history analysis results of two selected bridges considering in this study were given in Chapter 7. Conclusion, general comparison and recommendations of all studies were given in Chapter 8.

CHAPTER 2

DESCRIPTION OF INVESTIGATED BRIDGES

2.1 Introduction

The bridges studied as part of this thesis are located on the Kınalı-Tekirdağ-Çanakkale-Savaştepe highway, which is currently under construction. As shown in Figure 2.1 and Figure 2.2, the 354 km long highway runs from the North of Marmara Sea to the south and crosses the Dardanelles Strait. The highway line consists of 53 overpasses in total, but only six of them were selected in the current study for a detailed investigation of their seismic response.

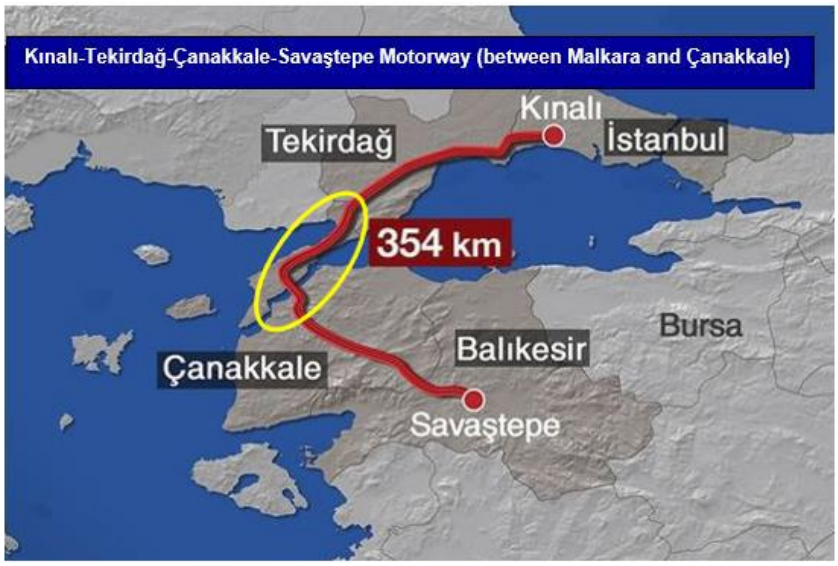

Figure 2.1 Kınalı-Tekirdağ-Çanakkale-Savaştepe Highway project line (retrieved from the Structural work design basis report)

Figure 2.2 Kınalı-Tekirdağ-Çanakkale-Savaştepe Highway project line (retrieved from the structural work design basis report)

Figure 2.3 and Figure 2.4 show the seismic hazard and active faults in the region that the investigated bridges are located. Structural design of the investigated bridges is based on earthquake design spectrum for a return period of 2475 years (2% probability of exceedance in 50 years). A detailed seismic investigation of the region had already been conducted in order to develop site-specific seismic design spectrums. Some of the results from this existing seismic investigation have been utilized in the current study.

Concrete material class of all structural elements is C30 except girders, whereas C45 is used for girders. S420 steel class is adopted for reinforcement used in design.

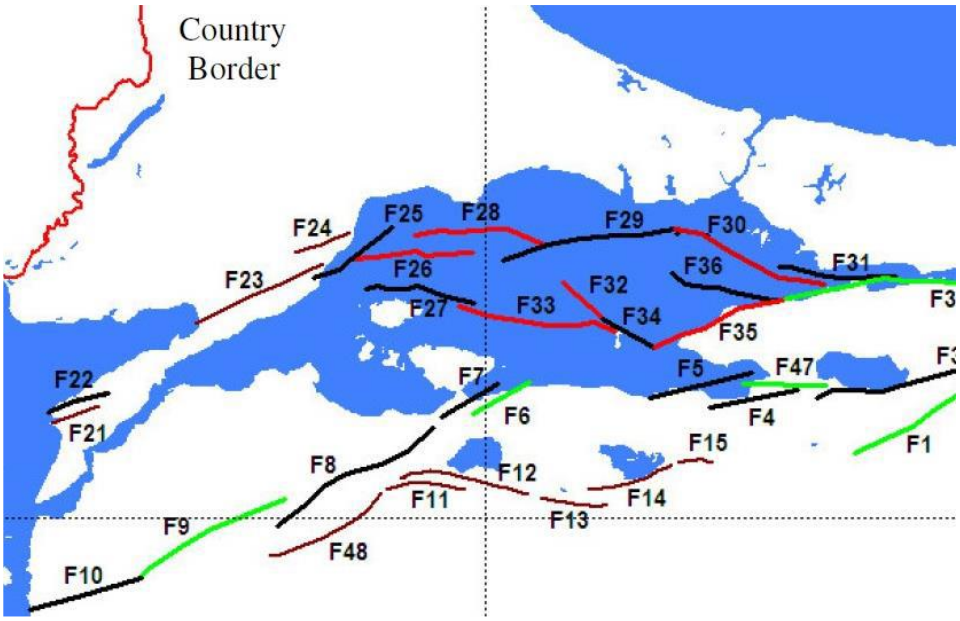

Figure 2.3 Active faults in Marmara region (retrieved from the structural work design basis report)

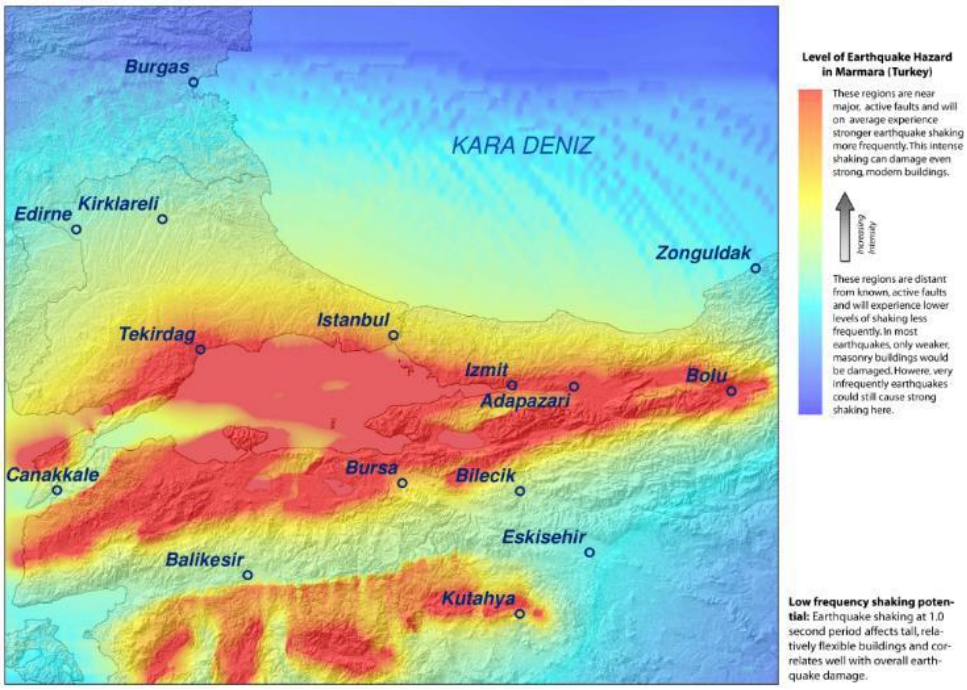

Figure 2.4 Level of earthquake hazard in Marmara region (retrieved from the structural work design basis report)

Earthquake hazard analysis report had already been prepared to determine earthquake hazard and design spectrum for each bridge. The report contains the findings of a comprehensive study of the probabilistic earthquake hazard for the Marmara, Thrace, and Northwestern Anatolia regions. The principle parameters required to determine the probability-based earthquake hazard are the sources of earthquake, the earthquake occurrence characteristics for each source, the ground motion prediction, and the probabilistic model. The time-dependent probabilistic seismic hazard model after the 1999 Kocaeli Earthquake has been studied in order to determine the probabilistic earthquake hazard of the related region. In the time dependent models, the earthquake occurrence probability increases depending on the time elapsed since the latest great earthquake in the fault controlling the regional earthquake hazard.

The probabilistic hazard analysis has been conducted for the average recurrence periods of 72, 475 and 2475 years (respectively 50%, 10% and 2% exceedance probability in 50 years) in the peak ground acceleration (PGA), the peak ground velocity (PGV), and the spectral accelerations corresponding to 0.2 s (S_s, spectral response acceleration parameter at short periods) and 1.0 s (S_1, spectral response acceleration parameter at a period of 1 s) with 5% damping. The site-specific design response spectrum for a return period of 2475 years has been determined based on the local ground conditions of bridge and the ground magnification coefficients in the ASCE 7-16 (2016) specifications. In addition to the probabilistic hazard studies, the deterministic earthquake hazard has been determined based on the probabilistic hazard deaggregation.

2.2 Geometric Details of Investigated Bridges

The investigated bridges have two simple spans, with A1 and A2 indicating abutment lines and P indicating pier line (Figure 2.5). All bridges are of precast concrete girder type, consisting of precast prestressed concrete girders and a cast-in-place reinforced concrete slab placed above the girders. The precast prestressed concrete girders are supported by piers at both ends. Girder ends are supported by elastomeric bearings that are placed on cast-in-place reinforced concrete cap beams. Each pier consists of three cast-in-place reinforced concrete circular cross section columns that are positioned next to each other at a certain spacing in the transverse direction of the bridge.

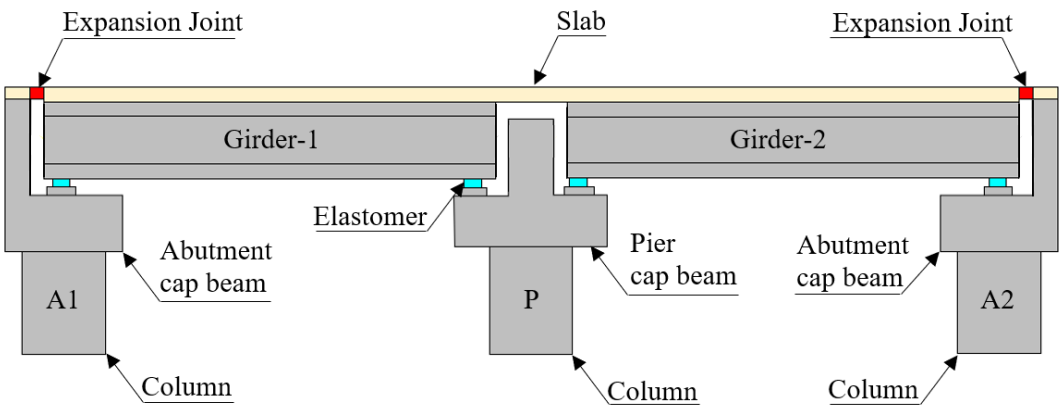

Figure 2.5 General structural layout for investigated bridges

The cross section of the bridges considered in this study is formed by seven 120 cm deep precast prestressed concrete girders that are positioned at 1.74 m spacing, as shown in the Figure 2.6 and Figure 2.7. A 25 cm thick cast in place concrete slab is placed above the girders. The bridges have a platform width of 12.00 m, and an asphalt thickness of 6 cm. Additional elements include curbs with 25 cm height and 1.50 m length, precast concrete side panels with 70×8 cm section, as well as guardrails and handrails. The total length and span length for each bridge considered in the study is tabulated in Table 2.1.

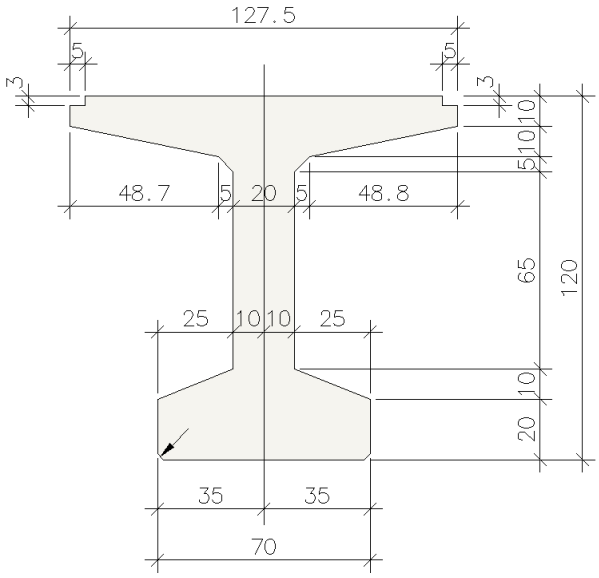

Figure 2.6 I-120 Precast prestressed concrete girder section used in bridges

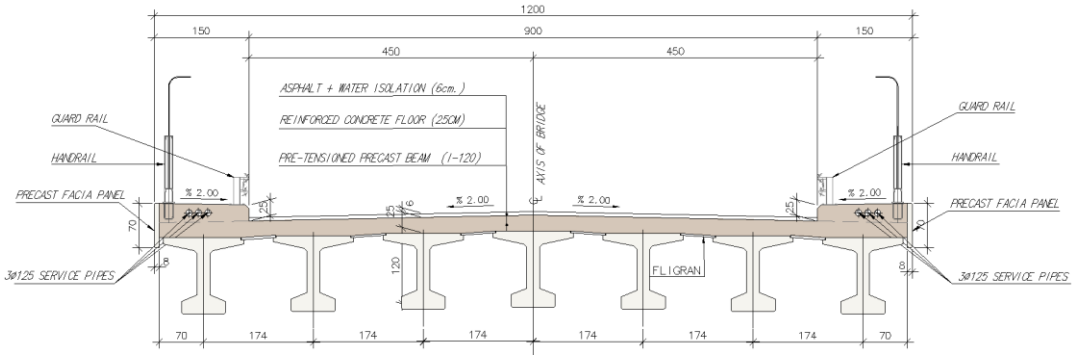

Figure 2.7 Superstructure section of the bridges

Each abutment and pier frame consist of three 1.80 m diameter cast in place reinforced concrete columns placed at a spacing of 4.50 m, as shown in Figure 2.8.

Column heights, column longitudinal reinforcement and column transversal reinforcement properties of the bridges are given in Table 2.2, Table 2.3 and Table 2.4 respectively.

Table 2.1 Total and span lengths in bridges

Bridge Name	Bridge Total Length (m)	A1-P Span (m)	P-A2 Span (m)
O2	52.00	26.00	26.00
O5	50.00	25.00	25.00
O7	50.00	25.00	25.00
O13	50.00	25.00	25.00
O15	48.00	24.00	24.00
O48	50.00	25.00	25.00

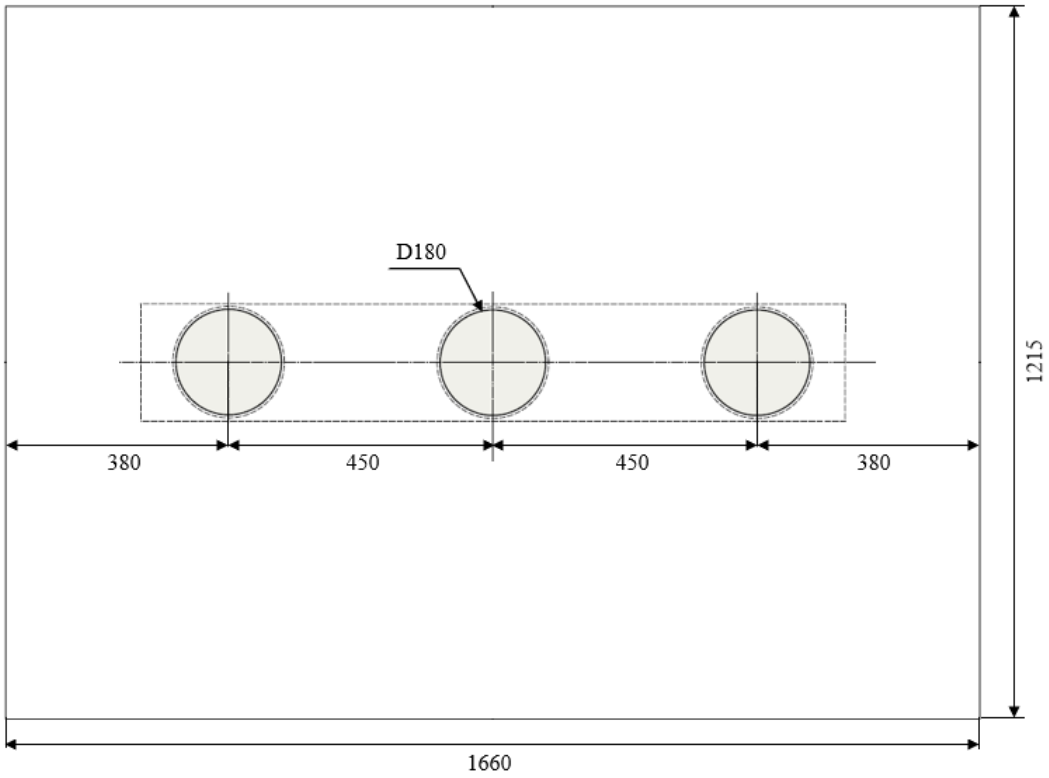

Figure 2.8: Column plan view of all bridges (units in cm)

Table 2.2 Column heights in bridges

Bridge Name	Number of Columns			Column Height (m)		
	A1	P	A2	A1	P	A2
O2	3	3	3	7.00	7.00	7.00
O5	3	3	3	7.70	8.00	6.80
O7	3	3	3	5.70	7.10	8.00
O13	3	3	3	6.80	6.80	6.80
O15	3	3	3	8.00	6.80	6.00
O48	3	3	3	8.00	8.00	7.00

Table 2.3 Longitudinal reinforcement in bridge columns

Bridge Name	Longitudinal Reinforcement			Additional Reinforcement Length (Bottom Reinforcement) (m)		
	A1	P	A2	A1	P	A2
O2	54ϕ32	58ϕ32	54ϕ32	-	-	-
O5	54ϕ32	54ϕ32	54ϕ32	-	-	-
O7	62ϕ32	62ϕ32+31ϕ25	62ϕ32	-	3.80	-
O13	62ϕ32	62ϕ32	62ϕ32	-	-	-
O15	54ϕ32	54ϕ32+27ϕ25	54ϕ32+27ϕ25	-	3.00	3.70
O48	62ϕ32	62ϕ32	62ϕ32	-	-	-

Table 2.4 Transversal reinforcement in all bridges columns

Bridge Name	Transversal Reinforcement for each Axis		
	A1	**P**	**A2**
O2	ϕ22/7.5 cm	ϕ22/7.5 cm	ϕ22/7.5 cm
O5	ϕ22/7.5 cm	ϕ22/7.5 cm	ϕ22/7.5 cm
O7	ϕ22/10 cm	ϕ22/10 cm	ϕ22/10 cm
O13	ϕ22/7.5 cm	ϕ22/7.5 cm	ϕ22/7.5 cm
O15	ϕ22/10 cm	ϕ22/10 cm	ϕ22/10 cm
O48	ϕ22/10 cm	ϕ20/10 cm	ϕ22/10 cm

The bridges have two types of 12 m long cap beams at girder supports. The cap beams used at abutment lines A1 and A2 have an L-shape cross section (Figure 2.9), while the beam used at pier line P has an inverted T-shape cross section (Figure 2.10).

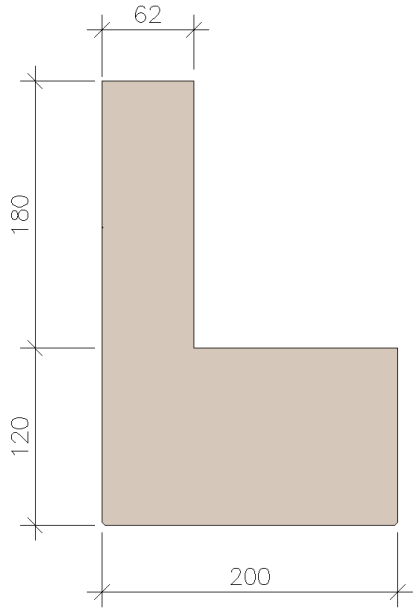

Figure 2.9 L-shape cap beam section at abutment lines A1 and A2 (units in cm)

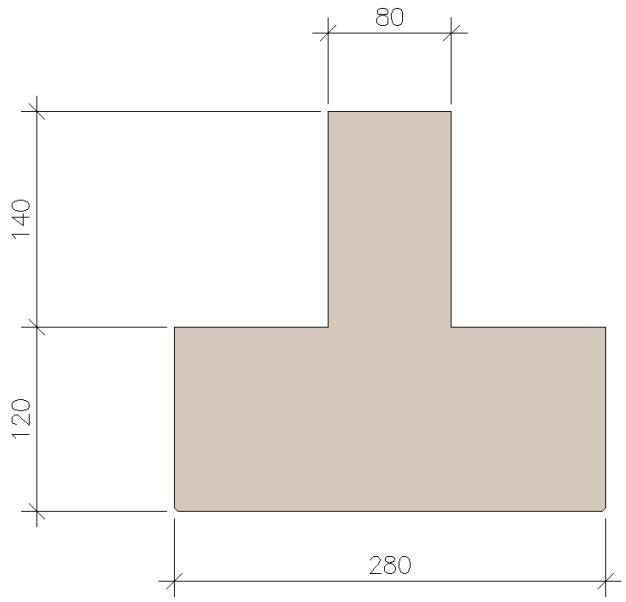

Figure 2.10 Inverted T-shape cap beam section at pier line P (units in cm)

Elastomeric bearing pads reinforced with steel plates are used under the precast prestressed girders. The elastomeric bearing pads used in all bridges have 400×400×130 mm dimensions (Figure 2.11).

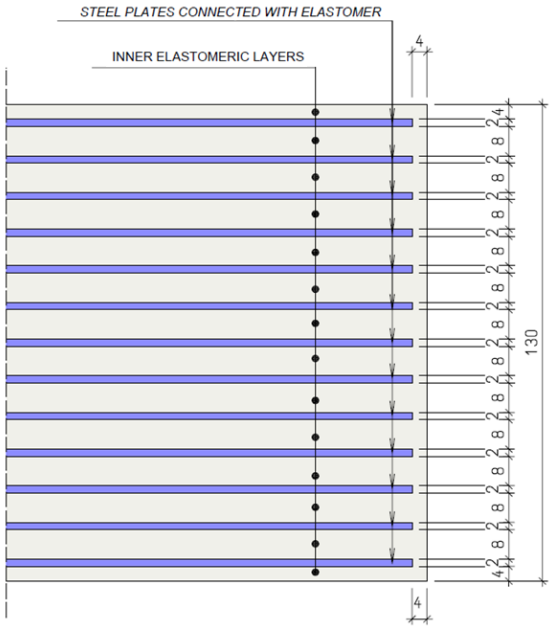

Figure 2.11 Elastomeric bearing pad details (units in mm)

2.3 Modeling Details and Design Spectrums used for Bridges

The “collapse prevention” seismic performance level has been considered during structural design of the investigated bridges. With this performance level, the bridge is expected to sustain damage during the design earthquake, but no thread to life safety is expected. Bridges designed based on this performance level are expected to allow the passage of emergency vehicles following the earthquake but may remain in operational for regular traffic for a short period of time (i.e., a few weeks). The other seismic performance levels often used in structural design are “controlled damage” and “limited damage”.

The AASHTO-LRFD Specification (2017) categorizes the bridges based on operational condition after a seismic event as “critical bridges”, “essential bridges”, and “other bridges”. Critical bridges are described as those that are expected to remain open to all traffic after a 1000 year return period earthquake and be usable by emergency vehicles immediately after a stronger earthquake (e.g., a 2500 year return period earthquake). Essential bridges, on the other hand, are expected to be open to emergency vehicles immediately after a 1000 year return period earthquake.

The collapse prevention seismic performance level adopted in the design of the investigated bridges for design level earthquake corresponds to the “other bridges” operational category in AASHTO Specification. For this category, the response modification factor (R) is specified as 3 and 5, respectively for the cases of single column piers and multiple column piers. Accordingly, a response modification factor of 3 was used for design of the bridge columns in the longitudinal direction of the bridge, while a factor of 5 was used in the transverse direction. It is important to note that these R factors were used for reduction of only the column axial loads and flexural moments with no reduction for earthquake forces in other structural members. In other words, cap beams, shear keys, and concrete blocks were designed as capacity protection elements with an R factor of 1.0.

Three-dimensional analysis model for each bridge was created by using Midas Civil software using the frame elements. Special attention was paid in modeling the relation between the girders and other elements at support locations. The effect of the gap between the superstructure and cap beams in longitudinal direction, as well as the gap between the girders and shear keys in transversal direction are reflected in the analysis model by utilizing an iterative procedure. Such an iterative analysis is required, because using the actual lateral stiffness of the elastomeric bearing pads results in relative displacements at girder supports that are much larger than the 8 cm physical gap that exists in actual bridges. Such excessive relative girder displacements indicate pounding of girder ends into cap beams and shear keys. In the procedure adopted in the analyses, stiffness of the elastomer is increased gradually until the relative displacement between girder ends and cap beams at the end of the response spectrum analysis is equal to the 8 cm physical gap that exists in the actual bridges. This procedure was repeated for the two principal directions and the elastomer stiffness determined this way was used in the subsequent analyses.

The method mentioned above is used for modeling the girder support conditions does not reflect the actual response in the longitudinal direction of bridges. In the longitudinal direction, when one end of girder comes into contact with the cap beam, a gap occurs at the other end. Therefore, for a given girder, simultaneous pounding does not occur at both ends. For example, for the earthquake direction indicated in Figure 2.12, there will be no contact between girder-1 and abutment line A1, as well as between girder-2 and pier line P. In other words, pounding is expected to occur only at the locations indicated with a black dot in the figure. This phenomenon has an important effect on the analysis results, therefore pounding conditions at girder ends must be reflected correctly in analysis models. In order to overcome this problem in response spectrum analysis, a separate model of the bridge should be created for each longitudinal earthquake direction and the correct elastomer stiffness values should be used.

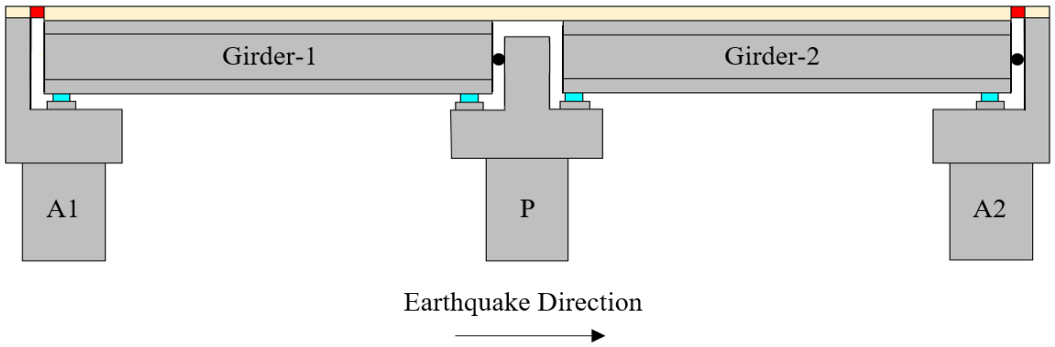

Figure 2.12 Representation of gaps existing at girder supports

The gravity load considered in the analyses consists of self-weight of girders, slab, cap beams and piers, as well as additional superimposed dead load including the weight of other elements such as asphalt pavement, guardrails, handrails, and side panels. The earthquake design spectrum used in the analyses was created for each bridge by considering the soil class, location, and the distance from the fault. The 2475-year return period response spectrums considered in the design of bridges are shown in Figure 2.13.

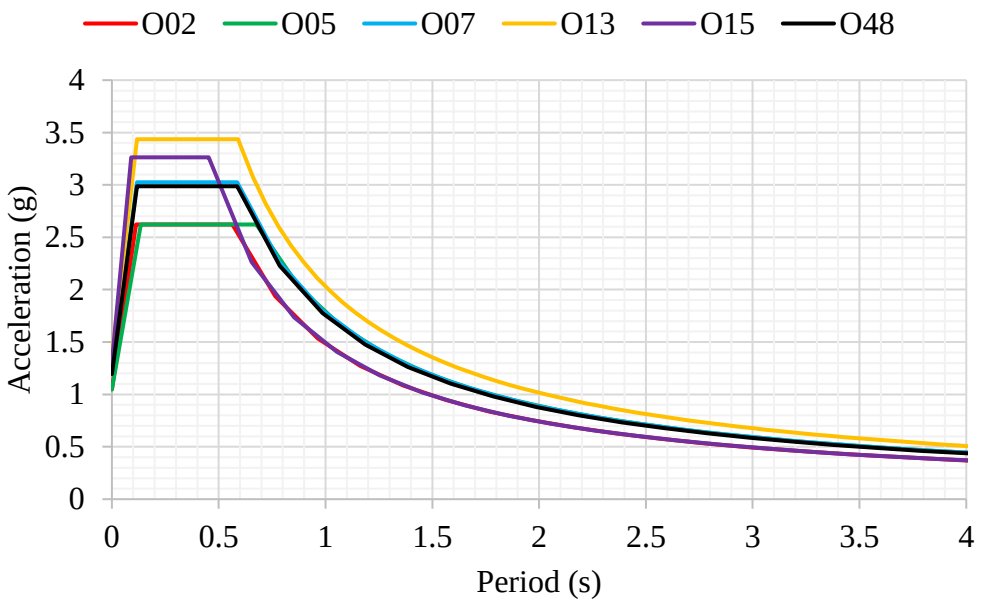

Figure 2.13 Response spectrum of all bridges

Information on soil class classified by NEHRP (2009), fault distance and peak ground acceleration (PGA) values, which are found from design response spectrums at 0 s period, are shown in Table 2.5

Table 2.5 Location properties and PGA values of each bridge

Bridge Name	**Soil Class**	**Fault Distance (km)**	**PGA (g)**
O02	C	25.00	1.05
O05	C	14.10	1.05
O07	C	10.00	1.21
O13	C	3.17	1.37
O15	B	4.00	1.31
O48	C	6.20	1.19

According to AASHTO LRFD (2017) and TBES (2020), elastic seismic force determined from the response spectrum analysis must be combined by considering the two perpendicular directions. To obtain the total design earthquake forces in the main direction, 100 percent of the absolute value of the forces in that direction must be considered and 30 percent of the absolute value of the forces in the other perpendicular direction must be added as shown in Eq. (2.1).

$$E^{Hx} = 1.00EQ_x + 0.30EQ_y$$
$$E^{Hy} = 0.30EQ_x + 1.00EQ_y \qquad \text{Eq. (2.1)}$$

E^{Hx}: Earthquake load combination in the X-direction

E^{Hy}: Earthquake load combination in the Y-direction

EQ_x: Spectrum load case in the X-direction

EQ_y: Spectrum load case in the Y-direction

Earthquake design forces were determined by considering these earthquake load combinations together with 30% of live load, which includes H30-S24 truck loading

and 3.6 kN/m^2 of pedestrian loading. Vertical earthquake action was not considered for original design of the bridges.

2.4 Design Procedure Used for Bridges

Member forces that are expected to develop after the formation of plastic deformations in bridge components were determined by using the simple procedure suggested in the AASHTO LRFD 8th edition. The column moment resistance considered in this procedure includes overstrength capacity. This expected resistance is calculated by considering the actual column actual size and reinforcement amount, as well as the expected material strengths for the concrete and steel reinforcing bars.

The procedure for determination of the plastic forces is different for two principal directions of the bridge. This is because of the fact that in the longitudinal direction bridge columns behave as individual cantilever members and plastic hinging occur only at the bottom of each column. In the transverse direction of the bridge, on the other hand, columns and cap beams form a frame at pier and abutment locations. In this case, plastic hinging is expected to occur at column top and bottom ends. It should be noted that in the transverse direction, columns in these support frames develop different levels of axial force as a result of the earthquake action. Such an unequal axial force distribution should be considered while determining the condition of plastic hinging on columns.

In the longitudinal direction, axial force of the column can be directly determined the from the gravity loading acting on the bridge. After determination of column axial forces, the corresponding column moment capacity is obtained from the nominal P-M interaction diagram of column cross sections. The nominal moment capacity determined this way for each column is then amplified with a factor of 1.3 to obtain the overstrength moment resistance. The corresponding plastic shear force is determined by dividing the overstrength moment resistance by the column height.

In the transverse direction, an iterative procedure is required to determine the plastic forces due to variability in column axial forces as a result of frame action. The procedure starts by determining the column axial forces under gravity loading. Nominal moment capacity value related to this level of axial force is obtained from P-M interaction diagram of column cross section. The change effect of the axial force values in order to determine the plastic forces is found from the following iteration procedure:

i) Each nominal moment values, which were found from nominal P-M interaction diagram, are increased with 1.3 times (overstrength resistance factor). After that, these moments were divided by half of the column height to determine the corresponding shear force.
ii) Column shear forces at each abutment locations were summed to determine the maximum shear force in the frame system.
iii) The frame shear force was applied to the mass center of the superstructure and column axial forces were determined due to overturning when the column overstrength moments are developed.
iv) Column overstrength moments were determined by using the column axial forces combined with the dead load axial forces. If the maximum shear force within the frame system is within 10 percent of the value previously determined, these forces were accepted as plastic forces of columns. Otherwise, the above procedure was repeated until this criteria was met.

The axial forces, shear forces and bending moments corresponding to plastic hinging and determined by utilizing the procedures explained above are presented in Table 2.6 and Table 2.7, respectively for the transverse and longitudinal directions. In these tables, the negative sign indicates a tensile axial force, which is valid for this study.

Table 2.6 Plastic forces of all bridges in the transverse direction

Plastic Hinge Forces in the Transverse Direction										
Bridge Name	**Column**	**Abutment line A1**			**Pier line P**			**Abutment line A2**		
		P_p (kN)	V_p (kN)	M_p (kN·m)	P_p (kN)	V_p (kN)	M_p (kN·m)	P_p (kN)	V_p (kN)	M_p (kN·m)
O02	**Right**	-8165	2742	9597	-7605	3405	11916	-8165	2742	9597
	Middle	1496	4915	17203	2819	5134	17969	1496	4915	17203
	Left	11156	6573	23004	13243	6816	23855	11156	6573	23004
O05	**Right**	-8603	3163	9490	-6556	2600	10400	-8603	3163	9490
	Middle	1364	5720	17160	2857	4550	18200	1364	5720	17160
	Left	11332	7280	21840	12271	5785	23140	11332	7280	21840
O07	**Right**	-8657	2925	11700	-10319	4211	14950	-8657	2925	11700
	Middle	1342	4810	19240	2802	6958	24700	1342	4810	19240
	Left	11342	6110	24440	15922	8349	29640	11342	6110	24440
O13	**Right**	-9193	3346	11375	-8113	3441	11700	-9193	3346	11375
	Middle	1423	5544	18850	2757	5735	19500	1423	5544	18850
	Left	12040	7169	24375	13626	7265	24700	12040	7169	24375
O15	**Right**	-7689	2470	9880	-9417	3824	13000	-10961	4312	12935
	Middle	1477	4388	17550	2663	6424	21840	1327	6825	20475
	Left	10643	5623	22490	14742	8056	27391	13614	8576	25727
O48	**Right**	-9312	3250	11375	-7754	3250	13000	-9312	3250	11375
	Middle	1412	5490	19214	2796	4875	19500	1412	5490	19214
	Left	12136	7057	24700	13346	6240	24960	12136	7057	24700

Table 2.7 Plastic forces of all bridges in the longitudinal direction

Plastic Hinge Forces in the Longitudinal Direction										
Bridge Name	**Column**	**Abutment line A1**			**Pier line P**			**Abutment line A2**		
		P_p (kN)	V_p (kN)	M_p (kN·m)	P_p (kN)	V_p (kN)	M_p (kN·m)	P_p (kN)	V_p (kN)	M_p (kN·m)
O02	**Right**	2373	2530	17711	2820	2567	17970	2373	2530	17711
	Middle	2373	2530	17711	2820	2567	17970	2373	2530	17711
	Left	2373	2530	17711	2820	2567	17970	2373	2530	17711
O05	**Right**	2246	2947	17680	2971	2291	18330	2246	2947	17680
	Middle	2246	2947	17680	2971	2291	18330	2246	2947	17680
	Left	2246	2947	17680	2971	2291	18330	2246	2947	17680
O07	**Right**	2637	2519	20150	3558	3479	24700	2637	2519	20150
	Middle	2637	2519	20150	3558	3479	24700	2637	2519	20150
	Left	2637	2519	20150	3558	3479	24700	2637	2519	20150
O13	**Right**	2587	2772	18850	2757	2868	19500	2587	2772	18850
	Middle	2587	2772	18850	2757	2868	19500	2587	2772	18850
	Left	2587	2772	18850	2757	2868	19500	2587	2772	18850
O15	**Right**	2484	2194	17550	2931	3212	21840	2442	3413	20475
	Middle	2484	2194	17550	2931	3212	21840	2442	3413	20475
	Left	2484	2194	17550	2931	3212	21840	2442	3413	20475
O48	**Right**	2865	2785	19500	3469	2600	20800	2865	2785	19500
	Middle	2865	2785	19500	3469	2600	20800	2865	2785	19500
	Left	2865	2785	19500	3469	2600	20800	2865	2785	19500

CHAPTER 3

BRIDGE MODELING

3.1 Introduction

For the evaluation of the seismic performance of bridge structures, three-dimensional frame elements were used by considering the cross-section properties to represent the superstructure, connection slab, cap beams, and columns. Midas Civil analysis software, a finite element (FE) analysis program developed by Midas IT, was used to assess the bridges in this study. Superstructure was modeled as a spline model, meaning that all structural members were represented as frame elements. Nodes connecting the superstructure were created at the centroid of the superstructure section. An illustration of the numerical model for the O13 bridge is given in Figure 3.1. Prestress forces inside the girders were not taken into account since all structural elements except for the columns are expected to remain elastic based on the adopted design approach.

According to AASHTO-LRFD Seismic Bridge Design (2011), no stiffness reduction is recommended for prestressed concrete superstructures. However, Turkish Bridge Earthquake Standard (2020) recommends 50% of gross stiffness as the effective stiffness in flexure and shear but no reduction for axial behavior. In this study, TBES (2020) was considered to determine the effective stiffness properties for superstructure elements.

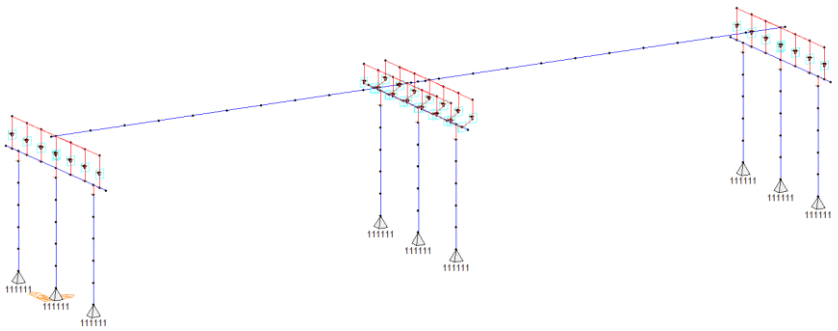

Figure 3.1 Analysis model in the Midas Civil software (O13 bridge)

3.2 Connection Slab Modeling

Connection slab provides the connection between the superstructure elements on the neighboring spans at the cap beam location. To reflect this condition, connection slab elements were provided in between the superstructure elements, as shown in Figure 3.2. Similar to the superstructure elements, the effective stiffnesses of the connection slab elements were taken as 50% of their gross stiffness.

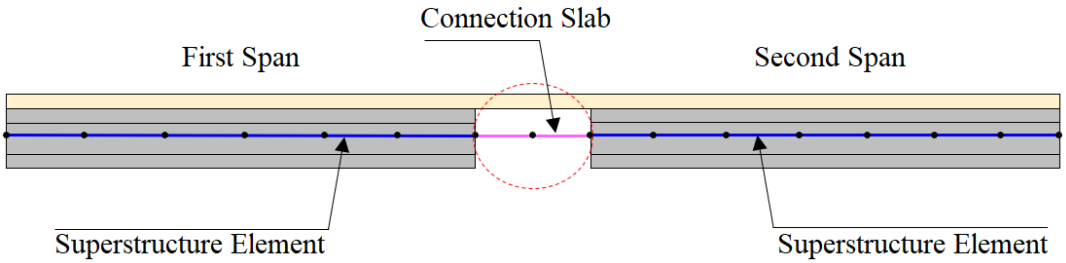

Figure 3.2 Modeling of superstructure and connection slab

3.3 Cap Beam Modeling

Cap beams are designed as capacity protective elements, in other words they are expected to remain elastic under earthquake actions. In the longitudinal direction of the bridge, each column acts as a cantilever member with the cap beam and other associated masses located at the top. In the transverse direction of the bridge, on the other hand, a frame system is formed at the pier and abutment locations by three

columns and the cap beam. As per TBES (2020), effective torsional and flexural stiffnesses of cap beams were taken respectively as 20% and 50% of the corresponding gross stiffnesses.

3.4 Column Modeling

Bridge columns are designed to yield under expected strong earthquake motions. Therefore, reflecting the nonlinear behavior of the columns in the analysis model is important for an accurate performance evaluation of the bridge system. Column clear height used in the analysis model was taken as the distance from the bottom level of the cap beam to the top of the foundation. Rigid links were provided between center of the cap beam to the node at the top of the column, as indicated in Figure 3.3. All six degrees of freedom were restrained at the base of the columns, as the boundary condition.

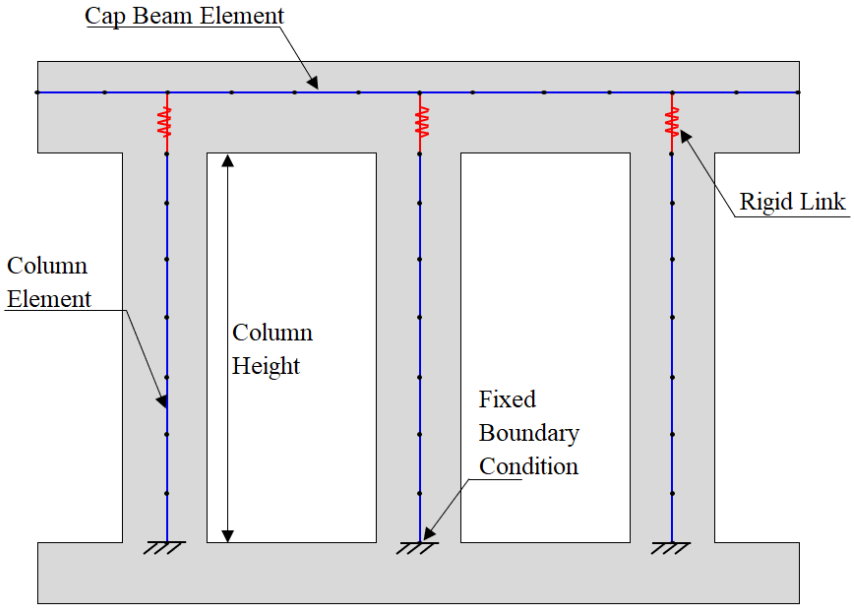

Figure 3.3 Column and cap beam element modeling

Columns are detailed to behave as ductile members according to the standards (AASHTO-LRFD (2017), TBES (2020), and EN-1998-1 (2014)) and effective flexural stiffness must be calculated to capture the realistic behavior of column

bending for nonlinear analysis. To calculate the effective flexural stiffness with Eq. (3.1), moment curvature analysis was performed by considering the inelastic material properties.

$$E \cdot I_{eff} = \frac{M_y}{\phi_y} \qquad \text{Eq. (3.1)}$$

Where:

E: Elastic modulus of column material

I_{eff}: Effective moment inertia

M_y: Yield moment determined from moment curvature analysis under dead load

ϕ_y: Yield curvature determined from moment curvature analysis under dead load

3.4.1 Moment – Curvature Analysis

Ductile column plastic moment capacity under the defined axial load can be determined from moment-curvature analysis by using the inelastic concrete and reinforcement bar properties. While performing the moment curvature analysis, expected material strengths must be considered instead of the characteristic values. The expected values for concrete compressive strength and steel yield strength were determined using Eq. (3.2), as specified in TBES (2020).

$$f_{ce} = 1.3 f_{ck}$$
$$f_{ye} = 1.2 f_{yk} \qquad \text{Eq. (3.2)}$$

Where:

f_{ce}: Expected concrete compressive strength

f_{ck}: Characteristic concrete compressive strength

f_{ye}: Expected yield strength for reinforcement steel

f_{yk}: Characteristic yield strength for reinforcement steel

Moment-curvature analysis utilizes equilibrium of internal forces and strain compatibility to derive the moment and the corresponding curvature values. The nonlinear moment-curvature response for reinforced concrete sections can be idealized with an elastic-perfectly plastic bilinear assumption as shown in Figure 3.4. The idealization is based on equal areas under the actual nonlinear and the idealized bilinear moment-curvature curves.

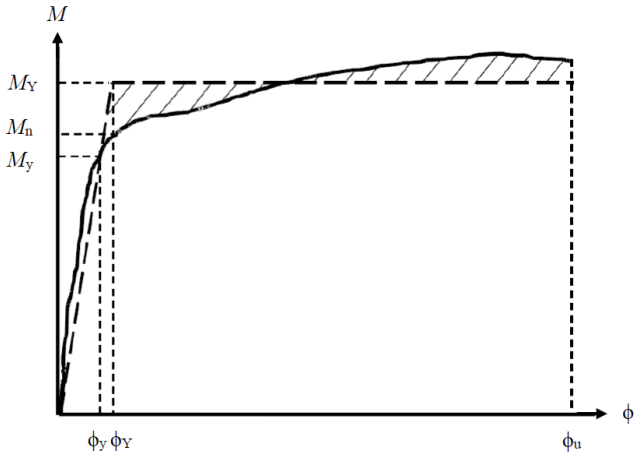

Figure 3.4 Bilinear idealization of moment-curvature curve (TBES, 2020)

3.4.2 Inelastic Concrete Material Model

The moment-curvature sectional analysis was performed with separate material models for the confined and unconfined parts of column cross section, as shown in Figure 3.5. Because of the confinement effect, compressive strength of the concrete and it's strain capacity increase. The unconfined concrete cover properties are different in terms of strength and strain since there is no confinement effect caused by transverse reinforcement. The unconfined concrete strength was taken as the expected concrete compressive strength, and strain at the maximum strength and the ultimate strain were taken as ε_{co}= 0.002 and ε_{sp}= 0.005.

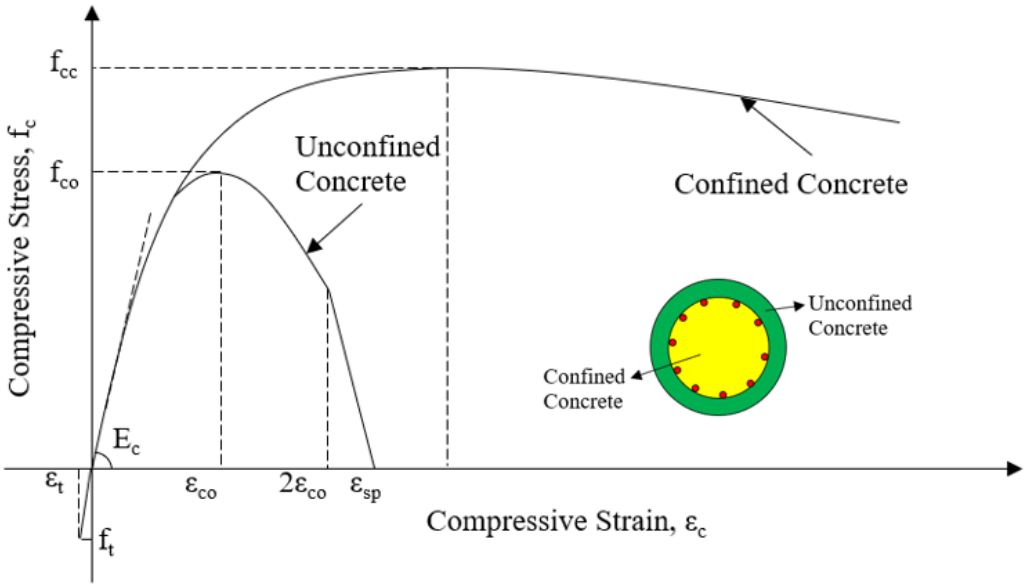

Figure 3.5 Confined and unconfined concrete stress-strain curves (Mander Model)

Mander equations were used to determine the elastic modulus, tensile strength and tensile strain of the concrete as shown in Eq. (3.3) (Mander et al., 1988).

$$E_c = 5000\sqrt{f_{co}}$$
$$f_t = 0.62\sqrt{f_{co}} \qquad \text{Eq. (3.3)}$$
$$\varepsilon_t = \frac{f_t}{E_c}$$

Where:

E_c: Elastic modulus of concrete

f_{co}: Unconfined concrete compressive strength

f_t: Concrete tensile strength

ε_t: Tensile strain of concrete

Considering the confinement effect provided by circular transverse reinforcement of column section, the maximum strength of the confined concrete was determined based on Mander confined concrete model with Eq. (3.4) (Mander et al., 1988).

$$f_{cc} = \lambda_c f_{co}$$

$$\lambda_c = 2.254\sqrt{1 + 7.94\frac{f_e}{f_{co}}} - 2\frac{f_e}{f_{co}} - 1.254 \qquad \text{Eq. (3.4)}$$

$$f_e = \frac{1}{2}k_e p_s f_{ywk}$$

$$p_s = \frac{4A_{sp}}{D_o s}$$

For circular transverse reinforcement, effective confinement coefficient is given in Eq. (3.5).

$$k_e = \left(1 - \frac{s}{2D_o}\right)^2 \left(1 - \frac{A_s}{\frac{\pi D_o^2}{4}}\right)^{-1} \qquad \text{Eq. (3.5)}$$

Where:

f_{cc}: Confined concrete strength (MPa)

λ_c: Confinement effect coefficient

f_{co}: Unconfined concrete strength (MPa)

f_e: Effective confinement pressure (MPa)

k_e: Effective confinement coefficient

p_s: Volumetric ratio for transverse reinforcement

f_{ywk}: Transverse reinforcement material strength (MPa)

A_{sp}: Transverse reinforcement area (mm^2)

D_o: Transverse reinforcement effective section diameter (mm)

s: Transverse reinforcement spacing (mm)

A_s: Longitudinal reinforcement area (mm^2)

3.4.3 Inelastic Reinforcement Material Model

Park strain hardening model, shown in Figure 3.6, was considered for nonlinear behavior of reinforcing steel in moment-curvature sectional analysis. In this model the relation between the reinforcement strain and stress is defined with the formulas given in Eq. (3.6).

$$f_s = E_s\varepsilon_s \; for \; \varepsilon_s < \varepsilon_{sy}$$
$$f_s = f_{sy} \; for \; \varepsilon_{sy} \leq \varepsilon_s < \varepsilon_{sh} \qquad \text{Eq. (3.6)}$$
$$f_s = f_{su} - (f_{su} - f_{sy})\frac{(\varepsilon_{su} - \varepsilon_s)^2}{(\varepsilon_{su} - \varepsilon_{sh})^2} \; for \; \varepsilon_{sh} \leq \varepsilon_s \leq \varepsilon_{su}$$

Where:

f_s: Reinforcement steel strength (MPa)

E_s: Elastic modulus of reinforcement (200 000 MPa)

ε_s: Reinforcement steel strain

f_{sy}: Reinforcement steel yield strength (MPa)

f_{su}: Reinforcement steel ultimate strength (MPa)

ε_{su}: Reinforcement steel ultimate strain

ε_{sh}: Reinforcement steel hardening strain

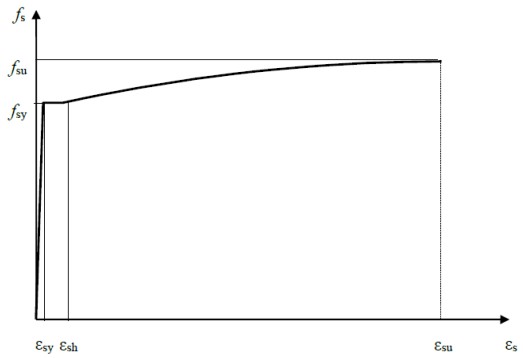

Figure 3.6 Reinforcement steel stress-strain curve according to Park strain hardening model (TBES, 2020)

3.5 Elastomeric Bearing Modeling

Elastomeric bearing pads are typically used to support precast concrete girders at the support locations in bridges. These pads are fabricated from high purity rubber and internal steel layers to prevent excessive bulging of the rubber under vertical loads (Figure 3.7). The elastomeric bearing pads used in the investigated bridges were 400×400×130 mm in dimension and were included in the analysis model as spring elements. Each of these support spring elements was connected to the superstructure by using a rigid link element. The support spring elements were assigned linear elastic material model with infinite stiffness in the vertical direction and in torsion. Horizontal stiffness of the elastomeric bearing pads in the longitudinal and transverse directions were computed by using Eq. (3.7).

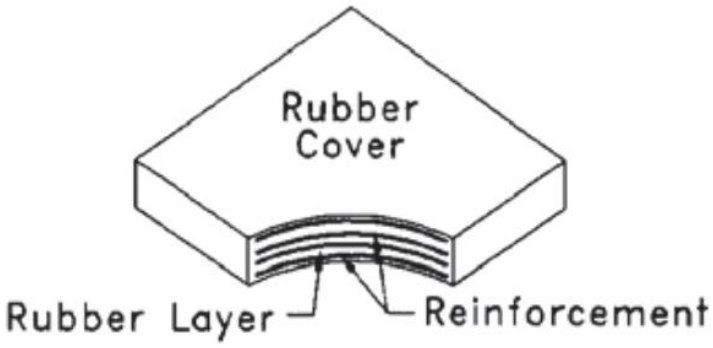

Figure 3.7 Elastomeric bearing (AASHTO LRFD 8th edition)

$$k_h = \frac{GA}{h} \qquad \text{Eq. (3.7)}$$

Where:

G: Shear modulus (1.00 MPa was used in this study)

A: Area of the elastomeric bearing (mm^2)

h: Thickness of the elastomeric bearing (mm)

3.6 Modeling of the Gap at Expansion Joint Locations

Gaps with sufficient widths are usually provided between the girders and the vertical walls of cap beams in order to allow for thermal deformations. A similar gap is also provided in the transversal direction of the bridge between girder ends and shear keys. A sudden increase in girder support stiffness occurs when these gaps close and the girder end comes into contact with the vertical walls of cap beams or shear keys under the design level earthquake. Such a pounding effect may have a significant effect on the seismic response of the bridge system and must be reflected in the analysis model.

The service level earthquake is usually considered to determine the required gap width. In other words, a sufficient gap width should be provided in order to prevent the pounding of girder ends against the cap beam or the shear keys, and avoid any damage in these members at service level earthquake. In the event of service level earthquake, elastomeric bearing pads are expected to absorb the earthquake energy without impact. Therefore, size of these bearing pads should be determined accordingly.

Details used in the investigated bridges at the pier and abutment locations are shown respectively in Figure 3.8 and Figure 3.9. An 8 cm gap is provided along the longitudinal axis of the bridge between the girder and the vertical walls of cap beams at both locations. As mentioned above, gaps in longitudinal direction is necessary for thermal deformations of superstructure. Therefore, gap length between girders and cap beam vertical wall is expected to change as a result of daily and seasonal movements. For this reason, it is hard to know the exact value of the gap width at the end of each girder at a given instant. In this study, gap length was taken as the design value of 8 cm in bridge modeling. A method has been provided by Muthukumar and DesRoches (2006) in order to reflect the effect of this type of gap in the bridge analysis model. Kelvin and Hertzs models have been used to capture the seismic pounding response. A simple analytical approach has been provided by Muthukumar and DesRoches (2006) to find the stiffness parameters in pounding action. They

conclude that axial stiffness of the superstructure can be used to determine the pounding stiffness as shown in Eq. (3.8).

$$k_h = \frac{EA}{L} \qquad \text{Eq. (3.8)}$$

Where**:**

k_h: Pounding stiffness for gap element (kN/m)

E: Elastic modulus of the superstructure concrete (kPa)

A: The cross-section of the superstructure (m^2)

L: Length of the superstructure in impact (m)

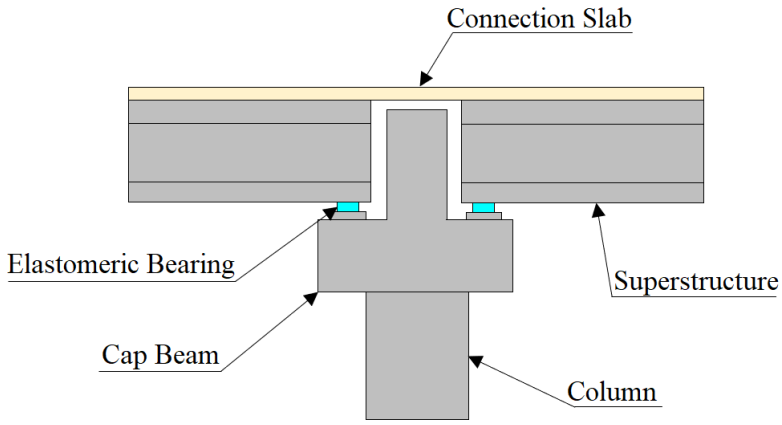

Figure 3.8 Gaps between girder ands and cap beam wall at pier lines

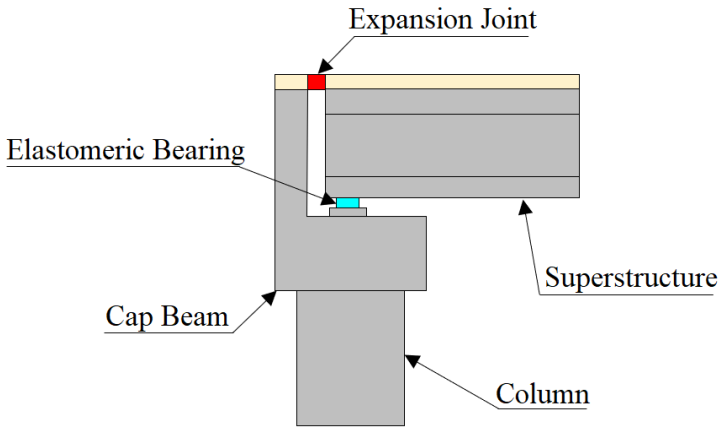

Figure 3.9 Gaps between girder ands and cap beam wall at abutment lines

In the analysis model, the girder support stiffness was taken as the stiffness provided by the elastomeric bearing pad. The girder support stiffness was increased to the pounding stiffness following the closing of the longitudinal gap between the girder end and the cap beam wall. Longitudinal gap was represented as a gap element in the analysis model. To capture the relative displacement of the elastomeric bearing pad, the gap element was connected to the top of the element and bottom of the elastomer. End of the gap element was connected by using rigid link as shown in the Figure 3.10 and Figure 3.11. When relative displacement of the girder support element exceeds the gap width of 8 cm pounding stiffness becomes effective. It is also noted that there is no damping on the gap elements.

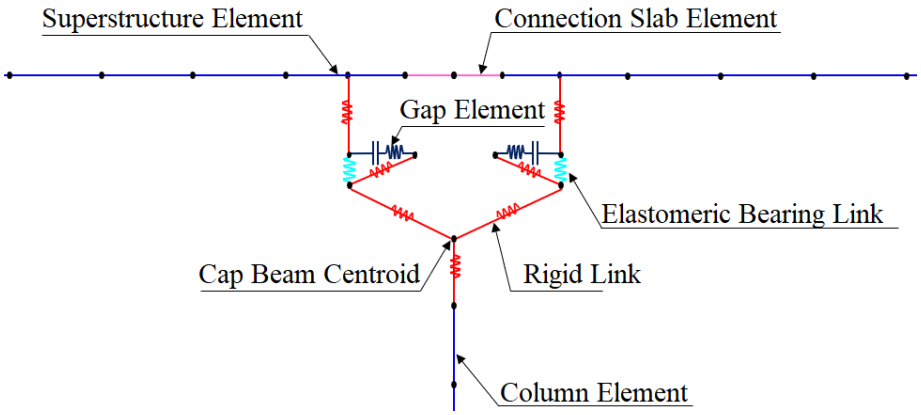

Figure 3.10 Modeling details used at pier lines

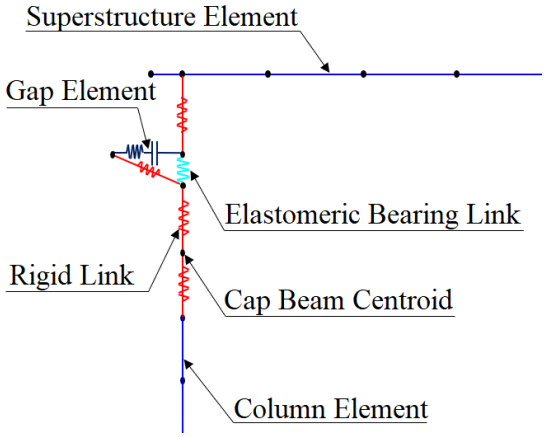

Figure 3.11 Modeling details used at abutment lines

The gaps exist in the transversal direction of the bridge between girder ends and shear keys are indicated in Figure 3.12. Under design level earthquake girder ends are expected to hit the shear keys and the resulting impact force is transferred to the columns. These shear keys serve as fuses to control further damage and behave as a transverse support for the superstructure (Kappos *et al.*, 2012).

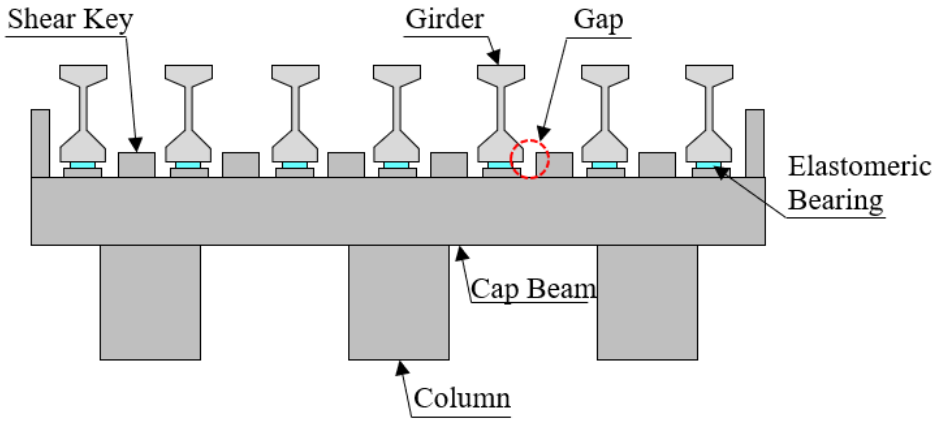

Figure 3.12 Typical shear keys provided on cap beam

Megalley *et al.* (2002) reported the results of an experimental study on the seismic response of interior and exterior shear keys. Based on these results, the empirical force versus shear deformation behavior shown in Figure 3.13 has been proposed to represent the behavior of interior shear keys. The shear key capacity and pounding stiffness as proposed by Megalley *et al.* (2002) are determined using Eq. (3.9). This stiffness becomes effective in the analysis model following the closing of the transverse gap between girder end and shear keys. The transversal gap was represented as a gap element in the analysis model. These gap elements were only assigned a stiffness value with no damping . The relation between the gap elements and the other elements of the model are shown in Figure 3.14.

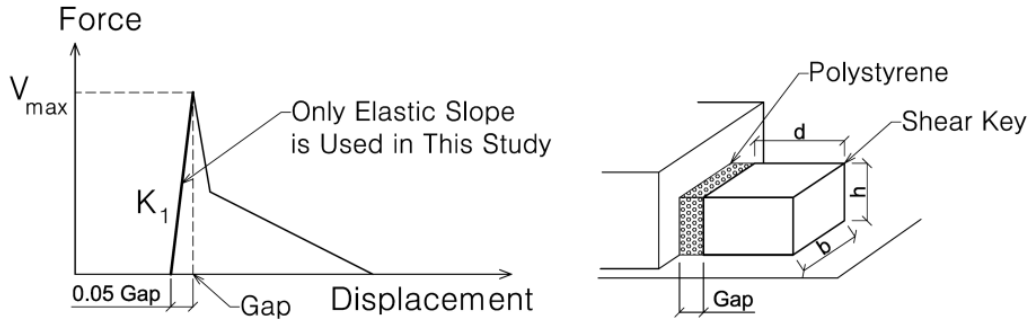

Figure 3.13 Interior shear key model (Bozorgzadeh *et al.*, 2007)

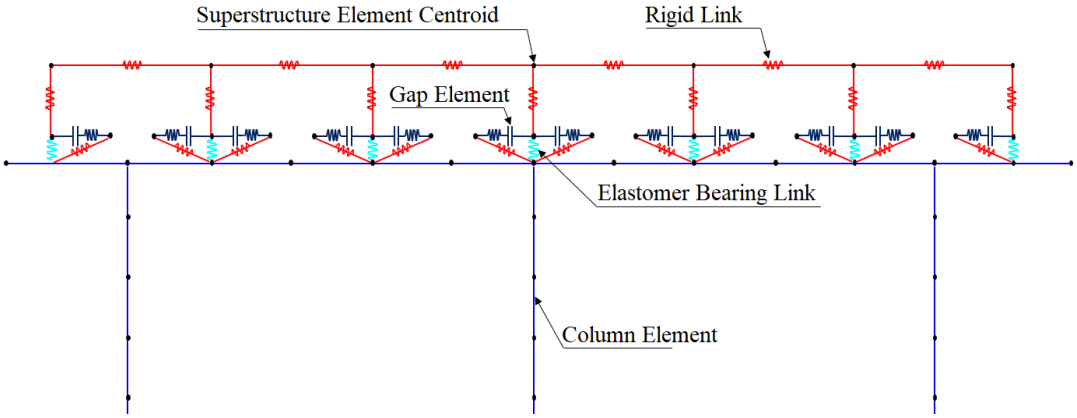

Figure 3.14 Transversal gap modeling in the analysis model

$$V_{max} = 11.3\sqrt{f_c'}\ b\ d$$

$$K_1 = \frac{V_{max}}{0.05\ g} \qquad \text{Eq. (3.9)}$$

Where:

V_{max}: Maximum shear force in the shear key (kip)

f_c': Concrete strength of the shear key (ksi)

b: Width of the shear key (in)

d: Length of the shear key (in)

K_1: Pounding stiffness (kip/in)

g: Gap length (in)

CHAPTER 4

PUSHOVER ANALYSIS DETAILS

4.1 Introduction

Pushover analysis has been widely used in recent years as a nonlinear static analysis method to predict the performance of structures under the effect of determined demand earthquake spectrum. The main advantage of this analysis method over dynamic time history analysis is that it takes less time and can be conducted with relatively less effort (Hajihashemi *et al.*, 2016). The main purpose of a pushover analysis is to determine the base shear versus displacement response, known as capacity curve, of the structure by using nonlinear properties of the structural elements under a selected loading scenario until the target displacement of a predetermined joint is reached. In the context of seismic performance evaluation of structural systems, the capacity curve determined at the end of a pushover analysis is then converted into a capacity spectrum. Meanwhile, a demand spectrum is determined by considering the expected earthquake intensity and appropriate soil properties. Having both the demand and capacity in spectral media, performance point can be obtained by overlapping the two spectra. This method is called as Capacity Spectrum Method (CSM). The performance point obtained from a CSM represents the behavior of the structure under the demand earthquake. The forces, displacements, rotations, and ductility levels occurring at this point are used for assessment of the structural performance during the expected earthquake by utilizing a set of predetermined performance limits. It should be noted that pushover analysis should start from an initial state where gravity loads, including self-weight and other applicable gravity loads, exist on the structure. No live load was considered in pushover analyses. Shaban et al. (2014) conducted an experimental study to

investigate the effect of vehicles on vibration response of bridges. Bridge shake tests on a large-scale model of a bridge with and without a vehicle were performed using harmonic motions and real time earthquake records. Test results indicate a favorable effect of vehicles on the seismic response of the bridge system due to damping effect provided by vehicle's tires and suspension system. Therefore, it is usually considered to be conservative not to include vehicle loading to monitor critical scenario during earthquake.

4.2 Lumped Plastic Hinge Model

As a generally accepted method in pushover analysis, nonlinear properties of structural elements are incorporated in the form of plastic hinges. One method of incorporating the plastic hinge properties in the analysis is through definition of lumped plastic hinges at appropriate locations along members. For members under flexural effects inelastic response is expected to localize at member ends. Accordingly, lumped plastic hinges are defined at locations close to the ends of members, with the rest of the elements remaining elastic. Because the plastic hinges are usually defined as zero-length elements there is no lengthwise variation of bending moment at the plastic hinge location. In reality, however plastic deformations at member ends take place along a certain length, known as the plastic hinge length. As a modeling assumption, the lumped plastic hinge is usually placed at the middle of the plastic hinge length. There are analytical expressions available in the literature to predict the length of plastic hinge region. According to AASHTO LRFD (2017) and TBES (2020) plastic hinge length formula as shown in Eq. (4.1) was used in this study.

$$L_p = 0.08L_k + 0.022f_{ye}d_{bl} \geq 0.044f_{ye}d_{bl} \qquad \text{Eq. (4.1)}$$

Where;

L_p: Plastic hinge length (m)

L_k: Member length for cantilever or half of the member length for frame system (m)

f_{ye}: Expected steel yield strength (MPa)

d_{bl}: Mean of longitudinal rebars diameter (m)

In this study, plastic hinges were utilized to represent the moment-rotation relationship of bridge columns. This relationship was determined by considering the moment-curvature analysis of column section with inelastic material properties. Bridge columns behave as cantilever members in the longitudinal direction of the bridge and as framed system in the transverse direction. Therefore, this difference was reflected in the plastic hinge properties and locations used in two perpendicular directions of the bridge.

For the cantilever column behavior, which is valid in the longitudinal direction of the investigated bridges, plastic hinging occurs only at the bottom of the member, as shown in Figure 4.1. In order to determine the plastic hinge moment-rotation behavior yield moment, yield curvature, and ultimate curvature values were determined from a moment-curvature analysis. In this analysis, the column axial load at plastic hinge location due to bridge self-weight and additional dead loads was considered, where additional dead loads are asphalt, shear keys, barriers, and guard rails. Curvature values determined from the sectional analysis were then converted to corresponding rotations by using the expresssions given in Eq. (4.2).

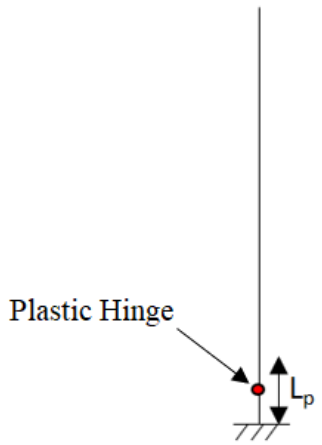

Figure 4.1. Column plastic hinge location in bridge longitudinal direction

$$\theta_y = \frac{\phi_y L}{3}$$
$$\theta_p = (\phi_u - \phi_y) L_p \qquad \text{Eq. (4.2)}$$
$$\theta_u = \theta_y + \theta_p$$

Where;

ϕ_y: Yield curvature (rad/m)

ϕ_u: Ultimate curvature (rad/m)

L: Length from contraflexure point (m) (*equal to L for cantilever and L/2 for frame system)*

L_p: Plastic hinge length (m)

θ_y: Yield rotation (rad)

θ_p: Plastic rotation (rad)

θ_u: Ultimate rotation (rad)

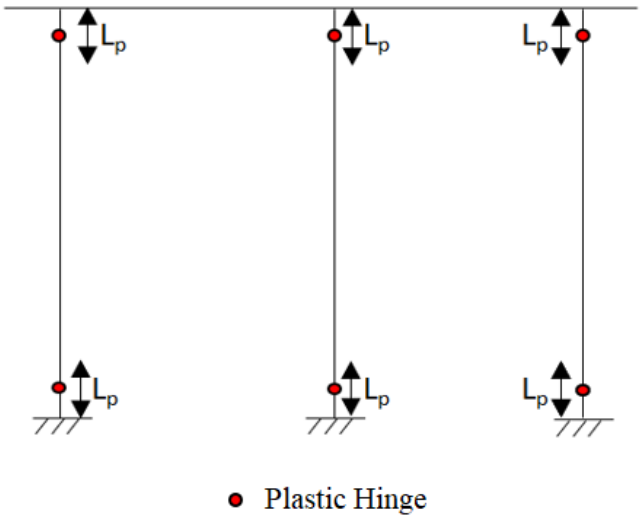

Figure 4.2. Column plastic hinge locations in bridge transverse direction

The procedure explained above has been repeated for the plastic hinge behavior in the transverse direction of the bridge by considering the frame shown in Figure 4.2. As shown, plastic hinges this time were assigned at both ends of column elements. Another major difference between the plastic hinge behaviors in the longitudinal and transverse directions is the level of axial load present in columns. Different than the longitudinal direction, the column axial load this time depends on the level and direction of the earthquake loading. For this reason, axial force and yield moment interaction diagram was obtained by using the moment-curvature analysis. The interaction diagram obtained this way was then assigned to the frame column system hinges in order to define the variation of column yield moment with the level of axial load present on the column, which is shown in Figure 4.3.

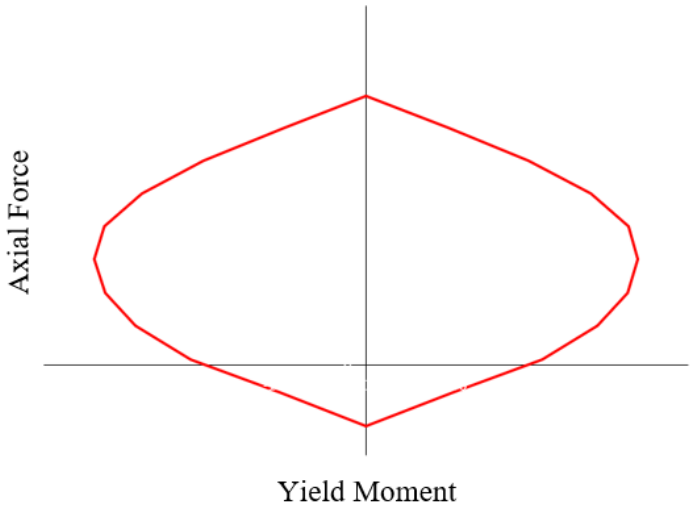

Figure 4.3. Axial force vs. yield moment interaction diagram

4.3 P-Delta Effect on Columns

Geometric nonlinearity caused by the so-called P-delta phenomenon must be considered in pushover analysis for accurate determination of load effects. Axial compressive force acting on columns results in additional moments when deformed shape of the frame is considered. As these moments develop due to deformation of members in the frame, they are often called second order moments. The total moment

that each column is subjected to is a combination of the first order moment, which is developed due to loading on the frame, and additional second order moment due to P-delta effects. Under the incremental lateral loading used in pushover analysis of the bridge system in the longitudinal direction, columns are expected to deform such that the lateral deformation at the top being equal to Δ, as illustrated in Figure 4.4. At this state deformed state, the total moments at column base are given in Eq. (4.3) as below:

$$M_1 = V \cdot L$$
$$M_2 = P \cdot \Delta \qquad \text{Eq. (4.3)}$$

Where;

M_1: Column first order moment due to external loading

M_2 Column second order moment due to P-delta

V: Lateral load on the column

P: Axial load on the column

Δ: Top displacement of the column

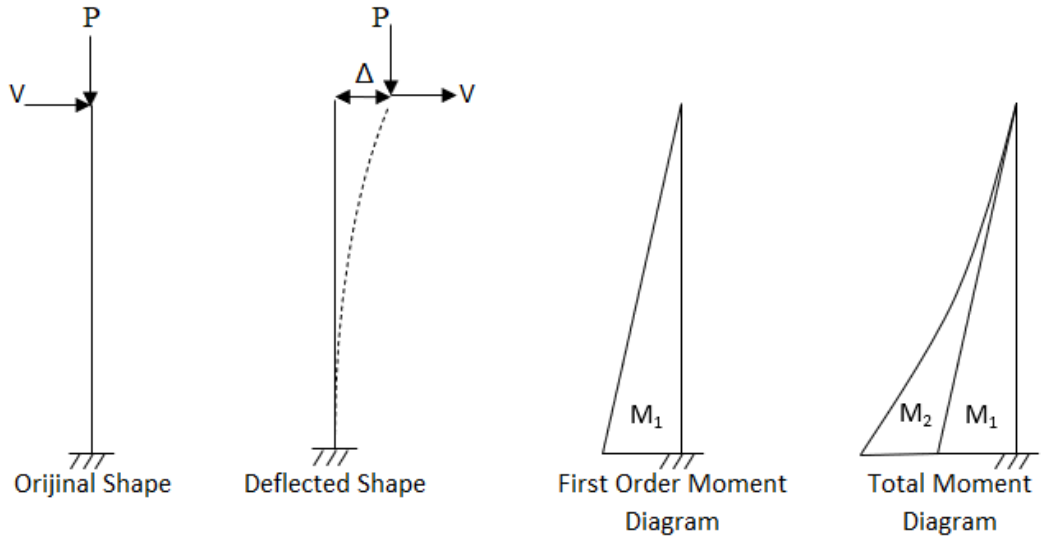

Figure 4.4. Effect of P-Delta on column moment

4.4 Incremental Loading Methods

The incremental loading in a pushover analysis can be applied in either load control or displacement control mode. In either method the loading is continued up to a predefined target value of load or displacement. In the current study, displacement-controlled loading has been used. In terms of the application of loading in pushover analysis the two most widely accepted methods are acceleration loading and force loading based on mode shapes of the structure. In the former method, a uniform acceleration distribution is assumed to develop in the structure, which means the loading consists of the inertia forces in the structure. Since the accelerations are assumed to be uniform, the load pattern is directly related to each element's mass. In the case of force loading based on mode shapes of the structure, mode shapes of the structure are determined first by an eigenvalue analysis and then these mode shapes are used to assign the load pattern for the pushover analysis. According to the pushover analysis direction, dominant mode must be selected for that direction. In the current study, all pushover analyses were conducted by using a load pattern that is based on the first and second mode shapes of bridges in two perpendicular directions.

4.5 Capacity Spectrum Method

According to the capacity spectrum method (CSM) as described by ATC-40 (1996), the performance point of the structure is obtained by overlapping of the capacity spectrum and demand spectrum is. The capacity curve reflects the nonlinear behavior of the bridge in the form of a load versus deformation curve, where load values indicate the base shear of the bridge and deformation represents the global displacement or monitored displacement according to the selection of incremental method. Figure 4.5 (a) represents a typical capacity curve of a bridge structure.

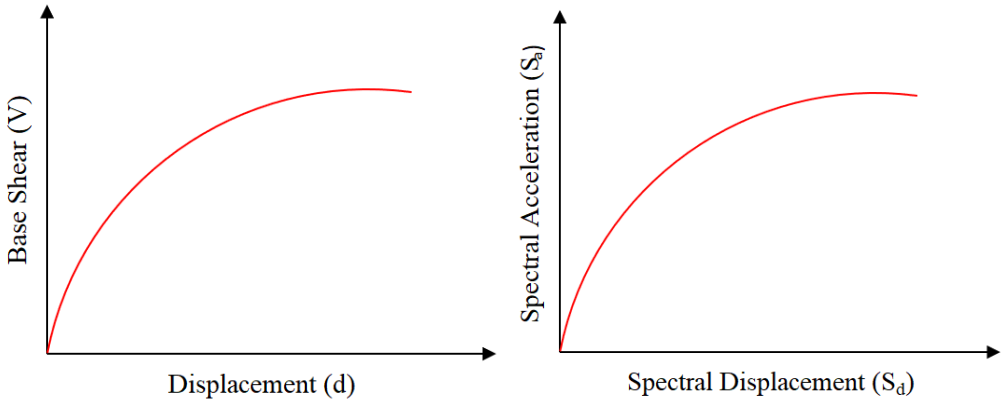

Figure 4.5. (a) Typical capacity curve, (b) Typical capacity spectrum

Capacity spectrum, as shown in Figure 4.5 (b), is a representation of the capacity curve in the form of spectral acceleration and spectral displacement. Eq. (4.4) gives the related formulation (ATC-40, 1996) for converting the base shear-displacement response into the corresponding capacity spectrum.

$$S_a = \frac{V}{M_1 g}$$

$$S_d = \frac{\Delta_{monitored\ node}}{\Gamma_1\ \phi_{1\ monitored\ node}} \qquad \text{Eq. (4.4)}$$

Where;

S_a: Spectral acceleration

V: Base Shear

M_1: Modal mass of the first natural mode

g: Gravitational acceleration

S_d: Spectral displacement

$\Delta_{monitored\ node}$: Displacement of monitored node

Γ_1: Modal participation factor of first natural mode

$\phi_{1\ monitored\ node}$: Amplitude of the first natural mode at monitored node

4.6 Response Spectrum and Demand Spectrum

Response spectrum is a function which contains the peak response of a structure under a transient event depending on the frequency (or period) and damping of the structure. It is commonly plotted as S_a (spectral acceleration) versus T (period) as show in Figure 4.6 (a). In order to illustrate the relationship with spectral acceleration and displacement, response spectrum periods are converted to spectral displacement by using Eq. (4.5) and it is called demand spectrum (Figure 4.6 (b)). By using this transformation, one could follow the spectral displacement trend of the ground motion in an easier way.

$$S_d = S_a g \left(\frac{T}{2\pi}\right)^2 \qquad \text{Eq. (4.5)}$$

Where;

S_d: Spectral displacement

S_a: Spectral acceleration

g: Gravitational acceleration

T: Period of the structure

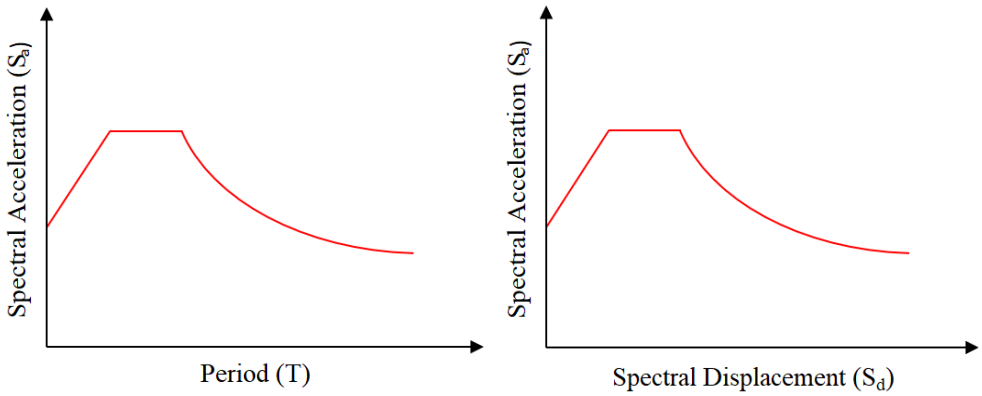

Figure 4.6. (a) Typical response spectrum, (b) Typical demand spectrum

4.7 Performance Point

Performance point is used to understand the behavior of the structure for demand earthquake as mentioned before. It is the point where capacity spectrum and demand spectrum with 5% damping ratio intersects each other, as shown in Figure 4.7.

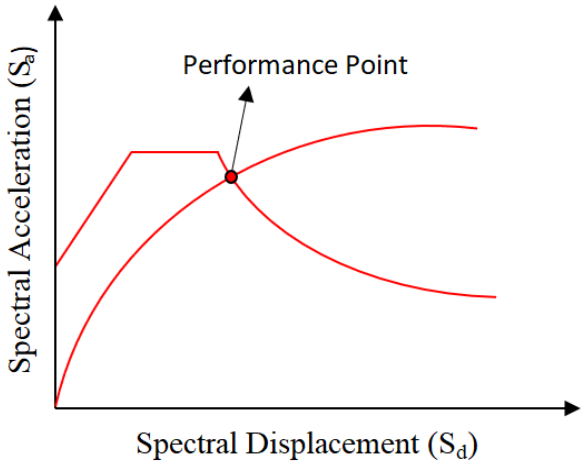

Figure 4.7. Performance point of structure

4.8 Performance Criteria of the Bridge for Pushover Analysis

Performance criteria of bridge columns were defined in terms of plastic rotations and drift ratios as per Turkish Bridge Earthquake Standard (TBES, 2020). The assessment was conducted separately for the longitudinal and transverse directions using the pushover analysis results. If bridge performance is not satisfied target performance level in either direction, it can be said that bridge performance does not satisfy target level.

TBES (2020) categorizes damage level into two classes for nonlinear analysis type. These classes are called Controlled Damage and Collapse Prevention. Furthermore, Limited Damage level is also considered for the first order analysis. In this study, all three performance levels were considered. Plastic rotation limits for these three performance levels can be found by using Eq. (4.6).

$$\theta_p^{(LD)} = \left(0.1875\phi_u - \phi_y\right)L_p$$
$$\theta_p^{(CD)} = \left(0.5\phi_u - \phi_y\right)L_p \qquad \text{Eq. (4.6)}$$
$$\theta_p^{(CP)} = \left(0.67\phi_u - \phi_y\right)L_p$$

Where;

$\theta_p^{(LD)}$: Plastic rotation limit for limited damage level (rad)

$\theta_p^{(CD)}$: Plastic rotation limit for controlled damage level (rad)

$\theta_p^{(CP)}$: Plastic rotation limit for collapse prevention damage level (rad)

ϕ_u: Ultimate curvature (rad/m)

ϕ_y: Yield curvature (rad/m)

L_p: Plastic hinge length (m)

CHAPTER 5

PUSHOVER ANALYSIS RESULTS

5.1 Introduction

In this chapter, the plastic hinge properties used in pushover analyses of the investigated bridges and the results obtained from these analyses are presented. Following the presentation of results, performance criteria of the bridges in two orthogonal directions was evaluated considering the performance limits given in Chapter 4. Finally, pushover response of the bridges was further evaluated to understand the properties that have a major effect on the response.

As mentioned in Section 4.4, in pushover analyses loading pattern was based on the main mode shapes considering the direction that is being analyzed. For the investigated bridges, the first and second mode shapes, respectively corresponds to translation in the longitudinal and transverse directions (Figure 5.1 and Figure 5.2). Therefore, pushover analyses in the longitudinal and transverse directions were conducted by considering these two mode shapes.

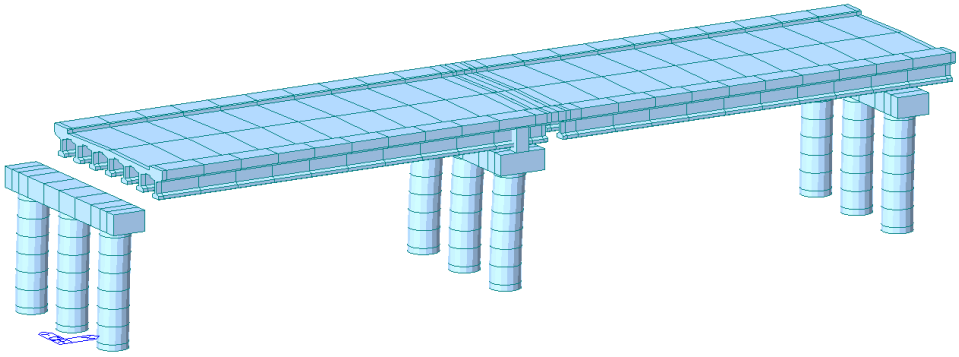

Figure 5.1 Typical mode shape in the longitudinal direction

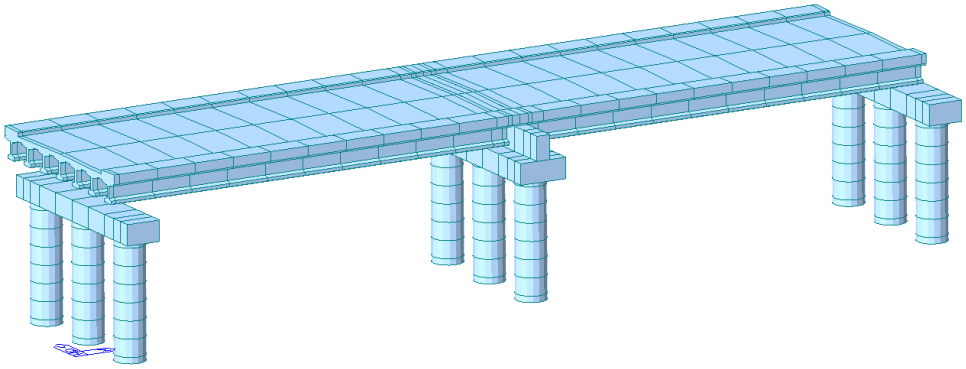

Figure 5.2 Typical mode shape in the transverse direction

The natural vibration periods and mass participation ratios in longitudinal and transverse directions are given in Table 5.1 for the investigated bridges. As evident, all the bridges have similar natural vibration periods and mass participation ratios, as a result of similar overall geometry, member sizes, and elastomeric bearing pad properties.

Table 5.1 Natural vibration periods and mass participation ratios for investigated bridges

Bridge	Mode 1			Mode 2		
	Period (s)	Mass Participation in Long. Direction (%)	Mass Participation in Trans. Direction (%)	Period (s)	Mass Participation in Long. Direction (%)	Mass Participation in Trans. Direction (%)
O02	1.06	67.33	0.00	1.02	0.00	63.95
O05	1.06	67.11	0.00	1.00	0.00	62.72
O07	1.04	66.44	0.00	1.00	0.00	63.15
O13	1.03	66.20	0.00	1.00	0.00	63.23
O15	1.02	65.84	0.00	0.98	0.00	62.30
O48	1.06	66.56	0.00	1.00	0.00	62.33

For bridges with unequal column heights, whether the pushover loading in the longitudinal direction is applied from one abutment to the other or vice versa affects

the overall bridge response. The difference results from the contact condition (i.e., pounding) used between girder ends and cap beams at support locations. Therefore, two separate longitudinal pushover analyses were conducted on bridges with unequal column heights, while for bridges with all columns having the same height a single analysis was conducted.

The center node located on bridge superstructure at the very end section of the bridge was chosen to monitor the displacements in the longitudinal direction pushover analysis. For the transverse direction pushover analysis, when the abutment and pier columns are of the same height, the center node at the middle section of the superstructure was used for monitoring the displacements. In bridges with different column height at pier and abutment locations, the center node located on the superstructure at the section of the tallest column was used for monitoring the pushover displacements.

5.2 Column Plastic Hinge Properties

Hinge properties used in the longitudinal and transverse direction pushover analyses and the corresponding analysis results are presented separately for each direction. Column hinge properties were calculated for each orthogonal direction by considering reinforcement properties, column height, and the axial force present on the column.

5.2.1 Hinge Properties for Analysis in Longitudinal Direction

As discussed earlier, bridge columns act as individual cantilever column members in the longitudinal direction of bridges. The axial loads considered to calculate the column plastic hinge properties in the longitudinal direction are those resulting from the self-weight of the bridge components. The column plastic hinge properties determined for the pushover analysis in the longitudinal direction of the investigated bridges are summarized in Table 5.2 for the two abutment (A1 and A2) and pier

locations. These hinge properties were assigned to column members at the location corresponding to the center of the plastic hinge length of each column, which are given in Table 5.3.

Table 5.2 Column plastic hinge properties for analysis in longitudinal direction of bridges

Bridge	Location	N (kN)	M_y (kN·m)	ϕ_y (1/m)	ϕ_u (1/m)	θ_y (rad)	θ_p (rad)	θ_u (rad)	$\frac{\theta_u}{\theta_y}$
O02	**A1**	1862	18855	0.0034	0.0604	0.0079	0.0522	0.0600	7.62
	P	3206	19537	0.0034	0.0610	0.0079	0.0527	0.0606	7.71
	A2	1862	18855	0.0034	0.0604	0.0079	0.0522	0.0600	7.62
O05	**A1**	1857	18852	0.0034	0.0604	0.0087	0.0554	0.0640	7.39
	P	3154	19510	0.0034	0.0610	0.0090	0.0573	0.0663	7.38
	A2	1817	18831	0.0034	0.0604	0.0077	0.0512	0.0589	7.69
O07	**A1**	1773	20989	0.0034	0.0596	0.0065	0.0456	0.0521	8.02
	P	3124	21507	0.0034	0.0542	0.0080	0.0456	0.0536	6.69
	A2	1872	21031	0.0034	0.0594	0.0091	0.0557	0.0648	7.12
O13	**A1**	1817	21150	0.0035	0.0610	0.0079	0.0517	0.0596	7.55
	P	3114	21782	0.0035	0.0616	0.0079	0.0522	0.0601	7.64
	A2	1817	21150	0.0035	0.0610	0.0079	0.0517	0.0596	7.55
O15	**A1**	1840	18728	0.0034	0.0607	0.0091	0.0570	0.0661	7.29
	P	3028	19300	0.0034	0.0590	0.0077	0.0485	0.0562	7.33
	A2	1748	18683	0.0034	0.0604	0.0068	0.0461	0.0529	7.79
O48	**A1**	1872	21031	0.0034	0.0594	0.0091	0.0557	0.0648	7.12
	P	3154	21332	0.0034	0.0500	0.0090	0.0464	0.0554	6.14
	A2	1826	21012	0.0034	0.0595	0.0080	0.0513	0.0593	7.44

Table 5.3 Longitudinal hinge plastic length of bridge columns

Bridge	Location	Plastic hinge length, L_p (m)
O02	A1	0.92
	P	0.92
	A2	0.92
O05	A1	0.97
	P	1.00
	A2	0.90
O07	A1	0.81
	P	0.90
	A2	1.00
O13	A1	0.90
	P	0.90
	A2	0.90
O15	A1	1.00
	P	0.87
	A2	0.81
O48	A1	1.00
	P	1.00
	A2	0.92

5.2.2 Hinge Properties for Analysis in Transverse Direction

Response of bridge columns in the transverse direction is different than the longitudinal direction because of the fact that three columns and the cap beam used at the abutment and pier locations form a frame in the transverse direction of bridges. In this case, different axial forces develop in each of these three columns when the bridge is subjected to lateral loading in the transverse direction. As mentioned in Section 4.2, axial force versus yield moment interaction diagram was obtained and

hinge properties for each axial force value were calculated for bottom and top cross sections of each column for all bridges. As an example, the column hinge properties for the two abutment (A1 and A2) and pier locations in bridge O13 are shown in Table 5.4. Because all columns at abutment and pier locations in this bridge have the same height and reinforcement layout the hinge properties for all columns happen to be the same. Column hinge properties used in transverse direction pushover analysis of other investigated bridges are provided in Appendix-A. Because of changes in column height and reinforcement layout between the abutment and pier locations, multiple column hinge properties had to be used in some of the bridges. The hinge properties determined this way were assigned to column members at the location corresponding to the center of the plastic hinge length of each column, which are given in Table 5.5. This table also shows the initial slope of the plastic hinge considering only the self-weight of the bridge system as the axial load. These stiffness values were used for definition of column plastic hinges in the analysis model. In some bridges, additional reinforcement has been provided at the bottom of pier columns. For these bridges, different the plastic hinge length and stiffness values were obtained at the top and bottom of pier columns.

Table 5.4 Bottom and top transverse column hinge properties in bridge O13

N (kN)	M_y (kN·m)	ϕ_y (1/m)	ϕ_u (1/m)	θ_y (rad)	θ_p (rad)	θ_u (rad)	$\frac{\theta_u}{\theta_y}$
150000	0	0.0000	0.0000	0.0000	0.0000	0.0000	0.00
131800	10161	0.0041	0.0142	0.0046	0.0072	0.0118	2.56
113600	20175	0.0046	0.0167	0.0053	0.0086	0.0138	2.63
95400	27879	0.0054	0.0193	0.0061	0.0099	0.0160	2.63
77200	32536	0.0061	0.0227	0.0069	0.0118	0.0187	2.71
59000	33723	0.0045	0.0273	0.0051	0.0161	0.0213	4.15
40400	32424	0.0038	0.0341	0.0044	0.0215	0.0258	5.94
21800	28624	0.0035	0.0456	0.0040	0.0299	0.0338	8.50
3200	21822	0.0035	0.0616	0.0039	0.0413	0.0452	11.49
-15400	10767	0.0034	0.0523	0.0039	0.0347	0.0386	9.87
-34000	0	0.0000	0.0000	0.0000	0.0000	0.0000	0.00

Table 5.5 Plastic hinge length and stiffness of bridge columns in transverse direction

Bridge	Location	L_p (m)	k (×10^6 kN·m)
O02	**A1**	0.71	4.76
	P	0.71	4.94
	A2	0.71	4.76
O05	**A1**	0.71	4.32
	P	0.71	4.32
	A2	0.71	4.89
O07	**A1**	0.71	6.44
	P Bottom	0.66	5.36
	P Top	0.71	5.33
	A2	0.71	4.60
O13	**A1**	0.71	5.34
	P	0.71	5.51
	A2	0.71	5.34
O15	**A1**	0.71	4.10
	P Bottom	0.66	5.02
	P Top	0.71	4.99
	A2	0.66	5.48
O48	**A1**	0.71	4.60
	P	0.71	4.70
	A2	0.71	5.25

5.3 Pushover Analysis Results

5.3.1 Longitudinal Pushover Analysis Results

Capacity curves from pushover analyses have been plotted with the points corresponding to the first and last yielding within the column members indicated on the curves. These capacity curves are then considered together with the corresponding response spectrum of bridges to determine the performance point. Detailed information on the procedure used to determine performance point is given Section 4.7. Considering the performance point, bridge column forces and rotations were determined, and these values were then compared with performance limits to determine the performance level of the columns.

According to pushover direction, bridge columns are labelled as “leading abutment”, “pier”, and “trailing abutment” for longitudinal pushover analysis as shown in Figure 5.3.

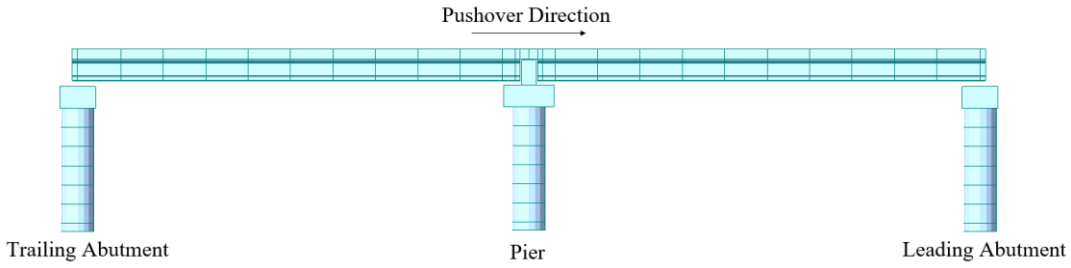

Figure 5.3 Naming convention for abutments with respect to longitudinal pushover direction

Longitudinal direction pushover results are presented in this section for only O02 and O07 bridges. The pushover behaviors of other bridges are similar to the behaviors explained for these two bridges. Plots, deformed shapes and tables summarizing the pushover analysis results for all of the investigated bridges are provided in Appendix B.

5.3.1.1 O02 Bridge Longitudinal Pushover Analysis Results

In the O02 Bridge all abutment and pier columns have the same height, therefore the longitudinal pushover analysis was conducted only in one direction. Capacity curve of this bridge is shown in Figure 5.4 with the yielding sequence of the columns indicated in Table 5.6. The increase in stiffness occurring at a displacement of approximately 9 cm is due to the girder ends coming into contact with the cap beams at the pier and the leading abutment. As indicated in Table 5.6, this contact condition occurred at the 22nd and 24th steps of the pushover analysis. Prior to the contact condition stiffness of the bridge system under pushover loading was governed almost entirely by the elastomeric bearing pads used at girder ends. Following the contact condition, bridge stiffness increases to the level corresponding to the lateral stiffness of the columns. With this stiffness level, lateral load resisting capability of the bridge system continues to increase until the formation of plastic hinging in the columns. For the O02 Bridge, plastic hinging occurred in pier columns and in leading abutment columns at 14 cm of total lateral displacement. Therefore, the columns at these locations were subjected to a lateral drift of approximately 5 cm ($14\ cm - 9\ cm = 5\ cm$) at the onset of yielding. Yielding occurred in the trailing abutment columns when the lateral displacement at the monitored node was equal to 74 cm. By this point, other columns of the bridge system suffered from a capacity drop, as evident in the capacity curve. Hinge behaviors that the columns at the pier and abutment locations followed during the pushover loading are shown in Figure 5.5. The plots in this figure clearly indicate the significant inelastic response of the pier and leading abutment columns as compared to the trailing abutment columns.

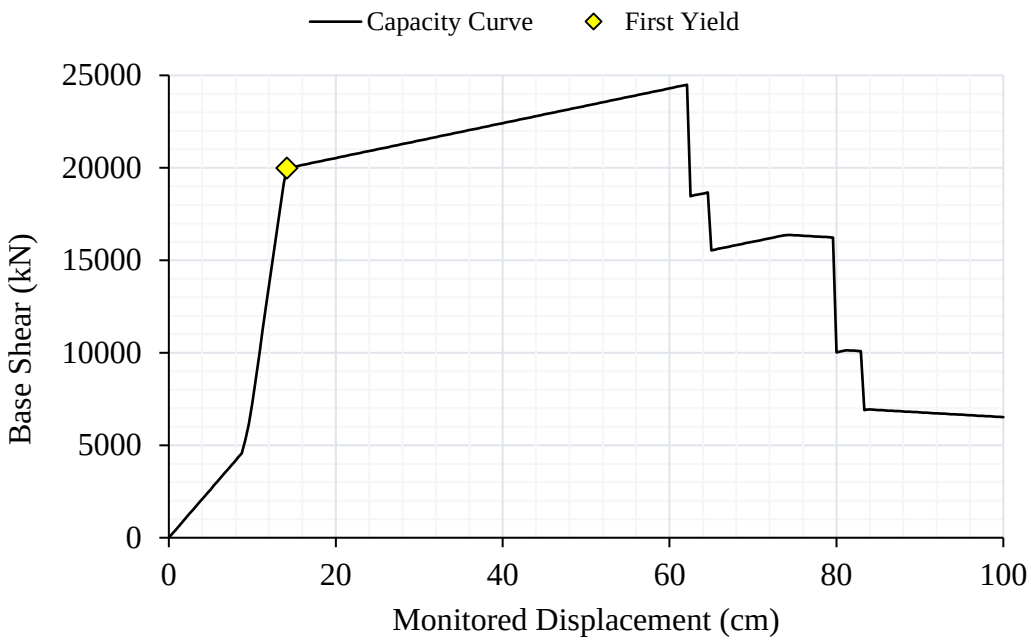

Figure 5.4 Capacity curve of O02 Bridge from longitudinal pushover analysis

Table 5.6 Longitudinal yield forces of O02 Bridge found from pushover analysis

Axis	Column Hinge	Pounding Step/Disp.	Yield Step/Disp.	P_y (kN)	V_y (kN)	M_y (kN·m)
A1	Left Column	-	178 / 74.2	1523	2882	18855
	Middle Column	-	178 / 74.2	1721	2882	18855
	Right Column	-	178 / 74.2	1529	2884	18855
P	Left Column	24 / 10.0	34 / 14.2	2832	2993	19537
	Middle Column	24 / 10.0	34 / 14.2	3198	2994	19537
	Right Column	24 / 10.0	34 / 14.2	2832	2998	19537
A2	Left Column	22 / 9.2	34 / 14.2	1663	2885	18855
	Middle Column	22 / 9.2	34 / 14.2	1881	2885	18855
	Right Column	22 / 9.2	34 / 14.2	1657	2887	18855

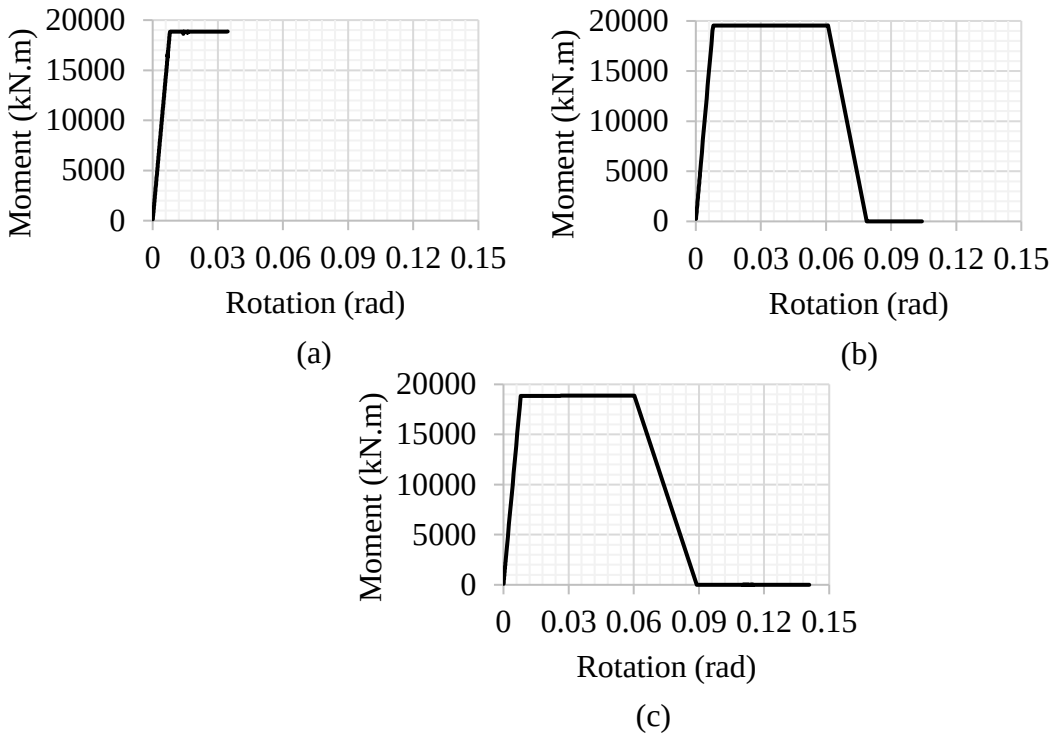

Figure 5.5 Column hinge behaviors in longitudinal pushover analysis of Bridge O02: (a) A1 columns, (b) P columns, (c) A2 columns

Although the pier and leading abutment (A2) columns yielded at the same loading step and they have same height, there is a slight difference in the yield moment and shear force values between these two sets of columns, as shown in Table 5.6. The reason for this behavior is twofold. The pier columns have larger axial force than the abutment columns because of a larger tributary area. Another reason for the difference in the moment and shear values of these two sets of columns is the small different in the amount of longitudinal reinforcement present in these columns. The abutment columns have 54ϕ32 longitudinal reinforcement, while the pier columns have 58ϕ32 reinforcement.

Ductility of the bridge system can be calculated as the ratio of the ultimate displacement to yield displacement in the pushover capacity curve. Ultimate displacement was taken as the displacement where the base shear drops to 80% of the load capacity. This value is equal to 62.5 cm for the O02 Bridge. Yield displacement was taken as the displacement corresponding to initiation of yielding

in the columns, which is 14 cm for the O02 Bridge. Therefore, this bridge possesses a ductility ratio of 4.5 in the longitudinal direction.

The performance point for the longitudinal direction of the bridge was determined by plotting the design spectrum and the pushover capacity curve in terms of spectral accelerations and displacements, as shown in Figure 5.6. It should be mentioned that the design spectrum considered here corresponds to a 2475-year return period earthquake. The performance point determined this way corresponds to a lateral displacement of 33.3 cm. Deformed shape of the bridge with the plastic rotation values at the performance point is given in Figure 5.7. Performance evaluation of the bridge conducted considering the performance point is summarized in Table 5.7. The plastic rotation obtained from the plastic hinge in each column was compared with the rotation limits specified in TBES (2020) for the performance levels of limited damage, controlled damage, and collapse prevention. No hinges developed in the trailing abutment columns at the performance point, as indicated by zero plastic rotation for these columns in Table 5.7. For the pier and leading abutment columns, the plastic rotation values fall between the corresponding limited damage and controlled damage limits, indicating that the response of these columns corresponds to the controlled damage performance level. Therefore, it is concluded that the O02 Bridge satisfies the target performance level of collapse prevention considering a 2475-year return period earthquake in the longitudinal direction.

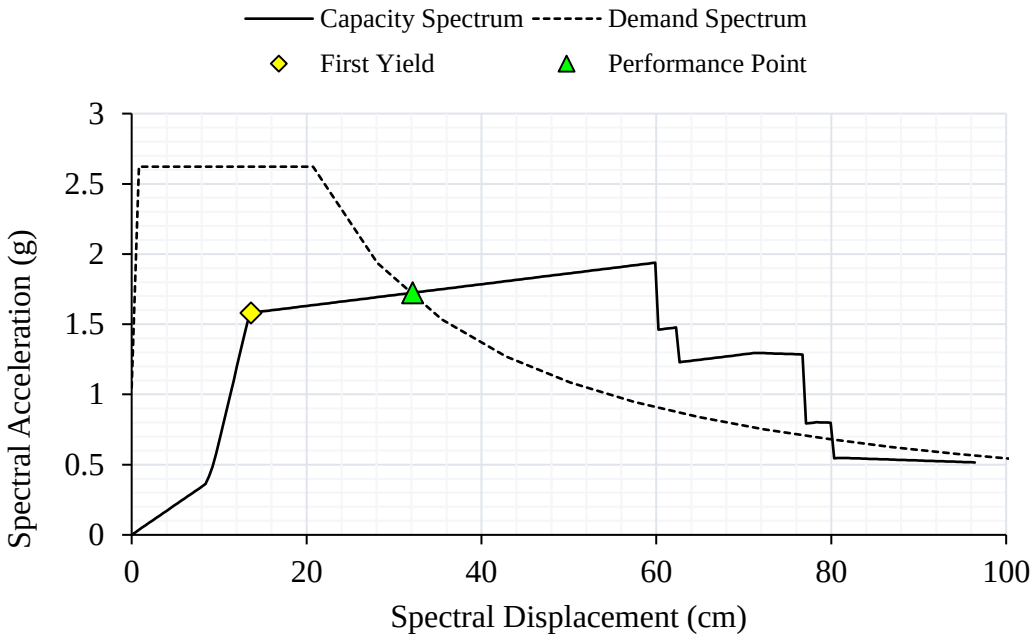

Figure 5.6 Performance point determination for O02 Bridge

Table 5.7 Performance evaluation of O02 Bridge

Location	Column	θ_p (rad)	θ_p^{LD} (rad)	θ_p^{CD} (rad)	θ_p^{CP} (rad)	Performance Level
A1	Left	0.0000	0.0073	0.0245	0.0339	No Damage
	Middle	0.0000	0.0073	0.0245	0.0339	No Damage
	Right	0.0000	0.0073	0.0245	0.0339	No Damage
P	Left	0.0158	0.0074	0.0248	0.0343	Controlled Damage
	Middle	0.0140	0.0074	0.0248	0.0343	Controlled Damage
	Right	0.0158	0.0074	0.0248	0.0343	Controlled Damage
A2	Left	0.0210	0.0073	0.0245	0.0339	Controlled Damage
	Middle	0.0199	0.0073	0.0245	0.0339	Controlled Damage
	Right	0.0210	0.0073	0.0245	0.0339	Controlled Damage

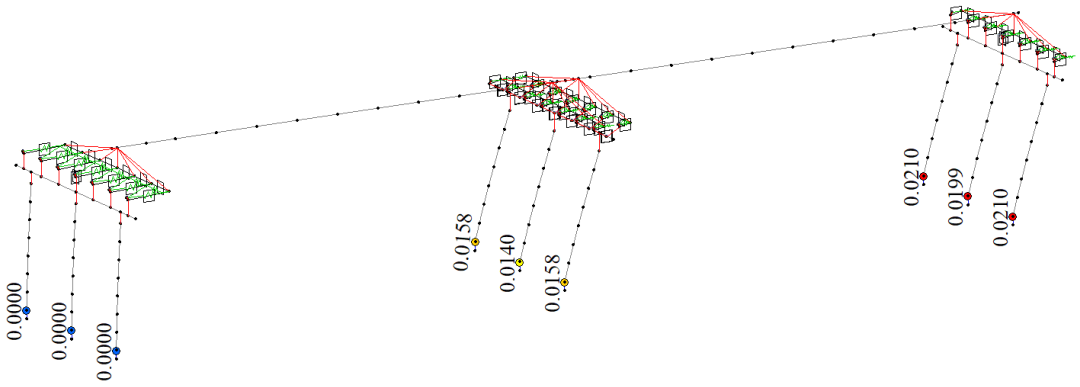

Figure 5.7 Deformed shape and plastic rotation values (rad) for O02 Bridge at the performance point in longitudinal pushover analysis

5.3.1.2 O07 Bridge Longitudinal Pushover Analysis Results

Different than the O02 Bridge, which was investigated in the previous section, different column heights were utilized at the pier and two abutment locations in the O07 Bridge. The column heights are 5.7 m, 7.1 m, and 8.0 m, respectively at the A1 abutment, pier, and A2 abutment locations. The longitudinal pushover analysis of this bridge was conducted in two directions, considering first A2 as the leading abutment (A1-P-A2 pushover direction) and then A1 as the leading abutment (A2-P-A1 pushover direction). Pushover capacity curves obtained from these two loading directions are shown in Figure 5.8. As evident, the bridge systems responded significantly different to the pushover loading depending on whether the leading abutment is the one with longer columns (A1-P-A2 pushover direction) or shorter columns (A2-P-A1 pushover direction). In the former case, columns at the trailing abutment (A1) did not develop plastic hinging due to their relatively short height. In the case of A2-P-A1 pushover direction, plastic hinging occurred in the columns at the trailing abutment towards the end of the analysis, as a result of the relatively long column height. Ductility ratio in the longitudinal direction of the bridge system was determined to be 4.4 for the A1-P-A2 pushover direction case and 3.4 for the A2-P-A1 pushover direction case.

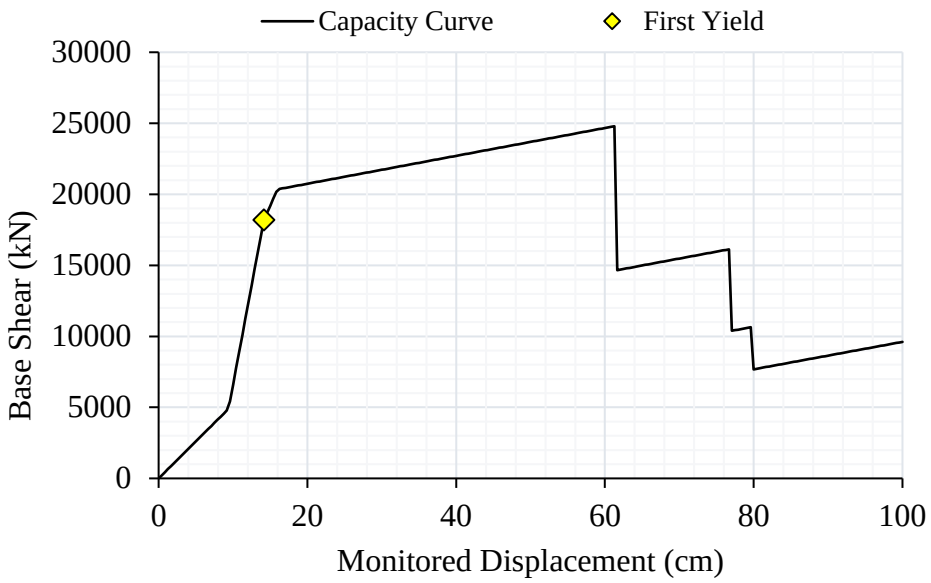

(a)

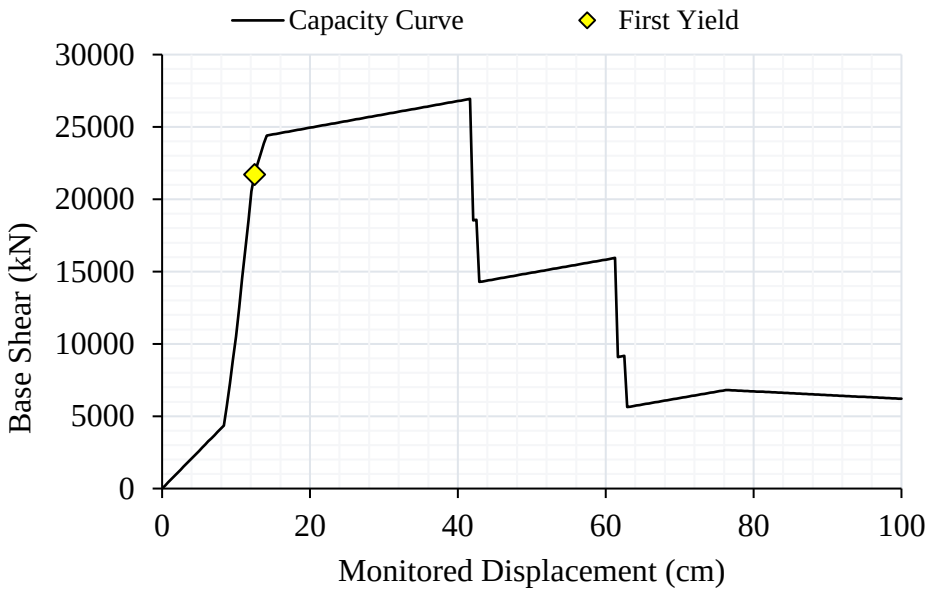

(b)

Figure 5.8 Capacity curves for O07 Bridge in longitudinal pushover analysis: (a) A1-P-A2 pushover direction, (b) A2-P-A1 pushover direction

The performance points for the A1-P-A2 pushover direction and A2-P-A1 pushover direction cases were determined to be 43.3 cm and 37.5 cm, respectively. Performance evaluation of the bridge conducted considering these performance points is summarized respectively in Table 5.8 and Table 5.9. Deformed shape of the bridge with the plastic rotation values at the performance point in both loading directions are given in Figure 5.9. No hinges developed in the trailing abutment columns in both loading directions at the performance point. The pier columns have collapse prevention performance level for both loading directions. For the A1-P-A2 pushover direction, where the leading abutment is the one with longer columns, these columns have controlled damage performance level. However, for the A2-P-A1 pushover direction, where the leading abutment is the one with shorter columns, these columns passed beyond the collapse prevention performance level. Therefore, it can be concluded that the O07 Bridge satisfies the target performance level of collapse prevention when the bridge is pushed towards the abutment with longer columns, while the target performance level is not satisfied when the bridge is pushed towards the abutment with shorter columns. The difference in the response in two loading directions arises from the fact that with the shorter columns in the leading abutment the column plastic rotations become excessive and go beyond the limit values.

Table 5.8 Performance evaluation of O07 Bridge in A1-P-A2 loading direction

Location	Column	θ_p (rad)	θ_p^{LD} (rad)	θ_p^{CD} (rad)	θ_p^{CP} (rad)	Performance Level
A1	Left	0.0000	0.0063	0.0214	0.0296	No Damage
	Middle	0.0000	0.0063	0.0214	0.0296	No Damage
	Right	0.0000	0.0063	0.0214	0.0296	No Damage
P	Left	0.0283	0.0061	0.0213	0.0295	Collapse Prevention
	Middle	0.0264	0.0061	0.0213	0.0295	Collapse Prevention
	Right	0.0283	0.0061	0.0213	0.0295	Collapse Prevention
A2	Left	0.0253	0.0077	0.0262	0.0362	Controlled Damage
	Middle	0.0241	0.0077	0.0262	0.0362	Controlled Damage
	Right	0.0254	0.0077	0.0262	0.0362	Controlled Damage

Table 5.9 Performance evaluation of O07 Bridge in A2-P-A1 loading direction

Location	Column	θ_p (rad)	θ_p^{LD} (rad)	θ_p^{CD} (rad)	θ_p^{CP} (rad)	Performance Level
A1	Left	0.0389	0.0063	0.0214	0.0296	Excessive Damage
	Middle	0.0375	0.0063	0.0214	0.0296	Excessive Damage
	Right	0.0390	0.0063	0.0214	0.0296	Excessive Damage
P	Left	0.0228	0.0061	0.0213	0.0295	Collapse Prevention
	Middle	0.0213	0.0061	0.0213	0.0295	Collapse Prevention
	Right	0.0228	0.0061	0.0213	0.0295	Collapse Prevention
A2	Left	0.0000	0.0077	0.0262	0.0362	No Damage
	Middle	0.0000	0.0077	0.0262	0.0362	No Damage
	Right	0.0000	0.0077	0.0262	0.0362	No Damage

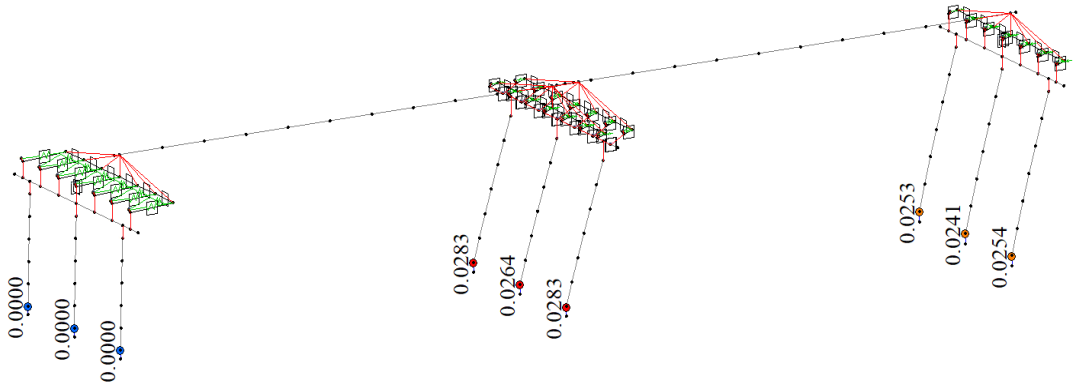

(a)

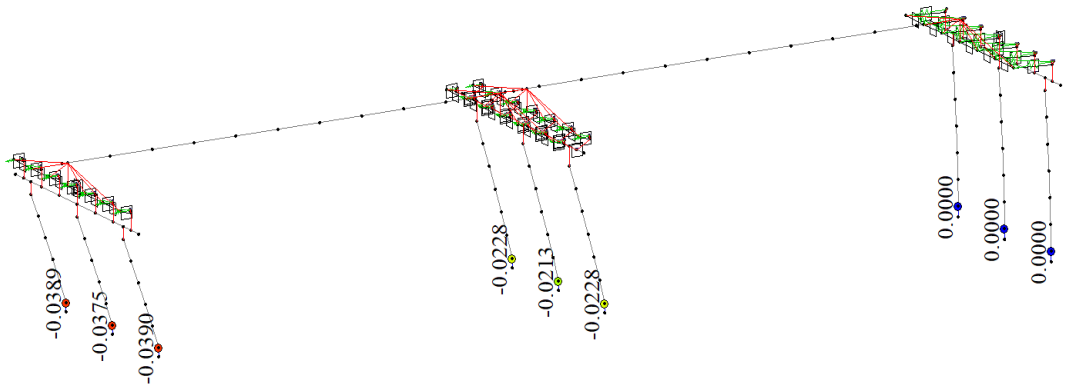

(b)

Figure 5.9: Deformed shape and plastic rotation values (rad) for O07 Bridge at performance point in longitudinal pushover analysis (a) A1-P-A2 direction, (b) A2-P-A1 direction

5.3.2 Transversal Pushover Analysis Results

Different than the longitudinal direction, the investigated bridges have a symmetric layout in the transverse direction. For this reason, a single transversal pushover analysis was conducted on each of the investigated bridges. As mentioned earlier, another difference between the longitudinal and transversal directions of the investigated bridges is that three columns and the cap beam used at the abutment and pier locations form a frame in the transverse direction of bridges. In this case, different axial forces developed in each of these three columns when the bridge was subjected to lateral loading in the transverse direction. Effect of this unequal axial force distribution among the columns was considered in the transversal pushover analyses. According to the transversal pushover direction, bridge columns in each abutment and pier locations were labelled as “leading column”, “middle column”, and “trailing column”, as shown in Figure 5.10.

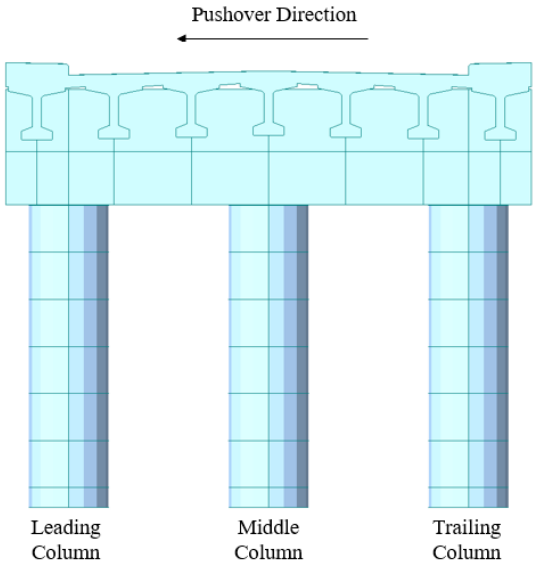

Figure 5.10 Convention used for column naming for transversal pushover analysis

All the investigated bridges exhibited similar pushover response in the transverse direction. For this reason, results for only the O02 Bridge are presented in this section. Plots and tables summarizing the pushover analysis results for all of the investigated bridges are provided in Appendix C.

5.3.2.1 O02 Bridge Transversal Pushover Analysis Results

Pushover capacity curve in the transverse direction of the bridge is shown in Figure 5.11. The increase in stiffness occurring at a displacement of approximately 8 cm is due to the girder ends coming in contact with shear keys at support locations. As indicated in Table 5.10, this contact condition occurred at abutment locations at the 33rd step and at pier location at the 34th step of the pushover analysis. These steps correspond to a pushover displacement on approximately 8.5 cm. Similar to the longitudinal direction response, prior to the contact condition stiffness of the bridge system under pushover loading was governed almost entirely by the elastomeric bearing pads used at girder ends. Following the contact condition, bridge stiffness increases to the level corresponding to the lateral stiffness of the support frames formed by three columns and the cap beam at the pier and abutment locations.

According to the results of the transversal pushover analysis, yielding initiated at the bottom of the trailing column at pier location at a pushover displacement of 10.7 cm. The last plastic hinge yielding occurred at the top of the leading column at both abutment locations at a pushover displacement of 14.0 cm. Therefore, the pier columns were subjected to a lateral drift of approximately 2.2 cm (10.7 cm – 8.5 cm = 2.2 cm) at the onset of yielding. This yield displacement value is significantly smaller than those observed in the longitudinal pushover analysis. The reason for such a difference is related with the column behavior of both pushover analyses. In the case of longitudinal pushover loading each column deformed as an individual cantilever member in single curvature mode. In the case of transverse pushover loading on the other hand, three support columns at each of the abutment and pier locations formed a frame and deformed in double curvature mode as a part of this frame. The ultimate and first yield displacements obtained from the pushover capacity curve indicate a ductility ratio of 2.9 in the transverse direction of the bridge. It should be noted that this value is significantly smaller than the ductility ratio of 4.5 for the longitudinal direction.

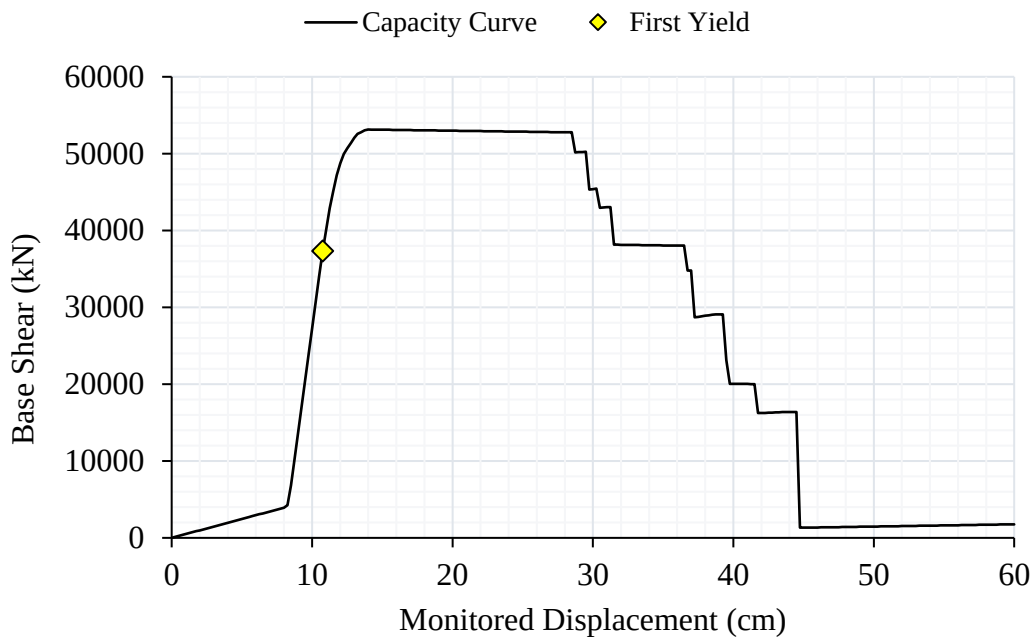

Figure 5.11 Capacity curve of O02 Bridge from transverse pushover analysis

Hinge behaviors that the columns at the pier and abutment locations followed during the pushover loading are shown in Figure 5.12. The plots indicate somehow symmetric response at the top and bottom plastic hinges. Another observation is that for both abutment and pier locations, trailing column has the largest inelastic deformation followed by the middle column. The reason for such a difference is the unequal axial force distribution among the columns under transverse pushover loading. The yield moment and shear force values given in Table 5.10 also show the effect of unequal axial force distribution among the three columns at support locations. The larger yield moment values for the pier columns than the abutment columns are due to the slight difference in the amount of longitudinal reinforcement present in these two groups of columns. Pier columns are reinforced with 58ϕ32 longitudinal bars, while 54ϕ32 reinforcing bars are used in abutment columns.

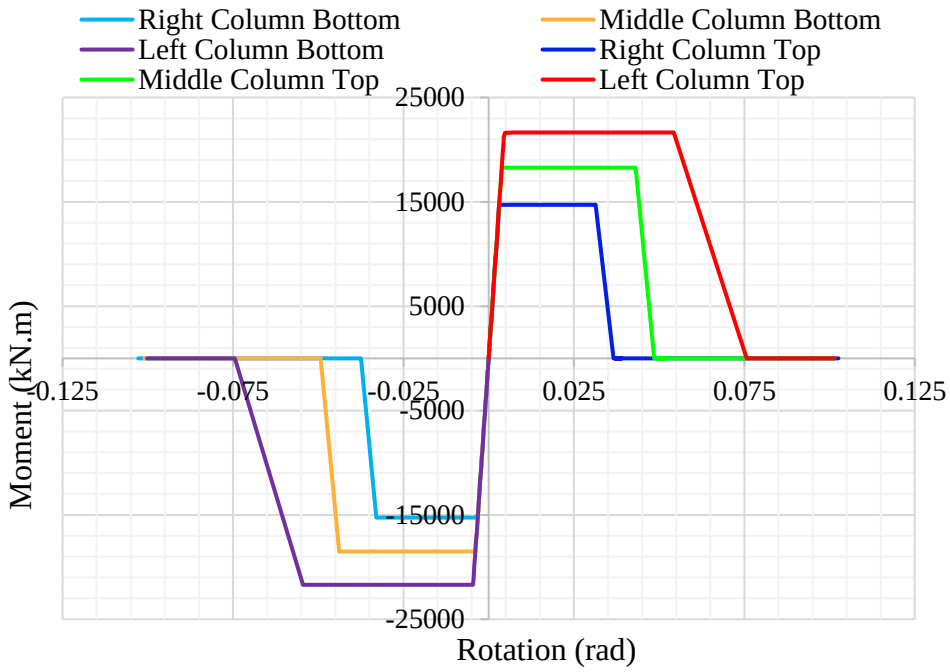

(a)

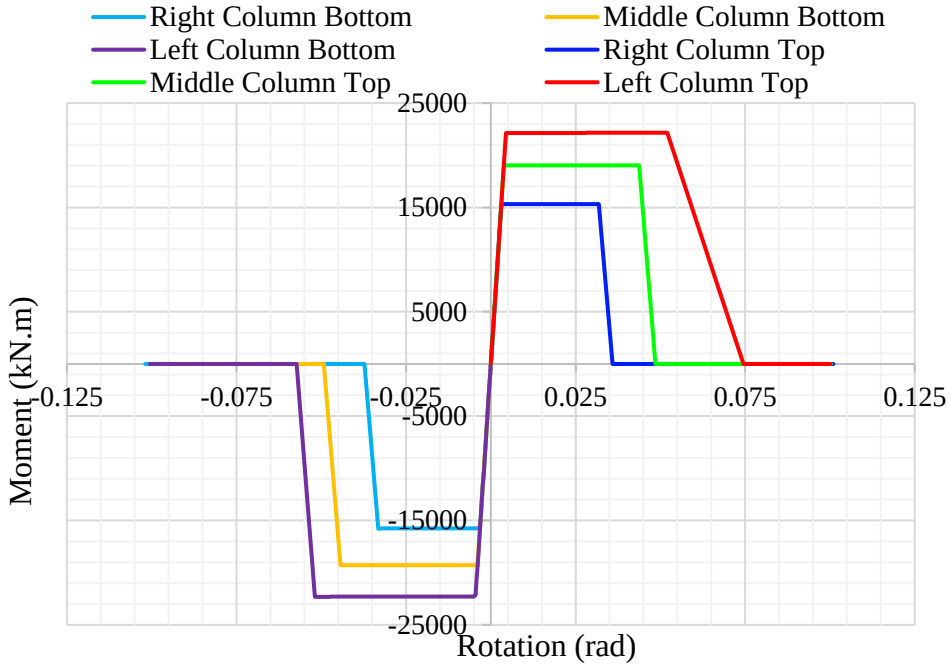

(b)

Figure 5.12 Column hinge behaviors in transverse pushover analysis of Bridge O02: (a) columns at A1 and A2 abutments, (b) columns at pier

Table 5.10 Column yield forces for O02 Bridge from transverse pushover analysis

Axis	Column Hinge	Pounding Step/Disp.	Yield Step/Disp.	P_y (kN)	V_y (kN)	M_y (kN·m)
A1	Left Column Bottom	33 / 8.3	53 / 13.3	8174	-6581	-21693
	Middle Column Bottom		49 / 12.3	1874	-5823	-18508
	Right Column Bottom		47 / 11.8	-3825	-4658	-15253
	Left Column Top		56 / 14.0	7991	-6812	21633
	Middle Column Top		50 / 12.5	1478	-5794	18270
	Right Column Top		49 / 12.3	-4770	-4726	14716
P	Left Column Bottom	34 / 8.5	48 / 12.0	9823	-7058	-22287
	Middle Column Bottom		45 / 11.3	3213	-6083	-19271
	Right Column Bottom		43 / 10.8	-2964	-4972	-15757
	Left Column Top		48 / 12.0	9423	-6953	22138
	Middle Column Top		46 / 11.5	2814	-6003	19030
	Right Column Top		44 / 11.0	-3715	-4877	15317
A2	Left Column Bottom	33 / 8.3	53 / 13.3	8174	-6581	-21693
	Middle Column Bottom		49 / 12.3	1874	-5823	-18508
	Right Column Bottom		47 / 11.8	-3825	-4658	-15253
	Left Column Top		56 / 14.0	7991	-6812	21633
	Middle Column Top		50 / 12.5	1478	-5794	18270
	Right Column Top		49 / 12.3	-4770	-4726	14716

The performance point corresponds to a pushover displacement of 10.3 cm, as illustrated in Figure 5.13. No column yielding occurred prior to this point, indicating that all columns in the bridge system are expected to remain elastic when the target displacement is reached. Therefore, it is concluded that the bridge satisfies the target performance level in the transverse direction by a large margin.

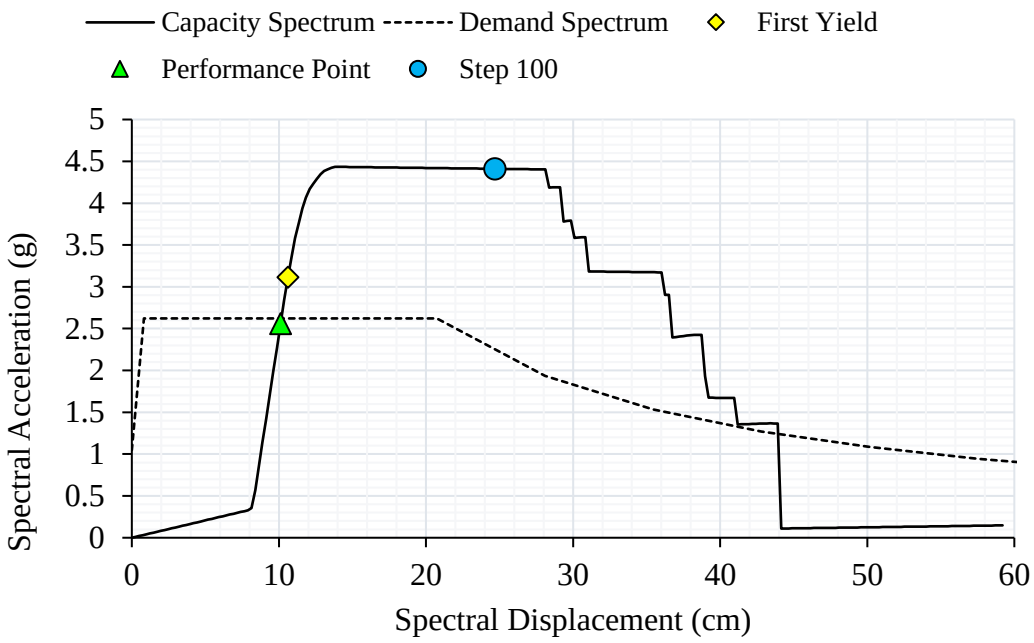

Figure 5.13 Performance point determination of O02 Bridge

Deformed shape of the bridge at the performance point and at 25 cm of transverse displacement are provided, respectively in Figure 5.14 and Figure 5.15. Since no column yielding occurred at the performance point (i.e., at 10.3 cm displacement) the plastic rotation values in Figure 5.14 are indicated as zero. In this case, the bridge superstructure undergoes a rigid translation in the transverse direction with no rotation. However, after yielding of the pier and abutment columns the deformed shape includes larger transverse displacement at the pier location than the abutments (Figure 5.15). The reason for such a deformed shape is yielding of the pier columns before the abutment columns. For bridges with unequal column height at pier and abutment locations, transverse displacement of columns at both abutments and pier would be different, resulting in twisting of the bridge superstructure in addition to translation.

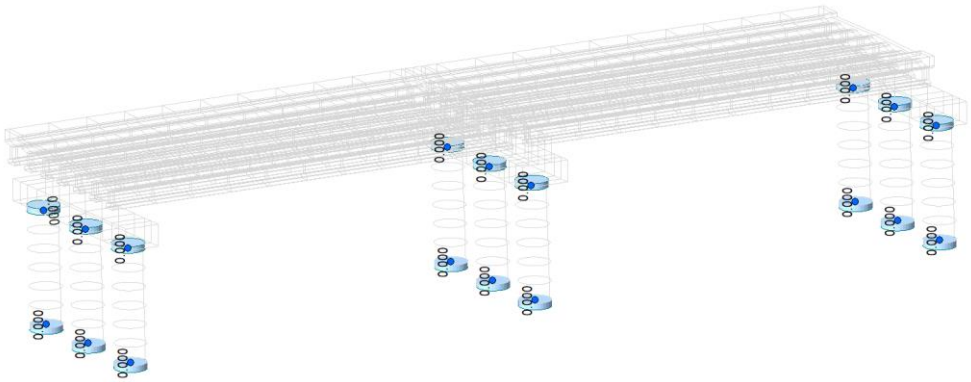

(a)

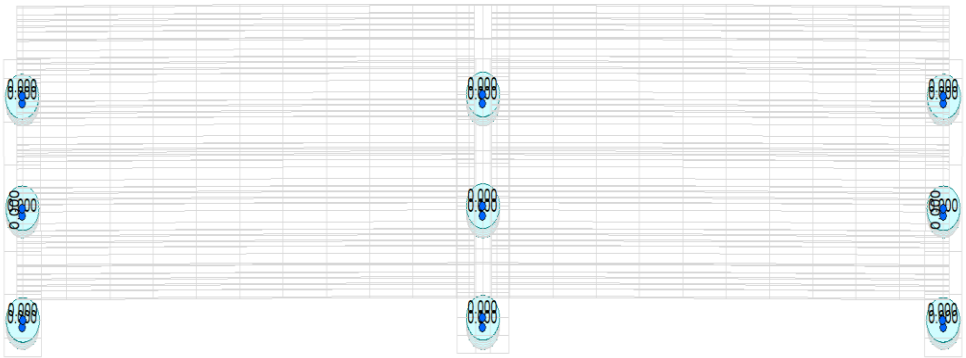

(b)

Figure 5.14 Deformed shape and plastic rotation values at the performance point of O02 Bridge (a) 3D-view (b) Plan view

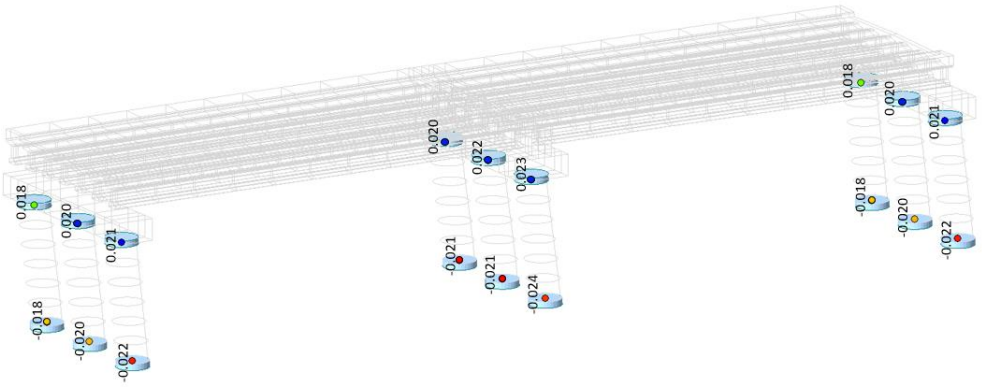

(a)

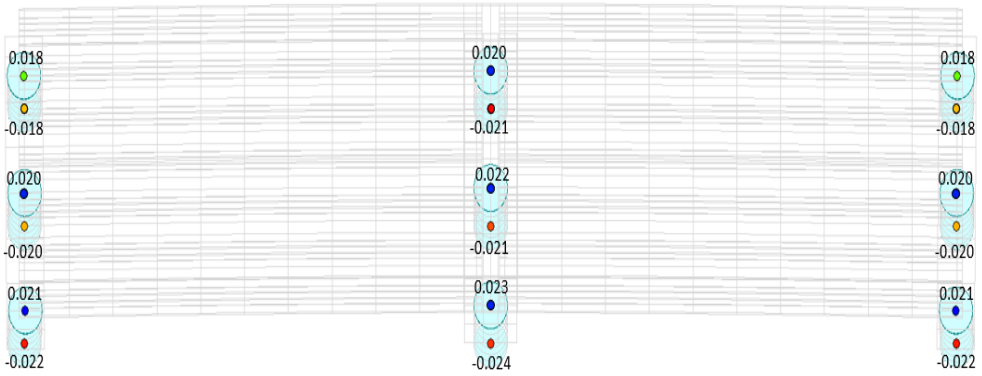

(b)

Figure 5.15 Deformed shape and plastic rotation values of O02 Bridge at 25 cm displacement (a) 3D-view (b) Plan view

5.4 Comparison of Capacity Curves in Longitudinal and Transverse Directions

A comparison of longitudinal and transverse direction capacity curves of O02 Bridge is provided in Figure 5.16. As can be seen the bridge has higher lateral stiffness in transverse direction. The first reason for such a difference in stiffness levels is due to presence of a frame system formed by bridge columns in transverse direction. Another reason for the relatively high transverse stiffness is that pounding between girder and shear key occurs in each axis for transverse direction, whereas pounding between girder end and abutment cap beam wall occurs only in two axes in the

longitudinal direction. Relatively high ductile behavior in the longitudinal direction, as a result of bridge columns behaving as a cantilever member is also valid in Figure 5.16.

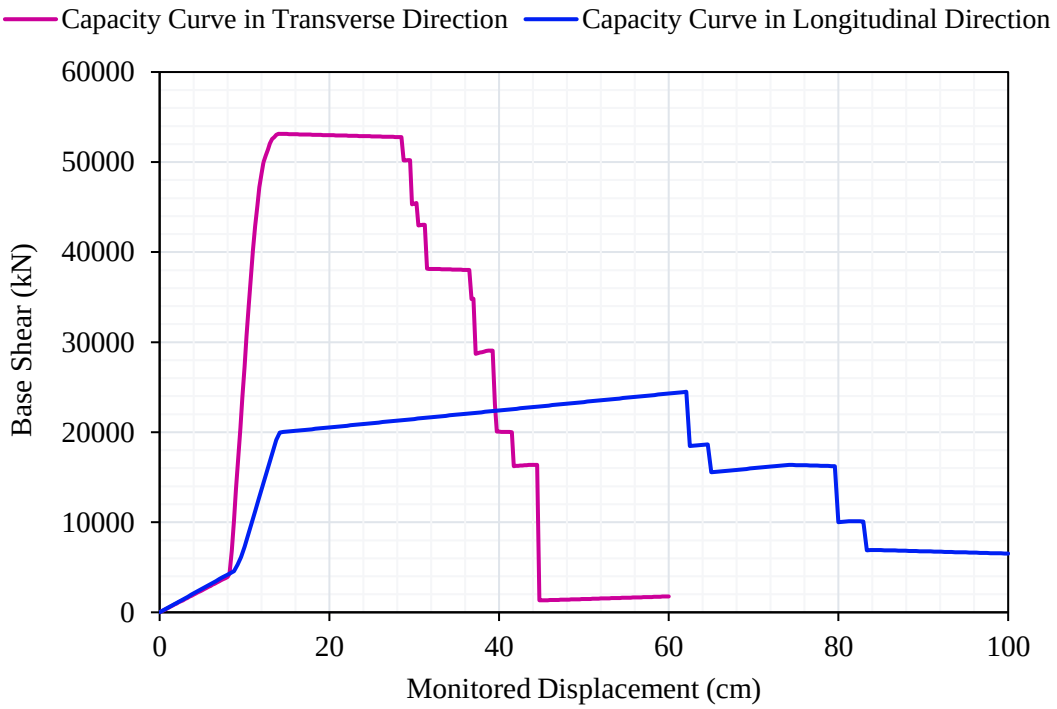

Figure 5.16 Capacity curves of O02 Bridge for both directions

5.5 Comparison of Plastic Forces

Plastic axial forces of pushover analyses and AASHTO iterations are given in Figure 5.17. Axial forces of columns found from longitudinal pushover analysis and AASHTO iteration are so similar because columns behave as cantilever in the longitudinal direction so axial load do not change. Same situation is not valid for transversal direction due to frame system and axial loads of right and left column change during earthquake in transversal direction. Axial force found from AASHTO iteration is 1.74 times higher than found from transversal pushover analysis for left column, also it can be named as compression column. Furthermore, there is a huge difference between axial force found from AASHTO iteration and transversal

pushover analysis for right column, also it can be named as tension column. AASHTO iteration axial force is 3.94 times higher than transversal pushover analysis. However, since middle column is present on the center of the frame system axial load does not change during the earthquake, so AASHTO iteration and longitudinal pushover analysis is almost same.

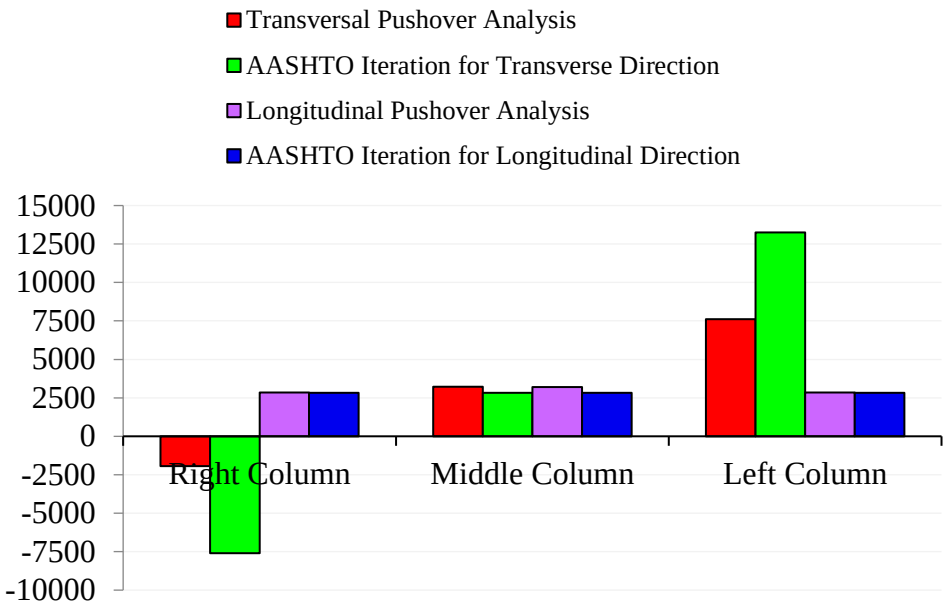

Figure 5.17 Plastic axial forces of O02 Bridge

Plastic moments found from pushover analyses and AASHTO iterations are shown in Figure 5.18. Because of the columns behavior on the longitudinal direction as mentioned before, there is no significant difference for longitudinal moments between longitudinal pushover analysis and AASHTO iteration. However, difference for transversal moment between transversal pushover analysis and AASHTO iteration can be seen apparently. Moment found from the transversal pushover analysis is 1.11 times higher than AASHTO iteration in the right column under the tension, whereas transversal moments of AASHTO iteration is 1.34 and 1.80 times higher than transversal pushover analysis for middle and left column, under the compression, respectively.

The main outcome can be retrieved from these comparisons is that axial forces and moments are similar in the longitudinal direction. Although axial forces are similar for middle column in transversal direction, there are huge difference for right (tension) and left (compression) column. Furthermore, difference in transverse moment is present for all columns clearly. The reason of AASHTO iteration has higher forces in transverse direction is that there is no yielding on the columns for transversal pushover analysis, so moments were not distributed among them. If foundation of columns is designed considered with these AASHTO iteration forces, it will be over design.

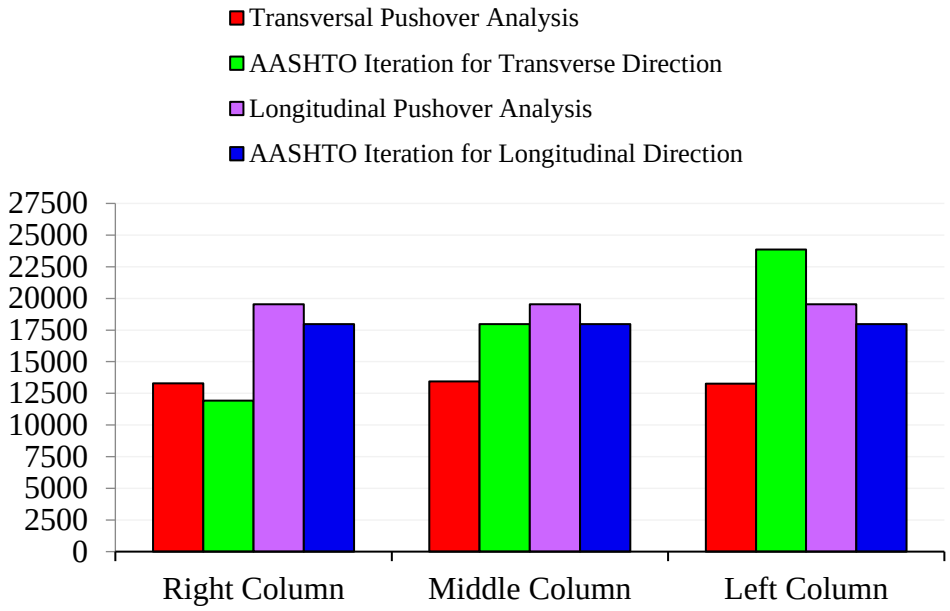

Figure 5.18 Plastic moments of O02 Bridge

CHAPTER 6

NONLINEAR TIME HISTORY ANALYSIS DETAILS

6.1 Introduction

Nonlinear time history analysis (NTHA) is a dynamic analysis of a structure under a ground motion that changes with time and by utilizing inelastic material properties of structural elements. As the dynamic response of the structure is captured with the inclusion of realistic nonlinear response of the members, this type of analysis is considered to produce more accurate structural response when compared with other structural analysis methods. In general principle, nonlinear properties of structural elements in a typical NTHA are assigned to the structure in the form of distributed plastic hinge based on the inelastic material behavior.

The main disadvantage of NTHA, especially when used with fiber section plastic hinge definition, is the fact that significantly large amount of data is produced at the end of the analysis and that post-processing of such data requires much effort. This issue has already been explained by Aviram *et al.* (2008). The execution of the analysis also requires relatively high computational effort as a result of nonlinear properties of each structural element together with the relatively small time increment used for the ground motion.

6.2 Distributed Plastic Hinge Model

Distributed plastic hinge model, which is widely used in NTHA, can be defined as either displacement or force-based formulation. As this model considers a distributed material nonlinearity across the member cross section, it provides a more accurate

representation of inelastic behavior than lumped hinge models (Spacone *et al.*, 1996). The member cross section is discretized into small size fibers at the locations of potential nonlinear behavior. Each of these fibers considers only axial deformations and is assigned a corresponding material property. In the current study, the bridge column cross sections were discretized such that the fibers were assigned either confined concrete material properties, unconfined concrete material properties, or reinforcing steel material properties, as illustrated in Figure 6.1.

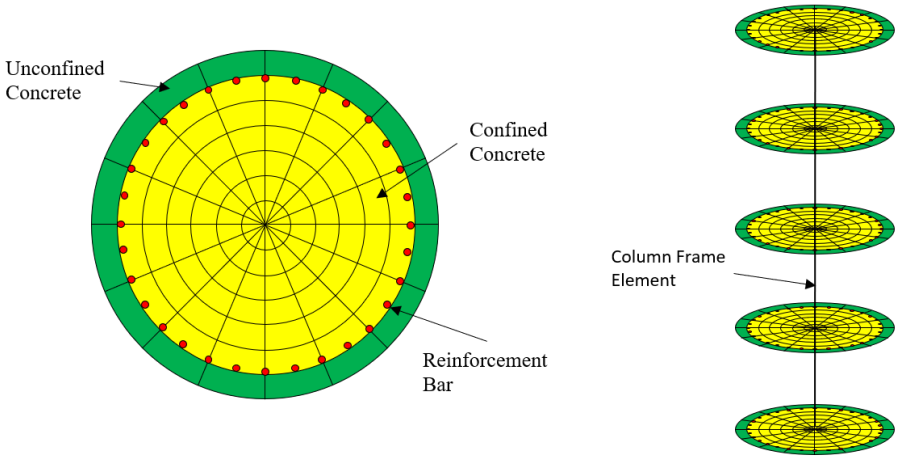

Figure 6.1 Typical Fiber Hinge Section

6.3 Analysis Methods

There are several analysis methods to solve the equation of motions to determine the dynamic response of structural systems. Complexity of the model to be analyzed is one of the factors in determining the analysis method. Step-by-step solution methods are employed to satisfy dynamic equilibrium at time steps with many iterations in order to be able to capture changing nonlinear properties such as degradation of stiffness and strength in the system. Nonlinearity associated with material yielding and the resulting stiffness reduction is considered at each time step and the stiffness matrix is updated accordingly. A direct implicit integration method was used in the current study for time history analyses. For numerical integration, Newmark method with constant acceleration was utilized. The numerical solution method adopted in

the current study appeared to be a reliable method with no numerical instability and accurate results.

Energy generated by earthquake is dissipated by the structural system mainly through plastic deformations and other types of damage, as well as damping. Compared with plastic deformations and damage, the energy dissipated through damping is usually not significant, but still needs to be considered in order to reflect the actual structural response (Xiaoming *et al.*, 2015).

Damping in numerical analysis is usually defined in one of the three methods of modal damping, mass and stiffness proportional damping, and strain energy proportional damping. In the current study, mass and stiffness proportional damping was used with Rayleigh damping model. The mass and stiffness proportional Rayleigh damping is defined by Eq. (6.1) (Chopra, 1995).

$$\zeta_n = \frac{a}{2}\frac{1}{\omega_n} + \frac{b}{2}\omega_n \qquad \text{Eq. (6.1)}$$

Where;

ζ_n : nth mode damping ratio

a: mass proportionality coefficient

b: stiffness proportionality coefficient

ω_n: nth mode circular frequency

The proportionality coefficients, a and b, can be determined for the pth and qth modes by using the system equation given in Eq. (6.2). The relations between the damping terms and natural frequency are shown in Figure 6.2.

$$\frac{1}{2}\begin{bmatrix} \frac{1}{\omega_p} & \omega_p \\ \frac{1}{\omega_q} & w_q \end{bmatrix}\begin{pmatrix} a \\ b \end{pmatrix} = \begin{pmatrix} \zeta_p \\ \zeta_q \end{pmatrix} \qquad \text{Eq. (6.2)}$$

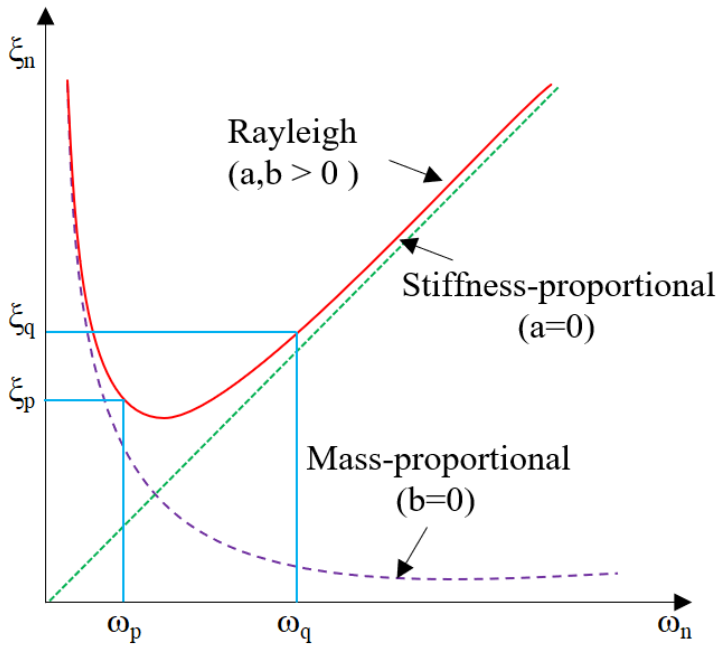

Figure 6.2 Damping ratio vs. frequency relationship from Rayleigh model

6.4 Ground Motion Selection and Scaling

Selection and scaling of the ground motions are probably the most controversial issues in time history analysis. The analysis results can be significantly affected from the selected ground motion records and the procedure used for scaling of these records. There are several ground motion scaling methods available in the literature based on Peak Ground Acceleration (PGA), first natural period (T_1), or spectral amplitudes (Vemuri and Kolluru, 2020). Different rules are also provided in different design codes for the period range to be considered in scaling procedure (ASCE 2005, ASCE 2010, ASCE 2016, ASCE 41-17, EUROCODE-8, TBES 2020). Furthermore, each code gives the different procedure to scale ground motions and minimum number of ground motions to be selected. Therefore, response to be obtained from a time history analysis for the same structure depends on subjective parameters defined by users and codes. A comparison of design codes in terms of ground motion selection and scaling to be used in NTHA is provided in Table 6.1.

Table 6.1 Selection and scaling rules specified in design documents

Code	Adopted method	Multiplication factor for design spectrum	Period range of scaling	Max. number of ground motion records
ASCE7-05	SRSS	1.30	$0.20T_1$-$1.50T_1$	7
ASCE 7-10	SRSS	1.00	$0.20T_1$-$1.50T_1$	7
ASCE 7-16	RotD100	0.90	$0.20T_1$-$2.00T_1$	11
ASCE 41-17	RotD100	0.90	$0.20T_1$-$1.50T_1$	11
Eurocode-8	SRSS	1.30	$0.20T_1$-$1.50T_1$	7
TBES-21	SRSS	1.30	$0.20T_1$-$1.50T_1$	7

Ground motion records can be retrieved by using Pacific Earthquake Engineering Research (PEER) Next Generation Attenuation (NGA) database (PEER, 2005). There are numerous records available in the database, and consideration of the characteristics of the expected earthquake (such as magnitude, distance to fault, fault type, soil type) is the key point for the selection of ground motions to be used in NTHA. It should be noted that each ground motion record has three components in two horizontal and vertical directions.

There are many approaches for scaling of ground motions so that all selected records represent similar level of seismic intensity that is compatible with the target design spectrum. One of the most common approaches to achieve this goal is using an amplitude scaling (Heo *et al.,* 2011), which is the method used in the current study. This method is based on the condition that average spectra of selected ground motion records does not fall below a target spectrum, which is obtained as a multiple of the design spectrum, for a specific period range. Spectra of ground motion records to be used for scaling are developed with adopted method such as the square root of the sum of the squares (SRSS) or maximum rotated component (RotD100) combination of the two horizontal components.

Among the rules presented in Table 6.1, the one specified in ASCE 41-17 was used in the current study. Accordingly, 11 ground motions records were considered with the RotD100 method for combination of the records in two perpendicular directions. The target spectra were defined as 90% of the design spectrum in the period range of $0.2T_1$-$1.5T_1$, where T_1 is the natural vibration period of the investigated bridge.

6.5 Performance Criteria

Cross-sectional strains were used as the parameter for assessment of the bridge performance in NTHA. Based on the procedure outlined in the recent Turkish Bridge Earthquake Standard (2020) the performance level is determined by comparing the maximum strains in the reinforcement and in the confined concrete with the corresponding limit values. This standard categorizes damage level into two classes as "controlled damage" and "collapse prevention". Furthermore, "limited damage" level is also considered for a linear analysis. In this study, all three damage levels were considered. It was considered that the bridge system fails to satisfy the target performance level if the target performance was not satisfied in either of the longitudinal or transverse directions.

Strain limits for the reinforcement and confined concrete for the considered performance levels are given in Eq. (6.3).

$$\begin{gathered} \varepsilon_c^{(LD)} = 0.003 \;\&\; \varepsilon_s^{(LD)} = 0.015 \\ \varepsilon_c^{(CD)} = 0.5\varepsilon_{cu} \leq 0.0135 \;\&\; \varepsilon_s^{(CD)} = 0.5\varepsilon_{su} = 0.040 \\ \varepsilon_c^{(CP)} = 0.67\varepsilon_{cu} \leq 0.018 \;\&\; \varepsilon_s^{(CP)} = 0.67\varepsilon_{su} \end{gathered} \qquad \text{Eq. (6.3)}$$

Where;

$\varepsilon_c^{(LD)}$: Confined concrete strain limit for limited damage level

$\varepsilon_s^{(LD)}$: Reinforcement strain limit for limited damage level

$\varepsilon_c^{(CD)}$: Confined concrete strain limit for controlled damage level

ε_{cu}: Ultimate strain for confined concrete

$\varepsilon_s^{(CD)}$: Reinforcement strain limit for controlled damage level

ε_{su}: Ultimate strain for reinforcement

$\varepsilon_c^{(CP)}$: Confined concrete strain limit for collapse prevention level

$\varepsilon_s^{(CP)}$: Reinforcement strain limit for collapse prevention level

CHAPTER 7

NONLINEAR TIME HISTORY ANALYSIS RESULTS

7.1 Introduction

In this chapter, selection and scaling of ground motion records used in the nonlinear time history analyses, fiber hinge properties, performance level strain limits and strain results of confined concrete and reinforcement fibers are given. Nonlinear time history analyses were conducted on O07 and O13 bridges. These two bridges represent, respectively the group of bridges with varying and constant column heights at pier and abutment locations.

7.2 Ground Motion Selection and Scaling

Ground motion records used in the time history analyses were retrieved from the Pacific Earthquake Engineering Research (PEER) Next Generation Attenuation (NGA) database (PEER, 2005) considering the expected earthquake characteristic of each bridge. As dictated by the ASCE 41-17 seismic performance evaluation procedure, eleven pairs of ground motion records were selected. Scaling of the raw ground motion records was conducted in the two horizontal and the vertical directions considering the procedure specified in ASCE 41-17.

Selection of the ground motion records from the database was done considering the expected earthquake magnitude, soil class, fault type, and fault proximity to the bridge location. According to the Earthquake Hazard Analysis Report for the Çanakkale Motorway project (2018), the expected earthquake magnitude at the site that the investigated bridges are located is 7.2. Based on this information, ground

motion records with earthquake magnitudes ranging between 6.0 and 8.0 were selected. Other parameters considered in the ground motion selection process are given in Table 7.1 and Table 7.2, respectively for the O07 and O13 bridges. It should be noted that the ground motions were selected such that there are no pulse effects.

Table 7.1 Ground motion record selection parameters for O07 Bridge

Fault Type	**Magnitude min, max**	**Fault Distance (km)**	**Soil Class**	**V_{s30} (m/s) min, max**
Strike Slip	6.00, 8.00	10	C	360, 720

Table 7.2 Ground motion records selection parameters for O13 Bridge

Fault Type	**Magnitude min, max**	**Fault Distance (km)**	**Soil Class**	**V_{s30} (m/s) min, max**
Strike Slip	6.00, 8.00	3.17	C	360, 720

Properties of the ground motions used in the time history analyses are presented in. Table 7.3. The acceleration versus time graph for these ground motion records in the three orthogonal directions are given in Appendix D.

In Table 7.3, R_{jb} is Joyner-Boore distance to rupture plane, R_{rup} is the closest distance to rupture plane and V_{s30} is the average shear wave velocity within the 30 m depth.

Table 7.3 Properties of ground motions used in time history analyses

Record Sequence Number	Earthquake Name	Year	Magnitude	R_{jb} (km)	R_{rup} (km)	V_{s30} (m/sec)
448	"Morgan Hill"	1984	6.19	3.22	3.26	488.8
864	"Landers"	1992	7.28	11.03	11.03	379.3
1612	"Duzce_ Turkey"	1999	7.14	4.17	4.17	551.3
1614	"Duzce_ Turkey"	1999	7.14	11.46	11.46	481
1787	"Duzce_ Turkey"	1999	7.14	3.58	3.58	425
3943	"Hector Mine"	1999	7.13	10.35	11.66	726
3966	"Tottori_ Japan"	2000	6.61	9.1	9.12	616.6
4068	"Tottori_ Japan"	2000	6.61	8.82	8.83	420.2
4071	"Parkfield-02_ CA"	2004	6.00	0.73	2.65	363.7
4132	"Parkfield-02_ CA"	2004	6.00	0.61	2.57	397.6
8166	"Parkfield-02_ CA"	2004	6.00	3.69	4.46	467.8

ASCE 41-17 considers the region of the spectrum bounded by the $0.2T_1$ – $1.5T_1$ period range for scaling. Average spectrum of the scaled records is expected to remain above the 90% of the design spectrum. In other words, the target spectrum was determined by multiplying the ordinates of the design spectrum by a factor of 0.9. RotD100 method is specified for combination of the records in two perpendicular directions. The natural vibration periods for the O07 Bridge and O13 Bridge are 1.04 sec and 1.03 sec, respectively. Accordingly, ground motion scaling

was performed within the 0.21 sec to 1.56 sec interval on the response spectrum for both bridges. Spectra corresponding to unscaled ground motion records and the arithmetic mean of these spectra are shown together with the target spectrum in Figure 7.1 and Figure 7.2 for the investigated bridges.

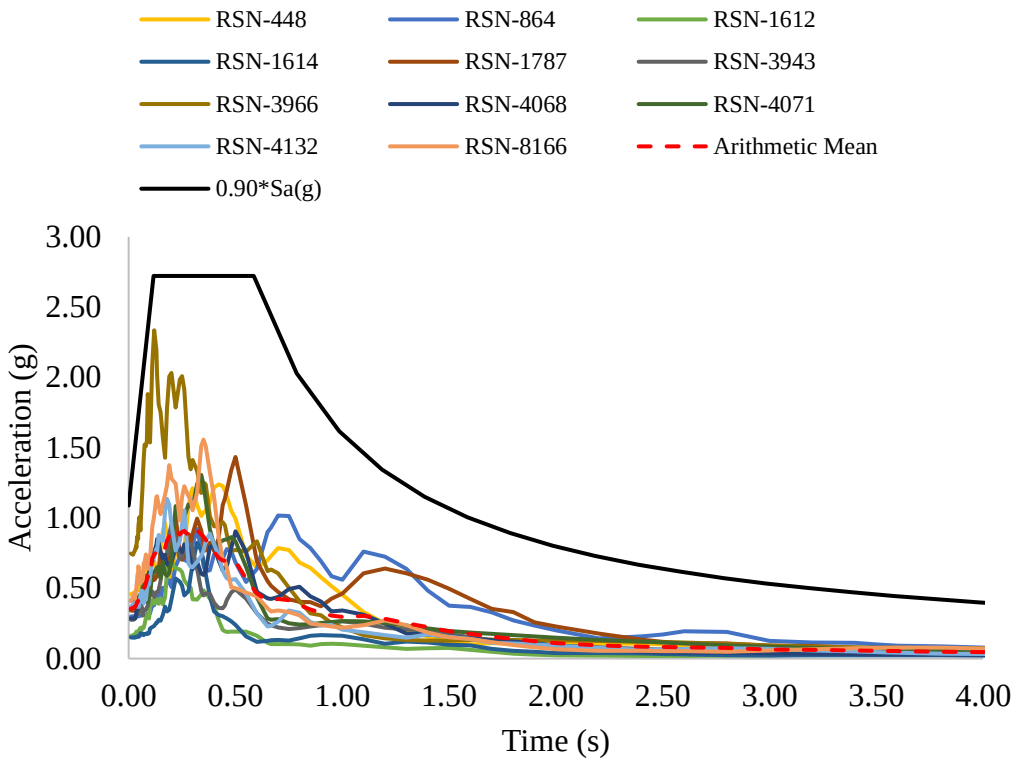

Figure 7.1 Unscaled ground motion spectra and target spectrum for O07 Bridge

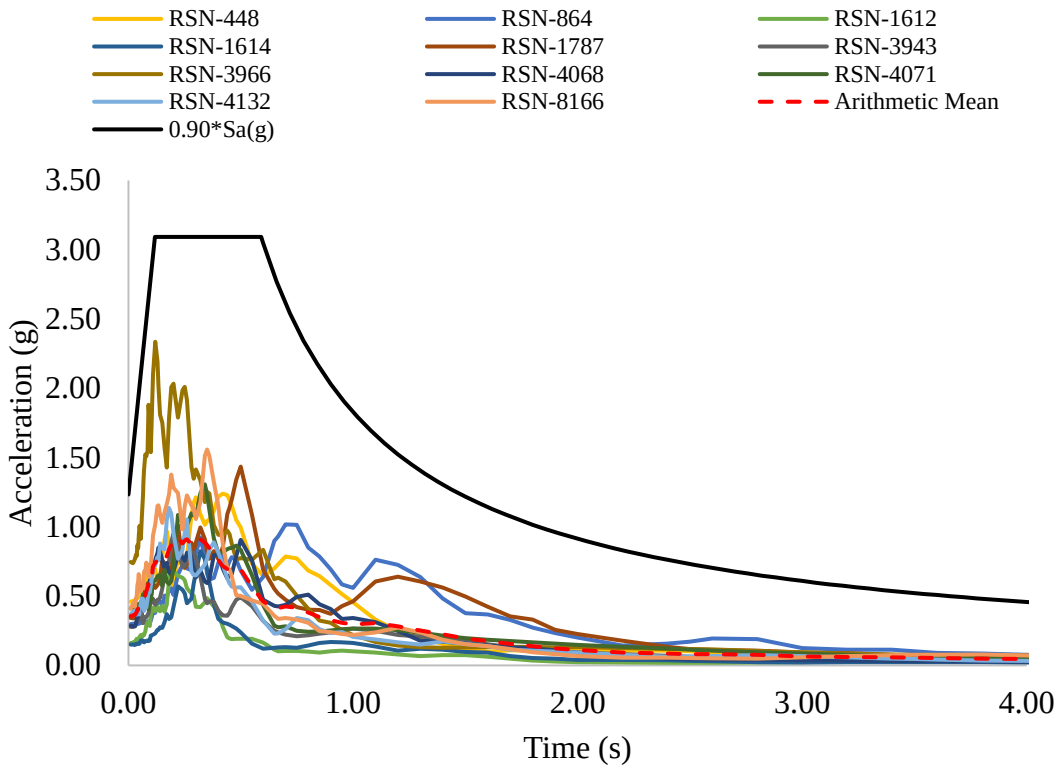

Figure 7.2 Unscaled ground motion spectra and target spectrum O13 Bridge

Scaling factors determined for each ground motion record for the investigated bridges are shown in Table 7.4 and Table 7.5. These scale factors were used both for the horizontal and vertical components of each record. The reason for the difference in the scale factors for O07 and O13 Bridges, is the fact that the bridges have different design spectra. The peak ground acceleration is 1.21g for the O07 Bridge, while it is 1.37g for the O13 Bridge. As a result, scale factors for the O13 Bridge are higher than those for the O07 Bridge. Spectra corresponding to the scaled ground motions are given in Figure 7.3 to Figure 7.6. Figure 7.4 and Figure 7.6 provide zoomed in views of the $0.2T_1$-$1.5T_1$ region of the spectra in order to better show the relation between the mean spectrum and the target spectrum.

Table 7.4 Scale factor for each ground motion record for O07 Bridge

RSN 448	RSN 864	RSN 1612	RSN 1614	RSN 1787	RSN 3943	RSN 3966	RSN 4068	RSN 4071	RSN 4132	RSN 8166
7.00	5.00	10.00	10.00	6.00	6.50	4.00	6.00	7.00	7.00	6.00

Table 7.5 Scale factor for each ground motion record for O13 Bridge

RSN 448	RSN 864	RSN 1612	RSN 1614	RSN 1787	RSN 3943	RSN 3966	RSN 4068	RSN 4071	RSN 4132	RSN 8166
10.00	5.00	12.50	12.50	6.25	6.50	5.00	6.00	7.00	7.00	6.00

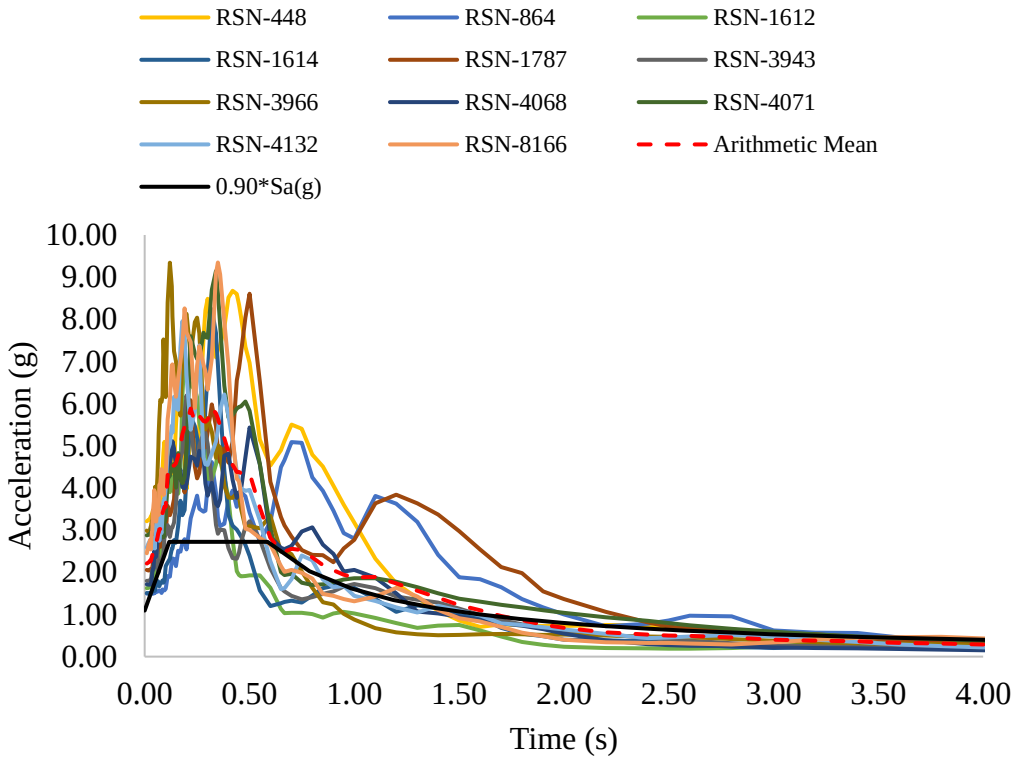

Figure 7.3 Scaled ground motion spectra and target spectrum for O07 Bridge

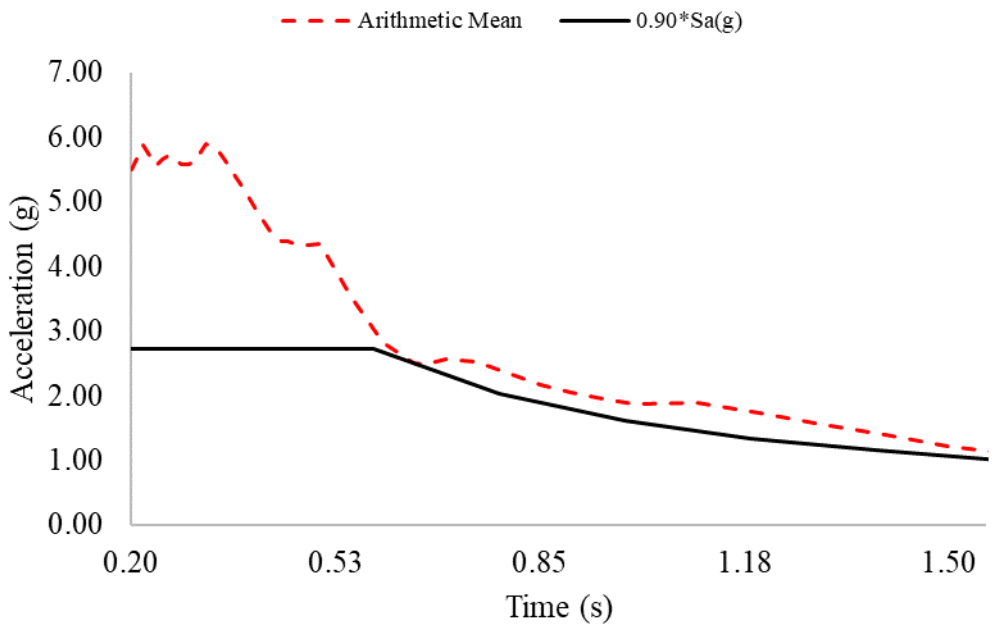

Figure 7.4 Target and mean spectra for O07 Bridge in $0.2T_1$ – $1.5T_1$ interval

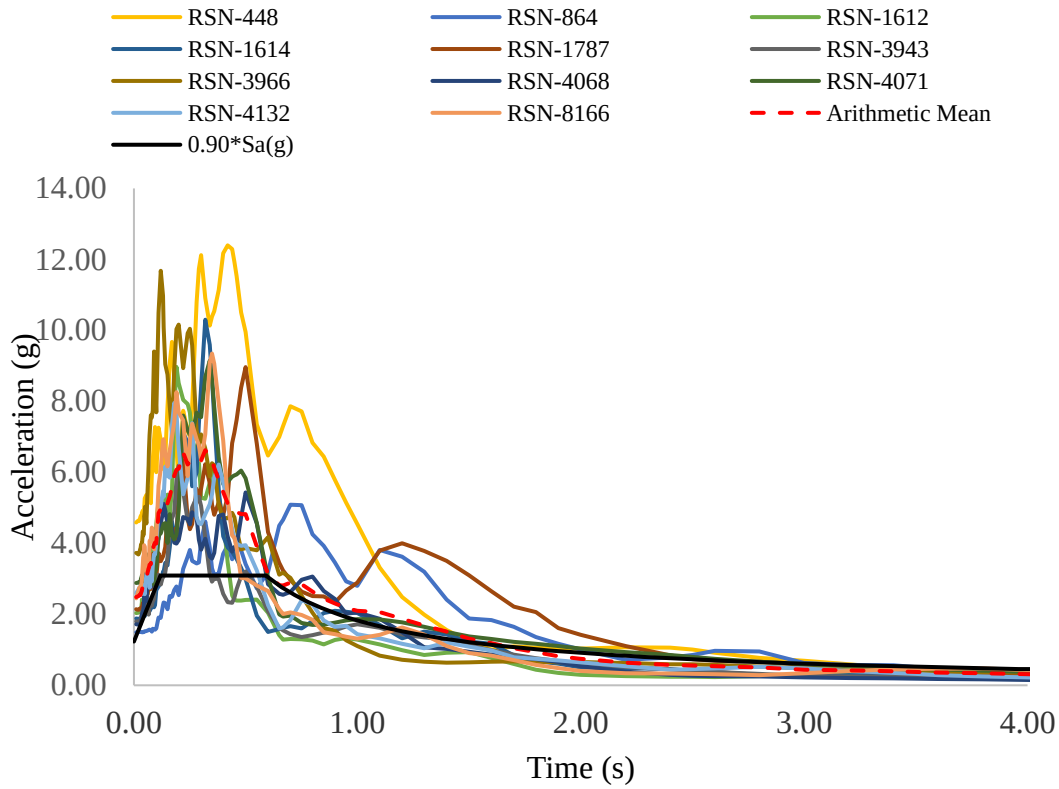

Figure 7.5 Scaled ground motion spectra and target spectrum for O13 Bridge

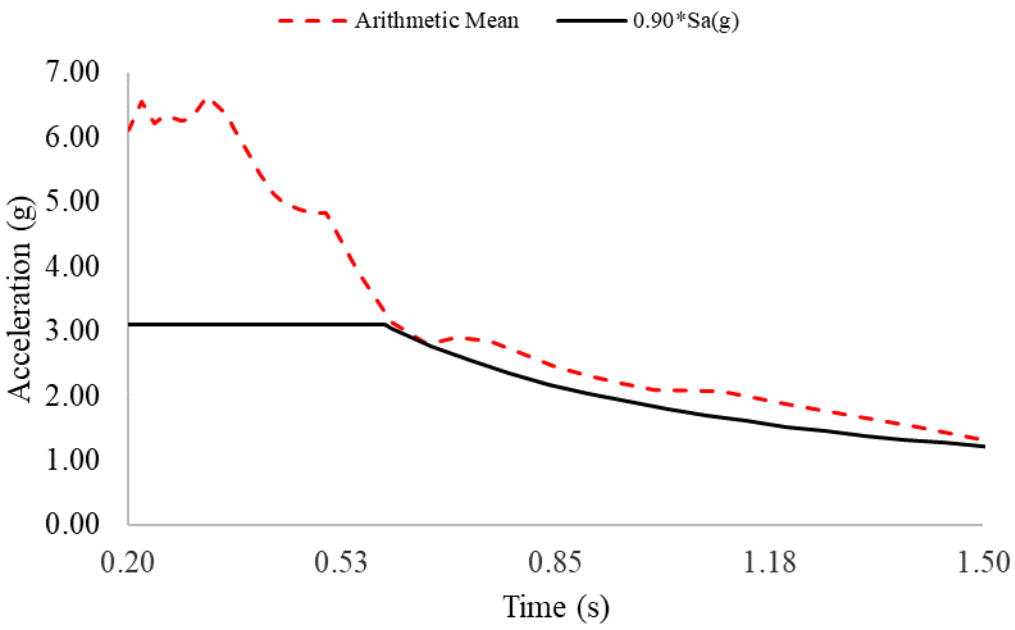

Figure 7.6 Target and mean spectra for O13 Bridge in $0.2T_1 - 1.5T_1$ interval

7.3 Fiber Hinges

Fiber hinges were used to reflect the inelastic response of bridge columns in nonlinear time history analysis. As mentioned in Chapter 6, column cross sections were discretized into fibers and inelastic properties of the corresponding materials were assigned to these fibers. Concrete fibers were divided into two groups as unconfined and confined. An example cross section discretization used for bridge columns is shown in Figure 7.7. Red dots represent the longitudinal reinforcement, yellow parts represent confined concrete and green parts represent unconfined concrete material.

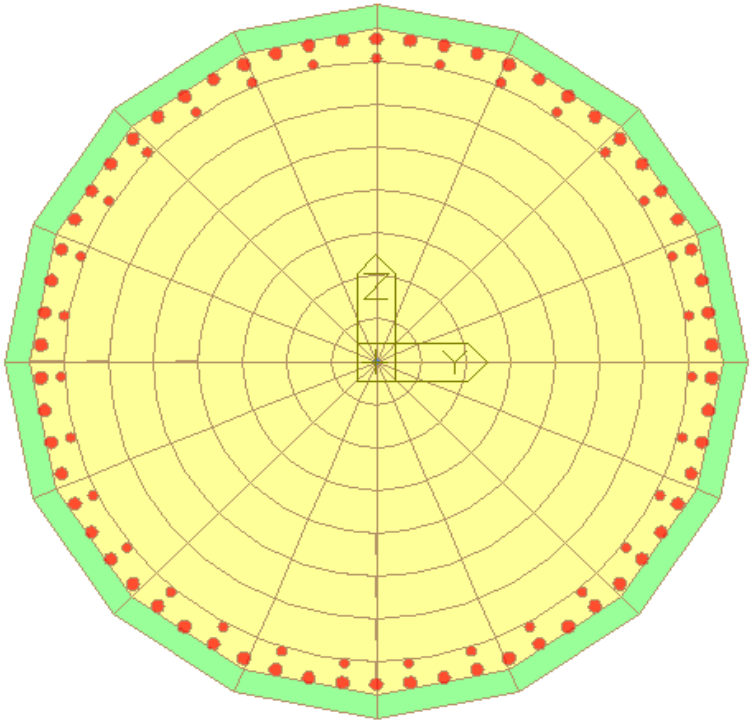

Figure 7.7 An example column cross section discretization for fiber hinge modeling

Inelastic concrete material properties were determined by using Mander model, while Park strain hardening model was considered for the nonlinear behavior of reinforcing steel, as explained in Sections 3.4.2 and 3.4.3 respectively. The material models are based on the expected material strengths for C30 concrete class and S420 steel class. As mentioned in Section 3.4.1, the 1.3 and 1.2 coefficients were used, respectively to convert the characteristic values of the concrete compressive strength and steel yield strength into corresponding expected strengths (TBES, 2020). The stress-strain behavior used for the reinforcement material in both bridges is shown in Figure 7.8.

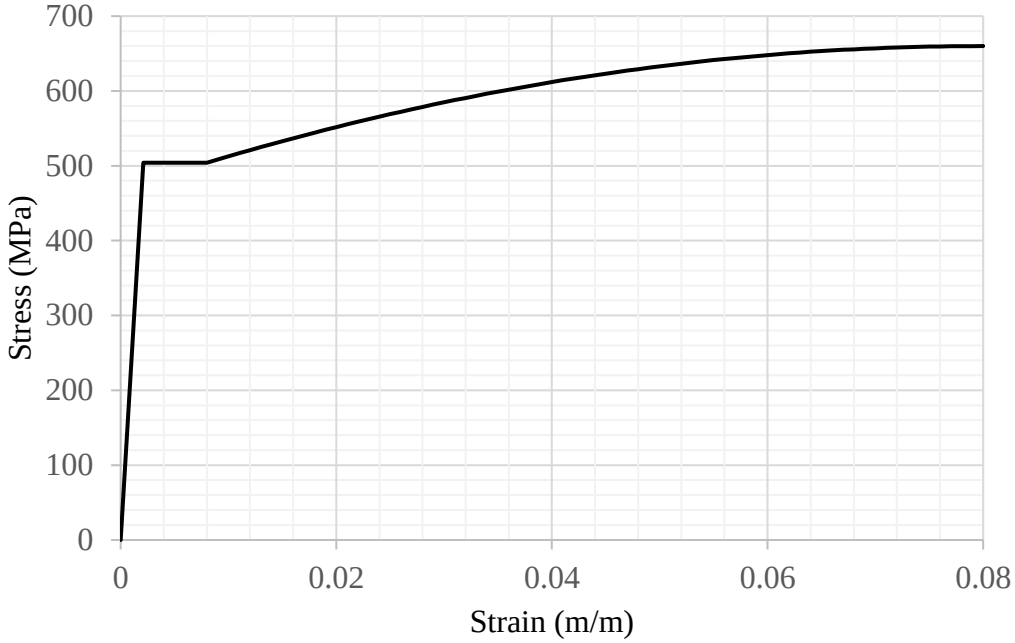

Figure 7.8 Inelastic reinforcement material behavior used for bridge columns

The unconfined and confined concrete stress-strain relations used for the O13 and O07 bridge columns are shown, respectively in Figure 7.9 and Figure 7.10. Since all columns in O13 Bridge have the same reinforcement detailing, the same confined concrete stress-strain model was used for all columns. In O07 Bridge, on the other hand, additional reinforcement was provided at the bottom cross section of pier columns. For this reason, two different confined concrete stress-strain models were used in the model of this bridge for definition of fiber hinges. Another observation that is valid in Figure 7.9 and Figure 7.10 is that the confined concrete strengths and maximum strains used for the two bridges are different. This difference occurs as a result of the amount of column transversal reinforcement used in the two bridges being different. Columns in O13 Bridge have ϕ22/7.5 transversal reinforcement, while it is ϕ22/10 in columns in O07 Bridge.

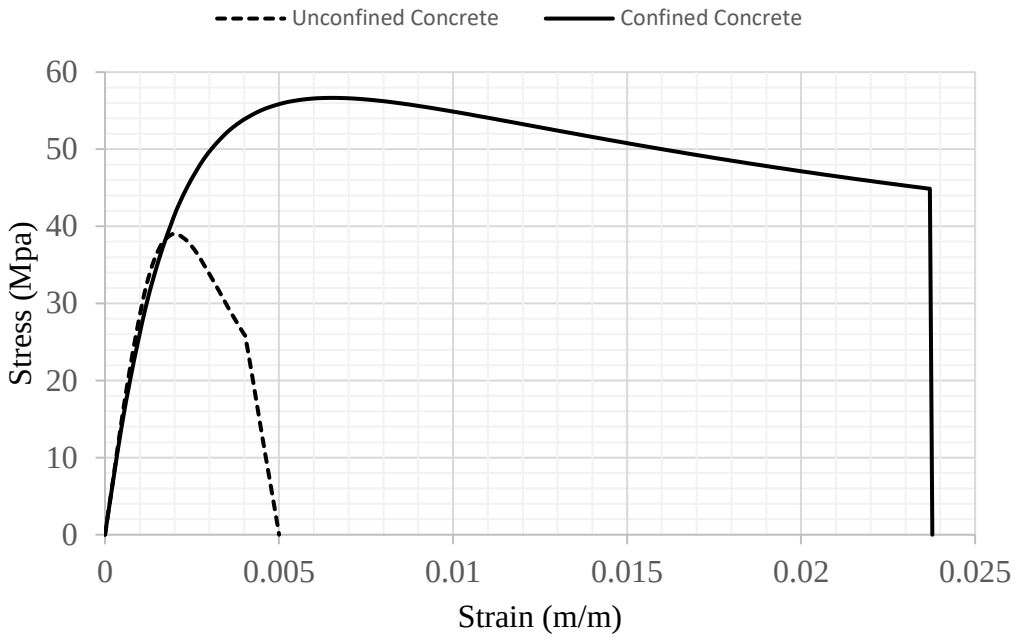

Figure 7.9 Inelastic concrete properties used for O13 Bridge columns

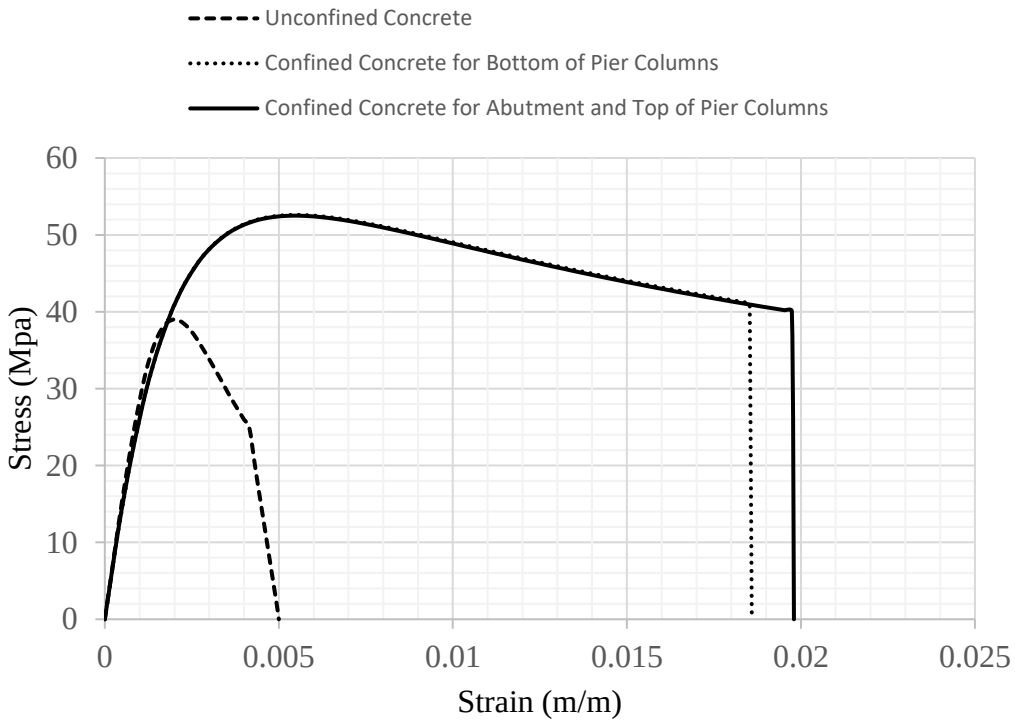

Figure 7.10 Inelastic concrete properties used for O07 Bridge columns

7.4 Performance Limits

Confined concrete and reinforcement strain limits for the performance levels of Limited Damage (LD), Controlled Damage (CD), and Collapse Prevention (CP) were determined by considering TBES (2020) as mentioned in Chapter 6. Reinforcement strain limit for each performance level is defined in terms of the ultimate tensile strain and is given in Table 7.6. Concrete strain limits for each performance level were determined by using the formulation provided in Section 6.5. Strain limits determined this way are presented in Table 7.7.

Table 7.6 Reinforcement strain limits (tensile) for different performance levels

Limited Damage	**Controlled Damage**	**Collapse Prevention**	**Ultimate Strain**
0.015	0.04	0.053	0.08

The relation between the performance levels and the reinforcement and confined concrete strain limits given in Table 7.6 and Table 7.7 are illustrated as color charts in Figure 7.11. Confined concrete and reinforcement strains in column fiber sections determined from time history analysis of the bridges are presented in the following section by using the same colors used in the charts given in Figure 7.11.

Table 7.7 Concrete strain limits (compressive) for different performance levels

Performance Level	O13 Bridge			O07 Bridge			
	A1	P	A2	A1	P		A2
					Bottom	Top	
Limited Damage	0.003	0.003	0.003	0.003	0.003	0.003	0.003
Controlled Damage	0.0119	0.0119	0.0119	0.0099	0.0093	0.0099	0.0099
Collapse Prevention	0.0159	0.0159	0.0159	0.0132	0.0124	0.0132	0.0132
Ultimate Strain	0.0237	0.0237	0.0237	0.0197	0.0185	0.0197	0.0197

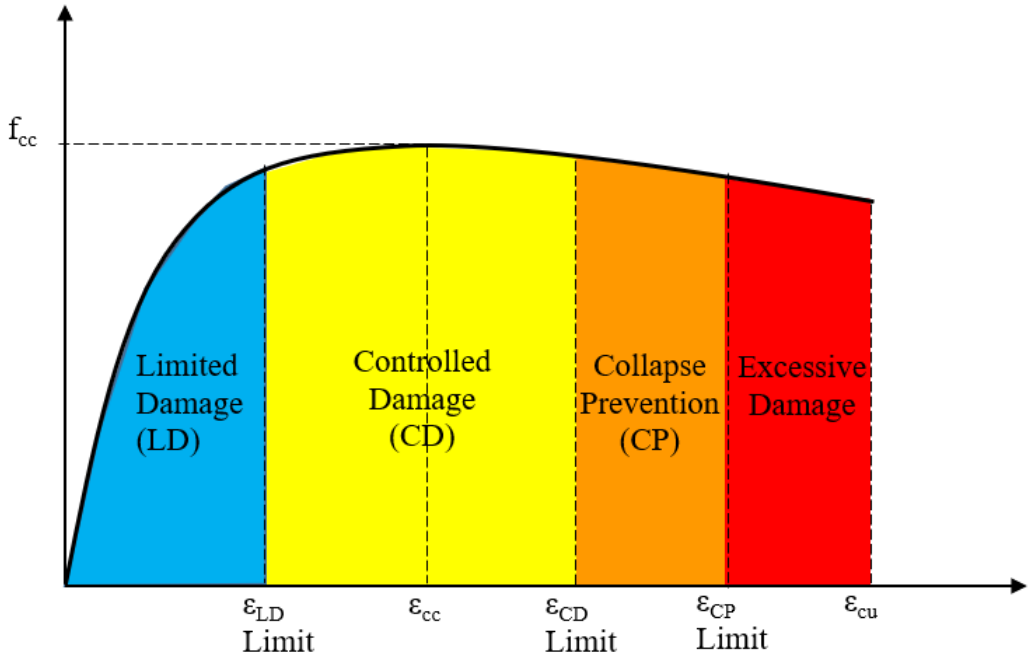

(a)

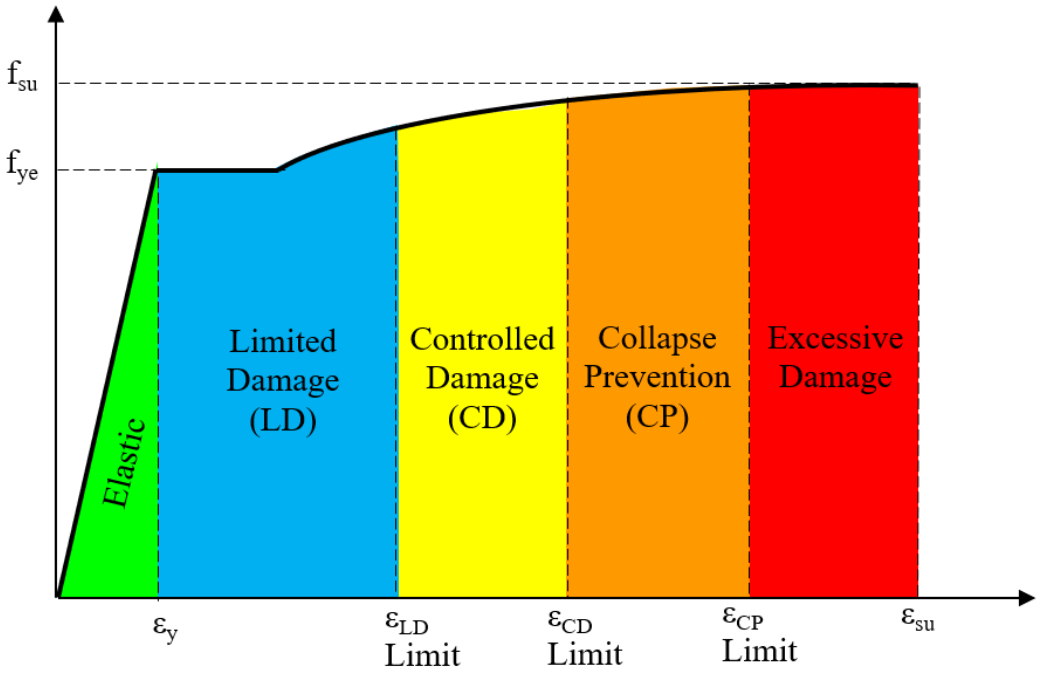

(b)

Figure 7.11 Relation between strain limits and performance levels: (a) confined concrete; (b) reinforcement

7.5 Analysis Results

According to the ASCE41-17, 22 time history analyses (11 records × 2 directions = 22 analyses) were conducted considering the scaled ground motion records for each bridge. It should be mentioned here that no vehicle loading on bridges were considered in time history analyses. For each of the 22 time history analyses, confined concrete and reinforcement strain histories on column fiber sections were determined. The maximum strain value from each analysis was then used to determine the average strain at each fiber of all the column cross sections. Performance evaluation was done based on these average confined concrete and reinforcement strain values. The average strain values determined this way are tabulated in Appendix E. Relative orientation of columns with respect to the longitudinal and transverse direction of bridge models is indicated in Figure 7.12.

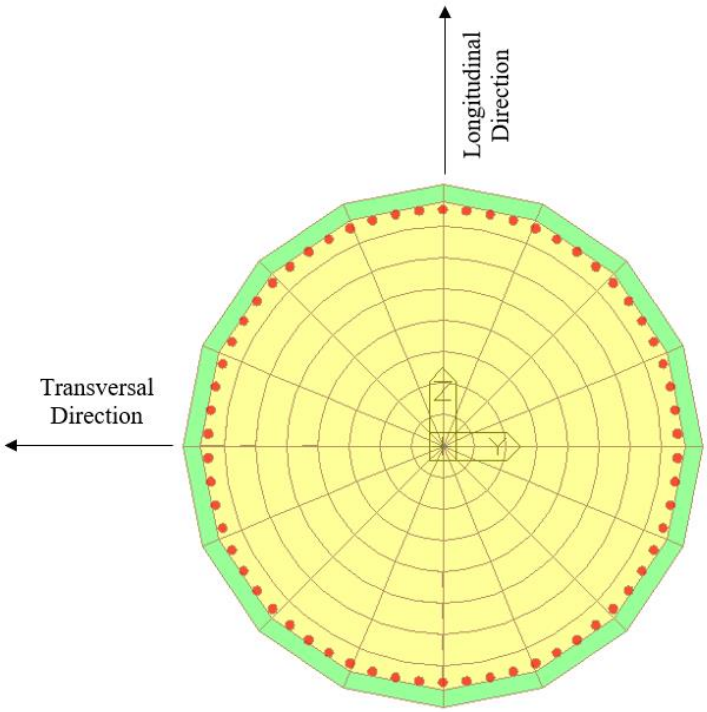

Figure 7.12 Longitudinal and transversal directions of bridge on the fiber column section

Performance assessment of pier and abutment columns for O07 Bridge based on the nonlinear time history analysis results is presented in Figure 7.13 to Figure 7.21. Values of the confined concrete and reinforcement strains at the top and bottom cross sections in each of the three columns at pier and two abutment locations are presented separately. Colors are used in Figure 7.13 to Figure 7.21 to indicate the interval in which column strains remain in relation to the stress-strain plots given in Figure 7.11. Column cross-sectional strain values for the top and bottom locations in both of the investigated bridges are provided in Appendix E.

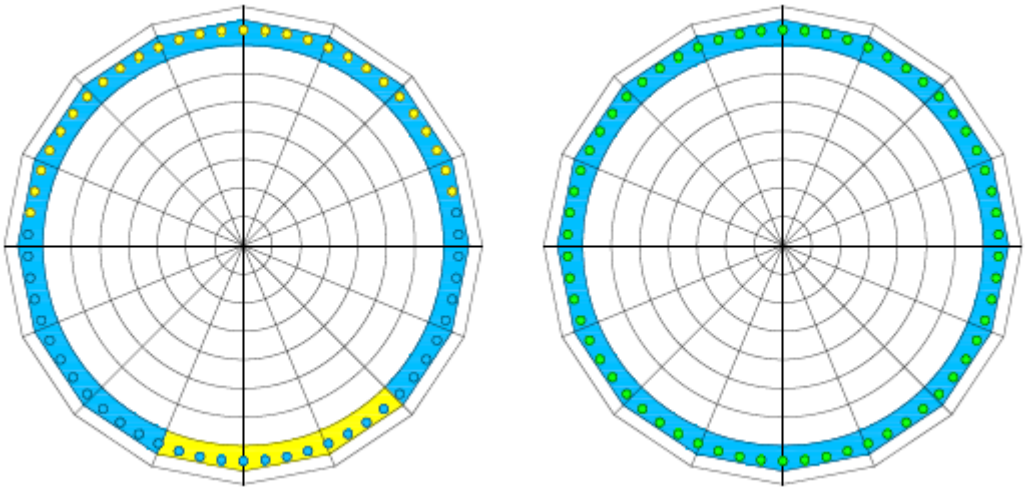

Figure 7.13 O07 Bridge A1 Axis right column bottom and top section performance evaluation

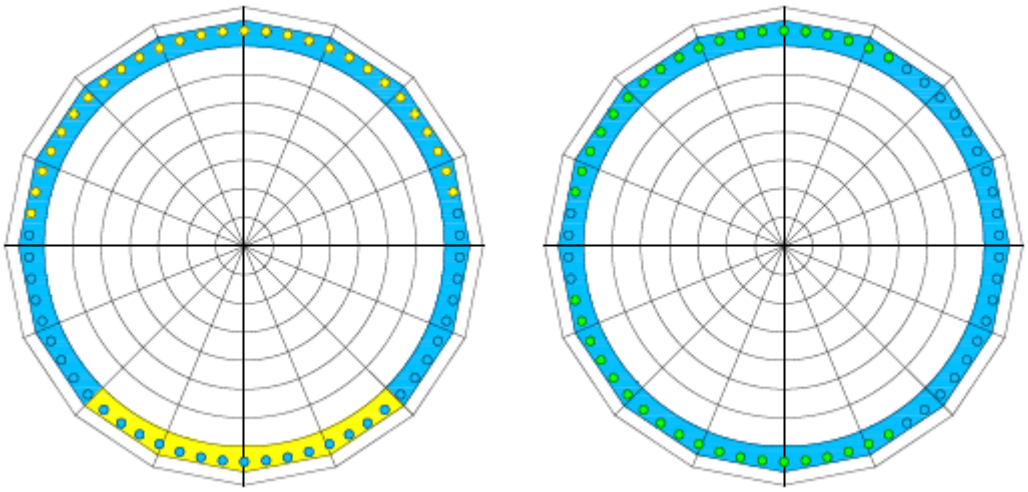

Figure 7.14 O07 Bridge A1 Axis middle column bottom and top section performance evaluation

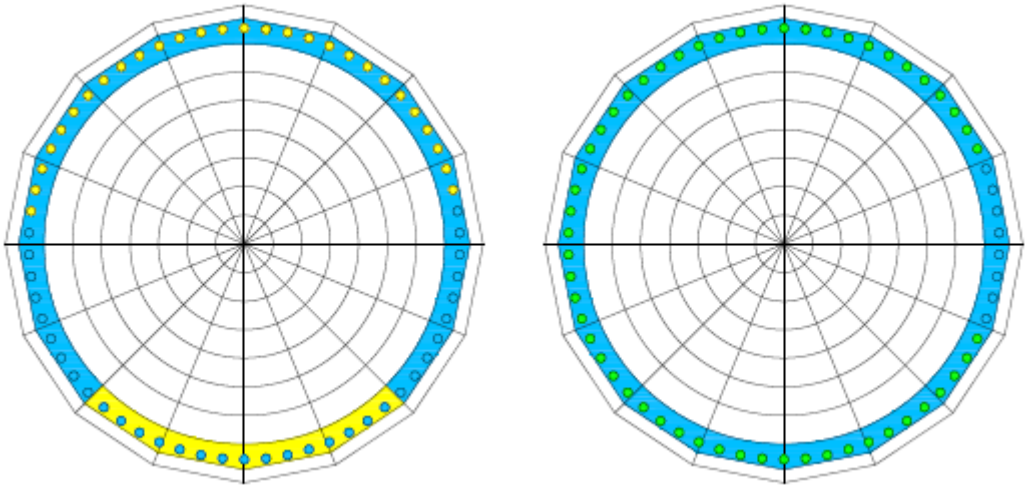

Figure 7.15 O07 Bridge A1 Axis left column bottom and top section performance evaluation

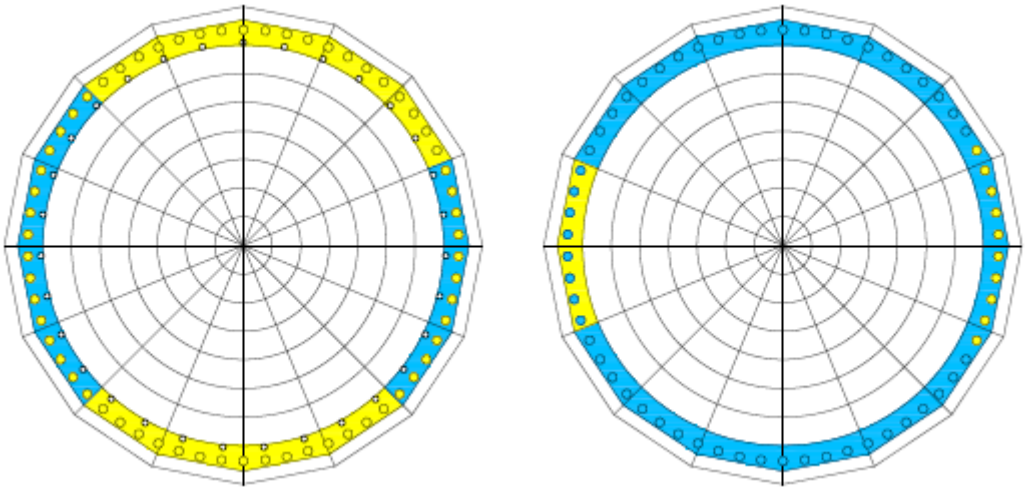

Figure 7.16 O07 Bridge P Axis right column bottom and top section performance evaluation

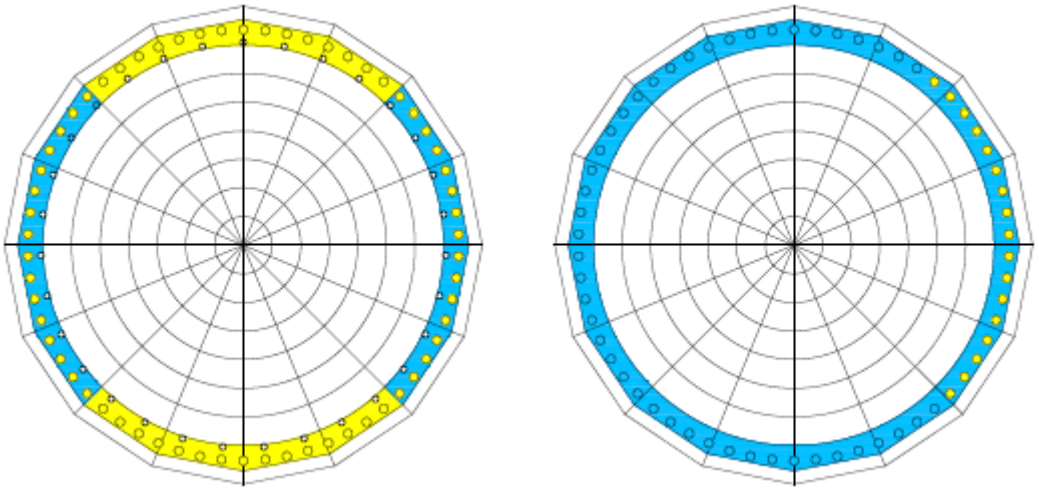

Figure 7.17 O07 Bridge P Axis middle column bottom and top section performance evaluation

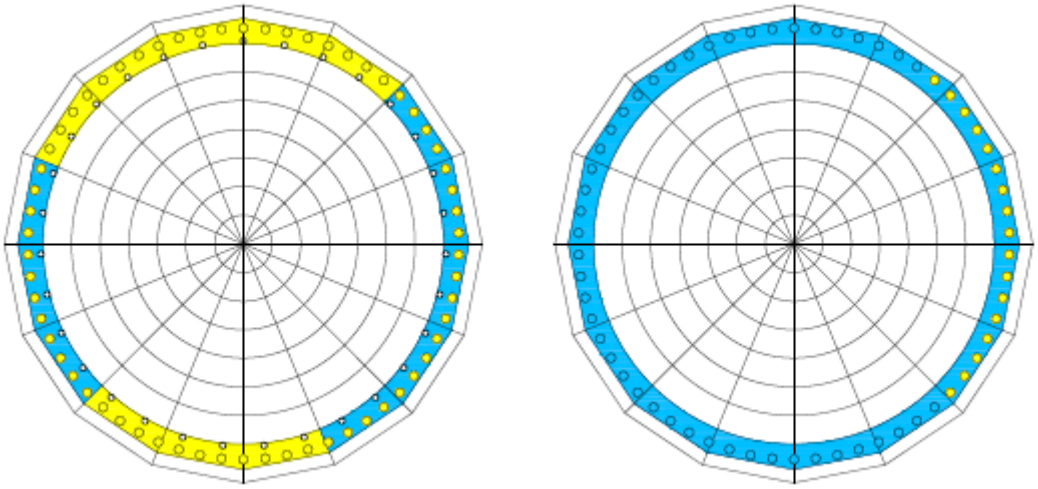

Figure 7.18 O07 Bridge P Axis left column bottom and top section performance evaluation

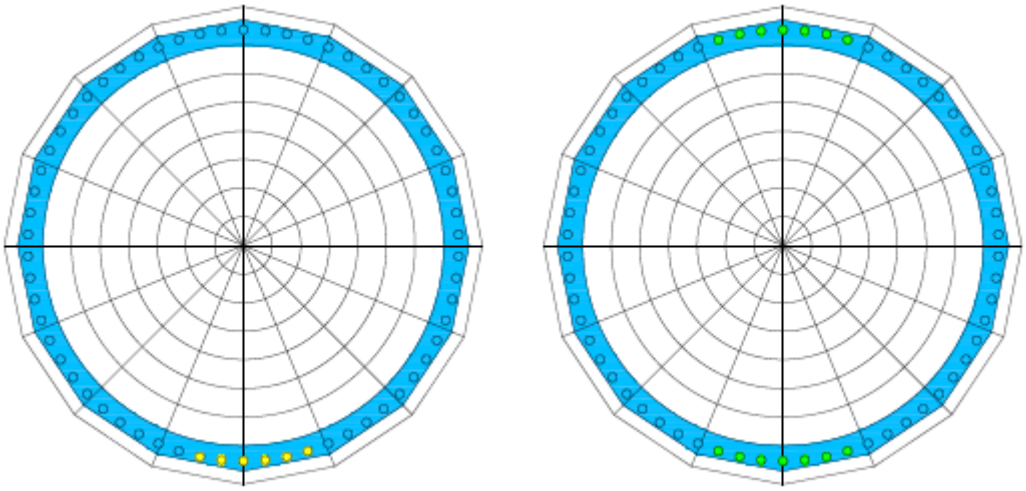

Figure 7.19 O07 Bridge A2 Axis right column bottom and top section performance evaluation

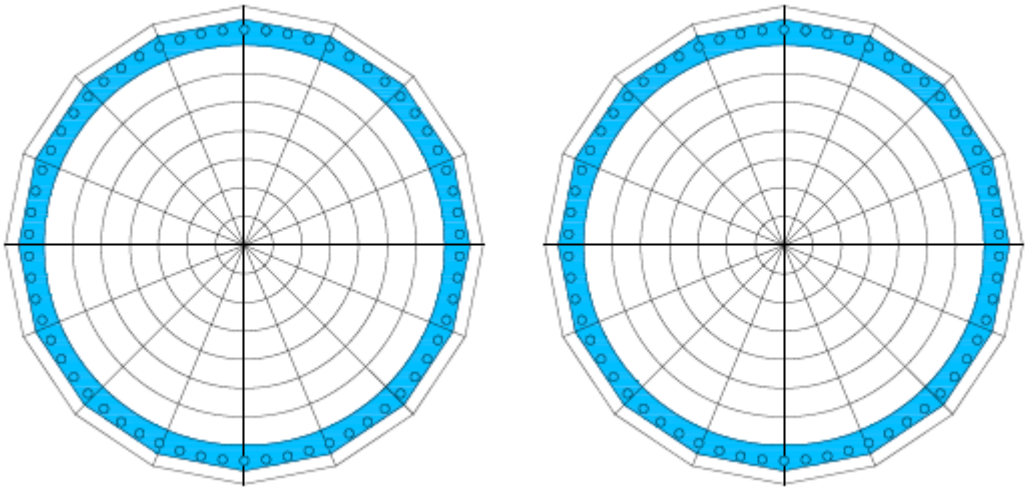

Figure 7.20 O07 Bridge A2 Axis middle column bottom and top section performance evaluation

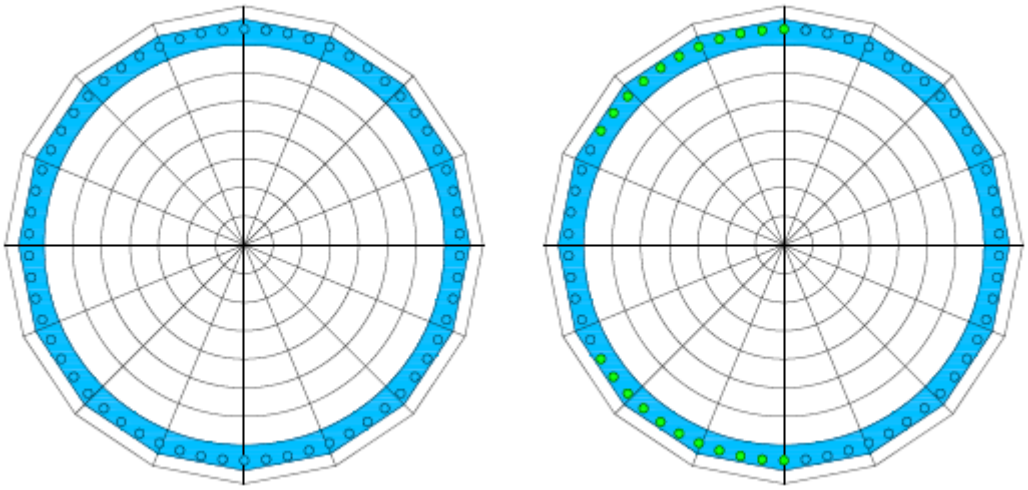

Figure 7.21 O07 Bridge A2 Axis left column bottom and top section performance evaluation

The analysis results presented in Figure 7.13 to Figure 7.21 clearly indicate that for all abutment and pier locations, bottom cross sections of columns are more critical than the top cross sections. It is also evident that in terms of the cross-sectional strains at column bottom location, longitudinal direction is more critical than transversal direction of the bridge. Smaller cross-sectional strains developed in the columns located at abutment A2 as a result of the height of these columns being taller than those of other columns. A nonsymmetrical cross-sectional strain distribution

occurred in the A1 abutment columns. The reason for such a distribution is because the contact condition between girder ends and cap beams occurring only in one direction of ground motion in the longitudinal direction of the bridge. For the pier columns, on the other hand, this contact condition occurred in both loading directions, producing a more symmetrical cross-sectional strain distribution. Considering results from all columns, both concrete and reinforcement strains satisfy the controlled damage performance level.

Performance assessment results for the columns in O13 Bridge are presented in Figure 7.22 to Figure 7.30. Different than the O07 Bridge, all columns in the O13 Bridge have the same column height. This shows itself in the form of similar column cross-sectional strain levels at both abutments. Longitudinal direction is also more critical for this bridge than the transverse direction due to the frame action occurring in the transverse direction. Another common response between this bridge and the O07 Bridge is that the cross sections at the bottom of all columns are more critical than those at the top. Considering results from all columns, both concrete and reinforcement strains satisfy the controlled damage performance level in the O13 Bridge.

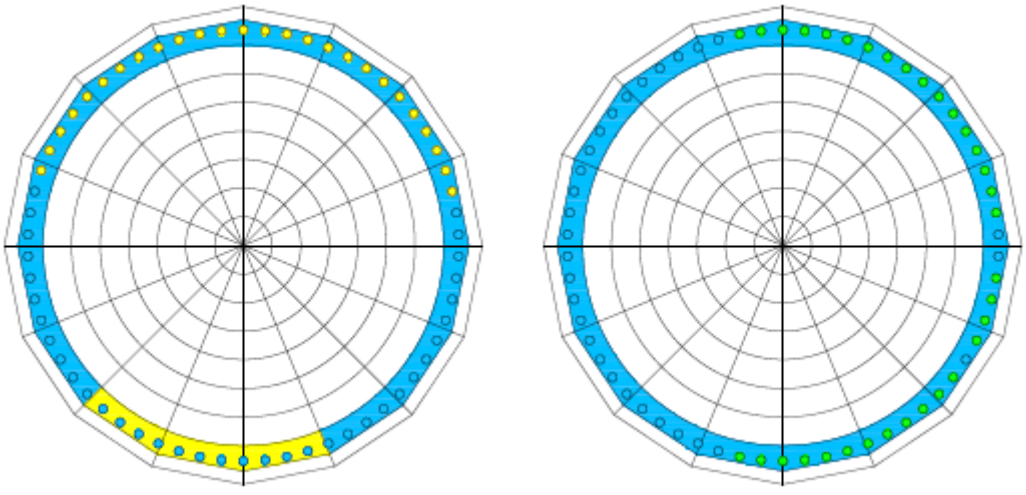

Figure 7.22 O13 Bridge A1 Axis right column bottom and top section performance evaluation

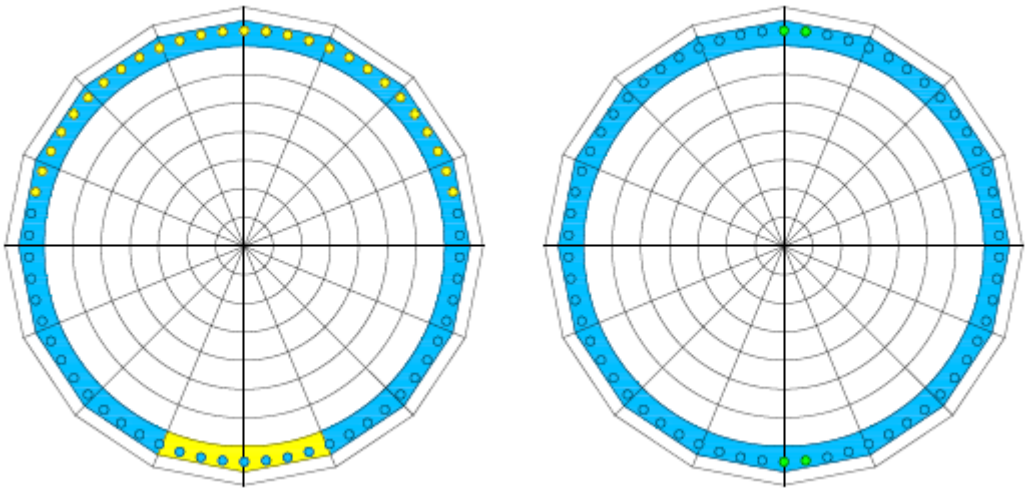

Figure 7.23 O13 Bridge A1 Axis middle column bottom and top section performance evaluation

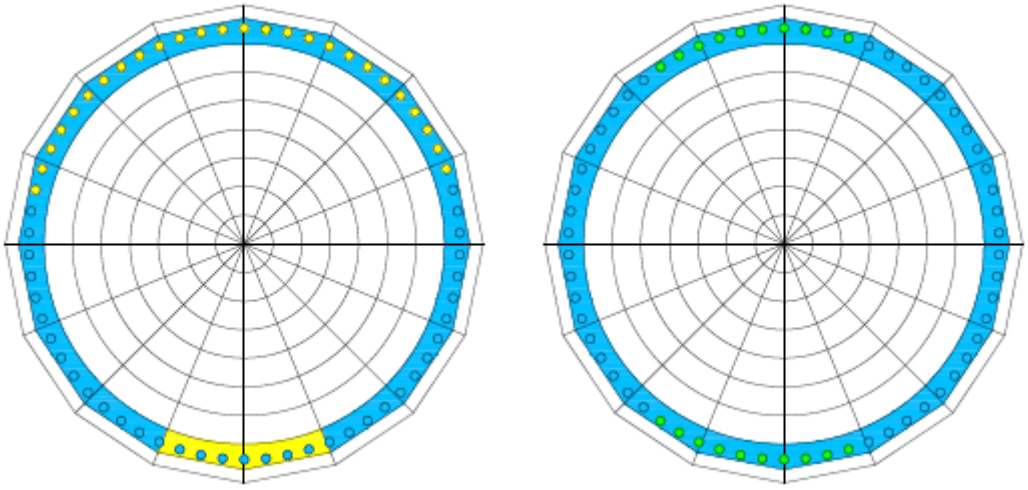

Figure 7.24 O13 Bridge A1 Axis left column bottom and top section performance evaluation

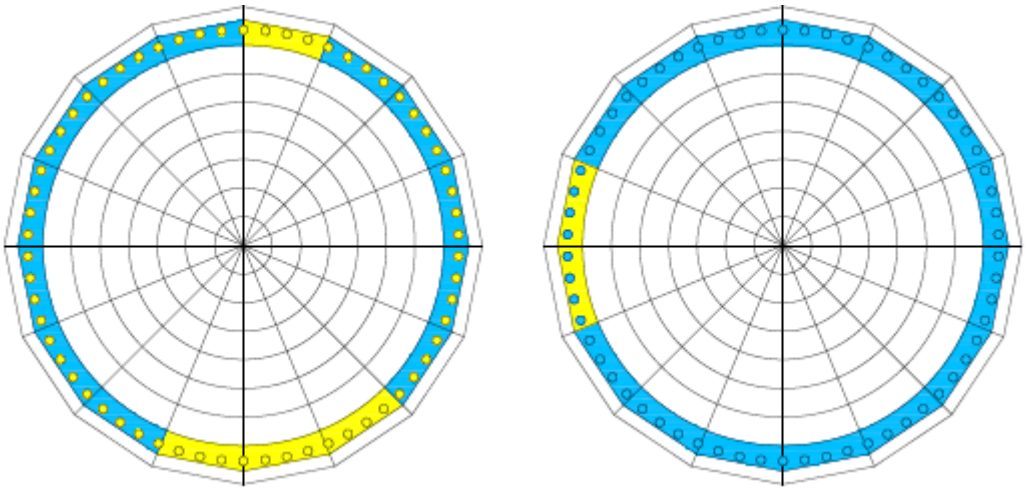

Figure 7.25 O13 Bridge P Axis right column bottom and top section performance evaluation

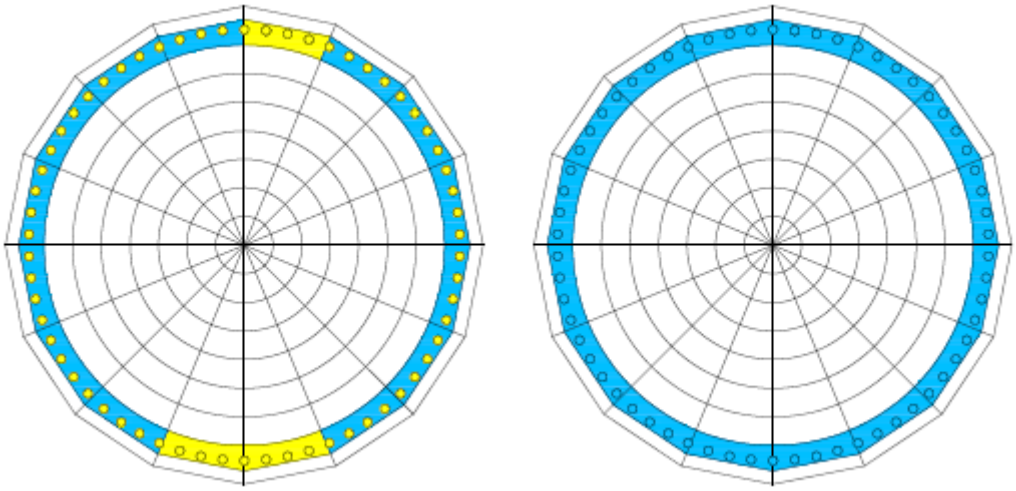

Figure 7.26 O13 Bridge P Axis middle column bottom and top section performance evaluation

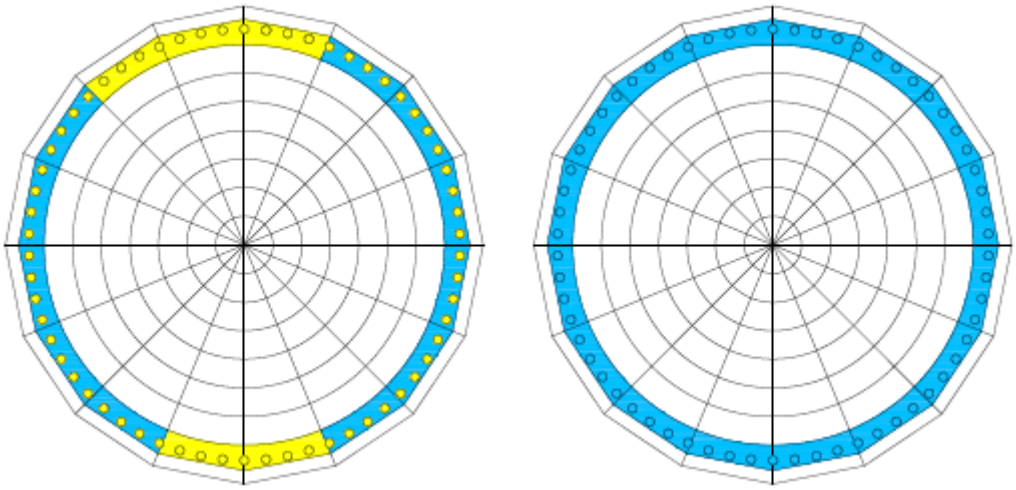

Figure 7.27 O13 Bridge P Axis left column bottom and top section performance evaluation

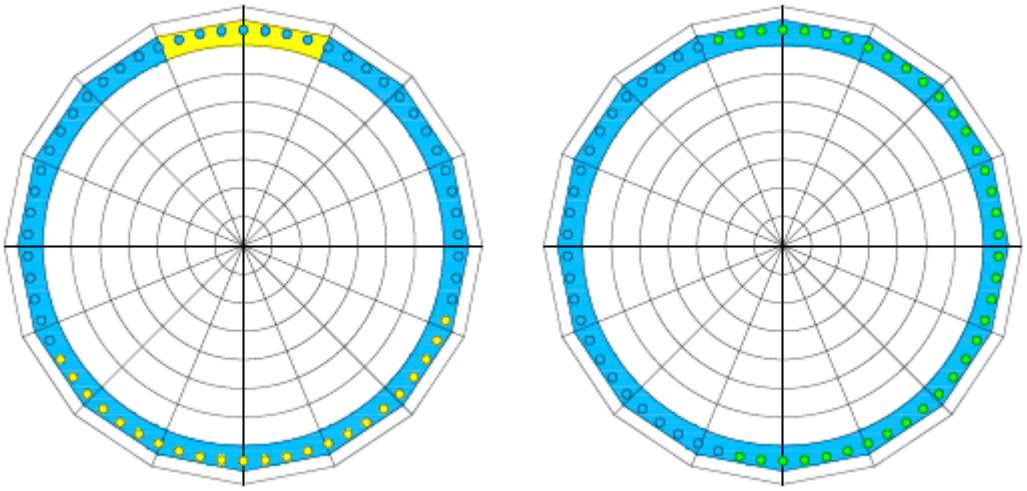

Figure 7.28 O13 Bridge A2 Axis right column bottom and top section performance evaluation

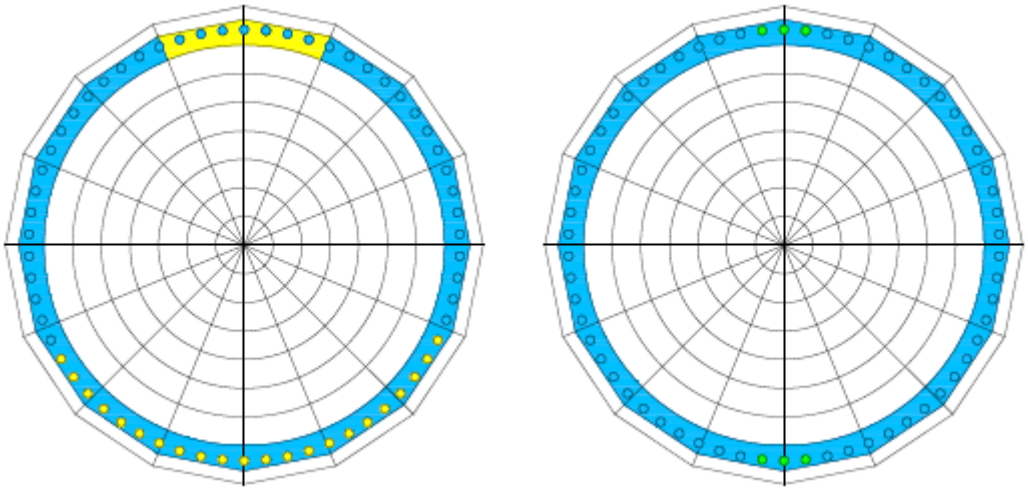

Figure 7.29 O13 Bridge A2 Axis middle column bottom and top section performance evaluation

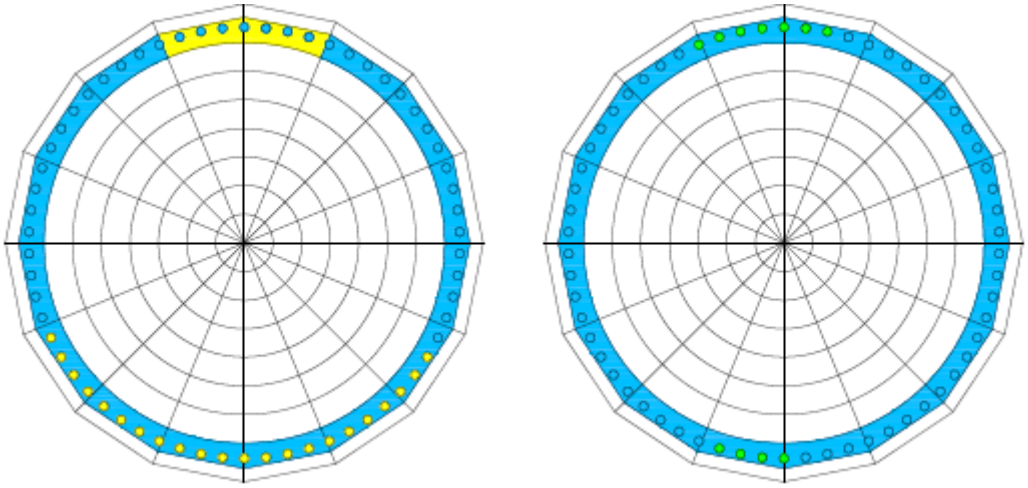

Figure 7.30 O13 Bridge A2 Axis left column bottom and top section performance evaluation

To compare column forces obtained from LRFD iteration, pushover analysis, and nonlinear time history analysis, only one column in each bridge was considered as an example. Axial force and moment values occurring at the bottom cross section of one of the pier columns are given in Table 7.8 and Table 7.9, respectively for O07 and O13 Bridge. To determine these values, the largest axial force and bending moment values were determined from each of the 22-time history analyses. The values given in Table 7.8 and Table 7.9 are the arithmetic mean of these 22 maximum

axial forces and bending moment values. As an example, the axial force and bending moment time histories obtained from the RSN-448 ground motion record are presented in Figure 7.31 and Figure 7.32.

Table 7.8 Axial force and moments values at the bottom of P axis right column in O07 Bridge

Axial Force, P (kN)		**Longitudinal Moment, M_y (kN·m)**		**Transversal Moment, M_z (kN·m)**	
Compression	**Tension**	**Negative Direction**	**Positive Direction**	**Negative Direction**	**Positive Direction**
10456	-3938	-22496	21637	-14688	19020

Table 7.9 Axial force and moments values at the bottom of P axis right column in O13 Bridge

Axial Force, P (kN)		**Longitudinal Moment, M_y (kN·m)**		**Transversal Moment, M_z (kN·m)**	
Compression	**Tension**	**Negative Direction**	**Positive Direction**	**Negative Direction**	**Positive Direction**
10812	-4003	-18787	17144	-11808	16568

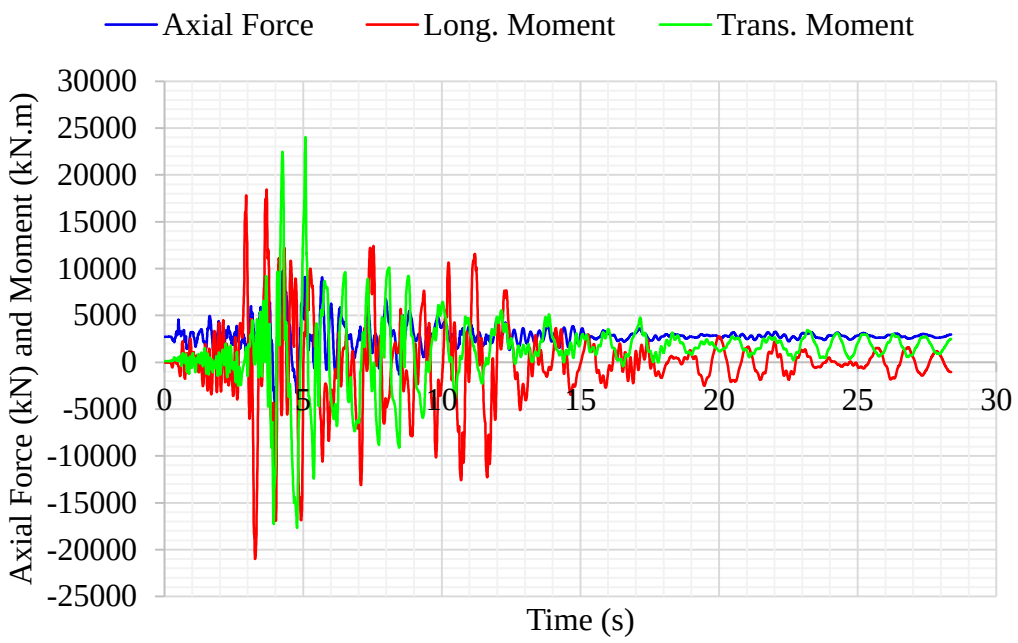

Figure 7.31 RSN-448 record axial force and moments for right column of P axis for O07 Bridge

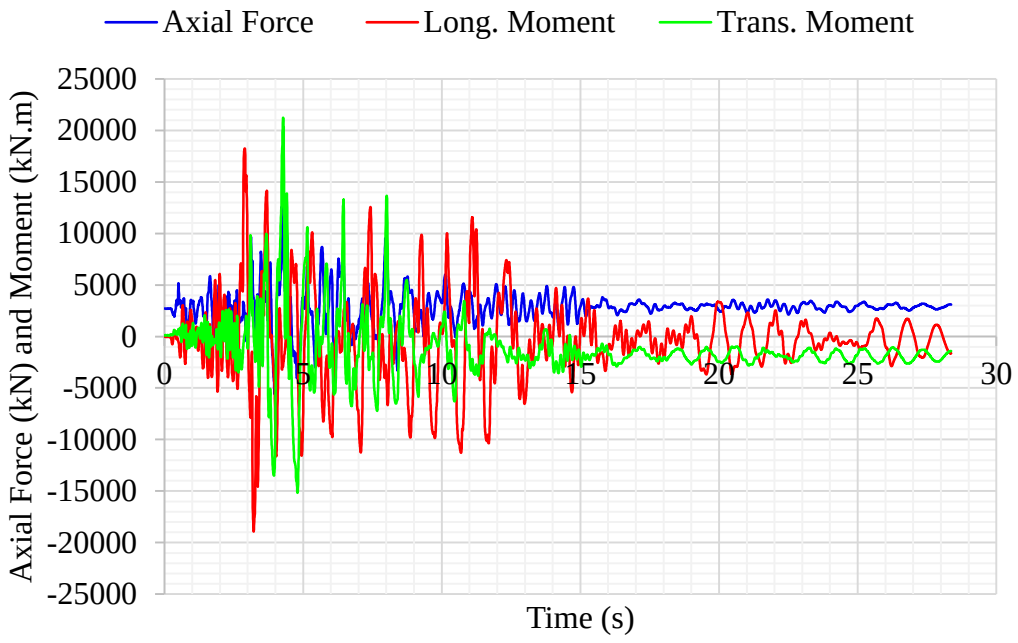

Figure 7.32 RSN-448 record axial force and moments for right column of P axis for O13 Bridge

Despite peak ground acceleration for O13 Bridge is higher than O07 Bridge, moment values of O13 are lower than O07 (Table 7.8 and Table 7.9). The main reason for this situation is that column heights of O07 Bridge are different at the abutment and pier locations. The column heights for A1, P, A2 locations are 5.70 m, 7.10 m, and 8.00 m, respectively. Because A2 axis columns are the most flexible columns in O07 Bridge, they have smaller bending moments compared to the other columns. This condition can be also seen in the fiber performance level results of A2 axis columns presented in Figure 7.19 to Figure 7.21. As a result of the A2 axis columns being so slender, the seismic load shares taken by the pier and A1 abutment columns increase. On the other hand, O13 Bridge has equal column height in each axis, so seismic forces were shared equally by the pier and abutments. As a result, the pier columns in O07 Bridge develops larger bending moments than the same column in O13 Bridge.

7.6 Comparison of Base Shear Values of O07 Bridge for Pushover Analysis and NTHA

Base shear values for O07 Bridge obtained from nonlinear time history and pushover analysis are shown in Figure 7.33. In transverse direction, only one pushover analysis because of the symmetric bridge layout in that direction. Therefore, base shear values in transverse direction are shown to be the same in positive and negative directions for pushover analysis. However, the same situation is not valid for nonlinear time history analysis, because acceleration values of ground motion records are not symmetric for positive and negative directions. In longitudinal directions, as mentioned in pushover analysis chapter, two pushover analyses must be done when columns heights are not same at all girder and pier locations. As a result, the time history analysis in positive and negative transverse directions yields unequal base shear values. The base shear value for the loading in A2-P-A1 direction, which is the case where the loading is towards to short column, is higher than the loading in A1-P-A2 direction. The main reason being the shorter columns having higher flexural

stiffness than the longer ones. As evident in Figure 7.33, pushover analysis produced higher base shear values than nonlinear time history analysis for all loading directions considered. A distributed plastic hinge model with fiber section used in nonlinear time history analyses provided more accurate force distribution on column sections than the lumped plastic hinge model used in pushover analyses. Such an accurate representation of column forces resulted in smaller base shear values when compared to pushover analyses.

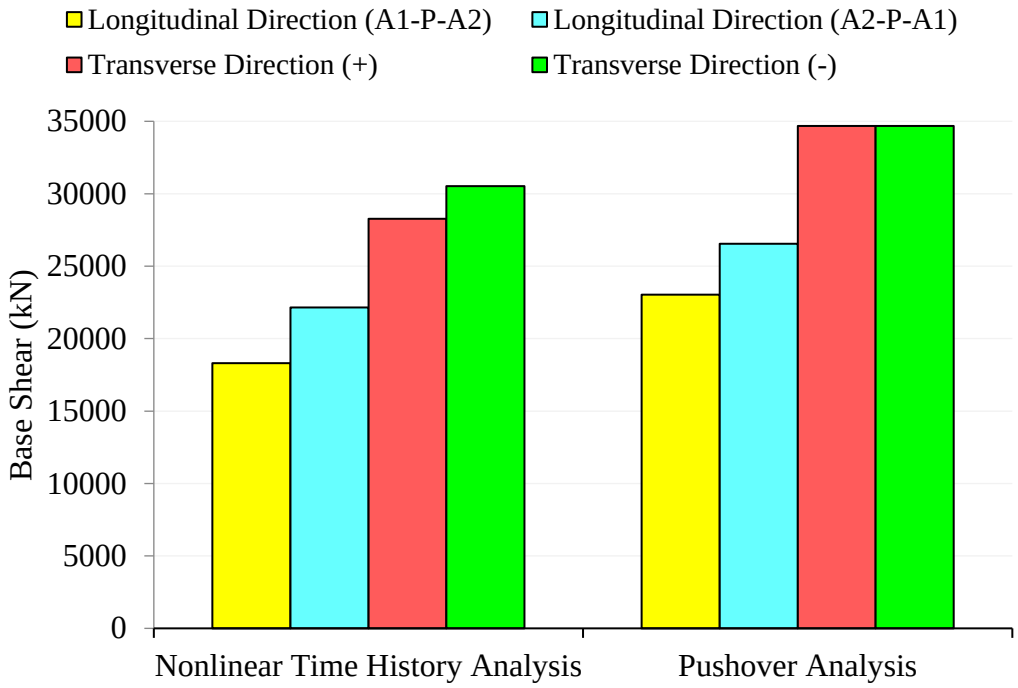

Figure 7.33 Base shear values of O07 Bridge from pushover analysis and NTHA

7.7 Comparison of Plastic Forces

Plastic axial force of nonlinear time history analysis, pushover analysis and AASHTO iteration are given in Figure 7.34 for O13 overpass bridge right column. As can be seen, axial force results are not important in longitudinal direction since only dead loads are considered in this direction. While compression and tension axial forces are similar for nonlinear time history analysis and transversal pushover analysis, these are highest value in AASHTO iteration for transverse direction.

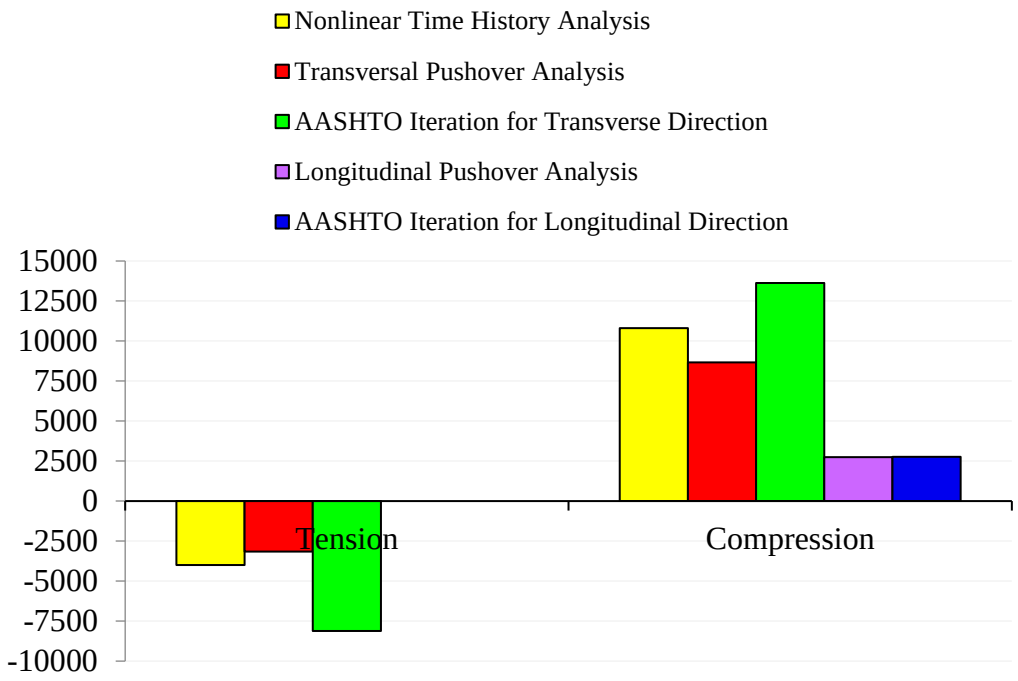

Figure 7.34 Plastic axial forces of O13 bridge right column

Plastic moments of nonlinear time history analysis, pushover analysis and AASHTO iteration are given in Figure 7.35 for O13 overpass bridge right column. There is no significant difference in the longitudinal moments because yielding occurred in the longitudinal direction. However, moment in transversal direction found from AASHTO iteration is 1.50 times higher than nonlinear time history and pushover analysis.

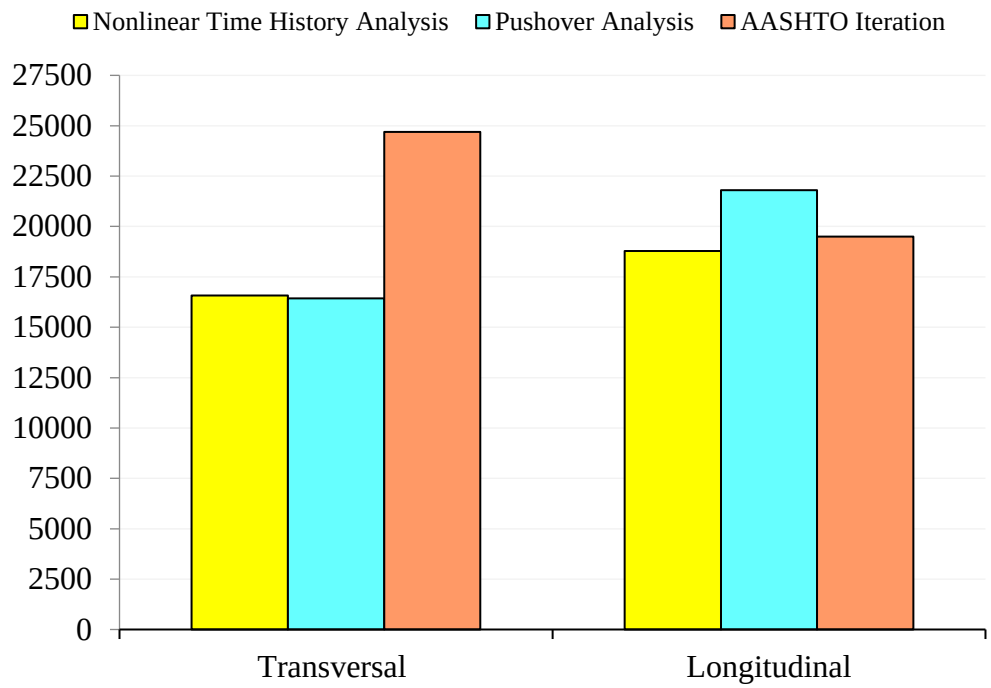

Figure 7.35 Plastic moments of O13 bridge right column

The main reason of moment and axial force difference in transversal direction is that there is no yielding on the columns in the transversal direction, so axial forces and moments were not distributed among them. Therefore, if overpass bridge has rigid frame system unrealistic forces in transversal direction may be obtained from AASHTO iteration procedure and it cause to over design foundation.

CHAPTER 8

CONCLUSIONS

In this study, seismic behavior of reinforced concrete overpass bridges located on the currently under construction Kınalı-Tekirdağ-Çanakkale-Savaştepe Highway were investigated by using nonlinear analysis methods. The bridges are located close to the North Anatolian Fault line, and their structural design is based on response spectrum analysis utilizing site specific design spectrums. Bridge numerical models were created for pushover and time history analyses by considering nonlinear effects. While lumped plastic hinge model was used for pushover analysis, distributed plastic hinge model with fiber section was used for nonlinear time history analysis.

Lumped plastic hinge model properties were determined from a moment-curvature analysis of the column cross section. Bridge columns behave as cantilever members in the longitudinal direction of the bridge. In this case, plastic hinging occurs only at the bottom of the columns. The yield moment, yield curvature, and ultimate curvature values were determined by considering the column axial load at plastic hinge location due to bridge self-weight and additional dead loads. In the transverse direction of the bridge, columns and cap beams form a frame at pier and abutment locations. In this case, plastic hinging is expected to occur at column top and bottom ends. In this case, columns in these support frames develop different levels of axial forces as a result of the earthquake action. Such an unequal axial force distribution was considered while determining the lumped plastic hinge properties for the analysis in the transverse direction.

For distributed plastic hinge modeling, column cross sections were discretized into small size fibers at the locations of potential nonlinear behavior. Each of these fibers considers only axial deformations and was assigned either confined concrete

material properties, unconfined concrete material properties, or reinforcing steel material properties

The following conclusions can be made on the basis of the analysis results:

- Vibration mode shapes and periods for the investigated bridges are similar to each other as a result of the similar superstructure layout, elastomeric bearings dimensions, and span length.
- The gaps present at girder supports between the superstructure and cap beams in longitudinal direction, as well as those between the girders and shear keys in transversal direction have a significant effect on seismic response of the bridge. A sudden increase in girder support stiffness occurs when these gaps close and the girder end comes into contact with the vertical wall of cap beams or shear keys under the design level earthquake. This type of response significantly affects the level of load transfer from superstructure to columns. Therefore, accurate modeling of bridge response requires realistic representation of these gaps in analysis models.
- Under longitudinal pushover loading each column deforms as an individual cantilever member in single curvature mode. In the case of transverse pushover loading, on the other hand, three support columns at each of the abutment and pier locations form a frame and deform in double curvature mode as a part of this frame. The ultimate and first yield displacements obtained from the pushover capacity curve indicate ductility ratios that are significantly smaller in the transverse direction than those in the longitudinal direction.
- No yielding of columns is observed at the performance point in transverse direction pushover analyses. On the contrary, plastic hinging to some extent occurs in the longitudinal direction pushover analyses. Therefore, the longitudinal bridge direction is more critical than the transverse direction. This condition arises from the fact that only one of the abutments gets

engaged in resisting the lateral loads in the longitudinal direction due to no contact between the girder ends and cap beams at the other abutment location.

- For bridges with unequal column height at abutments and pier, it is observed that the bridges usually satisfy the target performance level of collapse prevention when pushed towards the abutment with longer columns, while the target performance level is not satisfied when pushed towards the abutment with shorter columns. The difference in the response in two loading directions arises from the fact that with the shorter columns in the leading abutment the column plastic rotations become excessive and go beyond the limit values.
- Cross-sectional strain distributions obtained from nonlinear time history analyses indicate higher concrete and steel strains at bottom cross section of columns than the top cross sections. Similarly, larger cross-sectional strains are observed in the longitudinal bridge direction than the transverse direction. For bridges with unequal column height at abutments and pier, smaller cross-sectional strains develop in the taller columns compared to the shorter columns.
- Comparison of the bridge performance from pushover analysis and nonlinear time history analysis indicates that some bridge columns go beyond the required performance level in the longitudinal pushover analysis, however the performance limits are satisfied based on the nonlinear time history analysis results of the same bridges. The main reason for this behavior is that while nonlinear time history analysis provides results in terms of strain values for each fiber of column sections, pushover analysis provides the results as plastic rotations. Strain values provide more detailed results as the column section is discretized into small fibers and the distribution of strains/stresses within the cross section is obtained. On the other hand, plastic rotation values obtained at the end of pushover analysis represent the frame element results only at center of lumped plastic hinge length. Furthermore, after the occurrence of pounding at girder supports, vibration period of the bridge

system changes because of the increasing stiffness. While pushover analysis considers only dominant mode period of regarding direction, the effect of period change is reflected in nonlinear time history analysis results. For these reasons, the nonlinear time history analysis results are considered to be more reliable than the corresponding pushover analysis results.

- When the column plastic axial loads and bending moments determined following the iterative procedure as specified by AASHTO are compared with the results from the pushover and time history analyses, no significant difference is observed in the longitudinal bridge direction. However, a marked difference between the results is valid in the transverse direction, because pushover and time history analyses indicate no yielding in that direction. Therefore, the plastic forces determined from the AASHTO procedure are higher than those obtained from pushover and time history analyses.

Considering the results of the study for seismic performance assessment of reinforced concrete overpass bridges, the following recommendations can be made for future research:

- In this study, boundary conditions of all columns were modeled as fixed support. More detail analysis can be done considering soil structure interaction, especially for the cases where pile foundations are used.
- All of the investigated bridges had no skew angle and were located on a straight alignment. Effects of skew angle and curved alignment on the seismic performance of overpass bridges should be investigated.
- Number of spans should be investigated as a parameter to understand the seismic behavior of bridges with varying number of spans.
- Column cross sections other than circular section should be investigated to study the influence of this parameter on the seismic response of the overall bridge system. This way, the optimum cross-sectional geometries can be determined to provide target seismic performance level.

REFERENCES

AASHTO, 2011. AASHTO LRFD Seismic Bridge Design, 2nd edition. *American Association of State Highway and Transportation Officials*, Washington, D.C.

AASHTO, 2017. AASHTO LRFD Bridge Design Specifications, 8th edition. *American Association of State Highway and Transportation Officials*, Washington, D.C.

American Society of Civil Engineers, 2005. ASCE/SEI 7-5: Minimum Design Loads for Buildings and Other Structures.

American Society of Civil Engineers, 2010. ASCE/SEI 7-10: Minimum Design Loads for Buildings and Other Structures.

American Society of Civil Engineers, 2016. ASCE/SEI 7-16: Minimum Design Loads for Buildings and Other Structures.

American Society of Civil Engineers, 2017. ASCE/SEI 41-17: Seismic Evaluation and Retrofit of Existing Buildings.

ATC, 1996. ATC 32, Improved Seismic Design Criteria for Californian Bridges: Provisional Recommendations. *Applied Technology Council*, Redwood City, CA.

ATC, 1996. ATC 40, Seismic Evaluation and Retrofit of Concrete Buildings Volume 1. *Applied Technology Council*, Redwood City, CA.

Aviram, A., Mackie, K. R. & Stojadinovic, B. 2008. Guidelines for Nonlinear Analysis of Bridge Structures in California. Pacific Earthquake Engineering Research Center, University of California, Berkeley.

Bozorgzadeh, A., Megalley, S. H., Ashford, S. & Restrepo, J. I., 2007. Seismic Response of Sacrificial Exterior Keys in Bridge Abutments. Department of Structural Engineering, University of California, San Diego.

CALTRANS, 1999. Bridge Memo to Designers 20-1: Seismic Design Methodology, California Department of Transportation.

CALTRANS, 2006. Seismic Design Criteria Version 1.4, California Department of Transportation.

Canadian Standard Association - CSA 2019. CAN/CSA-S6-19: Canadian Highway Bridge Design Code.

Chopra, A. K. (1995). Dynamics of Structures: Theory and Applications to Earthquake Engineering. *Earthquake Engineering and Structural Dynamics*, 24(1173).

EN 1998-1, 2004. Eurocode 8: Design of structures for earthquake resistance – Part 1: General rules, seismic actions and rules for buildings. Authority: The European Union Per Regulation 305/2011, Directive 98/34/EC, Directive 2004/18/EC.

EN 1998-3, 2005. Eurocode 8: Design of structures for earthquake resistance – Part 3: Assessment and retrofitting of buildings. The European Union Per Regulation 305/2011, Directive 98/34/EC, Directive 2004/18/EC.

Federal Emergency Management Agency (FEMA), 2003. Multi-hazard Loss Estimation Methodology Earthquake Model, AZUS-MH MR1, Advanced Engineering Building Module, Technical and User's Manual, Washington, D.C.

Federal Highway Administration (FHWA) 2006. Seismic Retrofitting Manual for Highway Structures: Part 1 – Bridges. Research, Development, and Technology Turner-Fairbank Highway Research Center, McLean, VA.

Hajihashemi, A., Pezeshk, S., & Huff, T. 2017. Comparison of Nonlinear Static Procedures and Modeling Assumptions for the Seismic Design of Ordinary Bridges. *Practice Periodical on Structural Design and Construction*, 22(2), 04016022. doi:10.1061/(asce)sc.1943-5576.0000309.

Heo, Y., Kunnath, S.K., & Abrahamson, N. (2011). Amplitude-scaled versus spectrum-matched seismic ground motions for seismic performance assessment. *ASCE Journal of Structural Engineering*, 137(3), 278-288. doi:10.1061/ (ASCE)ST.1943-541X.0000340.

Hose, Y., Silva, P., & Seible, F. 2000. Development of a Performance Evaluation Database for Concrete Bridge Components and Systems under Simulated Seismic Loads. *Earthquake Spectra*, 16(2), 413-442. doi:10.1193/1.1586119.

Hwang H., Liu J.B. & Chiu Y.H., 2001. Seismic Fragility Analysis of Highway Bridges. Center for Earthquake Research and Information the University of Memphis, MAEC RR-4 Project, p. 117.

Japan Road Association, 2002. Specifications for Highway Bridges, Part V Seismic Design.

Kappos, A. J., Saiidi, M. S., Aydınoğlu, M. N., & Isaković, T. (Eds.). 2012. Seismic Design and Assessment of Bridges. *Geotechnical, Geological and Earthquake Engineering*. doi:10.1007/978-94-007-3943-7.

Kowalsky, M. J. 2000. Deformation Limit States for Circular Reinforced Concrete Bridge Columns. *Journal of Structural Engineering*, 126(8), 869-878. doi:10.1061/(asce)0733-9445(2000)126:8(869).

Mander, J. B., Priestley, M. J. N., & Park, R. 1988. Theoretical Stress-Strain Model for Confined Concrete. *Journal of Structural Engineering*, 114(8), 1804-1826. doi:10.1061/(asce)0733-9445(1988)114:8(1804).

Megalley, S. H., Silva, P. F. & Seible, F., 2002. Seismic Response of Sacrificial Exterior Keys in Bridge Abutments. Department of Structural Engineering, University of California, San Diego.

Muthukumar, S. & DesRoches, R., 2006. A Hertz contact model with non-linear damping for pounding simulation. *Earthquake Engineering & Structural Dynamics*, 35(7), 811–828. doi:10.1002/eqe.557.

NEHRP (2009), Recommended Seismic Provisions for New Buildings and Other Structures FEMA P-750 / 2009 Edition.

Pasific Earthquake Engineering Research Center, PEER Ground Motion Database. https://ngawest2.berkeley.edu/, [last visited on January 2022].

Shaban, N., Caner, A., Yakut, A., Askan, A., Naghshineh, A.K., Domanic, A. & Can, G. (2014). Vehicle effects on seismic response of a simple-span bridge during shake tests. *Earthquake Engineering & Structural Dynamics*, 44, 889-905. doi:10.1002/eqe.2491

Spacone, E., Filippou, F. C., & Taucer, F. F. (1996). Fibre Beam-Column Model for Non-Linear Analysis Of R/C Frames: Part I. Formulation. *Earthquake Engineering & Structural Dynamics*, 25(7), 711–725. doi:10.1002/(sici)1096-9845(199607)25:7<711::aid-eqe576>3.0.co;2-9.

Ulaştırma ve Altyapı Bakanlığı, (2020). Türkiye Köprü Deprem Yönetmeliği, Ek-1: Deprem Etkisi Altında Karayolu ve Demiryolu Köprü ve Viyadükleri Tasarımı için Esaslar.

Vemuri, J., & Kolluru, S. (2020). Evaluation of ground Motion Scaling Techniques. *Advances in Computer Methods and Geomechanics*, 55, 525–535. doi:10.1007/978-981-15-0886-8_43

Xiaoming, C., Jin, D., & Yungui, L. (2015). Mass proportional damping in nonlinear time-history analysis. 3rd International Conference on Material, Mechanical and Manufacturing Engineering (IC3ME 2015).

Yüksel Proje, 2018. Kınalı - Tekirdağ - Çanakkale - Savaştepe Motorway Project Malkara - Çanakkale (Including The 1915 Çanakkale Bridge) Construction, Structural Works Design Basis Report.

Yüksel Proje, 2018. Kınalı - Tekirdağ - Çanakkale - Savaştepe Motorway Project Malkara - Çanakkale (Including The 1915 Çanakkale Bridge) Construction, The Earthquake Hazard Analysis and Design-Based Earthquake Ground Motion Determination for The Viaduct Structures of The Çanakkale Motorway.

APPENDICES

A. Column Hinge Properties used in Transverse Direction Pushover Analyses

Table A.1 Bottom and top transverse hinge properties of A1 and A2 axis column of O02 Bridge

N (kN)	M_y (kN·m)	ϕ_y (1/m)	ϕ_u (1/m)	θ_y (rad)	θ_p (rad)	θ_u (rad)	$\frac{\theta_u}{\theta_y}$
147000	0	0.0000	0.0000	0.0000	0.0000	0.0000	0.00
129500	9476	0.0040	0.0144	0.0046	0.0074	0.0120	2.59
112000	19074	0.0046	0.0171	0.0054	0.0089	0.0143	2.65
94500	26423	0.0053	0.0198	0.0062	0.0103	0.0165	2.66
77000	30794	0.0055	0.0232	0.0064	0.0126	0.0190	2.98
59500	32076	0.0046	0.0278	0.0053	0.0165	0.0218	4.10
41800	30866	0.0038	0.0345	0.0045	0.0218	0.0262	5.85
24100	27316	0.0035	0.0457	0.0041	0.0300	0.0340	8.39
6400	21076	0.0034	0.0628	0.0039	0.0422	0.0461	11.76
-11300	11008	0.0039	0.0536	0.0046	0.0353	0.0398	8.70
-29000	0	0.0000	0.0000	0.0000	0.0000	0.0000	0.00

Table A.2 Bottom and top transverse hinge properties of P axis column of O02 Bridge

N (kN)	M_y (kN·m)	ϕ_y (1/m)	ϕ_u (1/m)	θ_y (rad)	θ_p (rad)	θ_u (rad)	$\frac{\theta_u}{\theta_y}$
147000	0	0.0000	0.0000	0.0000	0.0000	0.0000	0.00
129500	9505	0.0040	0.0137	0.0047	0.0069	0.0115	2.48
112000	19087	0.0046	0.0169	0.0054	0.0087	0.0141	2.63
94500	26439	0.0053	0.0195	0.0062	0.0101	0.0163	2.63
77000	30801	0.0055	0.0229	0.0064	0.0124	0.0188	2.95
59500	32083	0.0046	0.0274	0.0053	0.0162	0.0216	4.06
41800	30870	0.0038	0.0341	0.0045	0.0215	0.0259	5.78
24100	27312	0.0035	0.0451	0.0041	0.0296	0.0336	8.29
6400	21077	0.0034	0.0628	0.0039	0.0422	0.0461	11.76
-11300	11008	0.0039	0.0536	0.0046	0.0353	0.0398	8.70
-29000	0	0.0000	0.0000	0.0000	0.0000	0.0000	0.00

Table A.3 Bottom and top transverse hinge properties of A1 axis column of O05 Bridge

N (kN)	M_y (kN·m)	ϕ_y (1/m)	ϕ_u (1/m)	θ_y (rad)	θ_p (rad)	θ_u (rad)	$\frac{\theta_u}{\theta_y}$
147000	0	0.0000	0.0000	0.0000	0.0000	0.0000	0.00
129500	9476	0.0040	0.0144	0.0051	0.0074	0.0125	2.45
112000	19074	0.0046	0.0171	0.0059	0.0089	0.0148	2.50
94500	26423	0.0053	0.0198	0.0068	0.0103	0.0171	2.51
77000	30794	0.0055	0.0232	0.0070	0.0126	0.0196	2.80
59500	32076	0.0046	0.0278	0.0058	0.0165	0.0223	3.82
41800	30866	0.0038	0.0345	0.0049	0.0218	0.0267	5.41
24100	27316	0.0035	0.0457	0.0045	0.0300	0.0344	7.72
6400	21076	0.0034	0.0628	0.0043	0.0422	0.0465	10.78
-11300	11008	0.0039	0.0536	0.0050	0.0353	0.0403	8.00
-29000	0	0.0000	0.0000	0.0000	0.0000	0.0000	0.00

Table A.4 Bottom and top transverse hinge properties of P axis column of O05 Bridge

N (kN)	M_y (kN·m)	ϕ_y (1/m)	ϕ_u (1/m)	θ_y (rad)	θ_p (rad)	θ_u (rad)	$\frac{\theta_u}{\theta_y}$
147000	0	0.0000	0.0000	0.0000	0.0000	0.0000	0.00
129500	9476	0.0040	0.0144	0.0053	0.0074	0.0127	2.39
112000	19074	0.0046	0.0171	0.0061	0.0089	0.0150	2.45
94500	26423	0.0053	0.0198	0.0071	0.0103	0.0174	2.45
77000	30794	0.0055	0.0232	0.0073	0.0126	0.0199	2.73
59500	32076	0.0046	0.0278	0.0061	0.0165	0.0225	3.71
41800	30866	0.0038	0.0345	0.0051	0.0218	0.0269	5.24
24100	27316	0.0035	0.0457	0.0046	0.0300	0.0346	7.47
6400	21076	0.0034	0.0628	0.0045	0.0422	0.0467	10.42
-11300	11008	0.0039	0.0536	0.0052	0.0353	0.0405	7.74
-29000	0	0.0000	0.0000	0.0000	0.0000	0.0000	0.00

Table A.5 Bottom and top transverse hinge properties of A2 axis column of O05 Bridge

N (kN)	M_y (kN·m)	ϕ_y (1/m)	ϕ_u (1/m)	θ_y (rad)	θ_p (rad)	θ_u (rad)	$\frac{\theta_u}{\theta_y}$
147000	0	0.0000	0.0000	0.0000	0.0000	0.0000	0.00
129500	9476	0.0040	0.0144	0.0045	0.0074	0.0119	2.64
112000	19074	0.0046	0.0171	0.0052	0.0089	0.0141	2.70
94500	26423	0.0053	0.0198	0.0060	0.0103	0.0163	2.71
77000	30794	0.0055	0.0232	0.0062	0.0126	0.0188	3.03
59500	32076	0.0046	0.0278	0.0052	0.0165	0.0216	4.19
41800	30866	0.0038	0.0345	0.0044	0.0218	0.0261	5.99
24100	27316	0.0035	0.0457	0.0039	0.0300	0.0339	8.61
6400	21076	0.0034	0.0628	0.0038	0.0422	0.0460	12.08
-11300	11008	0.0039	0.0536	0.0044	0.0353	0.0397	8.93
-29000	0	0.0000	0.0000	0.0000	0.0000	0.0000	0.00

Table A.6 Bottom and top transverse hinge properties of A1 axis column of O07 Bridge

N (kN)	M_y (kN·m)	ϕ_y (1/m)	ϕ_u (1/m)	θ_y (rad)	θ_p (rad)	θ_u (rad)	$\frac{\theta_u}{\theta_y}$
143000	0	0.0000	0.0000	0.0000	0.0000	0.0000	0.00
125600	9458	0.0032	0.0115	0.0031	0.0059	0.0090	2.91
108200	18991	0.0038	0.0138	0.0036	0.0071	0.0107	2.96
90800	26406	0.0044	0.0159	0.0042	0.0081	0.0123	2.92
73400	31176	0.0052	0.0187	0.0049	0.0096	0.0145	2.93
56000	32531	0.0043	0.0224	0.0041	0.0129	0.0170	4.12
38100	31279	0.0037	0.0282	0.0035	0.0174	0.0209	5.96
20200	27577	0.0034	0.0378	0.0032	0.0244	0.0277	8.54
2300	21216	0.0034	0.0586	0.0032	0.0392	0.0424	13.11
-15600	10740	0.0033	0.0532	0.0031	0.0354	0.0385	12.34
-33500	0	0.0000	0.0000	0.0000	0.0000	0.0000	0.00

Table A.7 Bottom transverse hinge properties of P axis column of O07 Bridge

N (kN)	M_y (kN·m)	ϕ_y (1/m)	ϕ_u (1/m)	θ_y (rad)	θ_p (rad)	θ_u (rad)	$\frac{\theta_u}{\theta_y}$
143000	0	0.0000	0.0000	0.0000	0.0000	0.0000	0.00
125600	9580	0.0033	0.0108	0.0039	0.0049	0.0088	2.25
108200	19057	0.0038	0.0130	0.0045	0.0060	0.0106	2.33
90800	26459	0.0045	0.0149	0.0053	0.0069	0.0122	2.30
73400	31211	0.0052	0.0176	0.0062	0.0082	0.0143	2.32
56000	32545	0.0043	0.0212	0.0051	0.0111	0.0162	3.16
38100	31291	0.0037	0.0266	0.0044	0.0151	0.0194	4.45
20200	27549	0.0034	0.0358	0.0040	0.0213	0.0253	6.28
2300	21154	0.0034	0.0555	0.0041	0.0343	0.0383	9.44
-15600	10636	0.0034	0.0523	0.0040	0.0321	0.0362	8.97
-33500	0	0.0000	0.0000	0.0000	0.0000	0.0000	0.00

Table A.8 Top transverse hinge properties of P axis column of O07 Bridge

N (kN)	M_y (kN·m)	ϕ_y (1/m)	ϕ_u (1/m)	θ_y (rad)	θ_p (rad)	θ_u (rad)	$\frac{\theta_u}{\theta_y}$
143000	0	0.0000	0.0000	0.0000	0.0000	0.0000	0.00
125600	9458	0.0032	0.0115	0.0038	0.0059	0.0097	2.54
108200	18991	0.0038	0.0138	0.0045	0.0071	0.0116	2.57
90800	26406	0.0044	0.0159	0.0053	0.0081	0.0134	2.54
73400	31176	0.0052	0.0187	0.0062	0.0096	0.0157	2.55
56000	32531	0.0043	0.0224	0.0051	0.0129	0.0180	3.51
38100	31279	0.0037	0.0282	0.0044	0.0174	0.0217	4.98
20200	27577	0.0034	0.0378	0.0040	0.0244	0.0285	7.05
2300	21216	0.0034	0.0586	0.0040	0.0392	0.0432	10.72
-15600	10740	0.0033	0.0532	0.0039	0.0354	0.0393	10.10
-33500	0	0.0000	0.0000	0.0000	0.0000	0.0000	0.00

Table A.9 Bottom and top transverse hinge properties of A2 axis column of O07 Bridge

N (kN)	M_y (kN·m)	ϕ_y (1/m)	ϕ_u (1/m)	θ_y (rad)	θ_p (rad)	θ_u (rad)	$\frac{\theta_u}{\theta_y}$
143000	0	0.0000	0.0000	0.0000	0.0000	0.0000	0.00
125600	9458	0.0032	0.0115	0.0043	0.0059	0.0102	2.36
108200	18991	0.0038	0.0138	0.0051	0.0071	0.0121	2.39
90800	26406	0.0044	0.0159	0.0059	0.0081	0.0140	2.37
73400	31176	0.0052	0.0187	0.0069	0.0096	0.0165	2.38
56000	32531	0.0043	0.0224	0.0058	0.0129	0.0186	3.23
38100	31279	0.0037	0.0282	0.0049	0.0174	0.0223	4.54
20200	27577	0.0034	0.0378	0.0045	0.0244	0.0290	6.37
2300	21216	0.0034	0.0586	0.0045	0.0392	0.0437	9.63
-15600	10740	0.0033	0.0532	0.0044	0.0354	0.0398	9.08
-33500	0	0.0000	0.0000	0.0000	0.0000	0.0000	0.00

Table A.10 Bottom and top transverse hinge properties of A1 axis column of O15 Bridge

N (kN)	M_y (kN·m)	ϕ_y (1/m)	ϕ_u (1/m)	θ_y (rad)	θ_p (rad)	θ_u (rad)	$\frac{\theta_u}{\theta_y}$
139500	0	0.0000	0.0000	0.0000	0.0000	0.0000	0.00
122800	9100	0.0032	0.0108	0.0043	0.0054	0.0097	2.24
106100	18182	0.0038	0.0141	0.0051	0.0073	0.0124	2.45
89400	25165	0.0044	0.0163	0.0059	0.0084	0.0143	2.43
72700	29621	0.0051	0.0191	0.0068	0.0100	0.0167	2.48
56000	30910	0.0043	0.0230	0.0058	0.0132	0.0190	3.28
39000	29689	0.0037	0.0287	0.0049	0.0177	0.0226	4.60
22000	26175	0.0034	0.0382	0.0045	0.0247	0.0292	6.49
5000	20201	0.0033	0.0581	0.0044	0.0389	0.0433	9.78
-12000	10517	0.0037	0.0535	0.0049	0.0353	0.0403	8.14
-29000	0	0.0000	0.0000	0.0000	0.0000	0.0000	0.00

Table A.11 Bottom transverse hinge properties of P axis column of O15 Bridge

N (kN)	M_y (kN·m)	ϕ_y (1/m)	ϕ_u (1/m)	θ_y (rad)	θ_p (rad)	θ_u (rad)	$\frac{\theta_u}{\theta_y}$
140000	0	0.0000	0.0000	0.0000	0.0000	0.0000	0.00
123300	8874	0.0032	0.0107	0.0037	0.0049	0.0086	2.33
106600	18017	0.0038	0.0134	0.0043	0.0063	0.0106	2.46
89900	25049	0.0044	0.0154	0.0050	0.0072	0.0122	2.44
73200	29571	0.0051	0.0181	0.0057	0.0086	0.0143	2.49
56500	30930	0.0044	0.0217	0.0049	0.0114	0.0163	3.30
39400	29759	0.0037	0.0271	0.0042	0.0154	0.0196	4.66
22300	26249	0.0034	0.0361	0.0038	0.0215	0.0254	6.61
5200	20244	0.0033	0.0549	0.0038	0.0339	0.0377	10.03
-11900	10589	0.0037	0.0535	0.0042	0.0327	0.0370	8.75
-29000	0	0.0000	0.0000	0.0000	0.0000	0.0000	0.00

Table A.12 Top transverse hinge properties of P axis column of O15 Bridge

N (kN)	M_y (kN·m)	ϕ_y (1/m)	ϕ_u (1/m)	θ_y (rad)	θ_p (rad)	θ_u (rad)	$\frac{\theta_u}{\theta_y}$
139500	0	0.0000	0.0000	0.0000	0.0000	0.0000	0.00
122800	9100	0.0032	0.0108	0.0037	0.0054	0.0090	2.46
106100	18182	0.0038	0.0141	0.0043	0.0073	0.0116	2.70
89400	25165	0.0044	0.0163	0.0050	0.0084	0.0134	2.68
72700	29621	0.0051	0.0191	0.0057	0.0100	0.0157	2.74
56000	30910	0.0043	0.0230	0.0049	0.0132	0.0181	3.69
39000	29689	0.0037	0.0287	0.0042	0.0177	0.0219	5.24
22000	26175	0.0034	0.0382	0.0038	0.0247	0.0286	7.45
5000	20201	0.0033	0.0581	0.0038	0.0389	0.0427	11.33
-12000	10517	0.0037	0.0535	0.0042	0.0353	0.0395	9.40
-29000	0	0.0000	0.0000	0.0000	0.0000	0.0000	0.00

Table A.13 Bottom transverse hinge properties of A2 axis column of O15 Bridge

N (kN)	M_y (kN·m)	ϕ_y (1/m)	ϕ_u (1/m)	θ_y (rad)	θ_p (rad)	θ_u (rad)	$\frac{\theta_u}{\theta_y}$
140000	0	0.0000	0.0000	0.0000	0.0000	0.0000	0.00
123300	8874	0.0032	0.0107	0.0032	0.0049	0.0081	2.51
106600	18017	0.0038	0.0134	0.0038	0.0063	0.0101	2.66
89900	25049	0.0044	0.0154	0.0044	0.0072	0.0116	2.64
73200	29571	0.0051	0.0181	0.0051	0.0086	0.0136	2.69
56500	30930	0.0044	0.0217	0.0044	0.0114	0.0157	3.61
39400	29759	0.0037	0.0271	0.0037	0.0154	0.0191	5.15
22300	26249	0.0034	0.0361	0.0034	0.0215	0.0249	7.36
5200	20244	0.0033	0.0549	0.0033	0.0339	0.0373	11.24
-11900	10589	0.0037	0.0535	0.0037	0.0327	0.0365	9.78
-29000	0	0.0000	0.0000	0.0000	0.0000	0.0000	0.00

Table A.14 Top transverse hinge properties of A2 axis column of O15 Bridge

N (kN)	M_y (kN·m)	ϕ_y (1/m)	ϕ_u (1/m)	θ_y (rad)	θ_p (rad)	θ_u (rad)	$\frac{\theta_u}{\theta_y}$
139500	0	0.0000	0.0000	0.0000	0.0000	0.0000	0.00
122800	9100	0.0032	0.0108	0.0032	0.0054	0.0086	2.66
106100	18182	0.0038	0.0141	0.0038	0.0073	0.0111	2.93
89400	25165	0.0044	0.0163	0.0044	0.0084	0.0128	2.90
72700	29621	0.0051	0.0191	0.0051	0.0100	0.0151	2.97
56000	30910	0.0043	0.0230	0.0043	0.0132	0.0176	4.04
39000	29689	0.0037	0.0287	0.0037	0.0177	0.0214	5.80
22000	26175	0.0034	0.0382	0.0034	0.0247	0.0281	8.31
5000	20201	0.0033	0.0581	0.0033	0.0389	0.0422	12.71
-12000	10517	0.0037	0.0535	0.0037	0.0353	0.0390	10.53
-29000	0	0.0000	0.0000	0.0000	0.0000	0.0000	0.00

Table A.15 Bottom and top transverse hinge properties of A1 axis column of O48 Bridge

N (kN)	M_y (kN·m)	ϕ_y (1/m)	ϕ_u (1/m)	θ_y (rad)	θ_p (rad)	θ_u (rad)	$\frac{\theta_u}{\theta_y}$
143000	0	0.0000	0.0000	0.0000	0.0000	0.0000	0.00
125600	9458	0.0032	0.0115	0.0043	0.0059	0.0102	2.36
108200	18991	0.0038	0.0138	0.0051	0.0071	0.0121	2.39
90800	26406	0.0044	0.0159	0.0059	0.0081	0.0140	2.37
73400	31176	0.0052	0.0187	0.0069	0.0096	0.0165	2.38
56000	32531	0.0043	0.0224	0.0058	0.0129	0.0186	3.23
38100	31279	0.0037	0.0282	0.0049	0.0174	0.0223	4.54
20200	27577	0.0034	0.0378	0.0045	0.0244	0.0290	6.37
2300	21216	0.0034	0.0586	0.0045	0.0392	0.0437	9.63
-15600	10740	0.0033	0.0532	0.0044	0.0354	0.0398	9.08
-33500	0	0.0000	0.0000	0.0000	0.0000	0.0000	0.00

Table A.16 Bottom and top transverse hinge properties of P axis column of O48 Bridge

N (kN)	M_y (kN·m)	ϕ_y (1/m)	ϕ_u (1/m)	θ_y (rad)	θ_p (rad)	θ_u (rad)	$\frac{\theta_u}{\theta_y}$
138500	0	0.0000	0.0000	0.0000	0.0000	0.0000	0.00
121700	9468	0.0029	0.0102	0.0038	0.0052	0.0090	2.36
104900	18652	0.0034	0.0121	0.0045	0.0062	0.0107	2.37
88100	25714	0.0040	0.0139	0.0053	0.0071	0.0124	2.33
71300	30414	0.0046	0.0164	0.0061	0.0084	0.0145	2.36
54500	31915	0.0042	0.0197	0.0056	0.0110	0.0166	2.95
36900	30675	0.0036	0.0248	0.0048	0.0151	0.0199	4.12
19300	26998	0.0034	0.0335	0.0045	0.0214	0.0258	5.77
1700	20714	0.0034	0.0522	0.0045	0.0347	0.0392	8.70
-15900	10501	0.0032	0.0528	0.0043	0.0352	0.0395	9.21
-33500	0	0.0000	0.0000	0.0000	0.0000	0.0000	0.00

Table A.17 Bottom and top transverse hinge properties of A2 axis column of O48 Bridge

N (kN)	M_y (kN·m)	ϕ_y (1/m)	ϕ_u (1/m)	θ_y (rad)	θ_p (rad)	θ_u (rad)	$\frac{\theta_u}{\theta_y}$
143000	0	0.0000	0.0000	0.0000	0.0000	0.0000	0.00
125600	9458	0.0032	0.0115	0.0038	0.0059	0.0097	2.56
108200	18991	0.0038	0.0138	0.0044	0.0071	0.0115	2.59
90800	26406	0.0044	0.0159	0.0052	0.0081	0.0133	2.56
73400	31176	0.0052	0.0187	0.0061	0.0096	0.0156	2.57
56000	32531	0.0043	0.0224	0.0051	0.0129	0.0179	3.54
38100	31279	0.0037	0.0282	0.0043	0.0174	0.0217	5.04
20200	27577	0.0034	0.0378	0.0040	0.0244	0.0284	7.14
2300	21216	0.0034	0.0586	0.0040	0.0392	0.0432	10.86
-15600	10740	0.0033	0.0532	0.0038	0.0354	0.0392	10.23
-33500	0	0.0000	0.0000	0.0000	0.0000	0.0000	0.00

B. Longitudinal Pushover Analysis Results

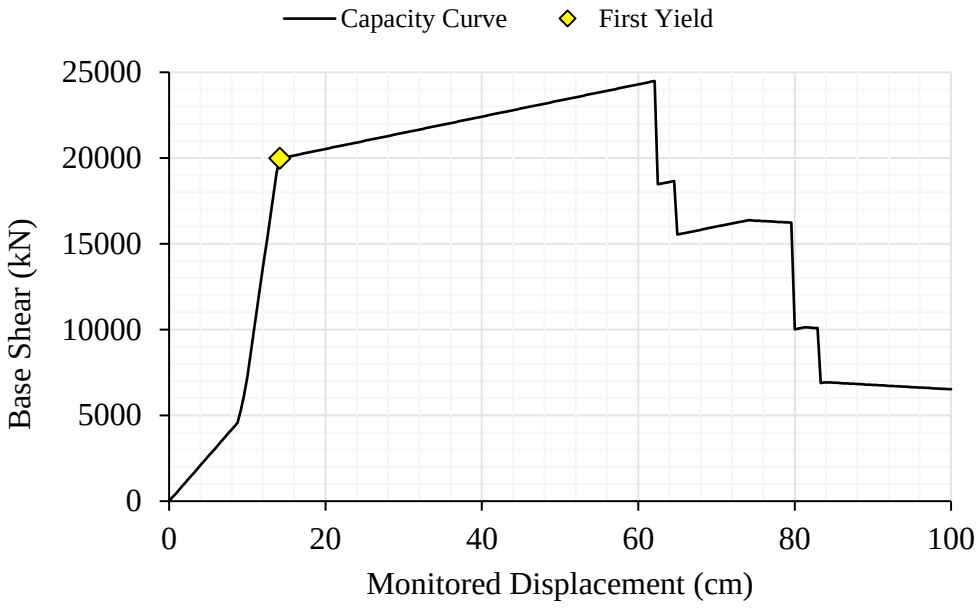

Figure B.1 Capacity curve for O02 Bridge in longitudinal pushover analysis

Table B.1 Longitudinal yield forces of O02 Bridge found from Pushover Analysis

Axis	Column Hinge	Pounding Step/Disp.	Yield Step/Disp.	P_y (kN)	V_y (kN)	M_y (kN·m)
A1	Left Column	-	178 / 74.2	1523	2882	18855
	Middle Column	-	178 / 74.2	1721	2882	18855
	Right Column	-	178 / 74.2	1529	2884	18855
P	Left Column	24 / 10.0	34 / 14.2	2832	2993	19537
	Middle Column	24 / 10.0	34 / 14.2	3198	2994	19537
	Right Column	24 / 10.0	34 / 14.2	2832	2998	19537
A2	Left Column	22 / 9.2	34 / 14.2	1663	2885	18855
	Middle Column	22 / 9.2	34 / 14.2	1881	2885	18855
	Right Column	22 / 9.2	34 / 14.2	1657	2887	18855

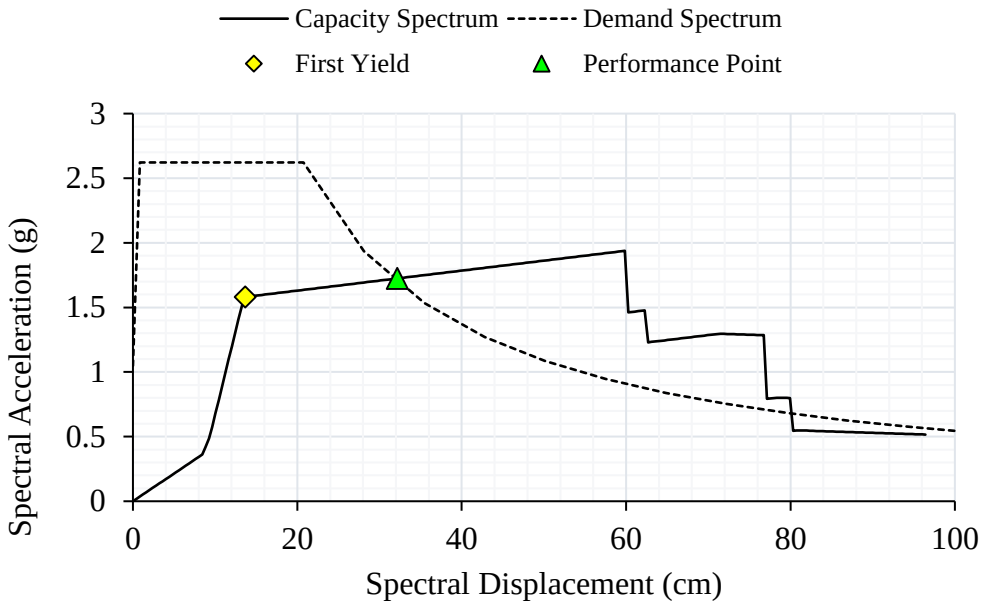

Figure B.2 Performance point determination for O02 Bridge

Table B.2 Performance point results of longitudinal pushover analysis for O02 Bridge

PO Results	A1 Columns			P Columns			A2 Columns		
	Left	**Middle**	**Right**	**Left**	**Middle**	**Right**	**Left**	**Middle**	**Right**
ϕ_y **(rad/m)**	0.0034	0.0034	0.0034	0.0034	0.0034	0.0034	0.0034	0.0034	0.0034
ϕ_p **(rad/m)**	0.0000	0.0000	0.0000	0.0173	0.0154	0.0174	0.0230	0.0219	0.0231
ϕ_u **(rad/m)**	0.0034	0.0034	0.0034	0.0207	0.0188	0.0207	0.0264	0.0253	0.0265
L **(m)**	7.000	7.000	7.000	7.000	7.000	7.000	7.000	7.000	7.000
L_p **(m)**	0.910	0.910	0.910	0.910	0.910	0.910	0.910	0.910	0.910
θ_y **(rad)**	0.0079	0.0079	0.0079	0.0079	0.0079	0.0079	0.0079	0.0079	0.0079
θ_p **(rad)**	0.0000	0.0000	0.0000	0.0158	0.0140	0.0158	0.0210	0.0199	0.0210
θ_c **(rad)**	0.0079	0.0079	0.0079	0.0237	0.0219	0.0237	0.0289	0.0278	0.0290
Δ_y **(m)**	0.056	0.056	0.056	0.055	0.055	0.055	0.056	0.056	0.056
Δ_{pd} **(m)**	0.000	0.000	0.000	0.103	0.092	0.103	0.137	0.130	0.138
Δ_{col} **(m)**	0.056	0.056	0.056	0.159	0.147	0.159	0.193	0.186	0.193
Δ **(%)**	0.793	0.793	0.793	2.265	2.099	2.268	2.754	2.654	2.759
μ_d	1.000	1.000	1.000	2.866	2.656	2.869	3.473	3.347	3.480
P_p **(kN)**	1603	1817	1609	2838	3206	2838	1687	1909	1680
V_p **(kN)**	1489	1498	1505	2927	2918	2932	2845	2839	2848
M_p **(kN·m)**	9676	9730	9765	19543	19542	19543	18863	18862	18863

Table B.3 Performance evaluation of O02 Bridge

Location	Column	θ_p (rad)	θ_p^{LD} (rad)	θ_p^{CD} (rad)	θ_p^{CP} (rad)	Performance Level
A1	**Left**	0.0000	0.0073	0.0245	0.0339	No Damage
	Middle	0.0000	0.0073	0.0245	0.0339	No Damage
	Right	0.0000	0.0073	0.0245	0.0339	No Damage
P	**Left**	0.0158	0.0074	0.0248	0.0343	Controlled Damage
	Middle	0.0140	0.0074	0.0248	0.0343	Controlled Damage
	Right	0.0158	0.0074	0.0248	0.0343	Controlled Damage
A2	**Left**	0.0210	0.0073	0.0245	0.0339	Controlled Damage
	Middle	0.0199	0.0073	0.0245	0.0339	Controlled Damage
	Right	0.0210	0.0073	0.0245	0.0339	Controlled Damage

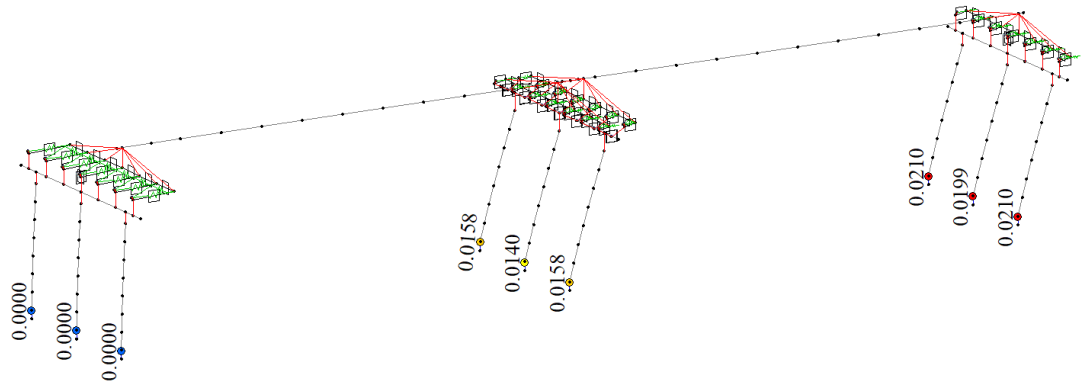

Figure B.3 Deformed shape and plastic rotation values (rad) for O02 Bridge at performance point in longitudinal pushover analysis

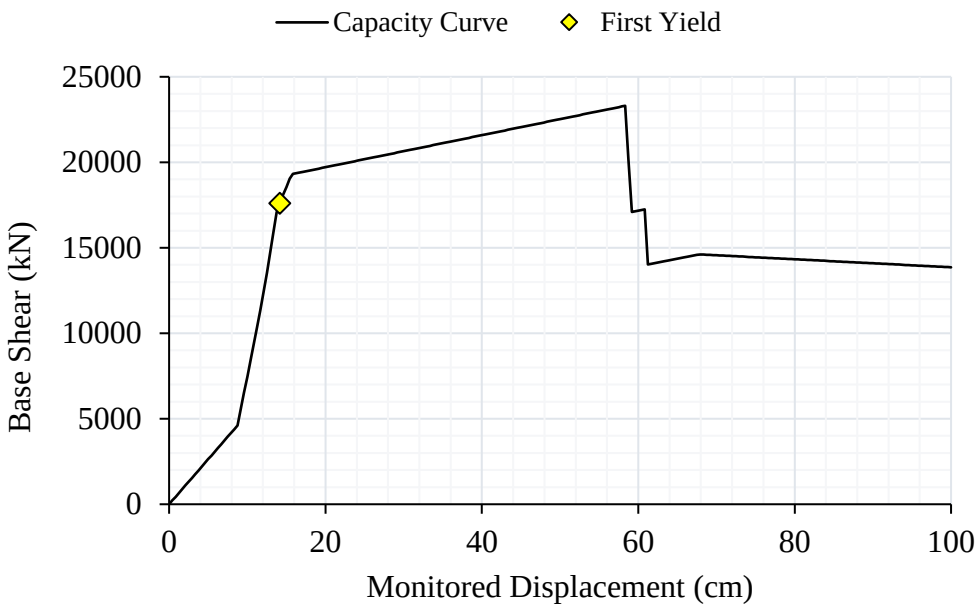

(a)

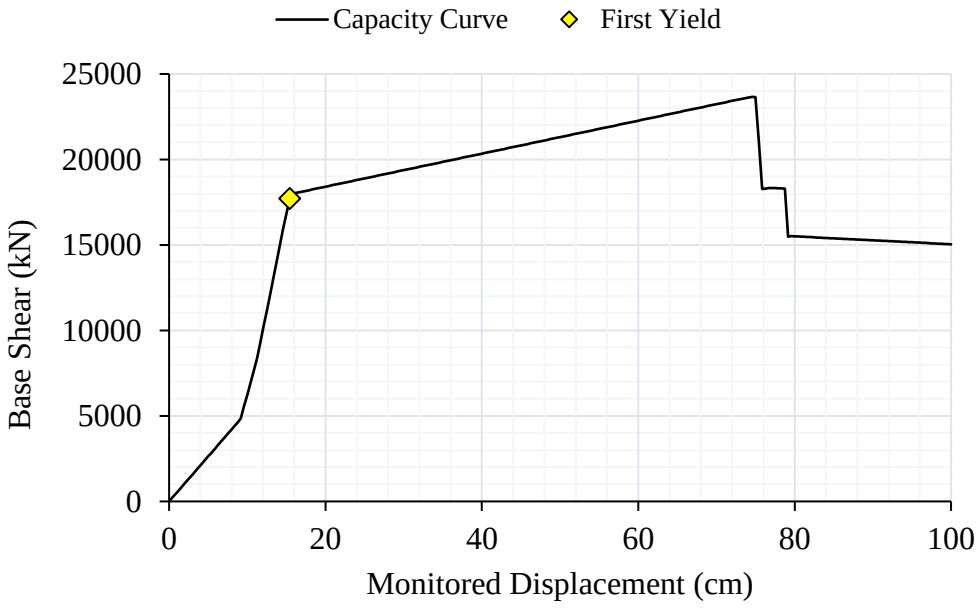

(b)

Figure B.4 Capacity curves for O05 Bridge in longitudinal pushover analysis: (a) A1-P-A2 pushover direction, (b) A2-P-A1 pushover direction

Table B.4 Yield forces of O05 Bridge found from Pushover Analysis (A1-P-A2 Direction)

Axis	Column Hinge	Pounding Step/Disp.	Yield Step/Disp.	P_y (kN)	V_y (kN)	M_y (kN·m)
A1	Left Column	-	163 / 67.9	1557	2612	18852
	Middle Column	-	163 / 67.9	1739	2612	18852
	Right Column	-	163 / 67.9	1565	2614	18852
P	Left Column	29 / 12.1	38 / 15.8	2823	2610	19510
	Middle Column	29 / 12.1	38 / 15.8	3136	2610	19510
	Right Column	29 / 12.1	38 / 15.8	2823	2614	19510
A2	Left Column	22 / 9.2	34 / 14.2	1624	2962	18831
	Middle Column	22 / 9.2	34 / 14.2	1843	2962	18831
	Right Column	22 / 9.2	34 / 14.2	1618	2964	18831

Table B.5 Yield forces of O05 Bridge found from Pushover Analysis (A2-P-A1 Direction)

Axis	Column Hinge	Pounding Step/Disp.	Yield Step/Disp.	P_y (kN)	V_y (kN)	M_y (kN·m)
A1	Left Column	23 / 9.6	37 / 15.4	1684	-2615	-18852
	Middle Column	23 / 9.6	37 / 15.4	1880	-2615	-18852
	Right Column	23 / 9.6	37 / 15.4	1677	-2617	-18852
P	Left Column	28 / 11.7	38 / 15.8	2829	-2608	-19510
	Middle Column	28 / 11.7	38 / 15.8	3143	-2608	-19510
	Right Column	28 / 11.7	38 / 15.8	2829	-2611	-19510
A2	Left Column	-	179 / 74.6	1500	-2965	-18831
	Middle Column	-	179 / 74.6	1704	-2966	-18831
	Right Column	-	179 / 74.6	1510	-2969	-18831

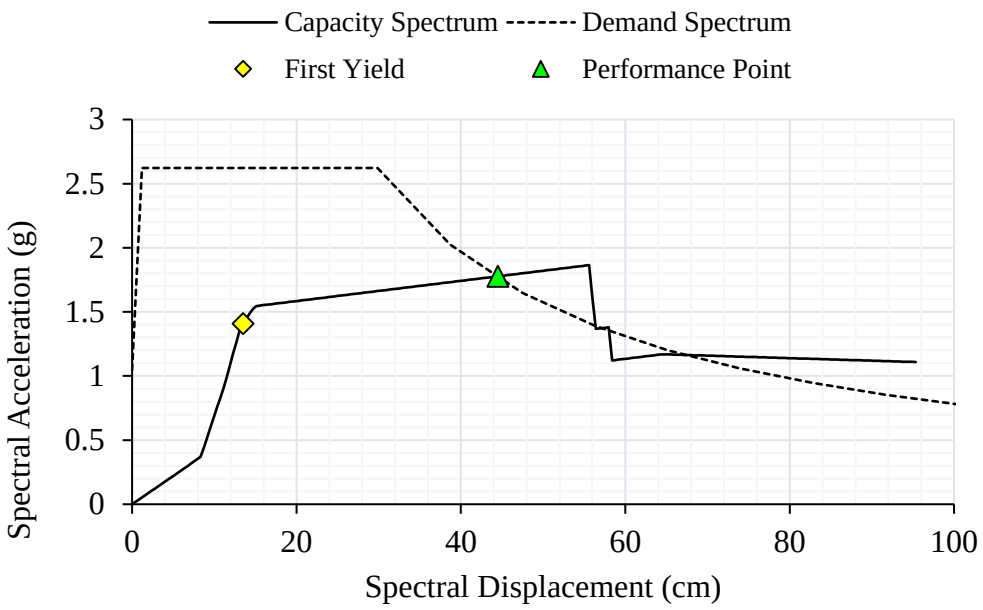

(a)

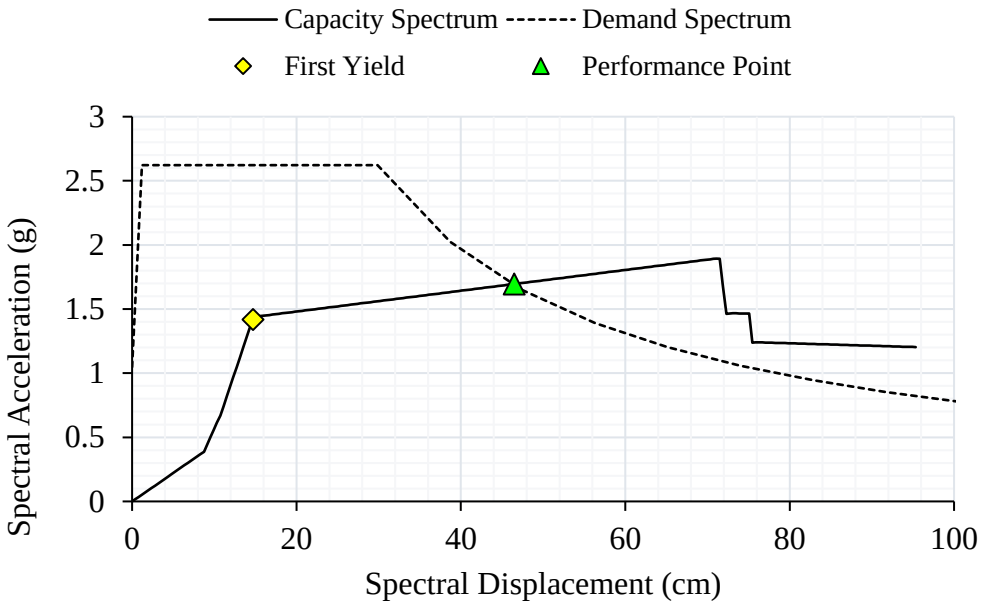

(b)

Figure B.5 Performance point determination for O05 Bridge in (a) A1-P-A2 Direction, (b) A2-P-A1 Direction

Table B.6 Performance point results of pushover analysis for O05 Bridge (A1-P-A2)

PO Results	A1 Columns			P Columns			A2 Columns		
	Left	Middle	Right	Left	Middle	Right	Left	Middle	Right
ϕ_y (rad/m)	0.0034	0.0034	0.0034	0.0034	0.0034	0.0034	0.0034	0.0034	0.0034
ϕ_p (rad/m)	0.0000	0.0000	0.0000	0.0186	0.0161	0.0186	0.0419	0.0399	0.0420
ϕ_u (rad/m)	0.0034	0.0034	0.0034	0.0220	0.0195	0.0220	0.0453	0.0433	0.0454
L (m)	7.700	7.700	7.700	8.000	8.000	8.000	6.800	6.800	6.800
L_p (m)	0.970	0.970	0.970	0.990	0.990	0.990	0.900	0.900	0.900
θ_y (rad)	0.0087	0.0087	0.0087	0.0090	0.0090	0.0090	0.0077	0.0077	0.0077
θ_p (rad)	0.0000	0.0000	0.0000	0.0184	0.0159	0.0185	0.0377	0.0359	0.0378
θ_c (rad)	0.0087	0.0087	0.0087	0.0275	0.0250	0.0275	0.0454	0.0436	0.0455
Δ_y (m)	0.067	0.067	0.067	0.072	0.072	0.072	0.052	0.052	0.052
Δ_{pd} (m)	0.000	0.000	0.000	0.138	0.119	0.139	0.239	0.228	0.240
Δ_{col} (m)	0.067	0.067	0.067	0.211	0.192	0.211	0.292	0.280	0.293
Δ (%)	0.872	0.872	0.872	2.632	2.397	2.635	4.291	4.120	4.302
μ_d	1.000	1.000	1.000	2.914	2.653	2.917	5.574	5.351	5.587
P_p (kN)	1606	1797	1616	2833	3147	2833	1661	1885	1652
V_p (kN)	1992	2003	2011	2518	2507	2523	2894	2884	2898
M_p (kN·m)	14315	14379	14422	19516	19515	19516	18845	18844	18845

Table B.7 Performance point results of pushover analysis for O05 Bridge (A2-P-A1)

PO Results	A1 Columns			P Columns			A2 Columns		
	Left	Middle	Right	Left	Middle	Right	Left	Middle	Right
ϕ_y (rad/m)	0.0034	0.0034	0.0034	0.0034	0.0034	0.0034	0.0034	0.0034	0.0034
ϕ_p (rad/m)	0.0321	0.0303	0.0322	0.0198	0.0171	0.0198	0.0000	0.0000	0.0000
ϕ_u (rad/m)	0.0355	0.0337	0.0356	0.0232	0.0205	0.0232	0.0034	0.0034	0.0034
L (m)	7.700	7.700	7.700	8.000	8.000	8.000	6.800	6.800	6.800
L_p (m)	0.970	0.970	0.970	0.990	0.990	0.990	0.900	0.900	0.900
θ_y (rad)	0.0087	0.0087	0.0087	0.0090	0.0090	0.0090	0.0077	0.0077	0.0077
θ_p (rad)	0.0311	0.0294	0.0312	0.0196	0.0169	0.0196	0.0000	0.0000	0.0000
θ_c (rad)	0.0398	0.0381	0.0399	0.0286	0.0259	0.0287	0.0077	0.0077	0.0077
Δ_y (m)	0.067	0.067	0.067	0.072	0.072	0.072	0.052	0.052	0.052
Δ_{pd} (m)	0.224	0.212	0.225	0.147	0.127	0.147	0.000	0.000	0.000
Δ_{col} (m)	0.292	0.279	0.292	0.219	0.199	0.220	0.052	0.052	0.052
Δ (%)	3.786	3.623	3.796	2.742	2.490	2.745	0.770	0.770	0.770
μ_d	4.341	4.154	4.351	3.035	2.756	3.038	1.000	1.000	1.000
P_p (kN)	1722	1923	1714	2840	3155	2840	1539	1749	1546
V_p (kN)	2553	2544	2555	2510	2497	2514	1997	2011	2020
M_p (kN·m)	18863	18862	18863	19517	19516	19517	12671	12746	12792

Table B.8 Performance evaluation of O05 Bridge in A1-P-A2 loading direction

Location	Column	θ_p (rad)	θ_p^{LD} (rad)	θ_p^{CD} (rad)	θ_p^{CP} (rad)	Performance Level
A1	Left	0.0000	0.0077	0.0260	0.0360	No Damage
	Middle	0.0000	0.0077	0.0260	0.0360	No Damage
	Right	0.0000	0.0077	0.0260	0.0360	No Damage
P	Left	0.0184	0.0080	0.0270	0.0373	Controlled Damage
	Middle	0.0159	0.0080	0.0270	0.0373	Controlled Damage
	Right	0.0185	0.0080	0.0270	0.0373	Controlled Damage
A2	Left	0.0377	0.0071	0.0241	0.0333	Excessive Damage
	Middle	0.0359	0.0071	0.0241	0.0333	Excessive Damage
	Right	0.0378	0.0071	0.0241	0.0333	Excessive Damage

Table B.9 Performance evaluation of O05 Bridge in A2-P-A1 loading direction

Location	Column	θ_p (rad)	θ_p^{LD} (rad)	θ_p^{CD} (rad)	θ_p^{CP} (rad)	Performance Level
A1	Left	0.0311	0.0077	0.0260	0.0360	Collapse Prevention
	Middle	0.0294	0.0077	0.0260	0.0360	Collapse Prevention
	Right	0.0312	0.0077	0.0260	0.0360	Collapse Prevention
P	Left	0.0196	0.0080	0.0270	0.0373	Controlled Damage
	Middle	0.0169	0.0080	0.0270	0.0373	Controlled Damage
	Right	0.0196	0.0080	0.0270	0.0373	Controlled Damage
A2	Left	0.0000	0.0071	0.0241	0.0333	No Damage
	Middle	0.0000	0.0071	0.0241	0.0333	No Damage
	Right	0.0000	0.0071	0.0241	0.0333	No Damage

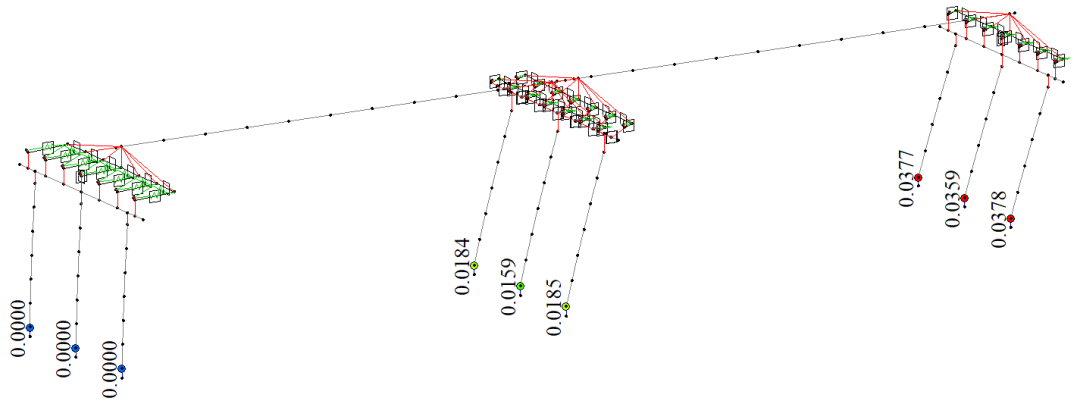

(a)

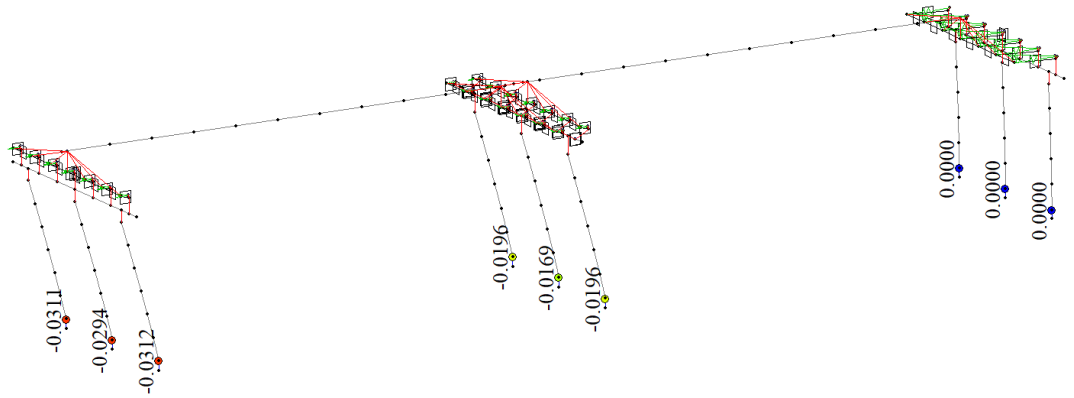

(b)

Figure B.6 Deformed shape and plastic rotation (rad) for O05 Bridge at performance point in longitudinal pushover analysis: (a) A1-P-A2 direction, (b) A2-P-A1 direction

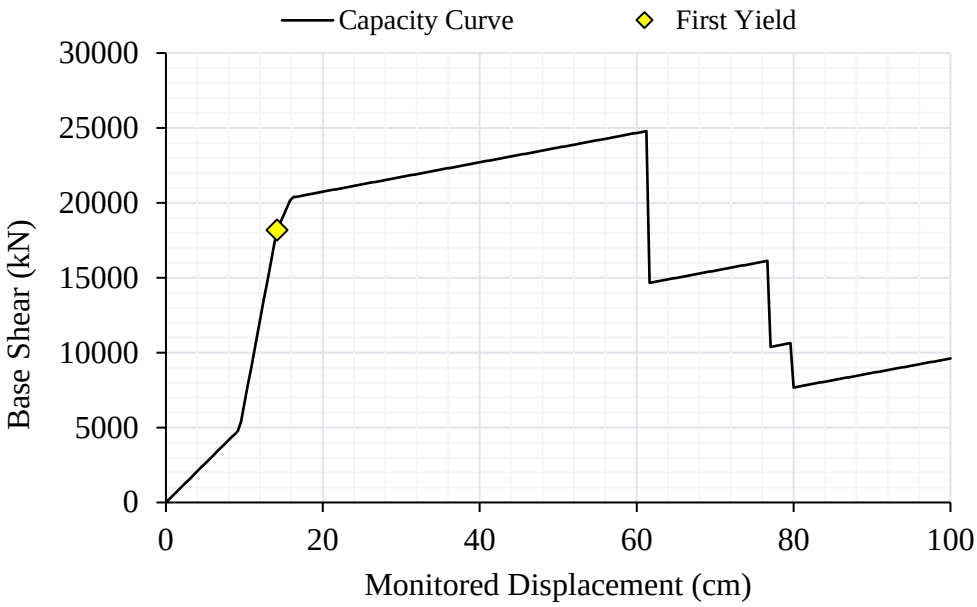

(a)

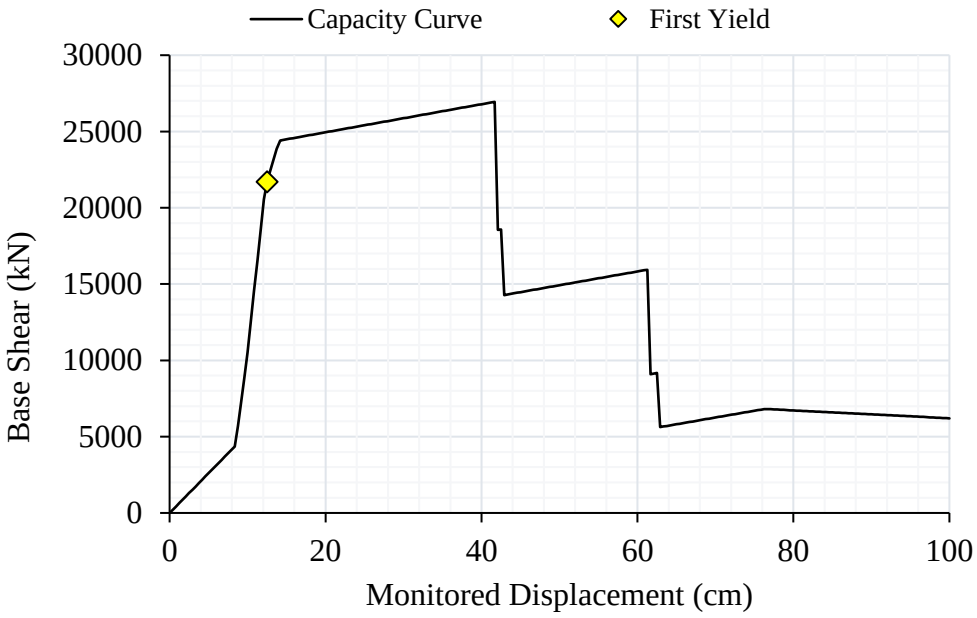

(b)

Figure B.7 Capacity curves for O07 Bridge in longitudinal pushover analysis: (a) A1-P-A2 pushover direction, (b) A2-P-A1 pushover direction

Table B.10 Yield forces of O07 Bridge found from Pushover Analysis (A1-P-A2 Direction)

Axis	Column Hinge	Pounding Step/Disp.	Yield Step/Disp.	P_y (kN)	V_y (kN)	M_y (kN·m)
A1	Left Column	-	-	-	-	-
	Middle Column	-	-	-	-	-
	Right Column	-	-	-	-	-
P	Left Column	24 / 10.0	34 / 14.2	2778	3237	21507
	Middle Column	24 / 10.0	34 / 14.2	3130	3238	21507
	Right Column	24 / 10.0	34 / 14.2	2778	3241	21507
A2	Left Column	23 / 9.6	39 / 16.3	1702	2808	21031
	Middle Column	23 / 9.6	39 / 16.3	1891	2807	21031
	Right Column	23 / 9.6	39 / 16.3	1696	2809	21031

Table B.11 Yield forces of O07 Bridge found from Pushover Analysis (A2-P-A1 Direction)

Axis	Column Hinge	Pounding Step/Disp.	Yield Step/Disp.	P_y (kN)	V_y (kN)	M_y (kN·m)
A1	Left Column	21 / 8.8	30 / 12.5	1547	-3959	-20989
	Middle Column	21 / 8.8	30 / 12.5	1802	-3961	-20989
	Right Column	21 / 8.8	30 / 12.5	1542	-3962	-20989
P	Left Column	25 / 10.4	34 / 14.2	2752	-3244	-21507
	Middle Column	25 / 10.4	34 / 14.2	3100	-3245	-21507
	Right Column	25 / 10.4	34 / 14.2	2752	-3249	-21507
A2	Left Column	-	184 / 76.7	1542	-2795	-21031
	Middle Column	-	184 / 76.7	1709	-2795	-21031
	Right Column	-	184 / 76.7	1545	-2796	-21031

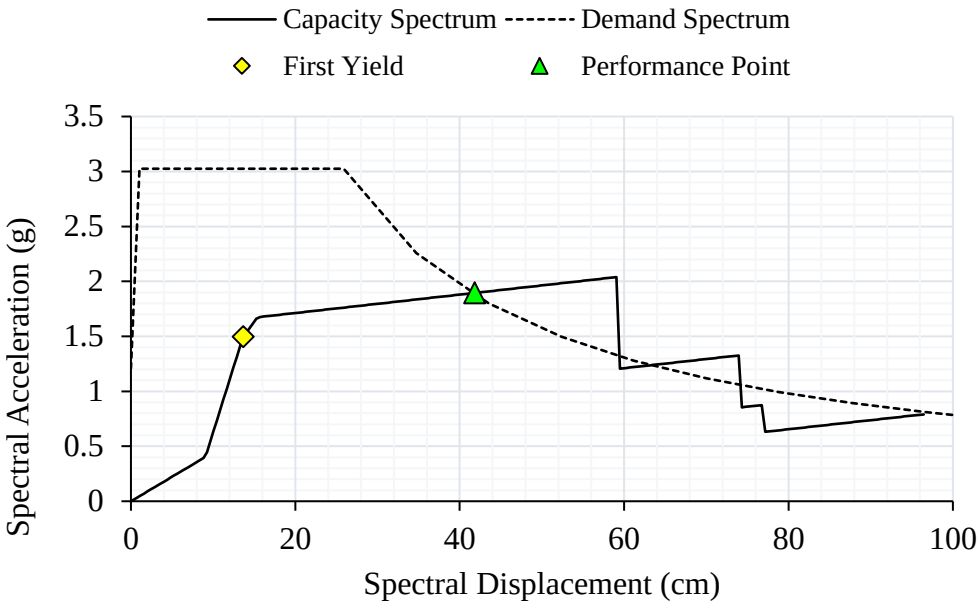

(a)

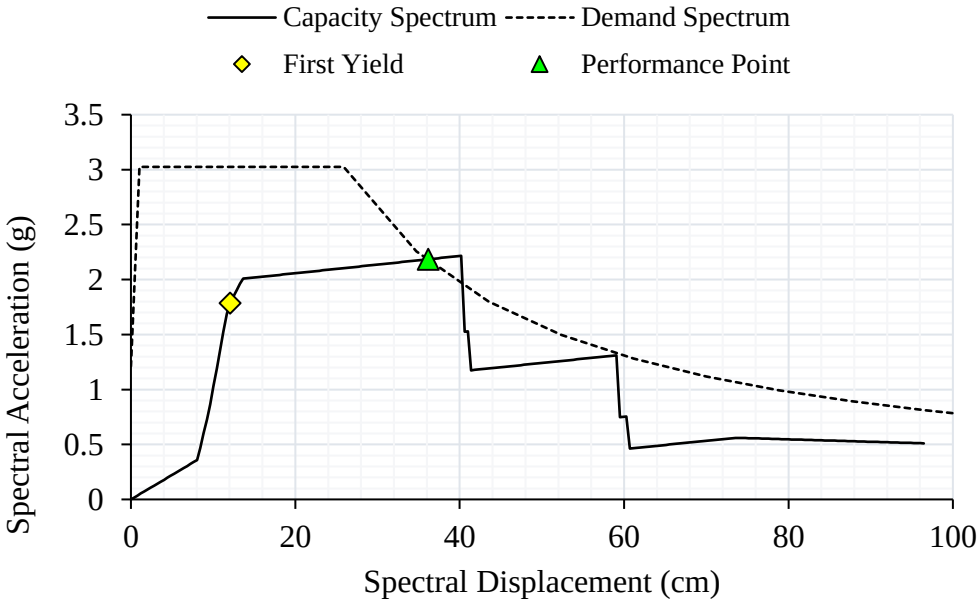

(b)

Figure B.8 Performance point determination for O07 Bridge in (a) A1-P-A2 Direction, (b) A2-P-A1 Direction

Table B.12 Performance point results of pushover analysis for O07 Bridge (A1-P-A2)

PO Results	A1 Columns			P Columns			A2 Columns		
	Left	**Middle**	**Right**	**Left**	**Middle**	**Right**	**Left**	**Middle**	**Right**
ϕ_y **(rad/m)**	0.0034	0.0034	0.0034	0.0034	0.0034	0.0034	0.0034	0.0034	0.0034
ϕ_p **(rad/m)**	0.0000	0.0000	0.0000	0.0315	0.0293	0.0315	0.0256	0.0244	0.0257
ϕ_u **(rad/m)**	0.0034	0.0034	0.0034	0.0349	0.0327	0.0349	0.0290	0.0278	0.0291
L **(m)**	5.700	5.700	5.700	7.100	7.100	7.100	8.000	8.000	8.000
L_p **(m)**	0.810	0.810	0.810	0.900	0.900	0.900	0.990	0.990	0.990
θ_y **(rad)**	0.0065	0.0065	0.0065	0.0080	0.0080	0.0080	0.0092	0.0092	0.0092
θ_p **(rad)**	0.0000	0.0000	0.0000	0.0283	0.0264	0.0284	0.0253	0.0241	0.0254
θ_c **(rad)**	0.0065	0.0065	0.0065	0.0364	0.0344	0.0364	0.0345	0.0333	0.0346
Δ_y **(m)**	0.037	0.037	0.037	0.057	0.057	0.057	0.073	0.073	0.073
Δ_{pd} **(m)**	0.000	0.000	0.000	0.188	0.175	0.189	0.190	0.181	0.191
Δ_{col} **(m)**	0.037	0.037	0.037	0.245	0.232	0.246	0.263	0.254	0.264
Δ **(%)**	0.651	0.651	0.651	3.456	3.273	3.458	3.292	3.179	3.298
μ_d	1.000	1.000	1.000	4.303	4.075	4.306	3.596	3.473	3.603
P_p **(kN)**	1460	1701	1465	2781	3133	2781	1737	1931	1730
V_p **(kN)**	1769	1788	1798	3144	3130	3148	2759	2752	2761
M_p **(kN·m)**	9362	9448	9496	21520	21519	21520	21041	21040	21041

Table B.13 Performance point results of pushover analysis for O07 Bridge (A2-P-A1)

PO Results	A1 Columns			P Columns			A2 Columns		
	Left	**Middle**	**Right**	**Left**	**Middle**	**Right**	**Left**	**Middle**	**Right**
ϕ_y **(rad/m)**	0.0034	0.0034	0.0034	0.0034	0.0034	0.0034	0.0034	0.0034	0.0034
ϕ_p **(rad/m)**	0.0480	0.0463	0.0481	0.0253	0.0236	0.0254	0.0000	0.0000	0.0000
ϕ_u **(rad/m)**	0.0514	0.0497	0.0516	0.0287	0.0270	0.0288	0.0034	0.0034	0.0034
L **(m)**	5.700	5.700	5.700	7.100	7.100	7.100	8.000	8.000	8.000
L_p **(m)**	0.810	0.810	0.810	0.900	0.900	0.900	0.990	0.990	0.990
θ_y **(rad)**	0.0065	0.0065	0.0065	0.0080	0.0080	0.0080	0.0092	0.0092	0.0092
θ_p **(rad)**	0.0389	0.0375	0.0390	0.0228	0.0213	0.0228	0.0000	0.0000	0.0000
θ_c **(rad)**	0.0454	0.0440	0.0455	0.0308	0.0293	0.0309	0.0092	0.0092	0.0092
Δ_y **(m)**	0.037	0.037	0.037	0.057	0.057	0.057	0.073	0.073	0.073
Δ_{pd} **(m)**	0.206	0.199	0.206	0.152	0.141	0.152	0.000	0.000	0.000
Δ_{col} **(m)**	0.243	0.236	0.244	0.209	0.198	0.209	0.073	0.073	0.073
Δ **(%)**	4.264	4.134	4.272	2.939	2.794	2.942	0.915	0.915	0.915
μ_d	6.546	6.346	6.559	3.659	3.479	3.664	1.000	1.000	1.000
P_p **(kN)**	1576	1837	1570	2760	3109	2760	1637	1824	1646
V_p **(kN)**	3900	3890	3904	3168	3158	3174	1784	1793	1800
M_p **(kN·m)**	21007	21006	21007	21518	21517	21518	13273	13332	13373

Table B.14 Performance evaluation of O07 Bridge in A1-P-A2 loading direction

Location	Column	θ_p (rad)	θ_p^{LD} (rad)	θ_p^{CD} (rad)	θ_p^{CP} (rad)	Performance Level
A1	Left	0.0000	0.0063	0.0214	0.0296	No Damage
	Middle	0.0000	0.0063	0.0214	0.0296	No Damage
	Right	0.0000	0.0063	0.0214	0.0296	No Damage
P	Left	0.0283	0.0061	0.0213	0.0295	Collapse Prevention
	Middle	0.0264	0.0061	0.0213	0.0295	Collapse Prevention
	Right	0.0283	0.0061	0.0213	0.0295	Collapse Prevention
A2	Left	0.0253	0.0077	0.0262	0.0362	Controlled Damage
	Middle	0.0241	0.0077	0.0262	0.0362	Controlled Damage
	Right	0.0254	0.0077	0.0262	0.0362	Controlled Damage

Table B.15 Performance evaluation of O07 Bridge in A2-P-A1 loading direction

Location	Column	θ_p (rad)	θ_p^{LD} (rad)	θ_p^{CD} (rad)	θ_p^{CP} (rad)	Performance Level
A1	Left	0.0389	0.0063	0.0214	0.0296	Excessive Damage
	Middle	0.0375	0.0063	0.0214	0.0296	Excessive Damage
	Right	0.0390	0.0063	0.0214	0.0296	Excessive Damage
P	Left	0.0228	0.0061	0.0213	0.0295	Collapse Prevention
	Middle	0.0213	0.0061	0.0213	0.0295	Collapse Prevention
	Right	0.0228	0.0061	0.0213	0.0295	Collapse Prevention
A2	Left	0.0000	0.0077	0.0262	0.0362	No Damage
	Middle	0.0000	0.0077	0.0262	0.0362	No Damage
	Right	0.0000	0.0077	0.0262	0.0362	No Damage

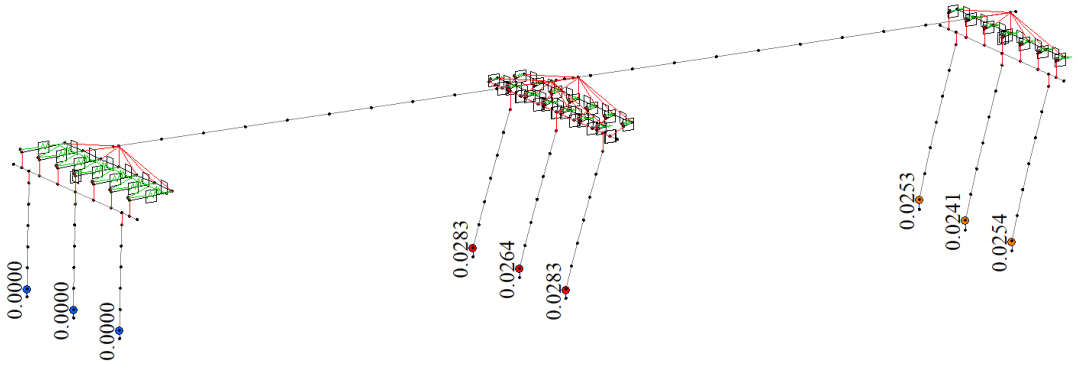

(a)

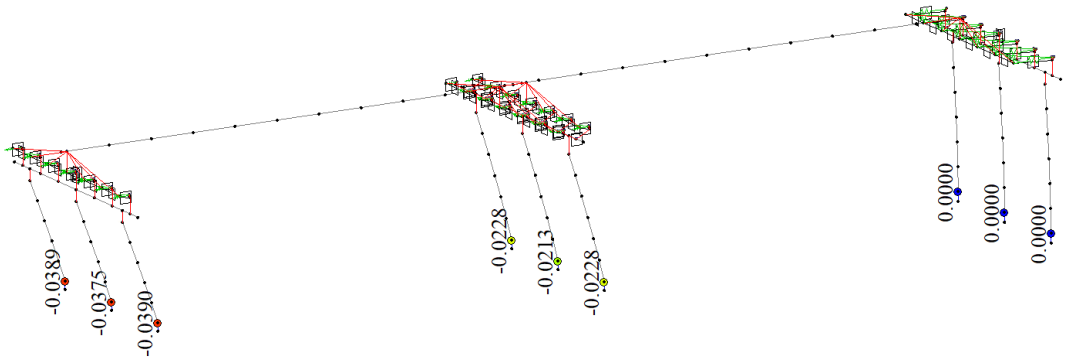

(b)

Figure B.9 Deformed shape and plastic rotation values (rad) for O07 Bridge at performance point in longitudinal pushover analysis: (a) A1-P-A2 direction, (b) A2-P-A1 direction

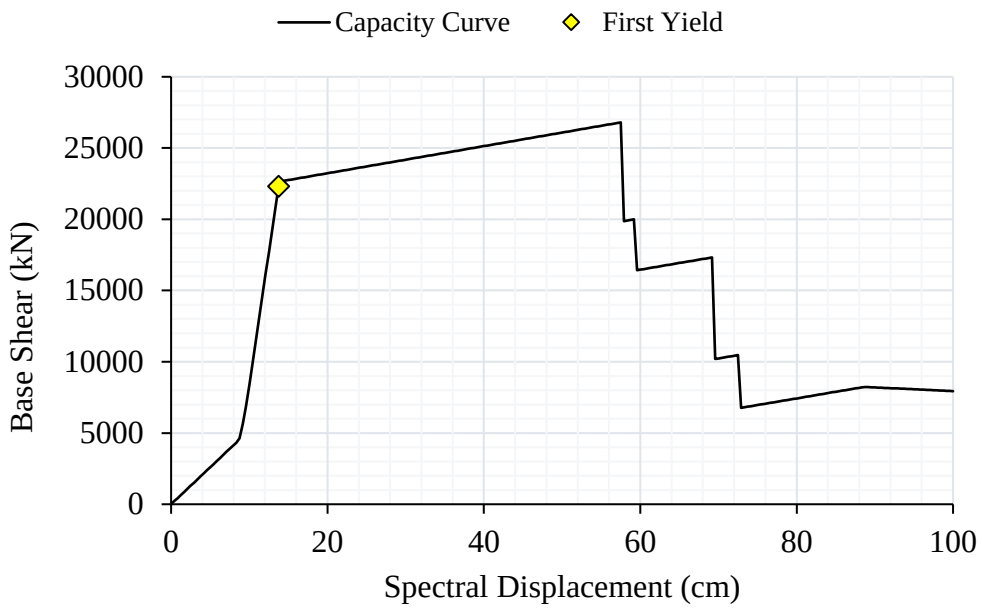

Figure B. 10 Capacity curve for O13 Bridge in longitudinal pushover analysis

Table B.16 Yield forces of O13 Bridge found from Pushover Analysis

Axis	Column Hinge	Pounding Step/Disp.	Yield Step/Disp.	P_y (kN)	V_y (kN)	M_y (kN·m)
A1	Left Column	-	213 / 88.8	1433	3325	21150
	Middle Column	-	213 / 88.8	1618	3325	21150
	Right Column	-	213 / 88.8	1435	3326	21150
P	Left Column	24 / 10.0	33 / 13.8	2741	3435	21782
	Middle Column	24 / 10.0	33 / 13.8	3106	3438	21782
	Right Column	24 / 10.0	33 / 13.8	2742	3441	21782
A2	Left Column	22 / 9.2	34 / 14.2	1619	3332	21150
	Middle Column	22 / 9.2	34 / 14.2	1837	3333	21150
	Right Column	22 / 9.2	34 / 14.2	1613	3335	21150

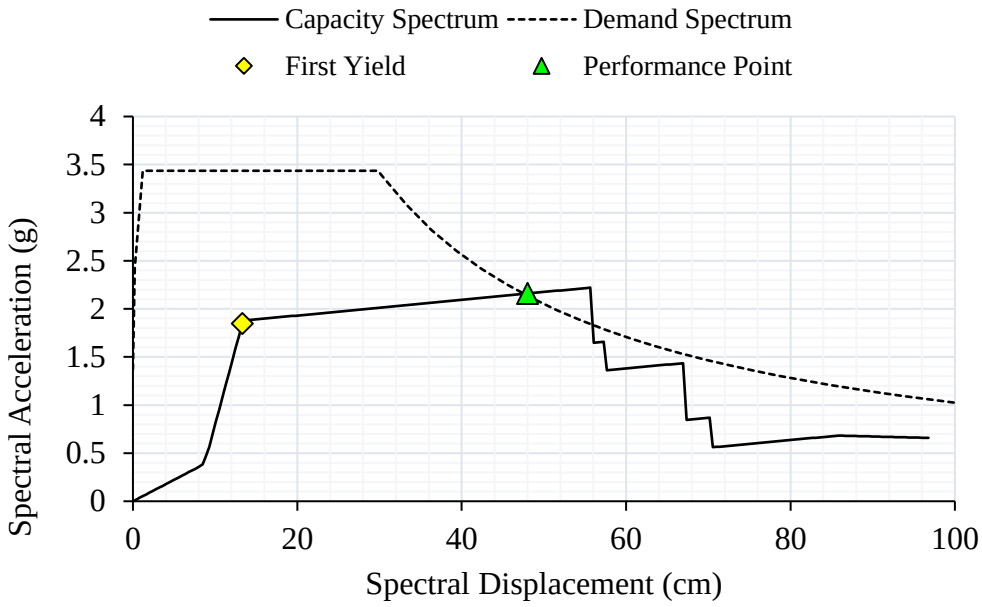

Figure B.11 Performance point determination for O13 Bridge

Table B.17 Performance point results of pushover analysis for O13 Bridge

PO Results	A1 Columns			P Columns			A2 Columns		
	Left	Middle	Right	Left	Middle	Right	Left	Middle	Right
ϕ_y (rad/m)	0.0035	0.0035	0.0035	0.0035	0.0034	0.0034	0.0034	0.0034	0.0034
ϕ_p (rad/m)	0.0000	0.0000	0.0000	0.0377	0.0236	0.0254	0.0000	0.0000	0.0000
ϕ_u (rad/m)	0.0035	0.0035	0.0035	0.0412	0.0270	0.0288	0.0034	0.0034	0.0034
L (m)	6.800	6.800	6.800	6.800	7.100	7.100	8.000	8.000	8.000
L_p (m)	0.900	0.900	0.900	0.900	0.900	0.900	0.990	0.990	0.990
θ_y (rad)	0.0079	0.0079	0.0079	0.0079	0.0080	0.0080	0.0092	0.0092	0.0092
θ_p (rad)	0.0000	0.0000	0.0000	0.0339	0.0213	0.0228	0.0000	0.0000	0.0000
θ_c (rad)	0.0079	0.0079	0.0079	0.0418	0.0293	0.0309	0.0092	0.0092	0.0092
Δ_y (m)	0.054	0.054	0.054	0.054	0.057	0.057	0.073	0.073	0.073
Δ_{pd} (m)	0.000	0.000	0.000	0.215	0.141	0.152	0.000	0.000	0.000
Δ_{col} (m)	0.054	0.054	0.054	0.269	0.198	0.209	0.073	0.073	0.073
Δ (%)	0.793	0.793	0.793	3.959	2.794	2.942	0.915	0.915	0.915
μ_d	1.000	1.000	1.000	5.004	3.479	3.664	1.000	1.000	1.000
P_p (kN)	1527	1734	1534	2753	3109	2760	1637	1824	1646
V_p (kN)	2110	2123	2131	3314	3158	3174	1784	1793	1800
M_p (kN·m)	13349	13421	13461	21796	21517	21518	13273	13332	13373

Table B.18 Performance evaluation of O13 Bridge

Location	Column	θ_p (rad)	θ_p^{LD} (rad)	θ_p^{CD} (rad)	θ_p^{CP} (rad)	Performance Level
A1	Left	0.0000	0.0071	0.0243	0.0336	No Damage
	Middle	0.0000	0.0071	0.0243	0.0336	No Damage
	Right	0.0000	0.0071	0.0243	0.0336	No Damage
P	Left	0.0339	0.0073	0.0246	0.0340	Collapse Prevention
	Middle	0.0309	0.0073	0.0246	0.0340	Collapse Prevention
	Right	0.0339	0.0073	0.0246	0.0340	Collapse Prevention
A2	Left	0.0424	0.0071	0.0243	0.0336	Excessive Damage
	Middle	0.0406	0.0071	0.0243	0.0336	Excessive Damage
	Right	0.0425	0.0071	0.0243	0.0336	Excessive Damage

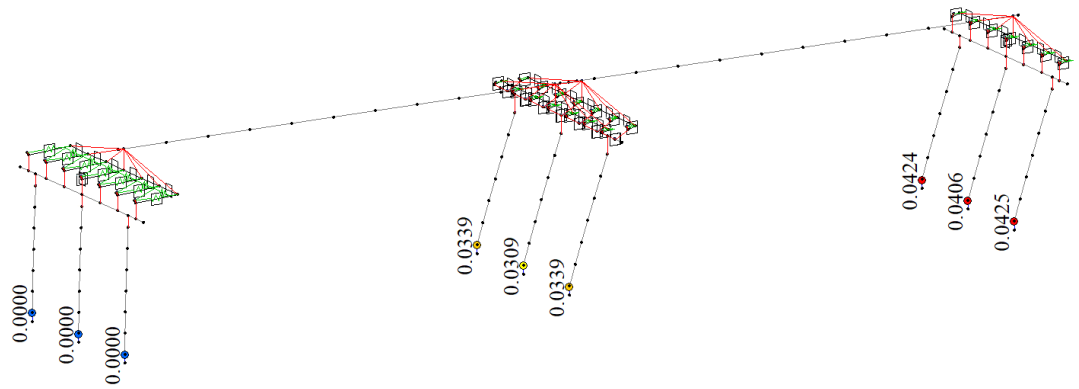

Figure B.12 Deformed shape and plastic rotation values (rad) for O13 Bridge at performance point in longitudinal pushover analysis

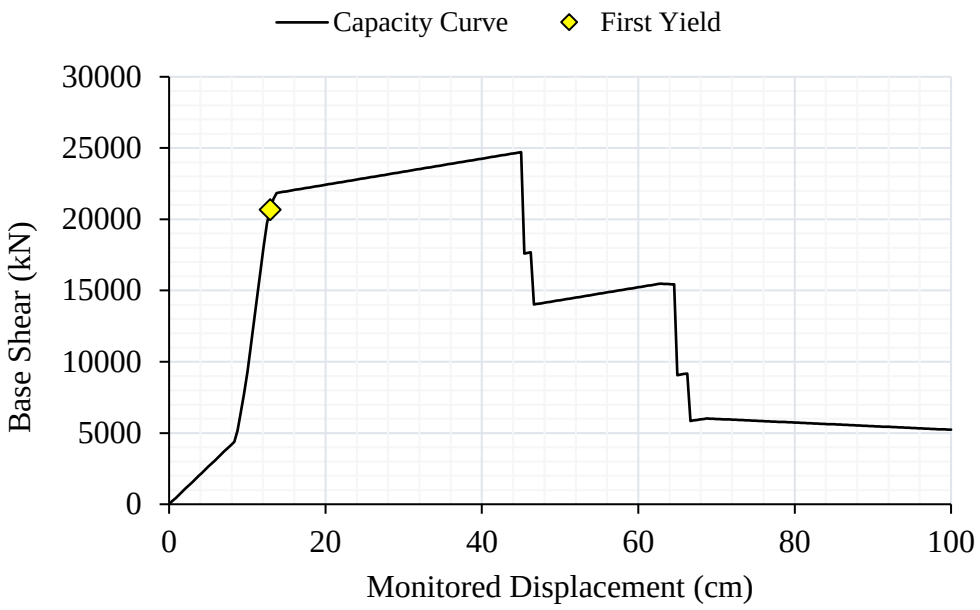

(a)

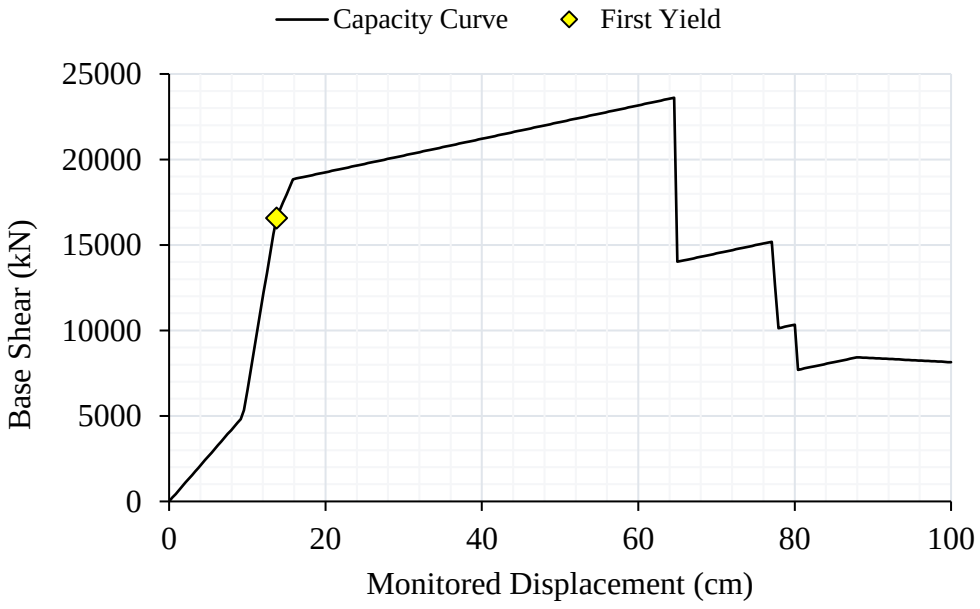

(b)

Figure B.13 Capacity curves for O15 Bridge in longitudinal pushover analysis: (a) A1-P-A2 pushover direction, (b) A2-P-A1 pushover direction

Table B.19 Yield forces of O15 Bridge found from Pushover Analysis (A1-P-A2 Direction)

Axis	Column Hinge	Pounding Step/Disp.	Yield Step/Disp.	P_y (kN)	V_y (kN)	M_y (kN·m)
A1	Left Column	-	151 / 62.9	1538	2472	18728
	Middle Column	-	151 / 62.9	1705	2471	18728
	Right Column	-	151 / 62.9	1544	2473	18728
P	Left Column	24 / 10.0	33 / 13.8	2661	3045	19300
	Middle Column	24 / 10.0	33 / 13.8	3011	3047	19300
	Right Column	24 / 10.0	33 / 13.8	2661	3051	19300
A2	Left Column	21 / 8.8	31 / 12.9	1536	3341	18683
	Middle Column	21 / 8.8	31 / 12.9	1772	3342	18683
	Right Column	21 / 8.8	31 / 12.9	1531	3344	18683

Table B.20 Yield forces of O15 Bridge found from Pushover Analysis (A2-P-A1 Direction)

Axis	Column Hinge	Pounding Step/Disp.	Yield Step/Disp.	P_y (kN)	V_y (kN)	M_y (kN·m)
A1	Left Column	23 / 9.6	39 / 16.3	1676	-2474	-18728
	Middle Column	23 / 9.6	39 / 16.3	1860	-2474	-18728
	Right Column	23 / 9.6	39 / 16.3	1670	-2476	-18728
P	Left Column	24 / 10.0	33 / 13.8	2683	-3038	-19300
	Middle Column	24 / 10.0	33 / 13.8	3038	-3039	-19300
	Right Column	24 / 10.0	33 / 13.8	2683	-3042	-19300
A2	Left Column	-	212 / 88.3	1338	-3334	-18683
	Middle Column	-	212 / 88.3	1536	-3335	-18683
	Right Column	-	212 / 88.3	1341	-3336	-18683

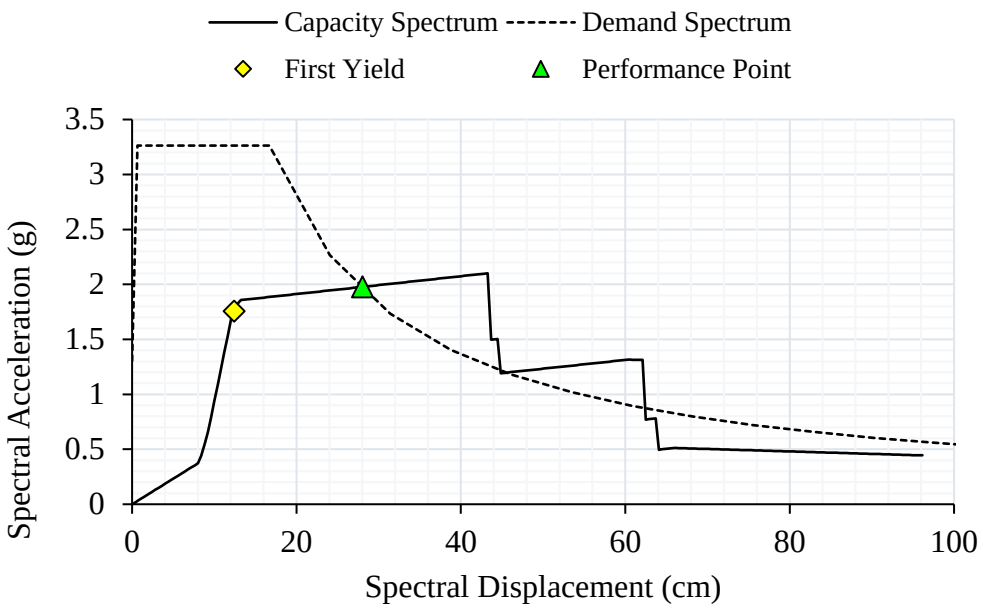

(a)

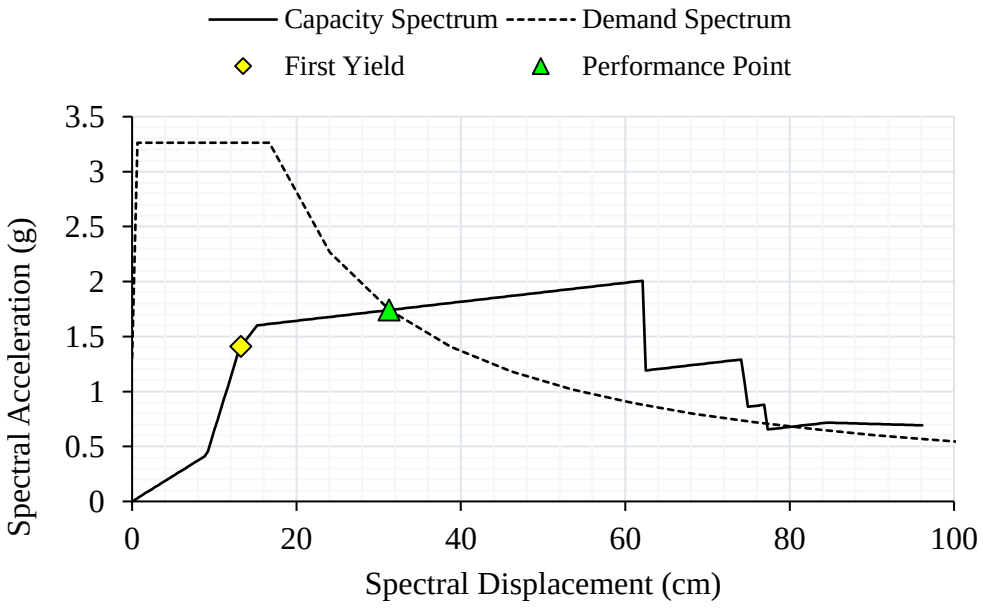

(b)

Figure B.14 Performance point determination for O15 Bridge in (a) A1-P-A2 Direction, (b) A2-P-A1 Direction

Table B.21 Performance point results of pushover analysis for O15 Bridge (A1-P-A2)

PO Results	A1 Columns			P Columns			A2 Columns		
	Left	**Middle**	**Right**	**Left**	**Middle**	**Right**	**Left**	**Middle**	**Right**
ϕ_y **(rad/m)**	0.0034	0.0034	0.0034	0.0034	0.0034	0.0034	0.0034	0.0034	0.0034
ϕ_p **(rad/m)**	0.0000	0.0000	0.0000	0.0171	0.0157	0.0172	0.0290	0.0278	0.0290
ϕ_u **(rad/m)**	0.0034	0.0034	0.0034	0.0205	0.0191	0.0206	0.0324	0.0312	0.0325
L **(m)**	8.000	8.000	8.000	6.800	6.800	6.800	6.000	6.000	6.000
L_p **(m)**	0.990	0.990	0.990	0.870	0.870	0.870	0.810	0.810	0.810
θ_y **(rad)**	0.0091	0.0091	0.0091	0.0077	0.0077	0.0077	0.0068	0.0068	0.0068
θ_p **(rad)**	0.0000	0.0000	0.0000	0.0149	0.0137	0.0150	0.0235	0.0226	0.0235
θ_c **(rad)**	0.0091	0.0091	0.0091	0.0226	0.0214	0.0226	0.0303	0.0294	0.0303
Δ_y **(m)**	0.073	0.073	0.073	0.052	0.052	0.052	0.041	0.041	0.041
Δ_{pd} **(m)**	0.000	0.000	0.000	0.095	0.087	0.095	0.131	0.126	0.132
Δ_{col} **(m)**	0.073	0.073	0.073	0.147	0.139	0.147	0.172	0.167	0.173
Δ **(%)**	0.913	0.913	0.913	2.165	2.049	2.168	2.870	2.785	2.876
μ_d	1.000	1.000	1.000	2.817	2.666	2.821	4.208	4.084	4.218
P_p **(kN)**	1619	1801	1627	2666	3018	2666	1558	1799	1552
V_p **(kN)**	1452	1460	1467	2995	2989	3001	3305	3300	3309
M_p **(kN·m)**	10903	10955	10992	19306	19305	19306	18692	18692	18692

Table B.22 Performance point results of pushover analysis for O15 Bridge (A2-P-A1)

PO Results	A1 Columns			P Columns			A2 Columns		
	Left	**Middle**	**Right**	**Left**	**Middle**	**Right**	**Left**	**Middle**	**Right**
ϕ_y **(rad/m)**	0.0034	0.0034	0.0034	0.0034	0.0034	0.0034	0.0034	0.0034	0.0034
ϕ_p **(rad/m)**	0.0158	0.0151	0.0158	0.0207	0.0189	0.0207	0.0000	0.0000	0.0000
ϕ_u **(rad/m)**	0.0192	0.0185	0.0193	0.0241	0.0223	0.0241	0.0034	0.0034	0.0034
L **(m)**	8.000	8.000	8.000	6.800	6.800	6.800	6.000	6.000	6.000
L_p **(m)**	0.990	0.990	0.990	0.870	0.870	0.870	0.810	0.810	0.810
θ_y **(rad)**	0.0091	0.0091	0.0091	0.0077	0.0077	0.0077	0.0068	0.0068	0.0068
θ_p **(rad)**	0.0156	0.0150	0.0157	0.0180	0.0165	0.0180	0.0000	0.0000	0.0000
θ_c **(rad)**	0.0248	0.0241	0.0248	0.0257	0.0242	0.0257	0.0068	0.0068	0.0068
Δ_y **(m)**	0.073	0.073	0.073	0.052	0.052	0.052	0.041	0.041	0.041
Δ_{pd} **(m)**	0.117	0.112	0.118	0.115	0.105	0.115	0.000	0.000	0.000
Δ_{col} **(m)**	0.190	0.185	0.191	0.167	0.157	0.167	0.041	0.041	0.041
Δ **(%)**	2.379	2.316	2.383	2.453	2.311	2.456	0.682	0.682	0.682
μ_d	2.607	2.538	2.611	3.193	3.008	3.196	1.000	1.000	1.000
P_p **(kN)**	1700	1887	1693	2682	3037	2682	1464	1691	1469
V_p **(kN)**	2446	2442	2448	2980	2971	2985	1392	1407	1416
M_p **(kN·m)**	18733	18733	18733	19307	19307	19307	7752	7820	7864

Table B.23 Performance evaluation of O15 Bridge in A1-P-A2 loading direction

Location	Column	θ_p (rad)	θ_p^{LD} (rad)	θ_p^{CD} (rad)	θ_p^{CP} (rad)	Performance Level
A1	Left	0.0000	0.0079	0.0268	0.0371	No Damage
	Middle	0.0000	0.0079	0.0268	0.0371	No Damage
	Right	0.0000	0.0079	0.0268	0.0371	No Damage
P	Left	0.0149	0.0067	0.0228	0.0315	Controlled Damage
	Middle	0.0137	0.0067	0.0228	0.0315	Controlled Damage
	Right	0.0150	0.0067	0.0228	0.0315	Controlled Damage
A2	Left	0.0235	0.0064	0.0217	0.0300	Collapse Prevention
	Middle	0.0225	0.0064	0.0217	0.0300	Collapse Prevention
	Right	0.0235	0.0064	0.0217	0.0300	Collapse Prevention

Table B.24 Performance evaluation of O15 Bridge in A2-P-A1 loading direction

Location	Column	θ_p (rad)	θ_p^{LD} (rad)	θ_p^{CD} (rad)	θ_p^{CP} (rad)	Performance Level
A1	Left	0.0156	0.0079	0.0268	0.0371	Controlled Damage
	Middle	0.0150	0.0079	0.0268	0.0371	Controlled Damage
	Right	0.0157	0.0079	0.0268	0.0371	Controlled Damage
P	Left	0.0180	0.0067	0.0228	0.0315	Controlled Damage
	Middle	0.0165	0.0067	0.0228	0.0315	Controlled Damage
	Right	0.0180	0.0067	0.0228	0.0315	Controlled Damage
A2	Left	0.0000	0.0064	0.0217	0.0300	No Damage
	Middle	0.0000	0.0064	0.0217	0.0300	No Damage
	Right	0.0000	0.0064	0.0217	0.0300	No Damage

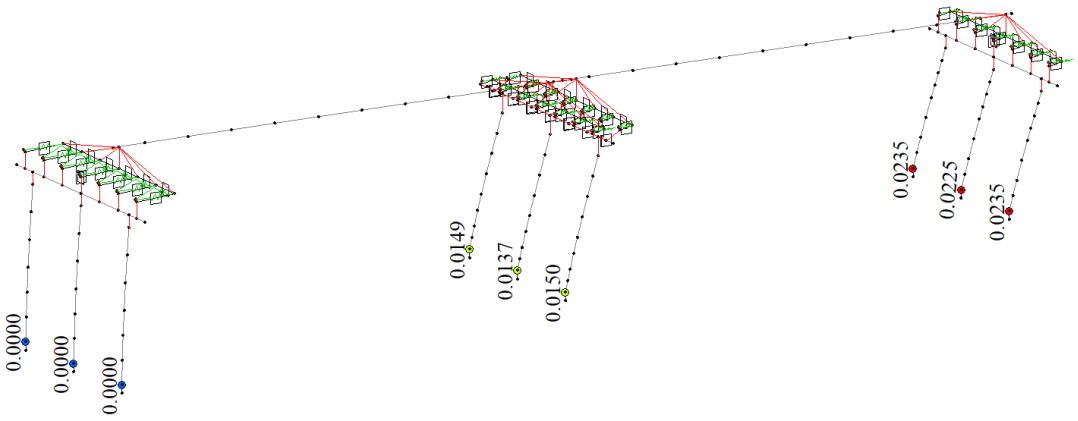

(a)

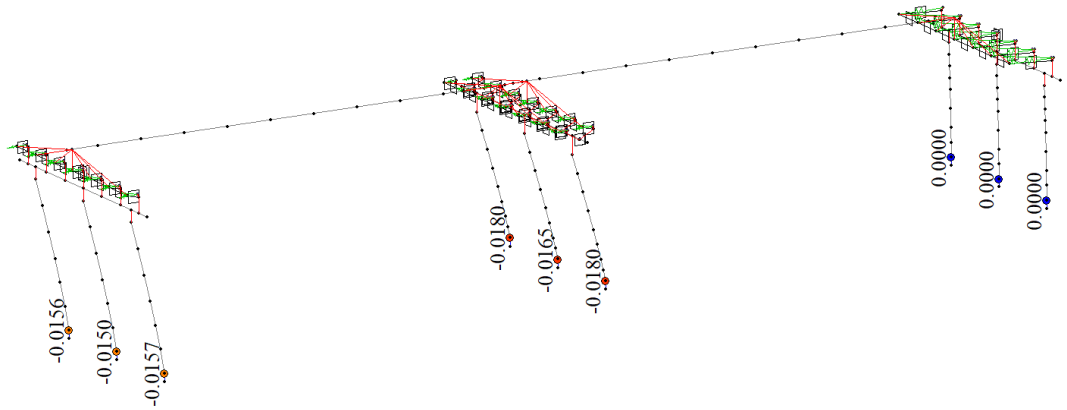

(b)

Figure B. 15 Deformed shape and plastic rotation values (rad) for O15 Bridge at performance point in longitudinal pushover analysis: (a) A1-P-A2 direction, (b) A2-P-A1 direction

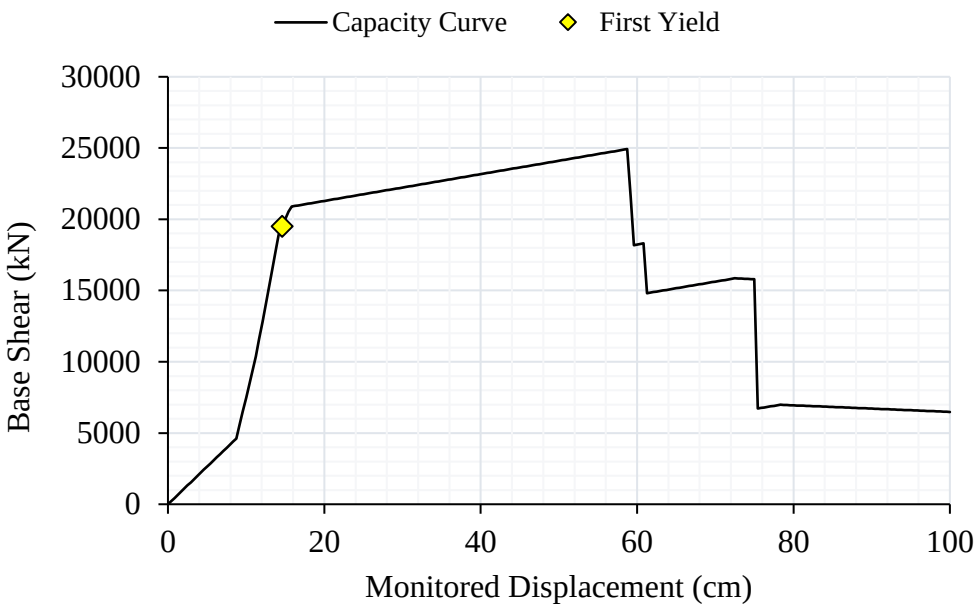

(a)

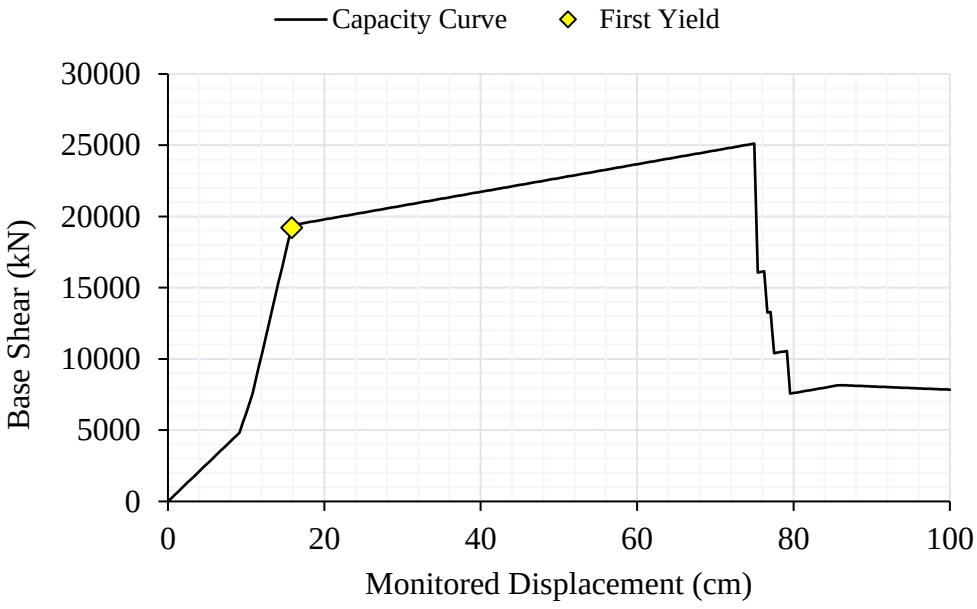

(b)

Figure B.16 Capacity curves for O48 Bridge in longitudinal pushover analysis: (a) A1-P-A2 pushover direction, (b) A2-P-A1 pushover direction

Table B.25 Yield forces of O48 Bridge found from Pushover Analysis (A1-P-A2 Direction)

Axis	Column Hinge	Pounding Step/Disp.	Yield Step/Disp.	P_y (kN)	V_y (kN)	M_y (kN·m)
A1	Left Column	-	174 / 72.5	1568	2802	21031
	Middle Column	-	174 / 72.5	1744	2803	21031
	Right Column	-	174 / 72.5	1577	2805	21031
P	Left Column	28 / 11.7	38 / 15.8	2823	2853	21332
	Middle Column	28 / 11.7	38 / 15.8	3136	2853	21332
	Right Column	28 / 11.7	38 / 15.8	2823	2857	21332
A2	Left Column	22 / 9.2	35 / 14.6	1639	3209	21012
	Middle Column	22 / 9.2	35 / 14.6	1852	3210	21012
	Right Column	22 / 9.2	35 / 14.6	1632	3212	21012

Table B.26 Yield forces of O48 Bridge found from Pushover Analysis (A2-P-A1 Direction)

Axis	Column Hinge	Pounding Step/Disp.	Yield Step/Disp.	P_y (kN)	V_y (kN)	M_y (kN·m)
A1	Left Column	23 / 9.6	39 / 16.3	1706	-2805	-21031
	Middle Column	23 / 9.6	39 / 16.3	1894	-2805	-21031
	Right Column	23 / 9.6	39 / 16.3	1698	-2807	-21031
P	Left Column	27 / 11.3	38 / 15.8	2830	-2850	-21332
	Middle Column	27 / 11.3	38 / 15.8	3144	-2851	-21332
	Right Column	27 / 11.3	38 / 15.8	2830	-2854	-21332
A2	Left Column	-	206 / 85.8	1472	-3203	-21012
	Middle Column	-	206 / 85.8	1659	-3204	-21012
	Right Column	-	206 / 85.8	1476	-3205	-21012

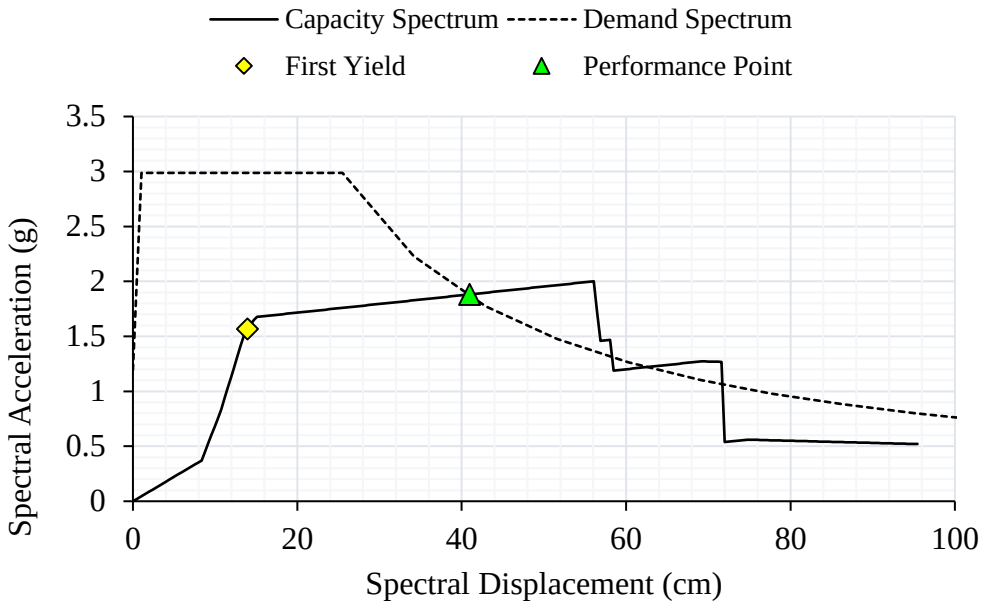

(a)

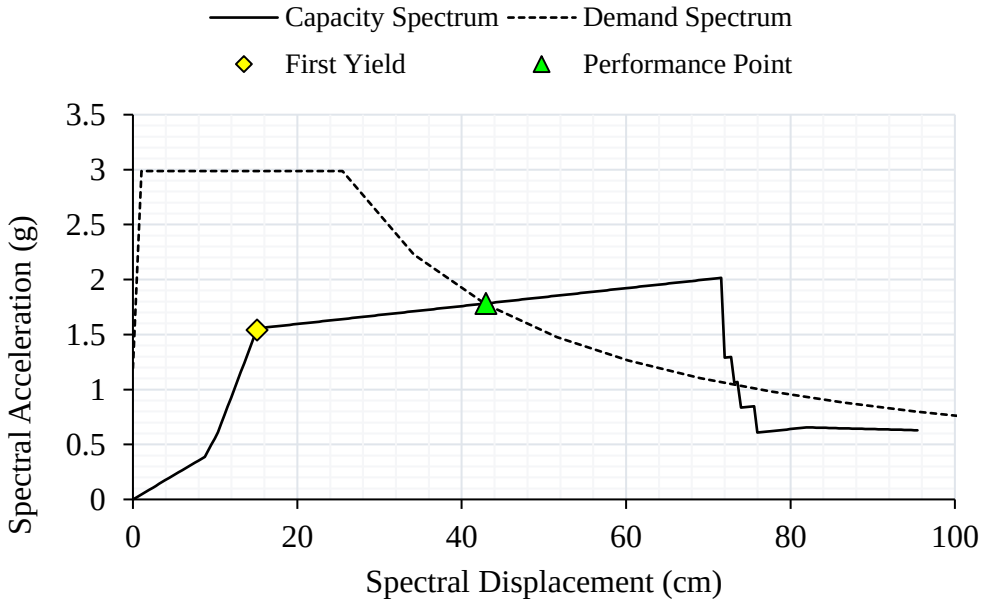

(b)

Figure B.17 Performance point determination for O48 Bridge in (a) A1-P-A2 Direction, (b) A2-P-A1 Direction

Table B.27 Performance point results of pushover analysis for O48 Bridge (A1-P-A2)

PO Results	A1 Columns			P Columns			A2 Columns		
	Left	**Middle**	**Right**	**Left**	**Middle**	**Right**	**Left**	**Middle**	**Right**
ϕ_y **(rad/m)**	0.0034	0.0034	0.0034	0.0034	0.0034	0.0034	0.0034	0.0034	0.0034
ϕ_p **(rad/m)**	0.0000	0.0000	0.0000	0.0216	0.0200	0.0217	0.0362	0.0347	0.0363
ϕ_u **(rad/m)**	0.0034	0.0034	0.0034	0.0250	0.0234	0.0251	0.0396	0.0381	0.0397
L **(m)**	8.000	8.000	8.000	8.000	8.000	8.000	7.000	7.000	7.000
L_p **(m)**	0.990	0.990	0.990	0.990	0.990	0.990	0.910	0.910	0.910
θ_y **(rad)**	0.0092	0.0092	0.0092	0.0091	0.0091	0.0091	0.0080	0.0080	0.0080
θ_p **(rad)**	0.0000	0.0000	0.0000	0.0214	0.0198	0.0214	0.0330	0.0316	0.0331
θ_c **(rad)**	0.0092	0.0092	0.0092	0.0305	0.0289	0.0305	0.0410	0.0396	0.0411
Δ_y **(m)**	0.073	0.073	0.073	0.073	0.073	0.073	0.056	0.056	0.056
Δ_{pd} **(m)**	0.000	0.000	0.000	0.161	0.148	0.161	0.216	0.207	0.216
Δ_{col} **(m)**	0.073	0.073	0.073	0.233	0.221	0.233	0.272	0.263	0.272
Δ **(%)**	0.915	0.915	0.915	2.915	2.763	2.918	3.881	3.753	3.891
μ_d	1.000	1.000	1.000	3.213	3.046	3.218	4.849	4.689	4.860
P_p **(kN)**	1631	1818	1642	2832	3146	2832	1671	1889	1662
V_p **(kN)**	1888	1898	1907	2773	2763	2778	3152	3144	3156
M_p **(kN·m)**	14093	14159	14205	21342	21341	21342	21025	21025	21025

Table B.28 Performance point results of pushover analysis for O48 Bridge (A2-P-A1)

PO Results	A1 Columns			P Columns			A2 Columns		
	Left	**Middle**	**Right**	**Left**	**Middle**	**Right**	**Left**	**Middle**	**Right**
ϕ_y **(rad/m)**	0.0034	0.0034	0.0034	0.0034	0.0034	0.0034	0.0034	0.0034	0.0034
ϕ_p **(rad/m)**	0.0271	0.0258	0.0272	0.0232	0.0214	0.0233	0.0000	0.0000	0.0000
ϕ_u **(rad/m)**	0.0306	0.0293	0.0307	0.0266	0.0248	0.0267	0.0034	0.0034	0.0034
L **(m)**	8.000	8.000	8.000	8.000	8.000	8.000	7.000	7.000	7.000
L_p **(m)**	0.990	0.990	0.990	0.990	0.990	0.990	0.910	0.910	0.910
θ_y **(rad)**	0.0092	0.0092	0.0092	0.0091	0.0091	0.0091	0.0080	0.0080	0.0080
θ_p **(rad)**	0.0269	0.0256	0.0270	0.0230	0.0212	0.0230	0.0000	0.0000	0.0000
θ_c **(rad)**	0.0360	0.0347	0.0361	0.0321	0.0303	0.0321	0.0080	0.0080	0.0080
Δ_y **(m)**	0.073	0.073	0.073	0.073	0.073	0.073	0.056	0.056	0.056
Δ_{pd} **(m)**	0.202	0.192	0.202	0.172	0.159	0.173	0.000	0.000	0.000
Δ_{col} **(m)**	0.275	0.265	0.275	0.245	0.232	0.245	0.056	0.056	0.056
Δ **(%)**	3.434	3.315	3.444	3.063	2.899	3.067	0.801	0.801	0.801
μ_d	3.752	3.622	3.762	3.377	3.196	3.381	1.000	1.000	1.000
P_p **(kN)**	1739	1932	1729	2840	3155	2840	1558	1764	1566
V_p **(kN)**	2753	2746	2756	2764	2754	2769	1883	1897	1906
M_p **(kN·m)**	21041	21041	21041	21343	21342	21343	12291	12368	12418

Table B.29 Performance evaluation of O48 Bridge in A1-P-A2 loading direction

Location	Column	θ_p (rad)	θ_p^{LD} (rad)	θ_p^{CD} (rad)	θ_p^{CP} (rad)	Performance Level
A1	Left	0.0000	0.0077	0.0262	0.0362	No Damage
	Middle	0.0000	0.0077	0.0262	0.0362	No Damage
	Right	0.0000	0.0077	0.0262	0.0362	No Damage
P	Left	0.0214	0.0060	0.0215	0.0300	Controlled Damage
	Middle	0.0198	0.0060	0.0215	0.0300	Controlled Damage
	Right	0.0214	0.0060	0.0215	0.0300	Controlled Damage
A2	Left	0.0329	0.0071	0.0241	0.0334	Collapse Prevention
	Middle	0.0316	0.0071	0.0241	0.0334	Collapse Prevention
	Right	0.0330	0.0071	0.0241	0.0334	Collapse Prevention

Table B.30 Performance evaluation of O48 Bridge in A2-P-A1 loading direction

Location	Column	θ_p (rad)	θ_p^{LD} (rad)	θ_p^{CD} (rad)	θ_p^{CP} (rad)	Performance Level
A1	Left	0.0269	0.0077	0.0262	0.0362	Collapse Prevention
	Middle	0.0256	0.0077	0.0262	0.0362	Controlled Damage
	Right	0.0269	0.0077	0.0262	0.0362	Collapse Prevention
P	Left	0.0230	0.0060	0.0215	0.0300	Collapse Prevention
	Middle	0.0212	0.0060	0.0215	0.0300	Controlled Damage
	Right	0.0230	0.0060	0.0215	0.0300	Collapse Prevention
A2	Left	0.0000	0.0071	0.0241	0.0334	No Damage
	Middle	0.0000	0.0071	0.0241	0.0334	No Damage
	Right	0.0000	0.0071	0.0241	0.0334	No Damage

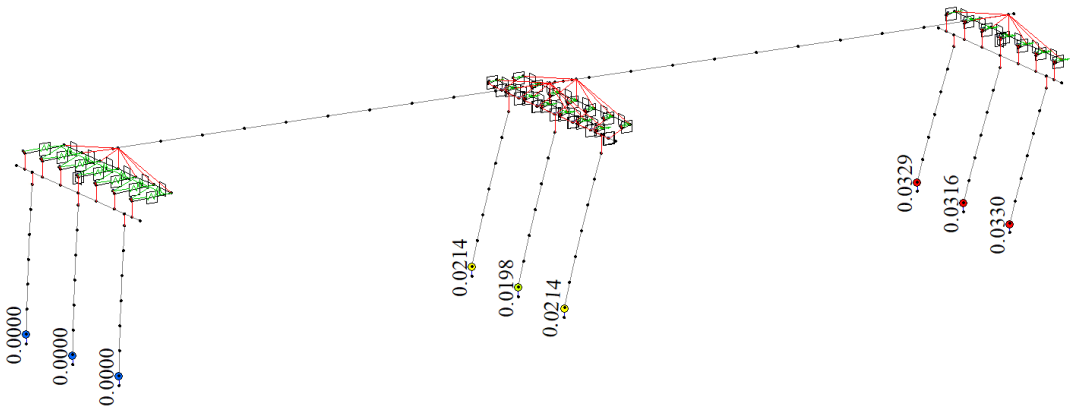

(a)

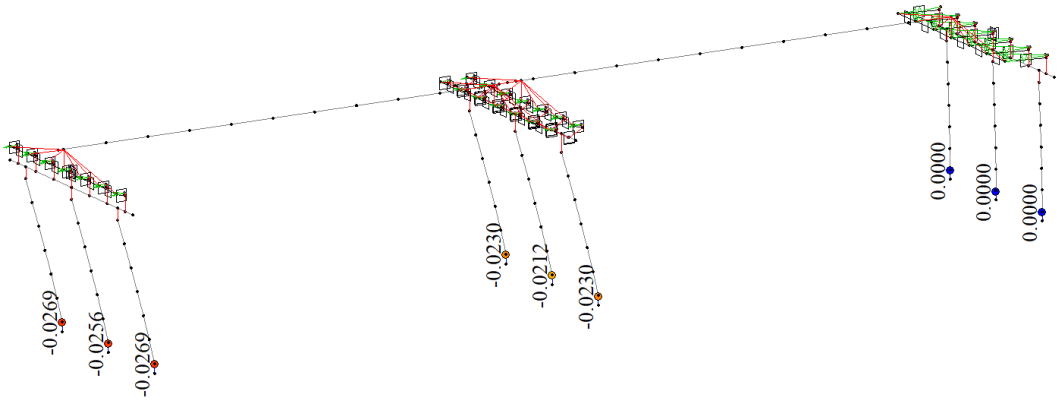

(b)

Figure B. 18 Deformed shape and plastic rotation values (rad) for O48 Bridge at performance point in longitudinal pushover analysis: (a) A1-P-A2 direction, (b) A2-P-A1 direction

C. Transversal Pushover Analysis Results

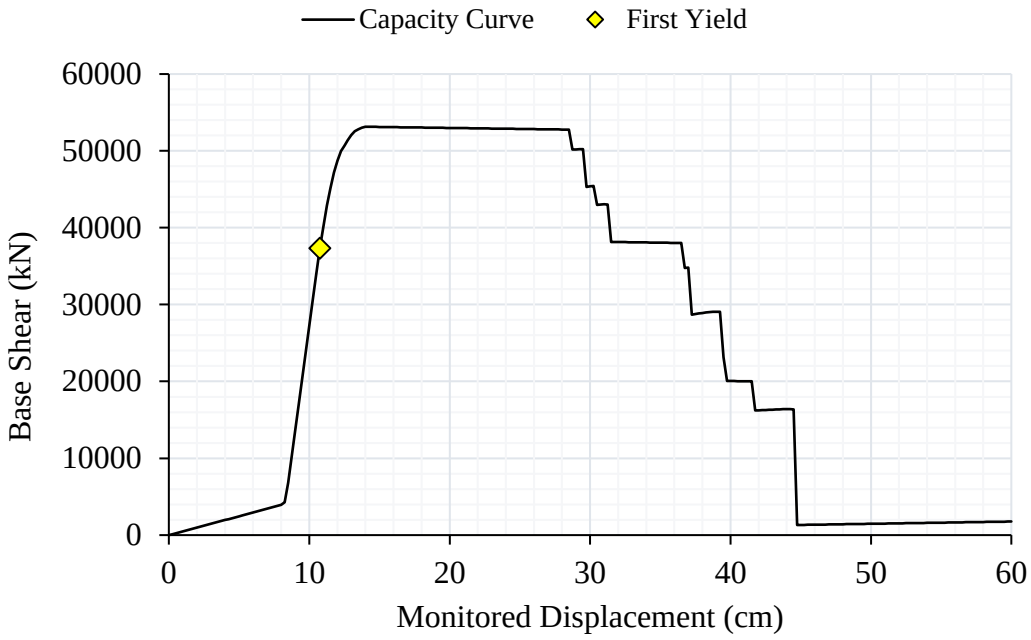

Figure C. 1 Capacity curve for O02 Bridge in transverse pushover analysis

Table C.1 Column yield forces for O02 Bridge from transverse pushover analysis

Axis	Column Hinge	Pounding Step/Disp.	Yield Step/Disp.	P_y (kN)	V_y (kN)	M_y (kN·m)
A1	**Left Column Bottom**	33/8.3	53/13.3	8174	-6581	-21693
	Middle Column Bottom		49/12.3	1874	-5823	-18508
	Right Column Bottom		47/11.8	-3825	-4658	-15253
	Left Column Top		56/14.0	7991	-6812	21633
	Middle Column Top		50/12.5	1478	-5794	18270
	Right Column Top		49/12.3	-4770	-4726	14716
P	**Left Column Bottom**	34/8.5	48/12.0	9823	-7058	-22287
	Middle Column Bottom		45/11.3	3213	-6083	-19271
	Right Column Bottom		43/10.8	-2964	-4972	-15757
	Left Column Top		48/12.0	9423	-6953	22138
	Middle Column Top		46/11.5	2814	-6003	19030
	Right Column Top		44/11.0	-3715	-4877	15317
A2	**Left Column Bottom**	33/8.3	53/13.3	8174	-6581	-21693
	Middle Column Bottom		49/12.3	1874	-5823	-18508
	Right Column Bottom		47/11.8	-3825	-4658	-15253
	Left Column Top		56/14.0	7991	-6812	21633
	Middle Column Top		50/12.5	1478	-5794	18270
	Right Column Top		49/12.3	-4770	-4726	14716

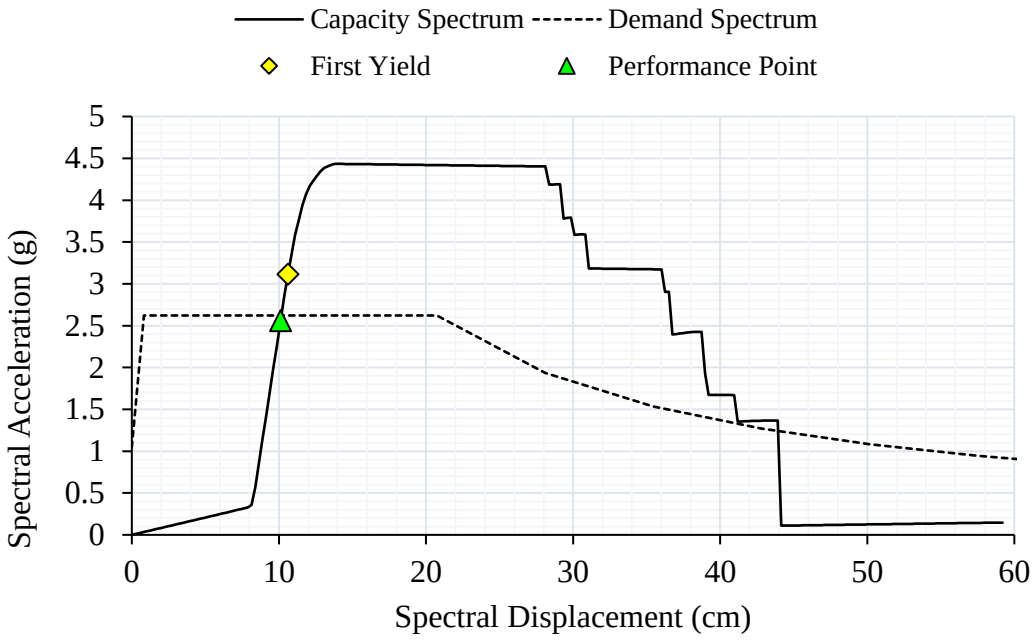

Figure C.2 Performance point determination of O02 Bridge

Table C.2 A1 Axis transverse pushover analysis results of O02 Bridge

PO Results	A1 Columns Bottom			A1 Columns Top		
	Left	**Middle**	**Right**	**Left**	**Middle**	**Right**
ϕ_y **(rad/m)**	-0.0037	-0.0033	-0.0030	0.0036	0.0033	0.0029
ϕ_p **(rad/m)**	0.0000	0.0000	0.0000	0.0000	0.0000	0.0000
ϕ_u **(rad/m)**	-0.0037	-0.0033	-0.0030	0.0036	0.0033	0.0029
L **(m)**	3.500	3.500	3.500	3.500	3.500	3.500
L_p **(m)**	0.710	0.710	0.710	0.710	0.710	0.710
θ_y **(rad)**	-0.0043	-0.0039	-0.0035	0.0042	0.0038	0.0034
θ_p **(rad)**	0.0000	0.0000	0.0000	0.0000	0.0000	0.0000
θ_c **(rad)**	-0.0043	-0.0039	-0.0035	0.0042	0.0038	0.0034
Δ_y **(m)**	-0.015	-0.014	-0.012	0.015	0.013	0.012
Δ_{pd} **(m)**	0.000	0.000	0.000	0.000	0.000	0.000
Δ_{col} **(m)**	-0.015	-0.014	-0.012	0.015	0.013	0.012
Δ **(%)**	0.427	0.389	0.346	0.422	0.384	0.341
μ_d	1.000	1.000	1.000	1.000	1.000	1.000
P_p **(kN)**	5039	1869	-1737	4639	1469	-2137
V_p **(kN)**	-2920	-3221	-2934	-2885	-3183	-2898
M_p **(kN·m)**	-9687	-10270	-9709	8665	9951	8687

Table C.3 P Axis transverse pushover analysis results of O02 Bridge

PO Results	A1 Columns Bottom			A1 Columns Top		
	Left	Middle	Right	Left	Middle	Right
ϕ_y (rad/m)	-0.0037	-0.0033	-0.0028	0.0037	0.0033	0.0028
ϕ_p (rad/m)	0.0000	0.0000	0.0000	0.0000	0.0000	0.0000
ϕ_u (rad/m)	-0.0037	-0.0033	-0.0028	0.0037	0.0033	0.0028
L (m)	3.500	3.500	3.500	3.500	3.500	3.500
L_p (m)	0.710	0.710	0.710	0.710	0.710	0.710
θ_y (rad)	-0.0044	-0.0039	-0.0033	0.0043	0.0038	0.0033
θ_p (rad)	0.0000	0.0000	0.0000	0.0000	0.0000	0.0000
θ_c (rad)	-0.0044	-0.0039	-0.0033	0.0043	0.0038	0.0033
Δ_y (m)	-0.015	-0.014	-0.012	0.015	0.013	0.011
Δ_{pd} (m)	0.000	0.000	0.000	0.000	0.000	0.000
Δ_{col} (m)	-0.015	-0.014	-0.012	0.015	0.013	0.011
Δ (%)	0.435	0.390	0.331	0.432	0.385	0.326
μ_d	1.000	1.000	1.000	1.000	1.000	1.000
P_p (kN)	7620	3213	-1930	7220	2813	-2330
V_p (kN)	-4138	-4233	-4156	-4072	-4166	-4089
M_p (kN·m)	-13266	-13446	-13284	12738	13121	12755

Table C.4 A2 Axis transverse pushover analysis results of O02 Bridge

PO Results	A1 Columns Bottom			A1 Columns Top		
	Left	**Middle**	**Right**	**Left**	**Middle**	**Right**
ϕ_y **(rad/m)**	-0.0037	-0.0033	-0.0030	0.0036	0.0033	0.0029
ϕ_p **(rad/m)**	0.0000	0.0000	0.0000	0.0000	0.0000	0.0000
ϕ_u **(rad/m)**	-0.0037	-0.0033	-0.0030	0.0036	0.0033	0.0029
L **(m)**	3.500	3.500	3.500	3.500	3.500	3.500
L_p **(m)**	0.710	0.710	0.710	0.710	0.710	0.710
θ_y **(rad)**	-0.0043	-0.0039	-0.0035	0.0042	0.0038	0.0034
θ_p **(rad)**	0.0000	0.0000	0.0000	0.0000	0.0000	0.0000
θ_c **(rad)**	-0.0043	-0.0039	-0.0035	0.0042	0.0038	0.0034
Δ_y **(m)**	-0.015	-0.014	-0.012	0.015	0.013	0.012
Δ_{pd} **(m)**	0.000	0.000	0.000	0.000	0.000	0.000
Δ_{col} **(m)**	-0.015	-0.014	-0.012	0.015	0.013	0.012
Δ **(%)**	0.427	0.389	0.346	0.422	0.384	0.341
μ_d	1.000	1.000	1.000	1.000	1.000	1.000
P_p **(kN)**	5039	1869	-1737	4639	1469	-2137
V_p **(kN)**	-2920	-3221	-2934	-2885	-3183	-2898
M_p **(kN·m)**	-9687	-10270	-9709	8665	9951	8687

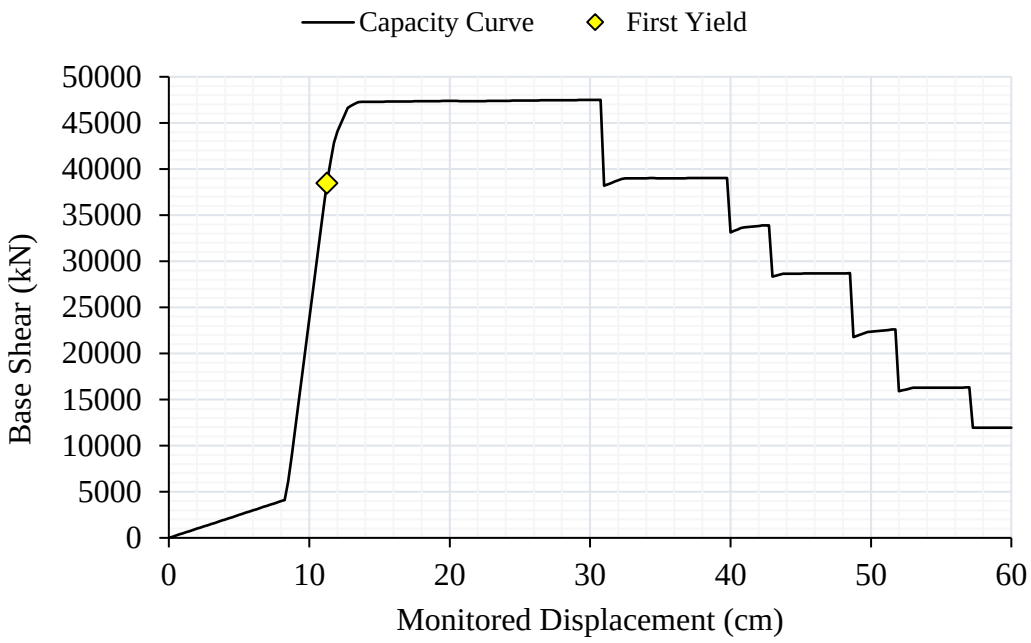

Figure C.3 Capacity curve for O05 Bridge in transverse pushover analysis

Table C.5 Column yield forces for O05 Bridge from transverse pushover analysis

Axis	Column Hinge	Pounding Step/Disp.	Yield Step/Disp.	P_y (kN)	V_y (kN)	M_y (kN·m)
A1	**Left Column Bottom**	34/8.5	51/12.8	8116	-5903	-21684
	Middle Column Bottom		48/12.0	1873	-5268	-18508
	Right Column Bottom		46/11.5	-3853	-4233	-15248
	Left Column Top		55/13.8	7895	-6105	21599
	Middle Column Top		48/12.0	1428	-5197	18242
	Right Column Top		47/11.8	-4639	-4252	14791
P	**Left Column Bottom**	35/8.8	51/12.8	9671	-6016	-22231
	Middle Column Bottom		48/12.0	3163	-5264	-19242
	Right Column Bottom		45/11.3	-2971	-4317	-15750
	Left Column Top		53/13.3	9263	-5930	22082
	Middle Column Top		48/12.0	2700	-5122	18965
	Right Column Top		45/11.3	-3435	-4193	15475
A2	**Left Column Bottom**	34/8.5	-	-	-	-
	Middle Column Bottom		107/26.8	1829	-5902	-18228
	Right Column Bottom		49/12.3	-3820	-4774	-15215
	Left Column Top		-	-	-	-
	Middle Column Top		-	-	-	-
	Right Column Top		110/27.5	-4727	-4886	14719

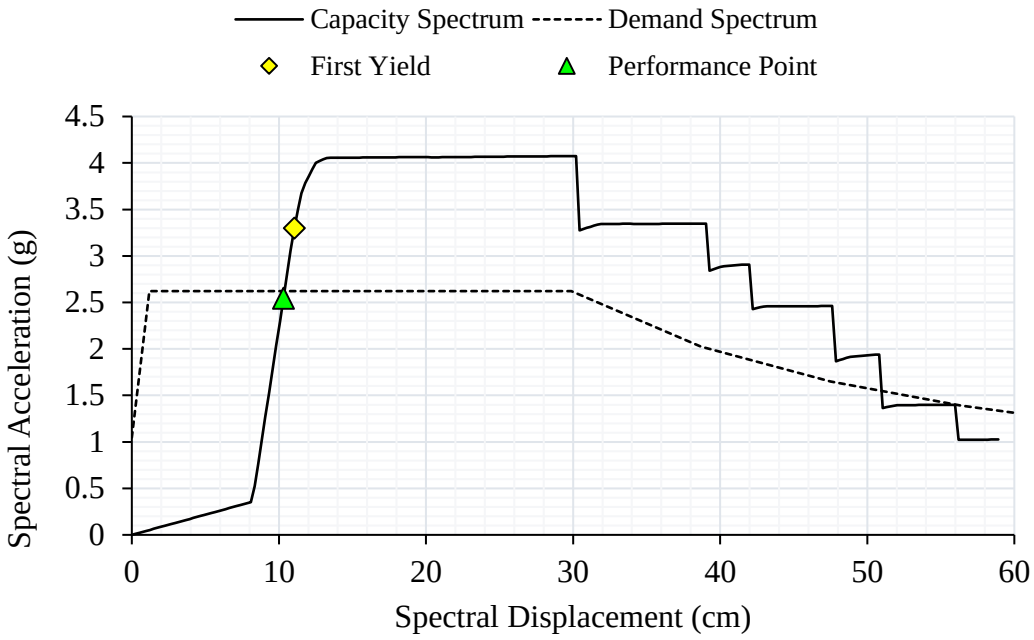

Figure C.4 Performance point determination of O05 Bridge

Table C.6 A1 Axis transverse pushover analysis results of O05 Bridge

PO Results	A1 Columns Bottom			A1 Columns Top		
	Left	**Middle**	**Right**	**Left**	**Middle**	**Right**
ϕ_y **(rad/m)**	-0.0037	-0.0033	-0.0029	0.0037	0.0033	0.0029
ϕ_p **(rad/m)**	0.0000	0.0000	0.0000	0.0000	0.0000	0.0000
ϕ_u **(rad/m)**	-0.0037	-0.0033	-0.0029	0.0037	0.0033	0.0029
L **(m)**	3.850	3.850	3.850	3.850	3.850	3.850
L_p **(m)**	0.710	0.710	0.710	0.710	0.710	0.710
θ_y **(rad)**	-0.0048	-0.0043	-0.0037	0.0047	0.0042	0.0037
θ_p **(rad)**	0.0000	0.0000	0.0000	0.0000	0.0000	0.0000
θ_c **(rad)**	-0.0048	-0.0043	-0.0037	0.0047	0.0042	0.0037
Δ_y **(m)**	-0.018	-0.016	-0.014	0.018	0.016	0.014
Δ_{pd} **(m)**	0.000	0.000	0.000	0.000	0.000	0.000
Δ_{col} **(m)**	-0.018	-0.016	-0.014	0.018	0.016	0.014
Δ **(%)**	0.478	0.428	0.373	0.472	0.422	0.367
μ_d	1.000	1.000	1.000	1.000	1.000	1.000
P_p **(kN)**	5641	1866	-2300	5196	1421	-2745
V_p **(kN)**	-3113	-3409	-3130	-3068	-3361	-3083
M_p **(kN·m)**	-11428	-12067	-11450	10314	11707	10335

Table C.7 P Axis transverse pushover analysis results of O05 Bridge

PO Results	P Columns Bottom			P Columns Top		
	Left	Middle	Right	Left	Middle	Right
ϕ_y (rad/m)	-0.0037	-0.0033	-0.0029	0.0037	0.0033	0.0028
ϕ_p (rad/m)	0.0000	0.0000	0.0000	0.0000	0.0000	0.0000
ϕ_u (rad/m)	-0.0037	-0.0033	-0.0029	0.0037	0.0033	0.0028
L (m)	4.000	4.000	4.000	4.000	4.000	4.000
L_p (m)	0.710	0.710	0.710	0.710	0.710	0.710
θ_y (rad)	-0.0050	-0.0045	-0.0038	0.0049	0.0044	0.0038
θ_p (rad)	0.0000	0.0000	0.0000	0.0000	0.0000	0.0000
θ_c (rad)	-0.0050	-0.0045	-0.0038	0.0049	0.0044	0.0038
Δ_y (m)	-0.020	-0.018	-0.015	0.020	0.018	0.015
Δ_{pd} (m)	0.000	0.000	0.000	0.000	0.000	0.000
Δ_{col} (m)	-0.020	-0.018	-0.015	0.020	0.018	0.015
Δ (%)	0.496	0.446	0.382	0.492	0.439	0.376
μ_d	1.000	1.000	1.000	1.000	1.000	1.000
P_p (kN)	7360	3163	-1664	6896	2699	-2128
V_p (kN)	-3434	-3505	-3452	-3340	-3409	-3356
M_p (kN·m)	-12730	-12883	-12745	12232	12552	12246

Table C.8 A2 Axis transverse pushover analysis results of O05 Bridge

PO Results	A2 Columns Bottom			A2 Columns Top		
	Left	**Middle**	**Right**	**Left**	**Middle**	**Right**
ϕ_y **(rad/m)**	-0.0037	-0.0033	-0.0029	0.0036	0.0033	0.0029
ϕ_p **(rad/m)**	0.0000	0.0000	0.0000	0.0000	0.0000	0.0000
ϕ_u **(rad/m)**	-0.0037	-0.0033	-0.0029	0.0036	0.0033	0.0029
L **(m)**	3.400	3.400	3.400	3.400	3.400	3.400
L_p **(m)**	0.710	0.710	0.710	0.710	0.710	0.710
θ_y **(rad)**	-0.0041	-0.0038	-0.0033	0.0041	0.0037	0.0033
θ_p **(rad)**	0.0000	0.0000	0.0000	0.0000	0.0000	0.0000
θ_c **(rad)**	-0.0041	-0.0038	-0.0033	0.0041	0.0037	0.0033
Δ_y **(m)**	-0.014	-0.013	-0.011	0.014	0.013	0.011
Δ_{pd} **(m)**	0.000	0.000	0.000	0.000	0.000	0.000
Δ_{col} **(m)**	-0.014	-0.013	-0.011	0.014	0.013	0.011
Δ **(%)**	0.415	0.378	0.334	0.411	0.373	0.330
μ_d	1.000	1.000	1.000	1.000	1.000	1.000
P_p **(kN)**	5109	1823	-1898	4722	1436	-2285
V_p **(kN)**	-3103	-3431	-3119	-3077	-3403	-3090
M_p **(kN·m)**	-9986	-10601	-10011	8913	10275	8937

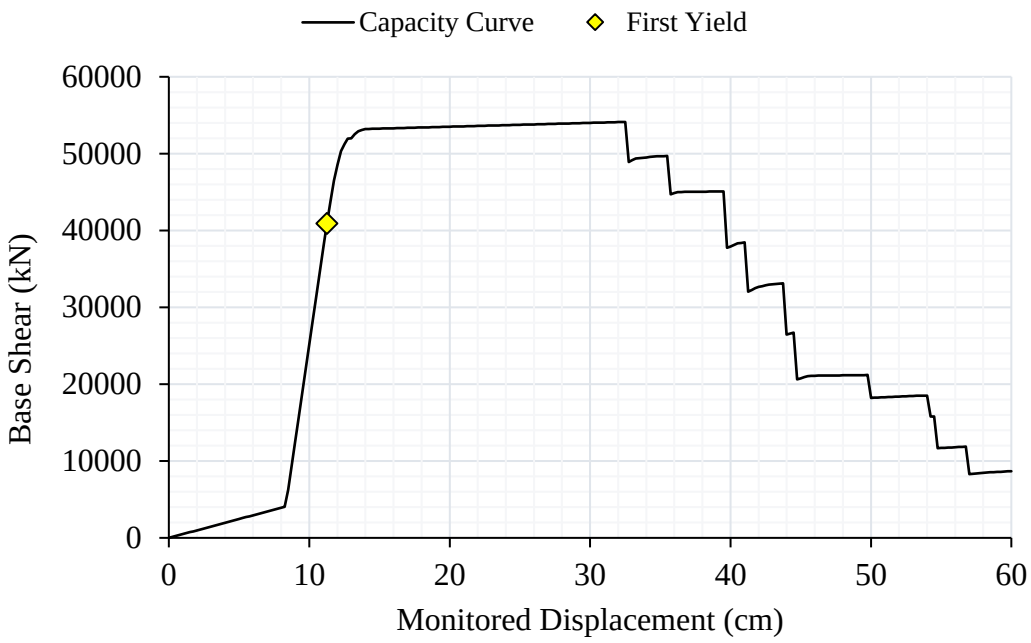

Figure C.5 Capacity curve for O07 Bridge in transverse pushover analysis

Table C.9 Column yield forces for O07 Bridge from transverse pushover analysis

Axis	Column Hinge	Pounding Step/Disp.	Yield Step/Disp.	P_y (kN)	V_y (kN)	M_y (kN·m)
A1	**Left Column Bottom**	34/8.5	-	-	-	-
	Middle Column Bottom		-	-	-	-
	Right Column Bottom		128/32.0	-3750	-5587	-14752
	Left Column Top		-	-	-	-
	Middle Column Top		-	-	-	-
	Right Column Top		-	-	-	-
P	**Left Column Bottom**	35/8.8	50/12.5	10410	-7376	-24040
	Middle Column Bottom		48/12.0	3132	-6699	-21455
	Right Column Bottom		45/11.25	-3587	-5430	-17686
	Left Column Top		52/13.0	10089	-7340	23980
	Middle Column Top		49/12.3	2724	-6553	21362
	Right Column Top		46/11.5	-4388	-5362	17294
A2	**Left Column Bottom**	34/8.5	54/13.5	8849	-6272	-23503
	Middle Column Bottom		50/12.5	1889	-5736	-20982
	Right Column Bottom		47/11.8	-4318	-4553	-17349
	Left Column Top		56/14.0	8515	-6329	23421
	Middle Column Top		50/12.5	1426	-5636	20697
	Right Column Top		49/12.3	-5454	-4603	16671

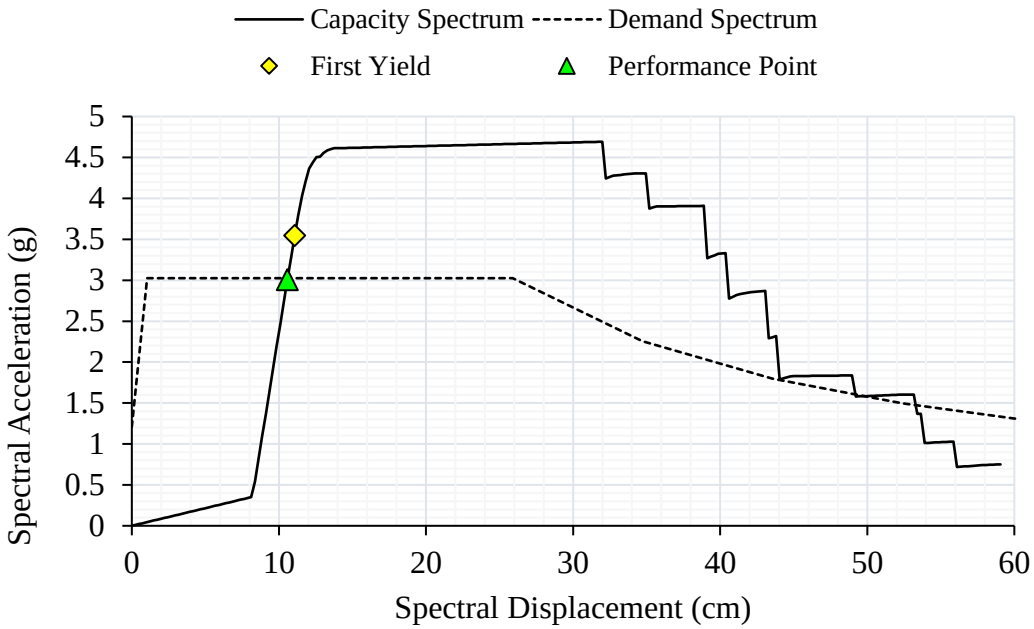

Figure C.6 Performance point determination of O07 Bridge

Table C.10 A1 Axis transverse pushover analysis results of O07 Bridge

PO Results	A1 Columns Bottom			A1 Columns Top		
	Left	**Middle**	**Right**	**Left**	**Middle**	**Right**
ϕ_y **(rad/m)**	-0.0036	-0.0034	-0.0031	0.0036	0.0034	0.0031
ϕ_p **(rad/m)**	0.0000	0.0000	0.0000	0.0000	0.0000	0.0000
ϕ_u **(rad/m)**	-0.0036	-0.0034	-0.0031	0.0036	0.0034	0.0031
L **(m)**	2.850	2.850	2.850	2.850	2.850	2.850
L_p **(m)**	0.710	0.710	0.710	0.710	0.710	0.710
θ_y **(rad)**	-0.0034	-0.0032	-0.0029	0.0034	0.0032	0.0029
θ_p **(rad)**	0.0000	0.0000	0.0000	0.0000	0.0000	0.0000
θ_c **(rad)**	-0.0034	-0.0032	-0.0029	0.0034	0.0032	0.0029
Δ_y **(m)**	-0.010	-0.009	-0.008	0.010	0.009	0.008
Δ_{pd} **(m)**	0.000	0.000	0.000	0.000	0.000	0.000
Δ_{col} **(m)**	-0.010	-0.009	-0.008	0.010	0.009	0.008
Δ **(%)**	0.338	0.325	0.290	0.340	0.322	0.291
μ_d	1.000	1.000	1.000	1.000	1.000	1.000
P_p **(kN)**	4623	1776	-1574	4305	1458	-1892
V_p **(kN)**	-3275	-3712	-3294	-3255	-3690	-3272
M_p **(kN·m)**	-8772	-9431	-8807	7566	9077	7600

Table C.11 P Axis transverse pushover analysis results of O07 Bridge

PO Results	P Columns Bottom			P Columns Top		
	Left	Middle	Right	Left	Middle	Right
ϕ_y (rad/m)	-0.0037	-0.0034	-0.0029	0.0037	0.0034	0.0029
ϕ_p (rad/m)	0.0000	0.0000	0.0000	0.0000	0.0000	0.0000
ϕ_u (rad/m)	-0.0037	-0.0034	-0.0029	0.0037	0.0034	0.0029
L (m)	3.550	3.550	3.550	3.550	3.550	3.550
L_p (m)	0.660	0.660	0.660	0.710	0.710	0.710
θ_y (rad)	-0.0043	-0.0040	-0.0034	0.0043	0.0040	0.0034
θ_p (rad)	0.0000	0.0000	0.0000	0.0000	0.0000	0.0000
θ_c (rad)	-0.0043	-0.0040	-0.0034	0.0043	0.0040	0.0034
Δ_y (m)	-0.015	-0.014	-0.012	0.015	0.014	0.012
Δ_{pd} (m)	0.000	0.000	0.000	0.000	0.000	0.000
Δ_{col} (m)	-0.015	-0.014	-0.012	0.015	0.014	0.012
Δ (%)	0.434	0.401	0.341	0.434	0.401	0.339
μ_d	1.000	1.000	1.000	1.000	1.000	1.000
P_p (kN)	8177	3131	-2617	7769	2723	-3025
V_p (kN)	-4631	-4746	-4655	-4532	-4645	-4554
M_p (kN·m)	-15233	-15458	-15259	14407	14875	14431

Table C.12 A2 Axis transverse pushover analysis results of O07 Bridge

PO Results	A2 Columns Bottom			A2 Columns Top		
	Left	**Middle**	**Right**	**Left**	**Middle**	**Right**
ϕ_y **(rad/m)**	-0.0037	-0.0034	-0.0030	0.0037	0.0034	0.0029
ϕ_p **(rad/m)**	0.0000	0.0000	0.0000	0.0000	0.0000	0.0000
ϕ_u **(rad/m)**	-0.0037	-0.0034	-0.0030	0.0037	0.0034	0.0029
L **(m)**	4.000	4.000	4.000	4.000	4.000	4.000
L_p **(m)**	0.710	0.710	0.710	0.710	0.710	0.710
θ_y **(rad)**	-0.0049	-0.0046	-0.0040	0.0049	0.0045	0.0039
θ_p **(rad)**	0.0000	0.0000	0.0000	0.0000	0.0000	0.0000
θ_c **(rad)**	-0.0049	-0.0046	-0.0040	0.0049	0.0045	0.0039
Δ_y **(m)**	-0.020	-0.018	-0.016	0.019	0.018	0.016
Δ_{pd} **(m)**	0.000	0.000	0.000	0.000	0.000	0.000
Δ_{col} **(m)**	-0.020	-0.018	-0.016	0.019	0.018	0.016
Δ **(%)**	0.491	0.457	0.398	0.487	0.450	0.392
μ_d	1.000	1.000	1.000	1.000	1.000	1.000
P_p **(kN)**	6103	1880	-2720	5639	1417	-3184
V_p **(kN)**	-3338	-3673	-3357	-3275	-3605	-3291
M_p **(kN·m)**	-12808	-13562	-12833	11478	13116	11501

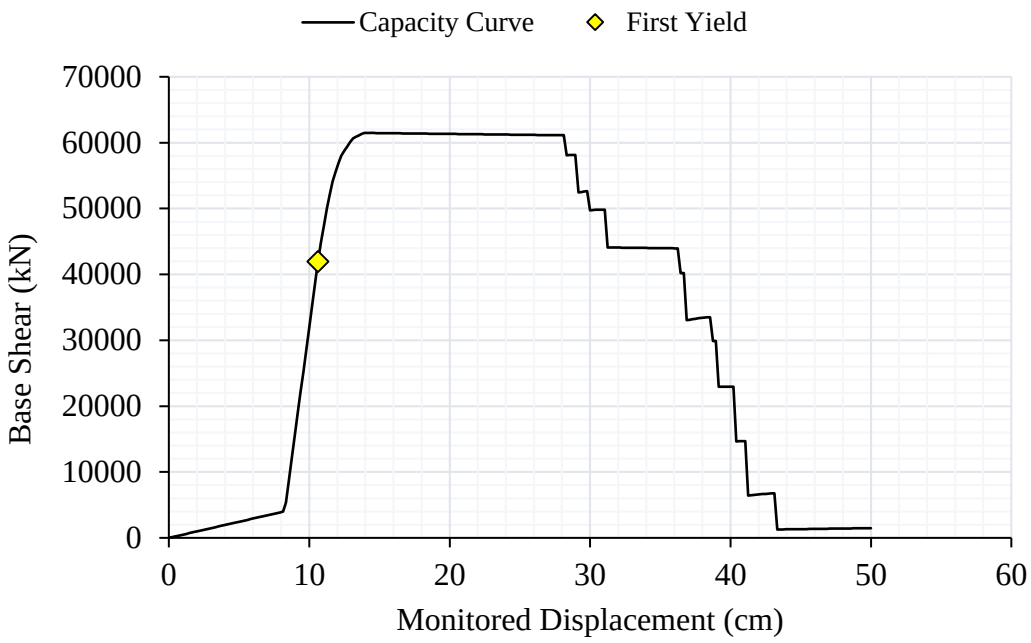

Figure C.7 Capacity curve for O13 Bridge in transverse pushover analysis

Table C.13 Column yield forces for O13 Bridge from transverse pushover analysis

Axis	Column Hinge	Pounding Step/Disp.	Yield Step/Disp.	P_y (kN)	V_y (kN)	M_y (kN·m)
A1	**Left Column Bottom**	40/8.3	63/13.1	8894	-7416	-23890
	Middle Column Bottom		59/12.3	1828	-6819	-21013
	Right Column Bottom		56/11.7	-4415	-5366	-17284
	Left Column Top		68/14.2	8791	-7761	23863
	Middle Column Top		60/12.5	1445	-6808	20773
	Right Column Top		59/12.3	-5582	-5524	16596
P	**Left Column Bottom**	41/8.5	56/11.7	10513	-7915	-24501
	Middle Column Bottom		54/11.3	3121	-7127	-21782
	Right Column Bottom		51/10.6	-3663	-5735	-17750
	Left Column Top		57/11.9	10201	-7914	24378
	Middle Column Top		54/11.3	2733	-7030	21538
	Right Column Top		52/10.8	-4424	-5692	17285
A2	**Left Column Bottom**	40/8.3	63/13.1	8894	-7416	-23890
	Middle Column Bottom		59/12.3	1828	-6819	-21013
	Right Column Bottom		56/11.7	-4415	-5366	-17284
	Left Column Top		68/14.2	8791	-7761	23863
	Middle Column Top		60/12.5	1445	-6808	20773
	Right Column Top		59/12.3	-5582	-5524	16596

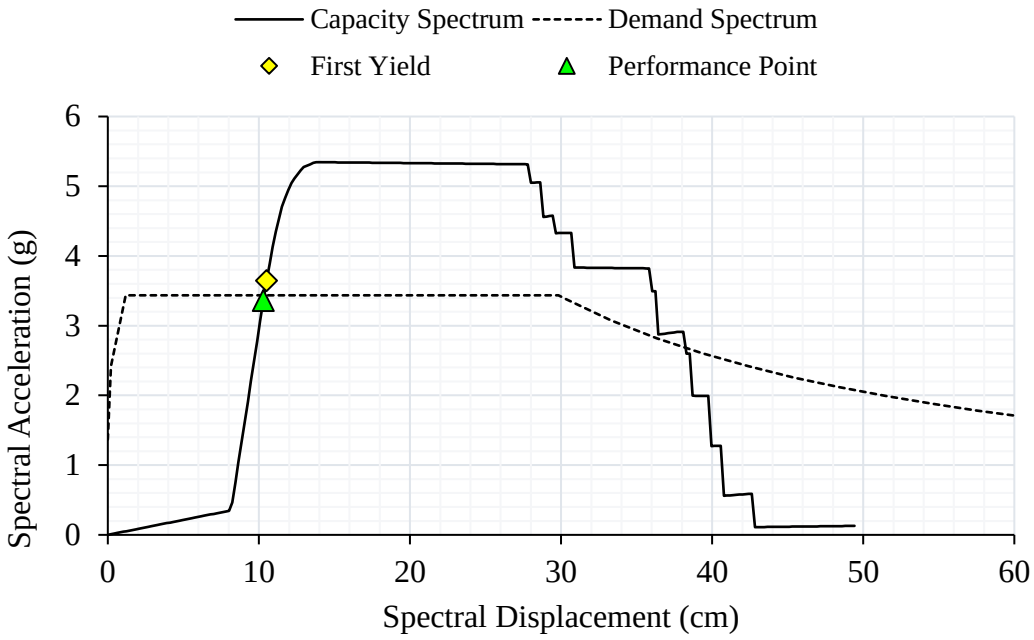

Figure C.8 Performance point determination of O13 Bridge

Table C.14 A1 Axis transverse pushover analysis results of O13 Bridge

PO Results	A1 Columns Bottom			A1 Columns Top		
	Left	**Middle**	**Right**	**Left**	**Middle**	**Right**
ϕ_y **(rad/m)**	-0.0038	-0.0035	-0.0030	0.0037	0.0034	0.0030
ϕ_p **(rad/m)**	0.0000	0.0000	0.0000	0.0000	0.0000	0.0000
ϕ_u **(rad/m)**	-0.0038	-0.0035	-0.0030	0.0037	0.0034	0.0030
L **(m)**	3.400	3.400	3.400	3.400	3.400	3.400
L_p **(m)**	0.710	0.710	0.710	0.710	0.710	0.710
θ_y **(rad)**	-0.0043	-0.0039	-0.0035	0.0042	0.0039	0.0034
θ_p **(rad)**	0.0000	0.0000	0.0000	0.0000	0.0000	0.0000
θ_c **(rad)**	-0.0043	-0.0039	-0.0035	0.0042	0.0039	0.0034
Δ_y **(m)**	-0.014	-0.013	-0.012	0.014	0.013	0.012
Δ_{pd} **(m)**	0.000	0.000	0.000	0.000	0.000	0.000
Δ_{col} **(m)**	-0.014	-0.013	-0.012	0.014	0.013	0.012
Δ **(%)**	0.426	0.394	0.345	0.423	0.389	0.341
μ_d	1.000	1.000	1.000	1.000	1.000	1.000
P_p **(kN)**	5700	1823	-2489	5312	1436	-2876
V_p **(kN)**	-3633	-4052	-3653	-3595	-4011	-3611
M_p **(kN·m)**	-11749	-12532	-11780	10362	12104	10392

Table C.15 P Axis transverse pushover analysis results of O13 Bridge

PO Results	P Columns Bottom			P Columns Top		
	Left	**Middle**	**Right**	**Left**	**Middle**	**Right**
ϕ_y **(rad/m)**	-0.0038	-0.0035	-0.0029	0.0038	0.0035	0.0029
ϕ_p **(rad/m)**	0.0000	0.0000	0.0000	0.0000	0.0000	0.0000
ϕ_u **(rad/m)**	-0.0038	-0.0035	-0.0029	0.0038	0.0035	0.0029
L **(m)**	3.400	3.400	3.400	3.400	3.400	3.400
L_p **(m)**	0.710	0.710	0.710	0.710	0.710	0.710
θ_y **(rad)**	-0.0043	-0.0040	-0.0033	0.0043	0.0039	0.0032
θ_p **(rad)**	0.0000	0.0000	0.0000	0.0000	0.0000	0.0000
θ_c **(rad)**	-0.0043	-0.0040	-0.0033	0.0043	0.0039	0.0032
Δ_y **(m)**	-0.015	-0.013	-0.011	0.015	0.013	0.011
Δ_{pd} **(m)**	0.000	0.000	0.000	0.000	0.000	0.000
Δ_{col} **(m)**	-0.015	-0.013	-0.011	0.015	0.013	0.011
Δ **(%)**	0.433	0.396	0.328	0.430	0.391	0.323
μ_d	1.000	1.000	1.000	1.000	1.000	1.000
P_p **(kN)**	8668	3120	-3158	8280	2732	-3546
V_p **(kN)**	-5274	-5411	-5300	-5201	-5336	-5225
M_p **(kN·m)**	-16411	-16662	-16438	15692	16228	15718

Table C.16 A2 Axis transverse pushover analysis results of O13 Bridge

PO Results	A2 Columns Bottom			A2 Columns Top		
	Left	**Middle**	**Right**	**Left**	**Middle**	**Right**
ϕ_y **(rad/m)**	-0.0038	-0.0035	-0.0030	0.0037	0.0034	0.0030
ϕ_p **(rad/m)**	0.0000	0.0000	0.0000	0.0000	0.0000	0.0000
ϕ_u **(rad/m)**	-0.0038	-0.0035	-0.0030	0.0037	0.0034	0.0030
L **(m)**	3.400	3.400	3.400	3.400	3.400	3.400
L_p **(m)**	0.710	0.710	0.710	0.710	0.710	0.710
θ_y **(rad)**	-0.0043	-0.0039	-0.0035	0.0042	0.0039	0.0034
θ_p **(rad)**	0.0000	0.0000	0.0000	0.0000	0.0000	0.0000
θ_c **(rad)**	-0.0043	-0.0039	-0.0035	0.0042	0.0039	0.0034
Δ_y **(m)**	-0.014	-0.013	-0.012	0.014	0.013	0.012
Δ_{pd} **(m)**	0.000	0.000	0.000	0.000	0.000	0.000
Δ_{col} **(m)**	-0.014	-0.013	-0.012	0.014	0.013	0.012
Δ **(%)**	0.426	0.394	0.345	0.423	0.389	0.341
μ_d	1.000	1.000	1.000	1.000	1.000	1.000
P_p **(kN)**	5700	1823	-2489	5312	1436	-2876
V_p **(kN)**	-3633	-4052	-3653	-3595	-4011	-3611
M_p **(kN·m)**	-11749	-12532	-11780	10362	12104	10392

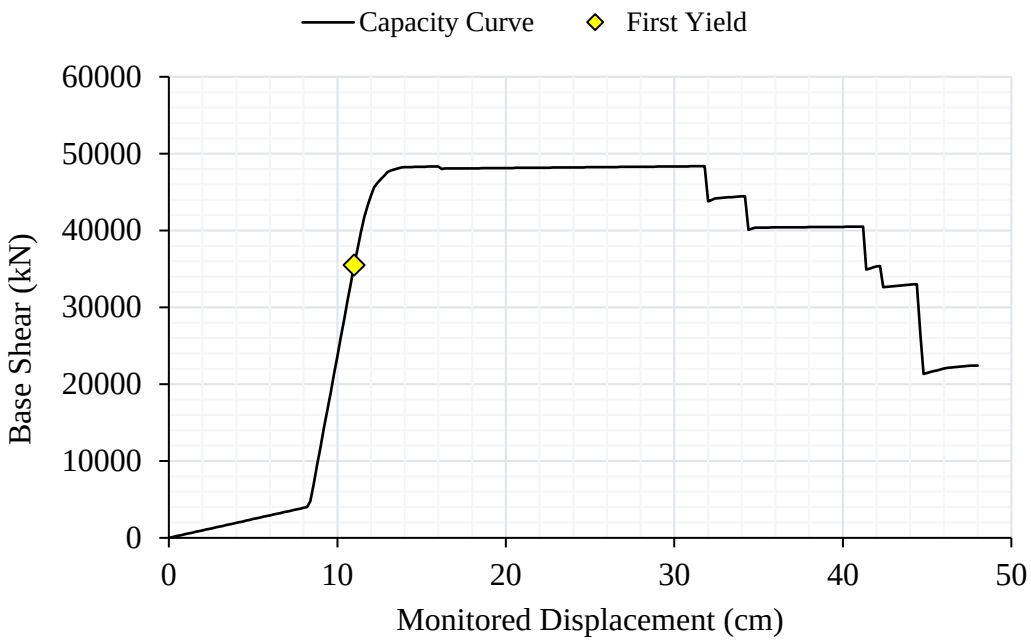

Figure C.9 Capacity curve for O15 Bridge in transverse pushover analysis

Table C.17 Column yield forces for O15 Bridge from transverse pushover analysis

Axis	Column Hinge	Pounding Step/Disp.	Yield Step/Disp.	P_y (kN)	V_y (kN)	M_y (kN·m)
A1	**Left Column Bottom**	42/8.4	66/13.2	8050	-5611	-21275
	Middle Column Bottom		61/12.2	1850	-5010	-18413
	Right Column Bottom		59/11.8	-3845	-4056	-15168
	Left Column Top		70/14.0	7756	-5725	21166
	Middle Column Top		62/12.4	1389	-4942	18138
	Right Column Top		61/12.2	-4748	-4033	14642
P	**Left Column Bottom**	43/8.6	61/12.2	9501	-6959	-21747
	Middle Column Bottom		58/11.6	3036	-6144	-19028
	Right Column Bottom		55/11.0	-2905	-5009	-15661
	Left Column Top		63/12.6	9208	-7004	21676
	Middle Column Top		59/11.8	2647	-6122	18854
	Right Column Top		56/11.2	-3608	-5010	15290
A2	**Left Column Bottom**	42/8.4	-	-	-	-
	Middle Column Bottom		-	-	-	-
	Right Column Bottom		-	-	-	-
	Left Column Top		-	-	-	-
	Middle Column Top		-	-	-	-
	Right Column Top		-	-	-	-

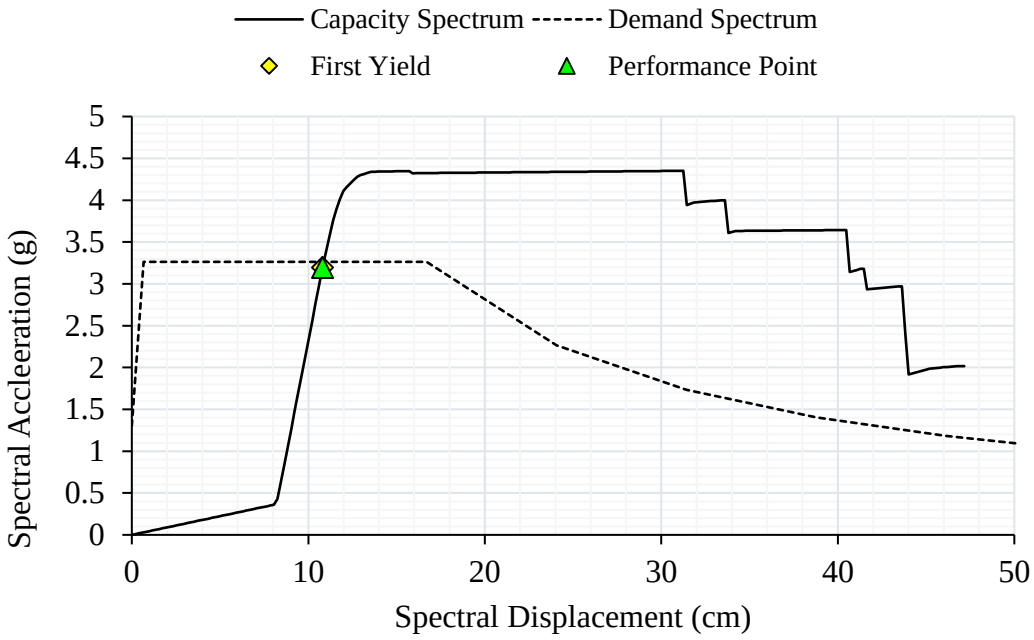

Figure C.10 Performance point determination of O15 Bridge

Table C.18 A1 Axis transverse pushover analysis results of O15 Bridge

PO Results	A1 Columns Bottom			A1 Columns Top		
	Left	**Middle**	**Right**	**Left**	**Middle**	**Right**
ϕ_y **(rad/m)**	-0.0038	-0.0034	-0.0029	0.0037	0.0033	0.0028
ϕ_p **(rad/m)**	0.0000	0.0000	0.0000	0.0000	0.0000	0.0000
ϕ_u **(rad/m)**	-0.0038	-0.0034	-0.0029	0.0037	0.0033	0.0028
L **(m)**	4.000	4.000	4.000	4.000	4.000	4.000
L_p **(m)**	0.710	0.710	0.710	0.710	0.710	0.710
θ_y **(rad)**	-0.0050	-0.0045	-0.0039	0.0050	0.0044	0.0038
θ_p **(rad)**	0.0000	0.0000	0.0000	0.0000	0.0000	0.0000
θ_c **(rad)**	-0.0050	-0.0045	-0.0039	0.0050	0.0044	0.0038
Δ_y **(m)**	-0.020	-0.018	-0.015	0.020	0.018	0.015
Δ_{pd} **(m)**	0.000	0.000	0.000	0.000	0.000	0.000
Δ_{col} **(m)**	-0.020	-0.018	-0.015	0.020	0.018	0.015
Δ **(%)**	0.501	0.449	0.385	0.497	0.442	0.379
μ_d	1.000	1.000	1.000	1.000	1.000	1.000
P_p **(kN)**	6037	1844	-2716	5573	1380	-3180
V_p **(kN)**	-3308	-3609	-3328	-3245	-3543	-3262
M_p **(kN·m)**	-12634	-13312	-12657	11444	12913	11465

Table C.19 P Axis transverse pushover analysis results of O15 Bridge

PO Results	P Columns Bottom			P Columns Top		
	Left	**Middle**	**Right**	**Left**	**Middle**	**Right**
ϕ_y **(rad/m)**	-0.0037	-0.0033	-0.0028	0.0038	0.0033	0.0027
ϕ_p **(rad/m)**	0.0000	0.0000	0.0000	0.0000	0.0000	0.0000
ϕ_u **(rad/m)**	-0.0037	-0.0033	-0.0028	0.0038	0.0033	0.0027
L **(m)**	3.400	3.400	3.400	3.400	3.400	3.400
L_p **(m)**	0.660	0.660	0.660	0.710	0.710	0.710
θ_y **(rad)**	-0.0042	-0.0038	-0.0031	0.0043	0.0038	0.0031
θ_p **(rad)**	0.0000	0.0000	0.0000	0.0000	0.0000	0.0000
θ_c **(rad)**	-0.0042	-0.0038	-0.0031	0.0043	0.0038	0.0031
Δ_y **(m)**	-0.014	-0.013	-0.011	0.014	0.013	0.011
Δ_{pd} **(m)**	0.000	0.000	0.000	0.000	0.000	0.000
Δ_{col} **(m)**	-0.014	-0.013	-0.011	0.014	0.013	0.011
Δ **(%)**	0.424	0.379	0.312	0.425	0.378	0.310
μ_d	1.000	1.000	1.002	1.000	1.000	1.000
P_p **(kN)**	8268	3035	-2905	7879	2646	-3294
V_p **(kN)**	-4986	-5104	-5009	-4921	-5037	-4942
M_p **(kN·m)**	-15650	-15869	-15661	14843	15298	14863

Table C.20 A2 Axis transverse pushover analysis results of O15 Bridge

PO Results	A2 Columns Bottom			A2 Columns Top		
	Left	**Middle**	**Right**	**Left**	**Middle**	**Right**
ϕ_y **(rad/m)**	-0.0036	-0.0033	-0.0030	0.0036	0.0033	0.0030
ϕ_p **(rad/m)**	0.0000	0.0000	0.0000	0.0000	0.0000	0.0000
ϕ_u **(rad/m)**	-0.0036	-0.0033	-0.0030	0.0036	0.0033	0.0030
L **(m)**	3.000	3.000	3.000	3.000	3.000	3.000
L_p **(m)**	0.660	0.660	0.660	0.660	0.660	0.660
θ_y **(rad)**	-0.0036	-0.0033	-0.0030	0.0036	0.0033	0.0030
θ_p **(rad)**	0.0000	0.0000	0.0000	0.0000	0.0000	0.0000
θ_c **(rad)**	-0.0036	-0.0033	-0.0030	0.0036	0.0033	0.0030
Δ_y **(m)**	-0.011	-0.010	-0.009	0.011	0.010	0.009
Δ_{pd} **(m)**	0.000	0.000	0.000	0.000	0.000	0.000
Δ_{col} **(m)**	-0.011	-0.010	-0.009	0.011	0.010	0.009
Δ **(%)**	0.363	0.334	0.296	0.365	0.333	0.297
μ_d	1.000	1.000	1.000	1.000	1.000	1.000
P_p **(kN)**	4765	1752	-1729	4427	1414	-2067
V_p **(kN)**	-3263	-3641	-3280	-3239	-3615	-3255
M_p **(kN·m)**	-9270	-9889	-9300	8071	9446	8100

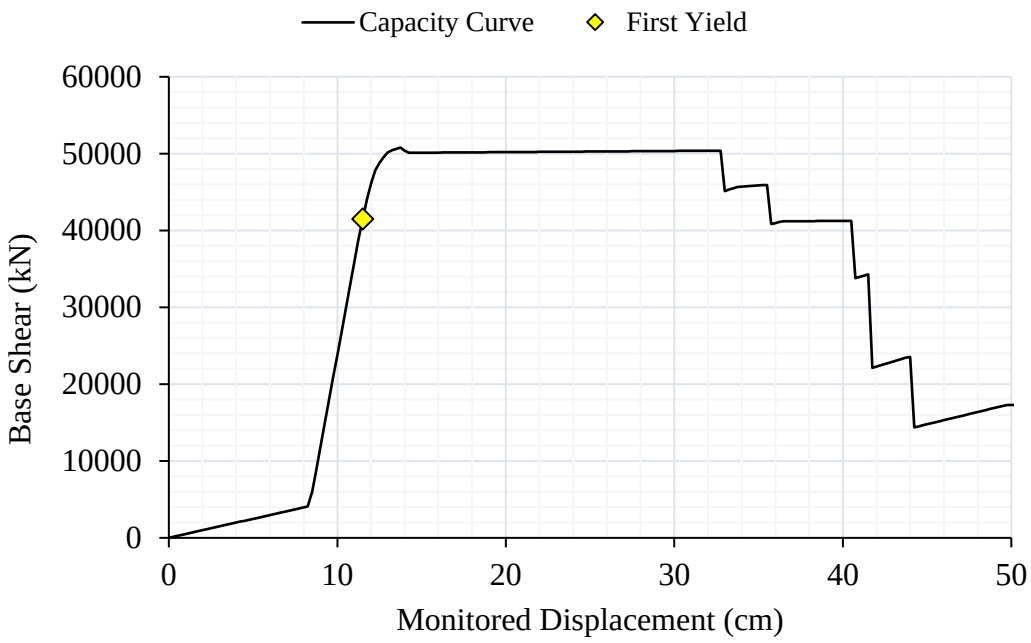

Figure C.11 Capacity curve for O48 Bridge in transverse pushover analysis

Table C.21 Column yield forces for O48 Bridge from transverse pushover analysis

Axis	Column Hinge	Pounding Step/Disp.	Yield Step/Disp.	P_y (kN)	V_y (kN)	M_y (kN·m)
A1	**Left Column Bottom**	34/8.5	53/13.3	8890	-6195	-23542
	Middle Column Bottom		49/12.3	1885	-5680	-20980
	Right Column Bottom		47/11.8	-4335	-4551	-17337
	Left Column Top		56/14	8645	-6354	23460
	Middle Column Top		50/12.5	1426	-5649	20697
	Right Column Top		49/12.3	-5467	-4614	16664
P	**Left Column Bottom**	35/8.8	51/12.8	10357	-6465	-23806
	Middle Column Bottom		48/12	3163	-5814	-21240
	Right Column Bottom		46/11.5	-3718	-4818	-17574
	Left Column Top		52/13	9932	-6361	23649
	Middle Column Top		49/12.3	2700	-5682	21067
	Right Column Top		46/11.5	-4182	-4693	17294
A2	**Left Column Bottom**	34/8.5	-	-	-	-
	Middle Column Bottom		-	-	-	-
	Right Column Bottom		51/12.8	-4432	-5201	-17220
	Left Column Top		-	-	-	-
	Middle Column Top		57/14.3	1254	-6366	20597
	Right Column Top		56/14.0	-5322	-5370	16748

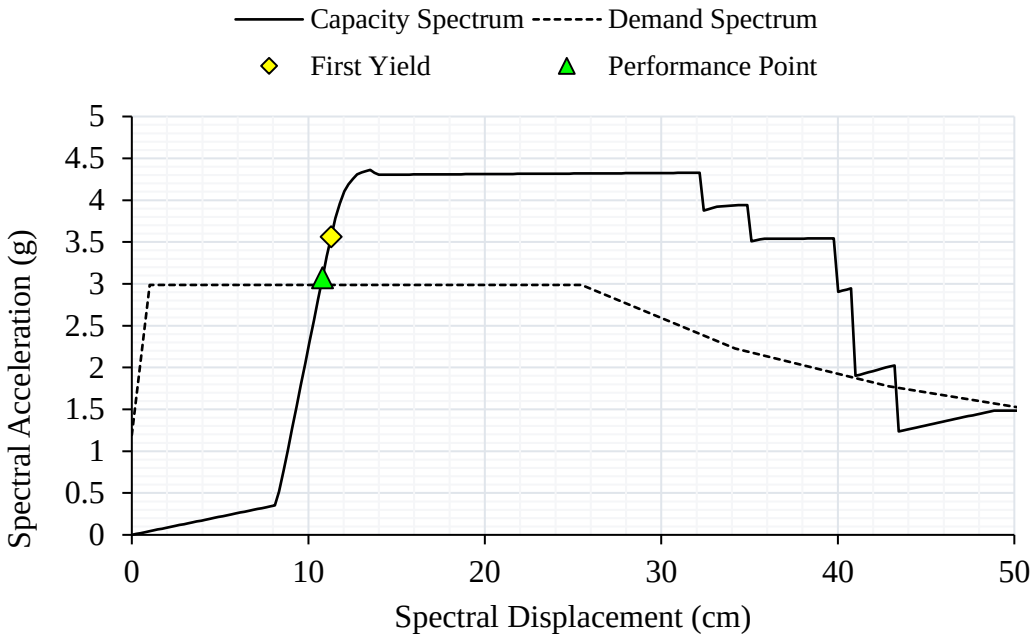

Figure C.12 Performance point determination of O48 Bridge

Table C.22 A1 Axis transverse pushover analysis results of O48 Bridge

PO Results	A1 Columns Bottom			A1 Columns Top		
	Left	**Middle**	**Right**	**Left**	**Middle**	**Right**
ϕ_y **(rad/m)**	-0.0037	-0.0034	-0.0029	0.0037	0.0034	0.0029
ϕ_p **(rad/m)**	0.0000	0.0000	0.0000	0.0000	0.0000	0.0000
ϕ_u **(rad/m)**	-0.0037	-0.0034	-0.0029	0.0037	0.0034	0.0029
L **(m)**	4.000	4.000	4.000	4.000	4.000	4.000
L_p **(m)**	0.710	0.710	0.710	0.710	0.710	0.710
θ_y **(rad)**	-0.0049	-0.0046	-0.0039	0.0049	0.0045	0.0039
θ_p **(rad)**	0.0000	0.0000	0.0000	0.0000	0.0000	0.0000
θ_c **(rad)**	-0.0049	-0.0046	-0.0039	0.0049	0.0045	0.0039
Δ_y **(m)**	-0.020	-0.018	-0.016	0.020	0.018	0.015
Δ_{pd} **(m)**	0.000	0.000	0.000	0.000	0.000	0.000
Δ_{col} **(m)**	-0.020	-0.018	-0.016	0.020	0.018	0.015
Δ **(%)**	0.494	0.457	0.393	0.491	0.450	0.386
μ_d	1.000	1.000	1.000	1.000	1.000	1.000
P_p **(kN)**	6519	1881	-3137	6055	1417	-3600
V_p **(kN)**	-3645	-4012	-3668	-3590	-3952	-3609
M_p **(kN·m)**	-13998	-14823	-14026	12557	14350	12582

Table C.23 P Axis transverse pushover analysis results of O48 Bridge

PO Results	P Columns Bottom			P Columns Top		
	Left	**Middle**	**Right**	**Left**	**Middle**	**Right**
ϕ_y **(rad/m)**	-0.0037	-0.0034	-0.0029	0.0037	0.0034	0.0028
ϕ_p **(rad/m)**	0.0000	0.0000	0.0000	0.0000	0.0000	0.0000
ϕ_u **(rad/m)**	-0.0037	-0.0034	-0.0029	0.0037	0.0034	0.0028
L **(m)**	4.000	4.000	4.000	4.000	4.000	4.000
L_p **(m)**	0.710	0.710	0.710	0.710	0.710	0.710
θ_y **(rad)**	-0.0049	-0.0045	-0.0038	0.0049	0.0045	0.0038
θ_p **(rad)**	0.0000	0.0000	0.0000	0.0000	0.0000	0.0000
θ_c **(rad)**	-0.0049	-0.0045	-0.0038	0.0049	0.0045	0.0038
Δ_y **(m)**	-0.020	-0.018	-0.015	0.020	0.018	0.015
Δ_{pd} **(m)**	0.000	0.000	0.000	0.000	0.000	0.000
Δ_{col} **(m)**	-0.020	-0.018	-0.015	0.020	0.018	0.015
Δ **(%)**	0.492	0.452	0.384	0.489	0.448	0.378
μ_d	1.000	1.000	1.000	1.000	1.000	1.000
P_p **(kN)**	8540	3163	-2845	8077	2699	-3309
V_p **(kN)**	-4329	-4427	-4354	-4223	-4319	-4247
M_p **(kN·m)**	-16077	-16287	-16100	15416	15855	15437

Table C.24 A2 Axis transverse pushover analysis results of O48 Bridge

PO Results	A2 Columns Bottom			A2 Columns Top		
	Left	**Middle**	**Right**	**Left**	**Middle**	**Right**
ϕ_y **(rad/m)**	-0.0037	-0.0034	-0.0030	0.0036	0.0034	0.0030
ϕ_p **(rad/m)**	0.0000	0.0000	0.0000	0.0000	0.0000	0.0000
ϕ_u **(rad/m)**	-0.0037	-0.0034	-0.0030	0.0036	0.0034	0.0030
L **(m)**	3.500	3.500	3.500	3.500	3.500	3.500
L_p **(m)**	0.710	0.710	0.710	0.710	0.710	0.710
θ_y **(rad)**	-0.0043	-0.0040	-0.0035	0.0043	0.0039	0.0034
θ_p **(rad)**	0.0000	0.0000	0.0000	0.0000	0.0000	0.0000
θ_c **(rad)**	-0.0043	-0.0040	-0.0035	0.0043	0.0039	0.0034
Δ_y **(m)**	-0.015	-0.014	-0.012	0.015	0.014	0.012
Δ_{pd} **(m)**	0.000	0.000	0.000	0.000	0.000	0.000
Δ_{col} **(m)**	-0.015	-0.014	-0.012	0.015	0.014	0.012
Δ **(%)**	0.427	0.399	0.349	0.425	0.394	0.345
μ_d	1.000	1.000	1.000	1.000	1.000	1.000
P_p **(kN)**	5844	1832	-2603	5443	1432	-3003
V_p **(kN)**	-3636	-4045	-3656	-3605	-4011	-3622
M_p **(kN·m)**	-12130	-12921	-12161	10744	12495	10772

D. Ground Motion Acceleration Figures and Fibers Strain Results for Confined Concrete and Reinforcement

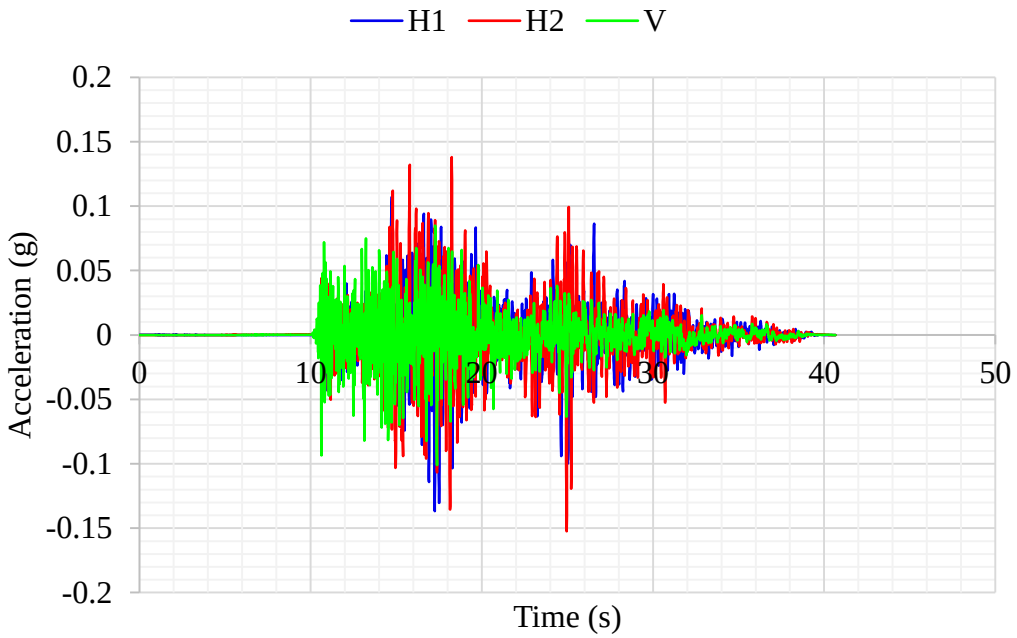

Figure D.1 RSN1612 Ground motion acceleration versus time graph

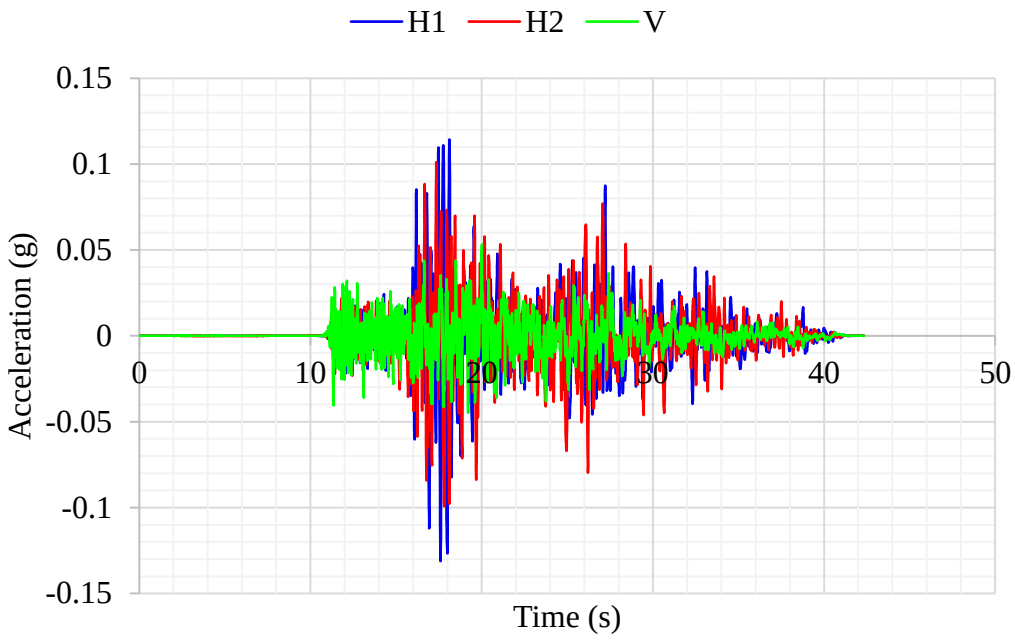

Figure D.2 RSN1614 Ground motion acceleration versus time graph

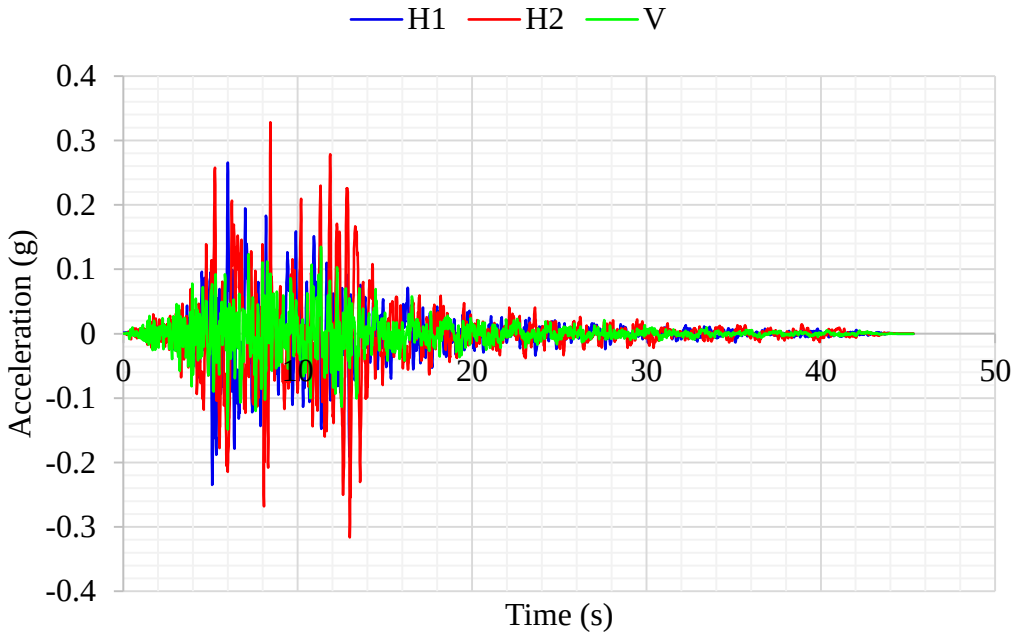

Figure D.3 RSN1787 Ground motion acceleration versus time graph

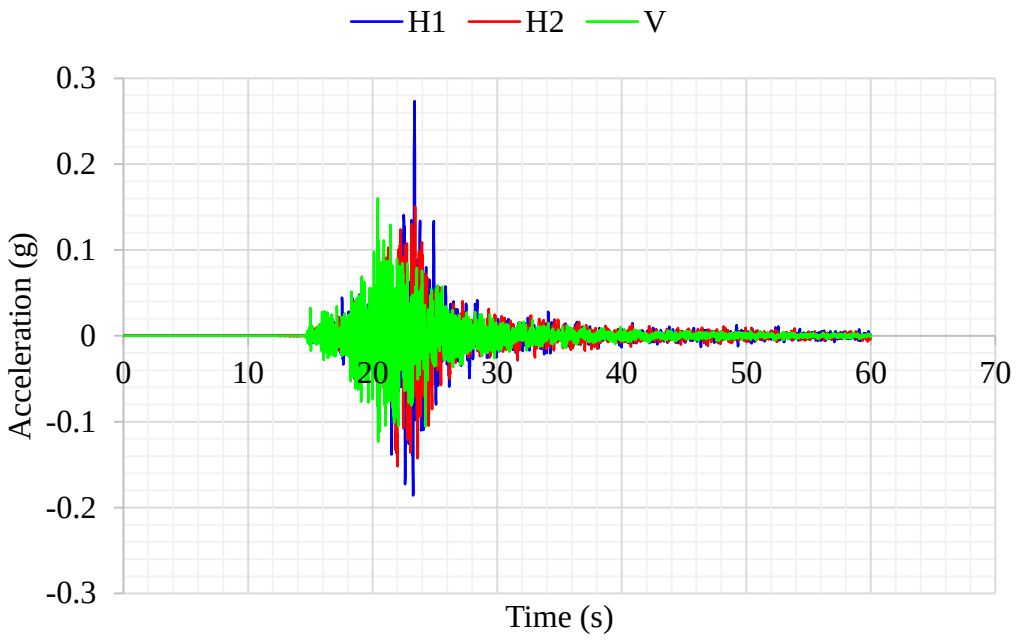

Figure D.4 RSN3943 Ground motion acceleration versus time graph

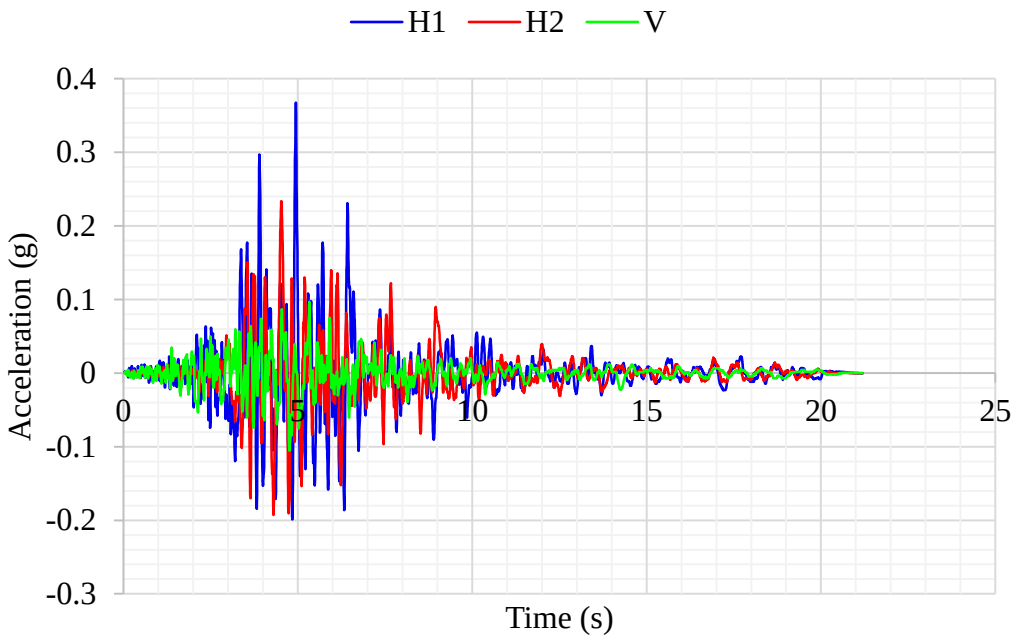

Figure D.5 RSN4132 Ground motion acceleration versus time graph

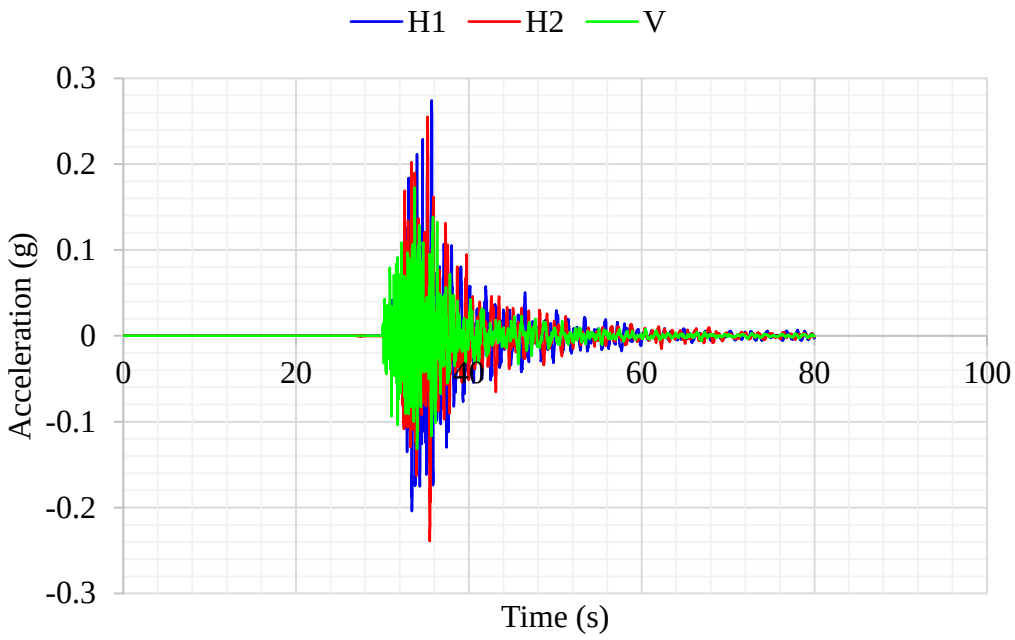

Figure D.6 RSN4068 Ground motion acceleration versus time graph

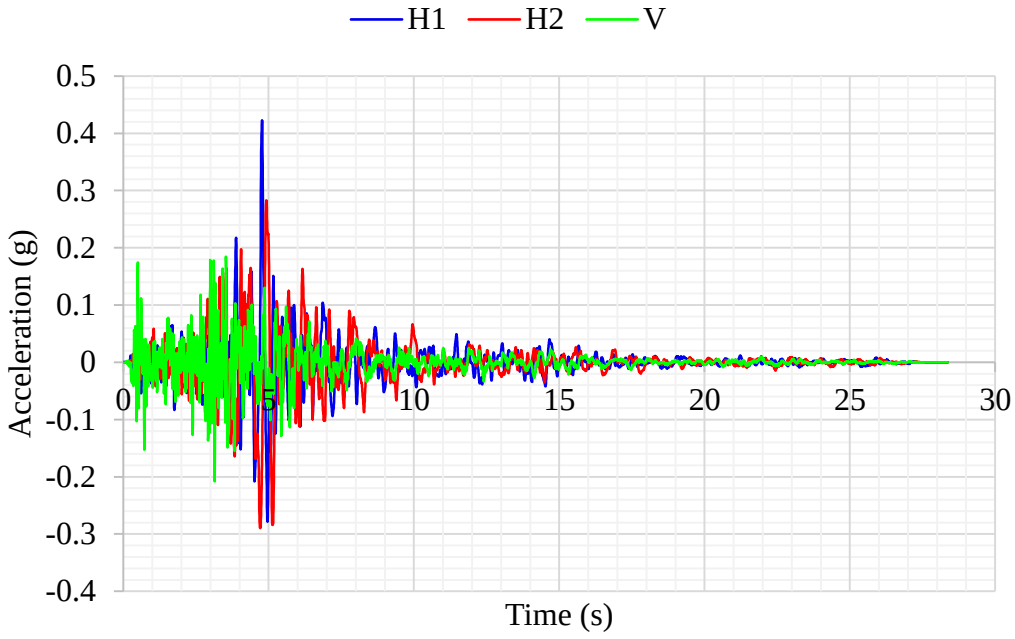

Figure D.7 RSN448 Ground motion acceleration versus time graph

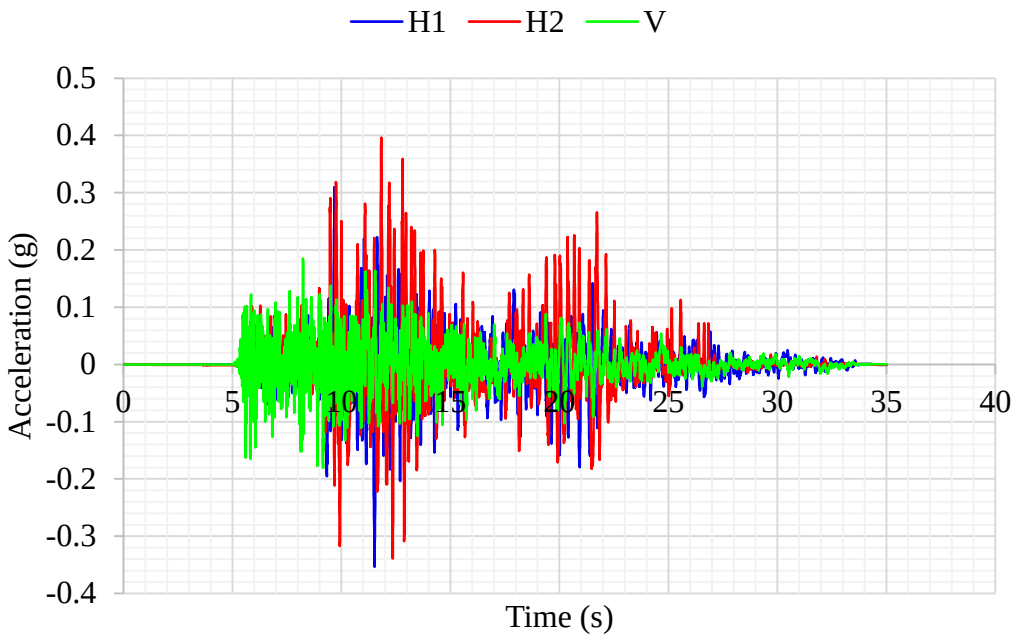

Figure D.8 RSN8166 Ground motion acceleration versus time graph

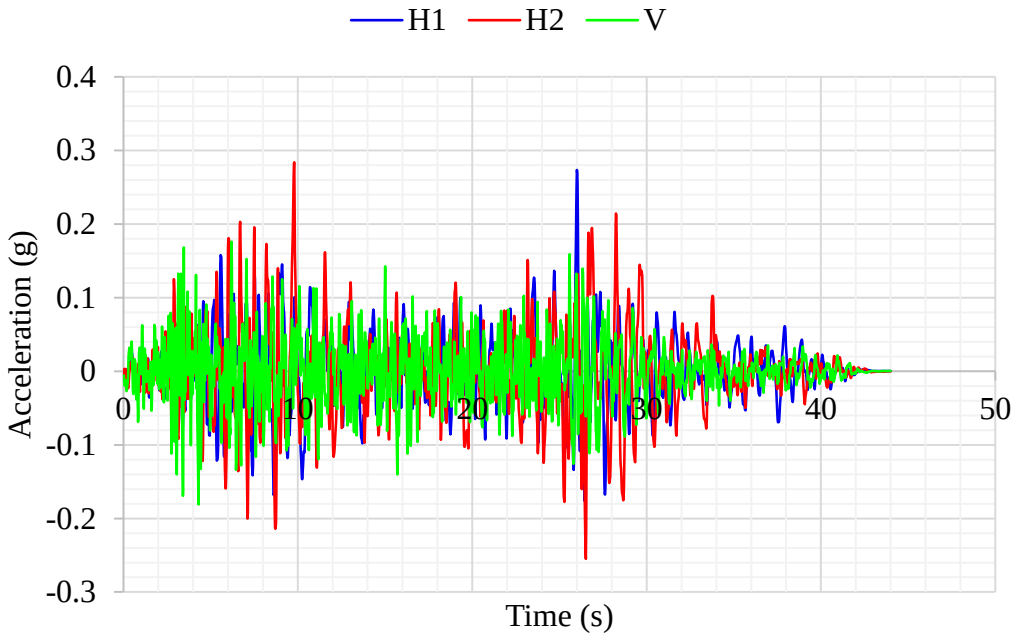

Figure D.9 RSN864 Ground motion acceleration versus time graph

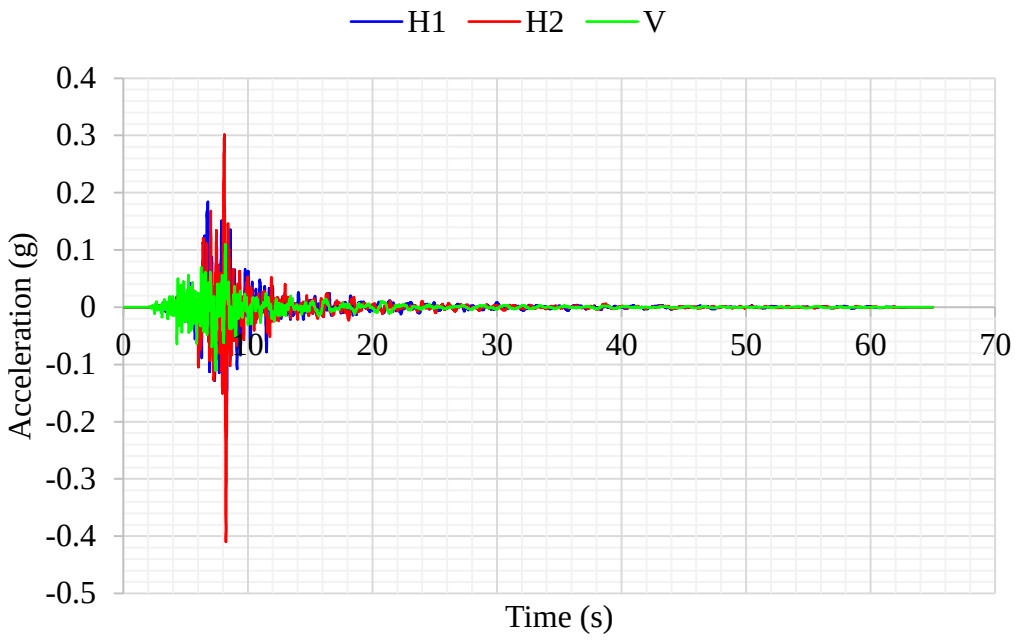

Figure D.10 RSN4071 Ground motion acceleration versus time graph

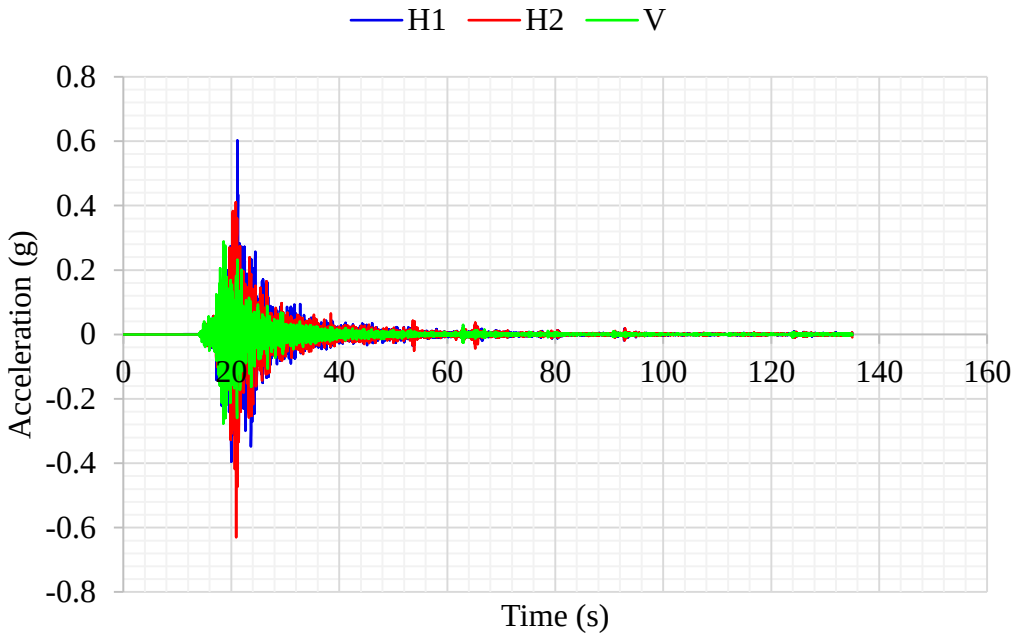

Figure D.11 RSN4071 Ground motion acceleration versus time graph

E. Fiber Results

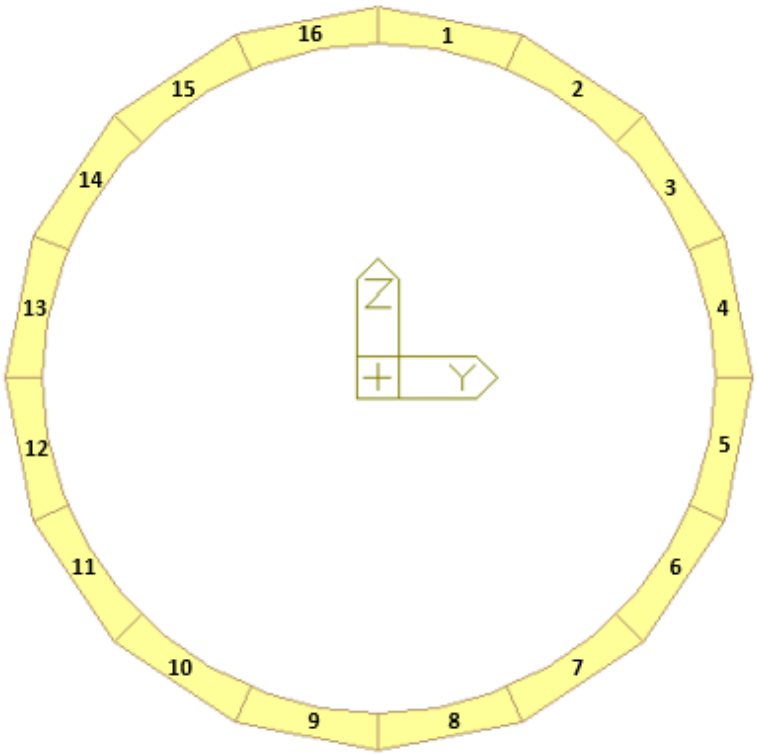

Figure E.1 Confined concrete part ID number for fiber column sections

Table E.1 Mean strain values and performance level for column bottom of A1 Axis for O07 Bridge

Concrete Fiber ID	Right Column		Middle Column		Left Column	
	Mean	Performance Level	Mean	Performance Level	Mean	Performance Level
1	0.00053	LD	0.00056	LD	0.00053	LD
2	0.00048	LD	0.00047	LD	0.00038	LD
3	0.00047	LD	0.00042	LD	0.00028	LD
4	0.00052	LD	0.00043	LD	0.00027	LD
5	0.00056	LD	0.00046	LD	0.00031	LD
6	0.00093	LD	0.00079	LD	0.00051	LD
7	0.00326	CD	0.00331	CD	0.00315	CD
8	0.00548	CD	0.00558	CD	0.00548	CD
9	0.00530	CD	0.00544	CD	0.00538	CD
10	0.00278	LD	0.00301	CD	0.00306	CD
11	0.00052	LD	0.00078	LD	0.00098	LD
12	0.00031	LD	0.00046	LD	0.00049	LD
13	0.00030	LD	0.00043	LD	0.00045	LD
14	0.00032	LD	0.00040	LD	0.00041	LD
15	0.00038	LD	0.00045	LD	0.00045	LD
16	0.00051	LD	0.00056	LD	0.00054	LD

Table E.2 Mean strain values and performance level for column bottom of P Axis for O07 Bridge

Concrete Fiber ID	Right Column		Middle Column		Left Column	
	Mean	Performance Level	Mean	Performance Level	Mean	Performance Level
1	0.00536	CD	0.00529	CD	0.00519	CD
2	0.00446	CD	0.00379	CD	0.00325	CD
3	0.00326	CD	0.00218	LD	0.00136	LD
4	0.00268	LD	0.00170	LD	0.00094	LD
5	0.00267	LD	0.00168	LD	0.00091	LD
6	0.00275	LD	0.00195	LD	0.00139	LD
7	0.00468	CD	0.00396	CD	0.00294	LD
8	0.00625	CD	0.00574	CD	0.00490	CD
9	0.00608	CD	0.00582	CD	0.00516	CD
10	0.00396	CD	0.00382	CD	0.00344	CD
11	0.00126	LD	0.00180	LD	0.00237	LD
12	0.00083	LD	0.00124	LD	0.00213	LD
13	0.00087	LD	0.00133	LD	0.00250	LD
14	0.00148	LD	0.00218	LD	0.00325	CD
15	0.00320	CD	0.00386	CD	0.00446	CD
16	0.00495	CD	0.00525	CD	0.00537	CD

Table E.3 Mean strain values and performance level for column bottom of A2 Axis for O07 Bridge

Concrete Fiber ID	Right Column		Middle Column		Left Column	
	Mean	Performance Level	Mean	Performance Level	Mean	Performance Level
1	0.00265	LD	0.00257	LD	0.00195	LD
2	0.00215	LD	0.00190	LD	0.00166	LD
3	0.00193	LD	0.00145	LD	0.00098	LD
4	0.00193	LD	0.00148	LD	0.00097	LD
5	0.00171	LD	0.00127	LD	0.00077	LD
6	0.00121	LD	0.00085	LD	0.00062	LD
7	0.00087	LD	0.00080	LD	0.00070	LD
8	0.00087	LD	0.00088	LD	0.00085	LD
9	0.00086	LD	0.00091	LD	0.00092	LD
10	0.00072	LD	0.00082	LD	0.00091	LD
11	0.00055	LD	0.00078	LD	0.00096	LD
12	0.00054	LD	0.00085	LD	0.00107	LD
13	0.00063	LD	0.00094	LD	0.00118	LD
14	0.00083	LD	0.00116	LD	0.00141	LD
15	0.00161	LD	0.00184	LD	0.00199	LD
16	0.00248	LD	0.00255	LD	0.00257	LD

Table E.4 Mean strain values and performance level for column top of A1 Axis for O07 Bridge

Concrete Fiber ID	Right Column		Middle Column		Left Column	
	Mean	Performance Level	Mean	Performance Level	Mean	Performance Level
1	0.00004	LD	0.00006	LD	0.00006	LD
2	0.00009	LD	0.00017	LD	0.00021	LD
3	0.00033	LD	0.00056	LD	0.00045	LD
4	0.00049	LD	0.00080	LD	0.00058	LD
5	0.00048	LD	0.00080	LD	0.00059	LD
6	0.00031	LD	0.00055	LD	0.00046	LD
7	0.00008	LD	0.00017	LD	0.00023	LD
8	0.00004	LD	0.00005	LD	0.00006	LD
9	0.00007	LD	0.00006	LD	0.00005	LD
10	0.00023	LD	0.00019	LD	0.00009	LD
11	0.00055	LD	0.00060	LD	0.00036	LD
12	0.00073	LD	0.00093	LD	0.00059	LD
13	0.00073	LD	0.00093	LD	0.00059	LD
14	0.00055	LD	0.00060	LD	0.00036	LD
15	0.00023	LD	0.00019	LD	0.00009	LD
16	0.00006	LD	0.00006	LD	0.00005	LD

Table E.5 Mean strain values and performance level for column top of P Axis for O07 Bridge

Concrete Fiber ID	Right Column		Middle Column		Left Column	
	Mean	Performance Level	Mean	Performance Level	Mean	Performance Level
1	0.00006	LD	0.00008	LD	0.00012	LD
2	0.00014	LD	0.00025	LD	0.00045	LD
3	0.00073	LD	0.00116	LD	0.00166	LD
4	0.00145	LD	0.00207	LD	0.00251	LD
5	0.00145	LD	0.00208	LD	0.00251	LD
6	0.00070	LD	0.00117	LD	0.00166	LD
7	0.00014	LD	0.00025	LD	0.00044	LD
8	0.00006	LD	0.00008	LD	0.00009	LD
9	0.00009	LD	0.00008	LD	0.00006	LD
10	0.00043	LD	0.00025	LD	0.00013	LD
11	0.00219	LD	0.00135	LD	0.00076	LD
12	0.00355	CD	0.00268	LD	0.00177	LD
13	0.00355	CD	0.00268	LD	0.00177	LD
14	0.00219	LD	0.00136	LD	0.00072	LD
15	0.00043	LD	0.00025	LD	0.00014	LD
16	0.00009	LD	0.00008	LD	0.00006	LD

Table E.6 Mean strain values and performance level for column top of A2 Axis for O07 Bridge

Concrete Fiber ID	Right Column		Middle Column		Left Column	
	Mean	Performance Level	Mean	Performance Level	Mean	Performance Level
1	0.00004	LD	0.00005	LD	0.00006	LD
2	0.00009	LD	0.00020	LD	0.00031	LD
3	0.00047	LD	0.00077	LD	0.00074	LD
4	0.00078	LD	0.00120	LD	0.00100	LD
5	0.00078	LD	0.00120	LD	0.00100	LD
6	0.00047	LD	0.00078	LD	0.00074	LD
7	0.00009	LD	0.00020	LD	0.00030	LD
8	0.00004	LD	0.00005	LD	0.00006	LD
9	0.00006	LD	0.00005	LD	0.00004	LD
10	0.00032	LD	0.00020	LD	0.00009	LD
11	0.00107	LD	0.00098	LD	0.00056	LD
12	0.00154	LD	0.00165	LD	0.00108	LD
13	0.00154	LD	0.00164	LD	0.00107	LD
14	0.00109	LD	0.00098	LD	0.00053	LD
15	0.00034	LD	0.00020	LD	0.00009	LD
16	0.00006	LD	0.00005	LD	0.00004	LD

Table E.7 Mean strain values and performance level for column bottom of A1 Axis for O13 Bridge

Concrete Fiber ID	Right Column		Middle Column		Left Column	
	Mean	Performance Level	Mean	Performance Level	Mean	Performance Level
1	0.00062	LD	0.00063	LD	0.00061	LD
2	0.00057	LD	0.00057	LD	0.00050	LD
3	0.00058	LD	0.00053	LD	0.00040	LD
4	0.00071	LD	0.00061	LD	0.00039	LD
5	0.00081	LD	0.00072	LD	0.00047	LD
6	0.00137	LD	0.00110	LD	0.00055	LD
7	0.00258	LD	0.00287	LD	0.00259	LD
8	0.00442	CD	0.00442	CD	0.00427	CD
9	0.00434	CD	0.00434	CD	0.00433	CD
10	0.00307	CD	0.00262	LD	0.00275	LD
11	0.00141	LD	0.00142	LD	0.00172	LD
12	0.00067	LD	0.00101	LD	0.00124	LD
13	0.00038	LD	0.00065	LD	0.00086	LD
14	0.00040	LD	0.00053	LD	0.00056	LD
15	0.00044	LD	0.00053	LD	0.00057	LD
16	0.00057	LD	0.00062	LD	0.00062	LD

Table E.8 Mean strain values and performance level for column bottom of P Axis for O13 Bridge

Concrete Fiber ID	Right Column		Middle Column		Left Column	
	Mean	Performance Level	Mean	Performance Level	Mean	Performance Level
1	0.00313	CD	0.00313	CD	0.00308	CD
2	0.00280	LD	0.00234	LD	0.00202	LD
3	0.00236	LD	0.00137	LD	0.00082	LD
4	0.00208	LD	0.00112	LD	0.00069	LD
5	0.00215	LD	0.00142	LD	0.00087	LD
6	0.00243	LD	0.00179	LD	0.00126	LD
7	0.00331	CD	0.00291	LD	0.00239	LD
8	0.00415	CD	0.00401	CD	0.00370	CD
9	0.00362	CD	0.00375	CD	0.00374	CD
10	0.00196	LD	0.00228	LD	0.00260	LD
11	0.00083	LD	0.00127	LD	0.00199	LD
12	0.00071	LD	0.00125	LD	0.00195	LD
13	0.00071	LD	0.00121	LD	0.00212	LD
14	0.00093	LD	0.00173	LD	0.00287	LD
15	0.00163	LD	0.00227	LD	0.00322	CD
16	0.00273	LD	0.00298	LD	0.00326	CD

Table E.9 Mean strain values and performance level for column bottom of A2 Axis for O13 Bridge

Concrete Fiber ID	Right Column		Middle Column		Left Column	
	Mean	Performance Level	Mean	Performance Level	Mean	Performance Level
1	0.00373	CD	0.00365	CD	0.00350	CD
2	0.00263	LD	0.00239	LD	0.00209	LD
3	0.00119	LD	0.00102	LD	0.00071	LD
4	0.00091	LD	0.00076	LD	0.00050	LD
5	0.00092	LD	0.00081	LD	0.00053	LD
6	0.00088	LD	0.00080	LD	0.00059	LD
7	0.00078	LD	0.00074	LD	0.00065	LD
8	0.00073	LD	0.00074	LD	0.00073	LD
9	0.00069	LD	0.00073	LD	0.00075	LD
10	0.00062	LD	0.00070	LD	0.00080	LD
11	0.00051	LD	0.00086	LD	0.00110	LD
12	0.00060	LD	0.00102	LD	0.00130	LD
13	0.00068	LD	0.00108	LD	0.00133	LD
14	0.00093	LD	0.00129	LD	0.00152	LD
15	0.00225	LD	0.00253	LD	0.00262	LD
16	0.00360	CD	0.00364	CD	0.00365	CD

Table E.10 Mean strain values and performance level for column top of A1 Axis for O13 Bridge

Concrete Fiber ID	Right Column		Middle Column		Left Column	
	Mean	Performance Level	Mean	Performance Level	Mean	Performance Level
1	0.00004	LD	0.00014	LD	0.00006	LD
2	0.00009	LD	0.00022	LD	0.00024	LD
3	0.00050	LD	0.00078	LD	0.00080	LD
4	0.00088	LD	0.00127	LD	0.00114	LD
5	0.00087	LD	0.00131	LD	0.00115	LD
6	0.00047	LD	0.00080	LD	0.00084	LD
7	0.00008	LD	0.00032	LD	0.00026	LD
8	0.00004	LD	0.00027	LD	0.00006	LD
9	0.00006	LD	0.00026	LD	0.00004	LD
10	0.00028	LD	0.00030	LD	0.00009	LD
11	0.00066	LD	0.00075	LD	0.00045	LD
12	0.00086	LD	0.00116	LD	0.00071	LD
13	0.00088	LD	0.00116	LD	0.00071	LD
14	0.00068	LD	0.00076	LD	0.00044	LD
15	0.00030	LD	0.00026	LD	0.00009	LD
16	0.00007	LD	0.00015	LD	0.00004	LD

Table E.11 Mean strain values and performance level for column top of P Axis for O13 Bridge

Concrete Fiber ID	Right Column		Middle Column		Left Column	
	Mean	Performance Level	Mean	Performance Level	Mean	Performance Level
1	0.00007	LD	0.00008	LD	0.00009	LD
2	0.00014	LD	0.00025	LD	0.00048	LD
3	0.00072	LD	0.00123	LD	0.00190	LD
4	0.00152	LD	0.00212	LD	0.00288	LD
5	0.00150	LD	0.00215	LD	0.00289	LD
6	0.00077	LD	0.00119	LD	0.00188	LD
7	0.00014	LD	0.00031	LD	0.00048	LD
8	0.00007	LD	0.00015	LD	0.00009	LD
9	0.00009	LD	0.00011	LD	0.00006	LD
10	0.00047	LD	0.00026	LD	0.00014	LD
11	0.00203	LD	0.00124	LD	0.00075	LD
12	0.00308	CD	0.00232	LD	0.00164	LD
13	0.00310	CD	0.00235	LD	0.00162	LD
14	0.00207	LD	0.00129	LD	0.00075	LD
15	0.00047	LD	0.00029	LD	0.00015	LD
16	0.00009	LD	0.00008	LD	0.00006	LD

Table E.12 Mean strain values and performance level for column top of A2 Axis for O13 Bridge

Concrete Fiber ID	Right Column		Middle Column		Left Column	
	Mean	Performance Level	Mean	Performance Level	Mean	Performance Level
1	0.00004	LD	0.00005	LD	0.00006	LD
2	0.00009	LD	0.00019	LD	0.00024	LD
3	0.00049	LD	0.00075	LD	0.00077	LD
4	0.00084	LD	0.00125	LD	0.00111	LD
5	0.00084	LD	0.00126	LD	0.00112	LD
6	0.00047	LD	0.00078	LD	0.00081	LD
7	0.00010	LD	0.00019	LD	0.00024	LD
8	0.00004	LD	0.00007	LD	0.00006	LD
9	0.00006	LD	0.00005	LD	0.00004	LD
10	0.00027	LD	0.00019	LD	0.00009	LD
11	0.00063	LD	0.00073	LD	0.00041	LD
12	0.00083	LD	0.00114	LD	0.00066	LD
13	0.00083	LD	0.00114	LD	0.00067	LD
14	0.00063	LD	0.00072	LD	0.00042	LD
15	0.00027	LD	0.00019	LD	0.00009	LD
16	0.00006	LD	0.00005	LD	0.00004	LD

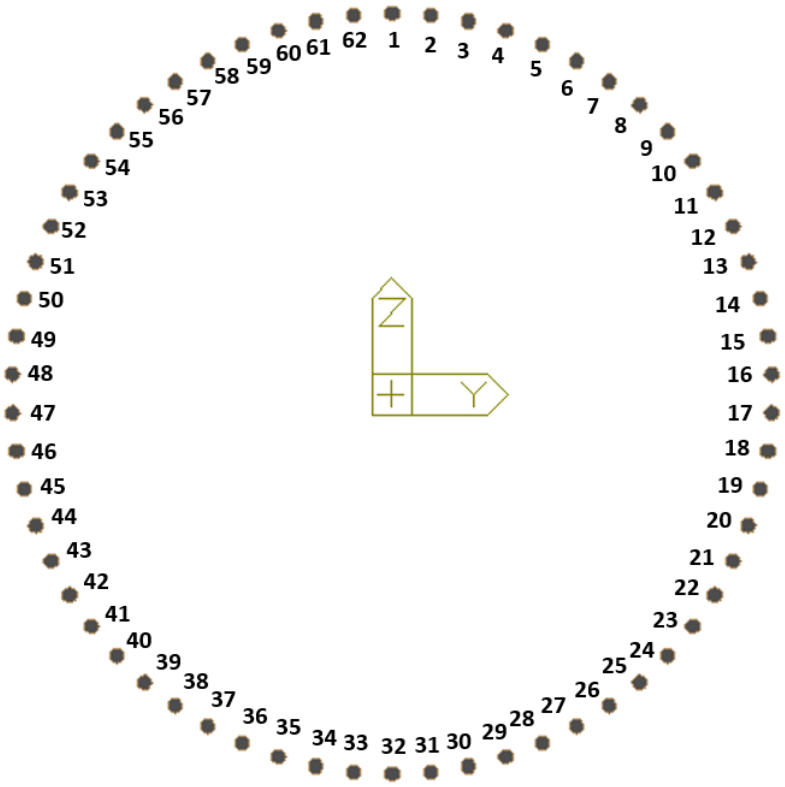

Figure E.2 Reinforcement part ID number for fiber column sections

Table E.13 Mean strain values and performance level for right column bottom reinforcements of A1 Axis for O07 Bridge

Reinf. Fiber ID	Mean	Performance Level	Reinf. Fiber ID	Mean	Performance Level
1	0.0297	CD	32	0.0039	LD
2	0.0295	CD	33	0.0039	LD
3	0.0292	CD	34	0.0038	LD
4	0.0287	CD	35	0.0039	LD
5	0.0281	CD	36	0.0039	LD
6	0.0273	CD	37	0.0040	LD
7	0.0263	CD	38	0.0042	LD
8	0.0251	CD	39	0.0044	LD
9	0.0239	CD	40	0.0049	LD
10	0.0225	CD	41	0.0054	LD
11	0.0210	CD	42	0.0059	LD
12	0.0194	CD	43	0.0067	LD
13	0.0178	CD	44	0.0078	LD
14	0.0162	CD	45	0.0092	LD
15	0.0147	LD	46	0.0107	LD
16	0.0132	LD	47	0.0123	LD
17	0.0118	LD	48	0.0140	LD
18	0.0103	LD	49	0.0156	CD
19	0.0090	LD	50	0.0173	CD
20	0.0078	LD	51	0.0189	CD
21	0.0067	LD	52	0.0204	CD
22	0.0059	LD	53	0.0219	CD
23	0.0054	LD	54	0.0233	CD
24	0.0050	LD	55	0.0246	CD

25	0.0047	LD	56	0.0257	CD
26	0.0045	LD	57	0.0267	CD
27	0.0043	LD	58	0.0277	CD
28	0.0042	LD	59	0.0284	CD
29	0.0041	LD	60	0.0290	CD
30	0.0040	LD	61	0.0294	CD
31	0.0039	LD	62	0.0296	CD

Table E.14 Mean strain values and performance level for middle column bottom reinforcements of A1 Axis for O07 Bridge

Reinf. Fiber ID	**Mean**	**Performance Level**	**Reinf. Fiber ID**	**Mean**	**Performance Level**
1	0.0297	CD	32	0.0036	LD
2	0.0296	CD	33	0.0036	LD
3	0.0293	CD	34	0.0037	LD
4	0.0288	CD	35	0.0038	LD
5	0.0281	CD	36	0.0040	LD
6	0.0273	CD	37	0.0041	LD
7	0.0263	CD	38	0.0044	LD
8	0.0252	CD	39	0.0047	LD
9	0.0240	CD	40	0.0052	LD
10	0.0226	CD	41	0.0058	LD
11	0.0211	CD	42	0.0064	LD
12	0.0195	CD	43	0.0074	LD
13	0.0179	CD	44	0.0084	LD
14	0.0162	CD	45	0.0097	LD
15	0.0146	LD	46	0.0112	LD
16	0.0131	LD	47	0.0128	LD

17	0.0116	LD	48	0.0144	LD
18	0.0102	LD	49	0.0160	CD
19	0.0088	LD	50	0.0176	CD
20	0.0076	LD	51	0.0192	CD
21	0.0064	LD	52	0.0207	CD
22	0.0055	LD	53	0.0221	CD
23	0.0050	LD	54	0.0235	CD
24	0.0046	LD	55	0.0247	CD
25	0.0043	LD	56	0.0258	CD
26	0.0041	LD	57	0.0268	CD
27	0.0039	LD	58	0.0277	CD
28	0.0038	LD	59	0.0284	CD
29	0.0037	LD	60	0.0290	CD
30	0.0037	LD	61	0.0294	CD
31	0.0036	LD	62	0.0296	CD

Table E.15 Mean strain values and performance level for left column bottom reinforcements of A1 Axis for O07 Bridge

Reinf. Fiber ID	**Mean**	**Performance Level**	**Reinf. Fiber ID**	**Mean**	**Performance Level**
1	0.0298	CD	32	0.0036	LD
2	0.0297	CD	33	0.0037	LD
3	0.0294	CD	34	0.0038	LD
4	0.0289	CD	35	0.0039	LD
5	0.0283	CD	36	0.0041	LD
6	0.0274	CD	37	0.0043	LD
7	0.0265	CD	38	0.0046	LD
8	0.0253	CD	39	0.0050	LD

9	0.0241	CD	40	0.0054	LD
10	0.0227	CD	41	0.0060	LD
11	0.0212	CD	42	0.0067	LD
12	0.0196	CD	43	0.0077	LD
13	0.0175	CD	44	0.0088	LD
14	0.0162	CD	45	0.0099	LD
15	0.0145	LD	46	0.0114	LD
16	0.0129	LD	47	0.0130	LD
17	0.0113	LD	48	0.0146	LD
18	0.0095	LD	49	0.0163	CD
19	0.0084	LD	50	0.0179	CD
20	0.0072	LD	51	0.0195	CD
21	0.0060	LD	52	0.0210	CD
22	0.0050	LD	53	0.0225	CD
23	0.0044	LD	54	0.0238	CD
24	0.0041	LD	55	0.0250	CD
25	0.0038	LD	56	0.0260	CD
26	0.0037	LD	57	0.0271	CD
27	0.0036	LD	58	0.0280	CD
28	0.0036	LD	59	0.0286	CD
29	0.0035	LD	60	0.0292	CD
30	0.0035	LD	61	0.0295	CD
31	0.0035	LD	62	0.0298	CD

Table E.16 Mean strain values and performance level for right column bottom reinforcements of P Axis for O07 Bridge

Reinf. Fiber ID	Mean	Performance Level	Reinf. Fiber ID	Mean	Performance Level
1	0.0357	CD	32	0.0362	CD
2	0.0358	CD	33	0.0363	CD
3	0.0357	CD	34	0.0362	CD
4	0.0353	CD	35	0.0362	CD
5	0.0348	CD	36	0.0360	CD
6	0.0340	CD	37	0.0356	CD
7	0.0332	CD	38	0.0352	CD
8	0.0322	CD	39	0.0336	CD
9	0.0310	CD	40	0.0337	CD
10	0.0298	CD	41	0.0329	CD
11	0.0286	CD	42	0.0319	CD
12	0.0274	CD	43	0.0309	CD
13	0.0265	CD	44	0.0298	CD
14	0.0259	CD	45	0.0289	CD
15	0.0260	CD	46	0.0281	CD
16	0.0262	CD	47	0.0276	CD
17	0.0263	CD	48	0.0273	CD
18	0.0271	CD	49	0.0277	CD
19	0.0272	CD	50	0.0281	CD
20	0.0282	CD	51	0.0286	CD
21	0.0294	CD	52	0.0293	CD
22	0.0305	CD	53	0.0303	CD
23	0.0317	CD	54	0.0312	CD
24	0.0327	CD	55	0.0321	CD

25	0.0335	CD	56	0.0328	CD
26	0.0342	CD	57	0.0335	CD
27	0.0349	CD	58	0.0342	CD
28	0.0354	CD	59	0.0347	CD
29	0.0347	CD	60	0.0351	CD
30	0.0361	CD	61	0.0353	CD
31	0.0362	CD	62	0.0355	CD

Table E.17 Mean strain values and performance level for middle column bottom reinforcements of P Axis for O07 Bridge

Reinf. Fiber ID	**Mean**	**Performance Level**	**Reinf. Fiber ID**	**Mean**	**Performance Level**
1	0.0361	CD	32	0.0365	CD
2	0.0360	CD	33	0.0369	CD
3	0.0358	CD	34	0.0371	CD
4	0.0354	CD	35	0.0372	CD
5	0.0349	CD	36	0.0371	CD
6	0.0341	CD	37	0.0367	CD
7	0.0332	CD	38	0.0363	CD
8	0.0321	CD	39	0.0346	CD
9	0.0309	CD	40	0.0349	CD
10	0.0295	CD	41	0.0340	CD
11	0.0282	CD	42	0.0331	CD
12	0.0268	CD	43	0.0321	CD
13	0.0256	CD	44	0.0312	CD
14	0.0248	CD	45	0.0302	CD
15	0.0243	CD	46	0.0293	CD
16	0.0240	CD	47	0.0292	CD

17	0.0242	CD	48	0.0294	CD
18	0.0245	CD	49	0.0297	CD
19	0.0252	CD	50	0.0300	CD
20	0.0264	CD	51	0.0305	CD
21	0.0277	CD	52	0.0309	CD
22	0.0290	CD	53	0.0318	CD
23	0.0302	CD	54	0.0326	CD
24	0.0313	CD	55	0.0335	CD
25	0.0324	CD	56	0.0343	CD
26	0.0333	CD	57	0.0347	CD
27	0.0341	CD	58	0.0353	CD
28	0.0348	CD	59	0.0357	CD
29	0.0343	CD	60	0.0361	CD
30	0.0358	CD	61	0.0363	CD
31	0.0362	CD	62	0.0363	CD

Table E.18 Mean strain values and performance level for left column bottom reinforcements of P Axis for O07 Bridge

Reinf. Fiber ID	**Mean**	**Performance Level**	**Reinf. Fiber ID**	**Mean**	**Performance Level**
1	0.0372	CD	32	0.0376	CD
2	0.0368	CD	33	0.0380	CD
3	0.0364	CD	34	0.0383	CD
4	0.0359	CD	35	0.0384	CD
5	0.0353	CD	36	0.0383	CD
6	0.0345	CD	37	0.0381	CD
7	0.0336	CD	38	0.0377	CD
8	0.0325	CD	39	0.0361	CD

9	0.0312	CD	40	0.0366	CD
10	0.0298	CD	41	0.0358	CD
11	0.0283	CD	42	0.0351	CD
12	0.0268	CD	43	0.0343	CD
13	0.0254	CD	44	0.0335	CD
14	0.0244	CD	45	0.0329	CD
15	0.0238	CD	46	0.0326	CD
16	0.0233	CD	47	0.0325	CD
17	0.0228	CD	48	0.0325	CD
18	0.0228	CD	49	0.0325	CD
19	0.0239	CD	50	0.0326	CD
20	0.0252	CD	51	0.0330	CD
21	0.0266	CD	52	0.0334	CD
22	0.0279	CD	53	0.0341	CD
23	0.0292	CD	54	0.0350	CD
24	0.0305	CD	55	0.0357	CD
25	0.0317	CD	56	0.0362	CD
26	0.0327	CD	57	0.0368	CD
27	0.0338	CD	58	0.0372	CD
28	0.0348	CD	59	0.0375	CD
29	0.0346	CD	60	0.0376	CD
30	0.0363	CD	61	0.0376	CD
31	0.0370	CD	62	0.0375	CD

Table E.19 Mean strain values and performance level for right column bottom reinforcements of A2 Axis for O07 Bridge

Reinf. Fiber ID	Mean	Performance Level	Reinf. Fiber ID	Mean	Performance Level
1	0.0067	LD	32	0.0153	CD
2	0.0067	LD	33	0.0153	CD
3	0.0067	LD	34	0.0151	CD
4	0.0067	LD	35	0.0149	LD
5	0.0068	LD	36	0.0148	LD
6	0.0070	LD	37	0.0147	LD
7	0.0072	LD	38	0.0144	LD
8	0.0074	LD	39	0.0141	LD
9	0.0075	LD	40	0.0137	LD
10	0.0077	LD	41	0.0133	LD
11	0.0079	LD	42	0.0129	LD
12	0.0082	LD	43	0.0124	LD
13	0.0085	LD	44	0.0119	LD
14	0.0088	LD	45	0.0114	LD
15	0.0092	LD	46	0.0110	LD
16	0.0096	LD	47	0.0105	LD
17	0.0101	LD	48	0.0100	LD
18	0.0105	LD	49	0.0095	LD
19	0.0109	LD	50	0.0090	LD
20	0.0113	LD	51	0.0087	LD
21	0.0117	LD	52	0.0085	LD
22	0.0122	LD	53	0.0082	LD
23	0.0127	LD	54	0.0080	LD
24	0.0132	LD	55	0.0078	LD

25	0.0136	LD	56	0.0076	LD
26	0.0141	LD	57	0.0074	LD
27	0.0144	LD	58	0.0072	LD
28	0.0148	LD	59	0.0071	LD
29	0.0150	CD	60	0.0070	LD
30	0.0152	CD	61	0.0069	LD
31	0.0153	CD	62	0.0068	LD

Table E.20 Mean values and performance level for middle column bottom reinforcements of A2 Axis for O07 Bridge

Reinf. Fiber ID	**Mean**	**Performance Level**	**Reinf. Fiber ID**	**Mean**	**Performance Level**
1	0.0066	LD	32	0.0148	LD
2	0.0064	LD	33	0.0147	LD
3	0.0063	LD	34	0.0146	LD
4	0.0063	LD	35	0.0147	LD
5	0.0063	LD	36	0.0146	LD
6	0.0065	LD	37	0.0145	LD
7	0.0067	LD	38	0.0143	LD
8	0.0069	LD	39	0.0140	LD
9	0.0071	LD	40	0.0138	LD
10	0.0073	LD	41	0.0134	LD
11	0.0075	LD	42	0.0131	LD
12	0.0078	LD	43	0.0127	LD
13	0.0081	LD	44	0.0124	LD
14	0.0084	LD	45	0.0120	LD
15	0.0087	LD	46	0.0115	LD
16	0.0091	LD	47	0.0111	LD

17	0.0095	LD	48	0.0106	LD
18	0.0099	LD	49	0.0101	LD
19	0.0103	LD	50	0.0098	LD
20	0.0107	LD	51	0.0094	LD
21	0.0113	LD	52	0.0091	LD
22	0.0118	LD	53	0.0088	LD
23	0.0123	LD	54	0.0086	LD
24	0.0128	LD	55	0.0084	LD
25	0.0132	LD	56	0.0082	LD
26	0.0136	LD	57	0.0079	LD
27	0.0140	LD	58	0.0076	LD
28	0.0143	LD	59	0.0074	LD
29	0.0145	LD	60	0.0072	LD
30	0.0147	LD	61	0.0070	LD
31	0.0147	LD	62	0.0068	LD

Table E.21 Mean strain values and performance level for left column bottom reinforcements of A2 Axis for O07 Bridge

Reinf. Fiber ID	**Mean**	**Performance Level**	**Reinf. Fiber ID**	**Mean**	**Performance Level**
1	0.0070	LD	32	0.0149	LD
2	0.0068	LD	33	0.0149	LD
3	0.0066	LD	34	0.0150	LD
4	0.0064	LD	35	0.0150	LD
5	0.0062	LD	36	0.0149	LD
6	0.0062	LD	37	0.0148	LD
7	0.0063	LD	38	0.0146	LD
8	0.0063	LD	39	0.0144	LD

9	0.0064	LD	40	0.0141	LD
10	0.0065	LD	41	0.0138	LD
11	0.0066	LD	42	0.0135	LD
12	0.0068	LD	43	0.0132	LD
13	0.0071	LD	44	0.0128	LD
14	0.0074	LD	45	0.0124	LD
15	0.0077	LD	46	0.0120	LD
16	0.0081	LD	47	0.0116	LD
17	0.0085	LD	48	0.0111	LD
18	0.0090	LD	49	0.0107	LD
19	0.0095	LD	50	0.0104	LD
20	0.0101	LD	51	0.0100	LD
21	0.0108	LD	52	0.0096	LD
22	0.0114	LD	53	0.0093	LD
23	0.0120	LD	54	0.0091	LD
24	0.0125	LD	55	0.0088	LD
25	0.0131	LD	56	0.0086	LD
26	0.0135	LD	57	0.0083	LD
27	0.0140	LD	58	0.0081	LD
28	0.0143	LD	59	0.0078	LD
29	0.0146	LD	60	0.0076	LD
30	0.0147	LD	61	0.0073	LD
31	0.0148	LD	62	0.0072	LD

Table E.22 Mean strain values and performance level for right column top reinforcements of A1 Axis for O07 Bridge

Reinf. Fiber ID	Mean	Performance Level	Reinf. Fiber ID	Mean	Performance Level
1	0.0007	Elastic	32	0.0007	Elastic
2	0.0007	Elastic	33	0.0008	Elastic
3	0.0008	Elastic	34	0.0009	Elastic
4	0.0009	Elastic	35	0.0009	Elastic
5	0.0010	Elastic	36	0.0010	Elastic
6	0.0011	Elastic	37	0.0012	Elastic
7	0.0012	Elastic	38	0.0013	Elastic
8	0.0013	Elastic	39	0.0014	Elastic
9	0.0014	Elastic	40	0.0014	Elastic
10	0.0015	Elastic	41	0.0015	Elastic
11	0.0016	Elastic	42	0.0016	Elastic
12	0.0016	Elastic	43	0.0016	Elastic
13	0.0017	Elastic	44	0.0016	Elastic
14	0.0017	Elastic	45	0.0016	Elastic
15	0.0017	Elastic	46	0.0017	Elastic
16	0.0017	Elastic	47	0.0017	Elastic
17	0.0017	Elastic	48	0.0017	Elastic
18	0.0017	Elastic	49	0.0017	Elastic
19	0.0017	Elastic	50	0.0016	Elastic
20	0.0017	Elastic	51	0.0016	Elastic
21	0.0016	Elastic	52	0.0016	Elastic
22	0.0016	Elastic	53	0.0016	Elastic
23	0.0015	Elastic	54	0.0015	Elastic
24	0.0014	Elastic	55	0.0014	Elastic

25	0.0013	Elastic	56	0.0014	Elastic
26	0.0012	Elastic	57	0.0012	Elastic
27	0.0011	Elastic	58	0.0011	Elastic
28	0.0010	Elastic	59	0.0011	Elastic
29	0.0009	Elastic	60	0.0009	Elastic
30	0.0008	Elastic	61	0.0008	Elastic
31	0.0007	Elastic	62	0.0007	Elastic

Table E.23 Mean strain values and performance level for middle column top reinforcements of A1 Axis for O07 Bridge

Reinf. Fiber ID	**Mean**	**Performance Level**	**Reinf. Fiber ID**	**Mean**	**Performance Level**
1	0.0013	Elastic	32	0.0013	Elastic
2	0.0015	Elastic	33	0.0013	Elastic
3	0.0018	Elastic	34	0.0013	Elastic
4	0.0021	Elastic	35	0.0014	Elastic
5	0.0022	Elastic	36	0.0016	Elastic
6	0.0024	Elastic	37	0.0017	Elastic
7	0.0026	LD	38	0.0018	Elastic
8	0.0028	LD	39	0.0020	Elastic
9	0.0029	LD	40	0.0020	Elastic
10	0.0031	LD	41	0.0022	Elastic
11	0.0032	LD	42	0.0022	Elastic
12	0.0033	LD	43	0.0024	Elastic
13	0.0034	LD	44	0.0024	Elastic
14	0.0035	LD	45	0.0025	Elastic
15	0.0035	LD	46	0.0026	LD
16	0.0036	LD	47	0.0026	LD

17	0.0036	LD	48	0.0026	LD
18	0.0035	LD	49	0.0026	LD
19	0.0035	LD	50	0.0025	Elastic
20	0.0034	LD	51	0.0024	Elastic
21	0.0033	LD	52	0.0024	Elastic
22	0.0032	LD	53	0.0022	Elastic
23	0.0031	LD	54	0.0022	Elastic
24	0.0030	LD	55	0.0020	Elastic
25	0.0028	LD	56	0.0019	Elastic
26	0.0026	LD	57	0.0018	Elastic
27	0.0024	Elastic	58	0.0017	Elastic
28	0.0022	Elastic	59	0.0016	Elastic
29	0.0021	Elastic	60	0.0014	Elastic
30	0.0018	Elastic	61	0.0013	Elastic
31	0.0015	Elastic	62	0.0013	Elastic

Table E.24 Mean strain values and performance level for left column top reinforcements of A1 Axis for O07 Bridge

Reinf. Fiber ID	**Mean**	**Performance Level**	**Reinf. Fiber ID**	**Mean**	**Performance Level**
1	0.0009	Elastic	32	0.0009	Elastic
2	0.0011	Elastic	33	0.0008	Elastic
3	0.0013	Elastic	34	0.0007	Elastic
4	0.0015	Elastic	35	0.0007	Elastic
5	0.0016	Elastic	36	0.0007	Elastic
6	0.0018	Elastic	37	0.0007	Elastic
7	0.0019	Elastic	38	0.0008	Elastic
8	0.0021	Elastic	39	0.0009	Elastic

9	0.0022	Elastic	40	0.0010	Elastic
10	0.0023	Elastic	41	0.0010	Elastic
11	0.0024	Elastic	42	0.0011	Elastic
12	0.0025	Elastic	43	0.0011	Elastic
13	0.0025	LD	44	0.0012	Elastic
14	0.0026	LD	45	0.0012	Elastic
15	0.0026	LD	46	0.0012	Elastic
16	0.0026	LD	47	0.0012	Elastic
17	0.0026	LD	48	0.0012	Elastic
18	0.0026	LD	49	0.0012	Elastic
19	0.0026	LD	50	0.0012	Elastic
20	0.0025	LD	51	0.0012	Elastic
21	0.0025	Elastic	52	0.0011	Elastic
22	0.0024	Elastic	53	0.0011	Elastic
23	0.0023	Elastic	54	0.0011	Elastic
24	0.0022	Elastic	55	0.0010	Elastic
25	0.0021	Elastic	56	0.0009	Elastic
26	0.0019	Elastic	57	0.0008	Elastic
27	0.0018	Elastic	58	0.0007	Elastic
28	0.0016	Elastic	59	0.0007	Elastic
29	0.0015	Elastic	60	0.0007	Elastic
30	0.0013	Elastic	61	0.0007	Elastic
31	0.0011	Elastic	62	0.0008	Elastic

Table E.25 Mean strain values and performance level for right column top reinforcements of P Axis for O07 Bridge

Reinf. Fiber ID	Mean	Performance Level	Reinf. Fiber ID	Mean	Performance Level
1	0.0080	LD	32	0.0077	LD
2	0.0080	LD	33	0.0078	LD
3	0.0084	LD	34	0.0080	LD
4	0.0091	LD	35	0.0085	LD
5	0.0100	LD	36	0.0092	LD
6	0.0109	LD	37	0.0098	LD
7	0.0117	LD	38	0.0104	LD
8	0.0125	LD	39	0.0110	LD
9	0.0133	LD	40	0.0115	LD
10	0.0140	LD	41	0.0120	LD
11	0.0145	LD	42	0.0124	LD
12	0.0150	CD	43	0.0128	LD
13	0.0154	CD	44	0.0131	LD
14	0.0158	CD	45	0.0133	LD
15	0.0160	CD	46	0.0135	LD
16	0.0161	CD	47	0.0136	LD
17	0.0161	CD	48	0.0136	LD
18	0.0160	CD	49	0.0135	LD
19	0.0158	CD	50	0.0133	LD
20	0.0155	CD	51	0.0131	LD
21	0.0151	CD	52	0.0128	LD
22	0.0146	LD	53	0.0125	LD
23	0.0140	LD	54	0.0121	LD
24	0.0133	LD	55	0.0116	LD

25	0.0126	LD	56	0.0111	LD
26	0.0118	LD	57	0.0106	LD
27	0.0110	LD	58	0.0101	LD
28	0.0100	LD	59	0.0095	LD
29	0.0092	LD	60	0.0089	LD
30	0.0083	LD	61	0.0084	LD
31	0.0078	LD	62	0.0081	LD

Table E.26 Mean strain values and performance level for middle column top reinforcements of P Axis for O07 Bridge

Reinf. Fiber ID	**Mean**	**Performance Level**	**Reinf. Fiber ID**	**Mean**	**Performance Level**
1	0.0083	LD	32	0.0084	LD
2	0.0091	LD	33	0.0081	LD
3	0.0101	LD	34	0.0081	LD
4	0.0111	LD	35	0.0083	LD
5	0.0122	LD	36	0.0088	LD
6	0.0132	LD	37	0.0095	LD
7	0.0141	LD	38	0.0101	LD
8	0.0150	CD	39	0.0108	LD
9	0.0158	CD	40	0.0113	LD
10	0.0165	CD	41	0.0118	LD
11	0.0172	CD	42	0.0123	LD
12	0.0177	CD	43	0.0127	LD
13	0.0181	CD	44	0.0130	LD
14	0.0185	CD	45	0.0132	LD
15	0.0187	CD	46	0.0134	LD
16	0.0188	CD	47	0.0134	LD

17	0.0188	CD	48	0.0134	LD
18	0.0187	CD	49	0.0134	LD
19	0.0185	CD	50	0.0132	LD
20	0.0181	CD	51	0.0130	LD
21	0.0177	CD	52	0.0127	LD
22	0.0171	CD	53	0.0123	LD
23	0.0165	CD	54	0.0118	LD
24	0.0158	CD	55	0.0113	LD
25	0.0150	LD	56	0.0108	LD
26	0.0141	LD	57	0.0102	LD
27	0.0132	LD	58	0.0095	LD
28	0.0122	LD	59	0.0088	LD
29	0.0111	LD	60	0.0083	LD
30	0.0101	LD	61	0.0081	LD
31	0.0092	LD	62	0.0081	LD

Table E.27 Mean strain values and performance level for left column top reinforcements of P Axis for O07 Bridge

Reinf. Fiber ID	**Mean**	**Performance Level**	**Reinf. Fiber ID**	**Mean**	**Performance Level**
1	0.0086	LD	32	0.0083	LD
2	0.0095	LD	33	0.0076	LD
3	0.0105	LD	34	0.0072	LD
4	0.0115	LD	35	0.0071	LD
5	0.0125	LD	36	0.0071	LD
6	0.0134	LD	37	0.0075	LD
7	0.0143	LD	38	0.0081	LD
8	0.0151	CD	39	0.0086	LD

9	0.0159	CD	40	0.0091	LD
10	0.0166	CD	41	0.0096	LD
11	0.0171	CD	42	0.0099	LD
12	0.0176	CD	43	0.0103	LD
13	0.0181	CD	44	0.0106	LD
14	0.0184	CD	45	0.0108	LD
15	0.0186	CD	46	0.0109	LD
16	0.0187	CD	47	0.0110	LD
17	0.0186	CD	48	0.0110	LD
18	0.0185	CD	49	0.0109	LD
19	0.0183	CD	50	0.0108	LD
20	0.0180	CD	51	0.0105	LD
21	0.0176	CD	52	0.0103	LD
22	0.0170	CD	53	0.0099	LD
23	0.0164	CD	54	0.0095	LD
24	0.0157	CD	55	0.0091	LD
25	0.0150	LD	56	0.0086	LD
26	0.0141	LD	57	0.0080	LD
27	0.0132	LD	58	0.0075	LD
28	0.0123	LD	59	0.0072	LD
29	0.0113	LD	60	0.0071	LD
30	0.0103	LD	61	0.0073	LD
31	0.0093	LD	62	0.0077	LD

Table E.28 Mean strain values and performance level for right column top reinforcements of A2 Axis for O07 Bridge

Reinf. Fiber ID	Mean	Performance Level	Reinf. Fiber ID	Mean	Performance Level
1	0.0020	Elastic	32	0.0020	Elastic
2	0.0020	Elastic	33	0.0020	Elastic
3	0.0022	Elastic	34	0.0021	Elastic
4	0.0025	Elastic	35	0.0024	Elastic
5	0.0028	LD	36	0.0026	LD
6	0.0030	LD	37	0.0028	LD
7	0.0033	LD	38	0.0030	LD
8	0.0036	LD	39	0.0032	LD
9	0.0038	LD	40	0.0034	LD
10	0.0040	LD	41	0.0035	LD
11	0.0042	LD	42	0.0037	LD
12	0.0044	LD	43	0.0038	LD
13	0.0045	LD	44	0.0039	LD
14	0.0046	LD	45	0.0040	LD
15	0.0047	LD	46	0.0040	LD
16	0.0047	LD	47	0.0040	LD
17	0.0047	LD	48	0.0040	LD
18	0.0047	LD	49	0.0040	LD
19	0.0046	LD	50	0.0040	LD
20	0.0045	LD	51	0.0039	LD
21	0.0044	LD	52	0.0038	LD
22	0.0042	LD	53	0.0037	LD
23	0.0040	LD	54	0.0035	LD
24	0.0038	LD	55	0.0034	LD

25	0.0036	LD	56	0.0032	LD
26	0.0033	LD	57	0.0030	LD
27	0.0031	LD	58	0.0028	LD
28	0.0028	LD	59	0.0026	LD
29	0.0025	Elastic	60	0.0024	Elastic
30	0.0022	Elastic	61	0.0021	Elastic
31	0.0020	Elastic	62	0.0020	Elastic

Table E.29 Mean strain values and performance level for middle column top reinforcements of A2 Axis for O07 Bridge

Reinf. Fiber ID	**Mean**	**Performance Level**	**Reinf. Fiber ID**	**Mean**	**Performance Level**
1	0.0030	LD	32	0.0030	LD
2	0.0033	LD	33	0.0028	LD
3	0.0037	LD	34	0.0028	LD
4	0.0041	LD	35	0.0030	LD
5	0.0046	LD	36	0.0033	LD
6	0.0050	LD	37	0.0036	LD
7	0.0054	LD	38	0.0039	LD
8	0.0058	LD	39	0.0041	LD
9	0.0061	LD	40	0.0044	LD
10	0.0064	LD	41	0.0046	LD
11	0.0067	LD	42	0.0048	LD
12	0.0069	LD	43	0.0049	LD
13	0.0071	LD	44	0.0051	LD
14	0.0072	LD	45	0.0052	LD
15	0.0073	LD	46	0.0052	LD
16	0.0074	LD	47	0.0052	LD

17	0.0074	LD	48	0.0053	LD
18	0.0073	LD	49	0.0052	LD
19	0.0072	LD	50	0.0052	LD
20	0.0071	LD	51	0.0051	LD
21	0.0069	LD	52	0.0049	LD
22	0.0067	LD	53	0.0048	LD
23	0.0064	LD	54	0.0046	LD
24	0.0061	LD	55	0.0044	LD
25	0.0058	LD	56	0.0041	LD
26	0.0054	LD	57	0.0039	LD
27	0.0050	LD	58	0.0036	LD
28	0.0046	LD	59	0.0033	LD
29	0.0041	LD	60	0.0030	LD
30	0.0037	LD	61	0.0028	LD
31	0.0033	LD	62	0.0028	LD

Table E.30 Mean strain values and performance level for left column top reinforcements of A2 Axis for O07 Bridge

Reinf. Fiber ID	**Mean**	**Performance Level**	**Reinf. Fiber ID**	**Mean**	**Performance Level**
1	0.0025	Elastic	32	0.0025	Elastic
2	0.0029	LD	33	0.0021	Elastic
3	0.0032	LD	34	0.0019	Elastic
4	0.0036	LD	35	0.0018	Elastic
5	0.0040	LD	36	0.0017	Elastic
6	0.0043	LD	37	0.0018	Elastic
7	0.0046	LD	38	0.0020	Elastic
8	0.0049	LD	39	0.0021	Elastic

9	0.0052	LD	40	0.0023	Elastic
10	0.0054	LD	41	0.0024	Elastic
11	0.0056	LD	42	0.0025	Elastic
12	0.0058	LD	43	0.0026	LD
13	0.0060	LD	44	0.0027	LD
14	0.0061	LD	45	0.0027	LD
15	0.0062	LD	46	0.0028	LD
16	0.0062	LD	47	0.0028	LD
17	0.0062	LD	48	0.0028	LD
18	0.0062	LD	49	0.0028	LD
19	0.0061	LD	50	0.0027	LD
20	0.0060	LD	51	0.0027	LD
21	0.0058	LD	52	0.0026	LD
22	0.0056	LD	53	0.0025	Elastic
23	0.0054	LD	54	0.0024	Elastic
24	0.0052	LD	55	0.0023	Elastic
25	0.0049	LD	56	0.0021	Elastic
26	0.0046	LD	57	0.0020	Elastic
27	0.0043	LD	58	0.0018	Elastic
28	0.0039	LD	59	0.0017	Elastic
29	0.0036	LD	60	0.0018	Elastic
30	0.0032	LD	61	0.0019	Elastic
31	0.0028	LD	62	0.0022	Elastic

Table E.31 Mean strain values and performance level for right column bottom reinforcements of A1 Axis for O13 Bridge

Reinf. Fiber ID	Mean	Performance Level	Reinf. Fiber ID	Mean	Performance Level
1	0.0243	CD	32	0.0068	LD
2	0.0245	CD	33	0.0068	LD
3	0.0243	CD	34	0.0067	LD
4	0.0240	CD	35	0.0067	LD
5	0.0236	CD	36	0.0067	LD
6	0.0231	CD	37	0.0068	LD
7	0.0225	CD	38	0.0070	LD
8	0.0217	CD	39	0.0071	LD
9	0.0208	CD	40	0.0074	LD
10	0.0199	CD	41	0.0078	LD
11	0.0188	CD	42	0.0081	LD
12	0.0177	CD	43	0.0085	LD
13	0.0165	CD	44	0.0090	LD
14	0.0154	CD	45	0.0096	LD
15	0.0146	LD	46	0.0103	LD
16	0.0138	LD	47	0.0112	LD
17	0.0130	LD	48	0.0124	LD
18	0.0122	LD	49	0.0135	LD
19	0.0115	LD	50	0.0146	LD
20	0.0109	LD	51	0.0158	CD
21	0.0104	LD	52	0.0170	CD
22	0.0099	LD	53	0.0181	CD
23	0.0094	LD	54	0.0192	CD
24	0.0090	LD	55	0.0201	CD

25	0.0086	LD	56	0.0210	CD
26	0.0082	LD	57	0.0218	CD
27	0.0079	LD	58	0.0225	CD
28	0.0075	LD	59	0.0232	CD
29	0.0073	LD	60	0.0237	CD
30	0.0070	LD	61	0.0241	CD
31	0.0069	LD	62	0.0244	CD

Table E.32 Mean strain values and performance level for middle column bottom reinforcements of A1 Axis for O13 Bridge

Reinf. Fiber ID	**Mean**	**Performance Level**	**Reinf. Fiber ID**	**Mean**	**Performance Level**
1	0.0244	CD	32	0.0065	LD
2	0.0243	CD	33	0.0065	LD
3	0.0242	CD	34	0.0065	LD
4	0.0238	CD	35	0.0066	LD
5	0.0234	CD	36	0.0068	LD
6	0.0228	CD	37	0.0069	LD
7	0.0222	CD	38	0.0071	LD
8	0.0214	CD	39	0.0075	LD
9	0.0206	CD	40	0.0078	LD
10	0.0196	CD	41	0.0083	LD
11	0.0186	CD	42	0.0087	LD
12	0.0175	CD	43	0.0091	LD
13	0.0163	CD	44	0.0097	LD
14	0.0151	CD	45	0.0104	LD
15	0.0139	LD	46	0.0113	LD
16	0.0130	LD	47	0.0121	LD

17	0.0123	LD	48	0.0132	LD
18	0.0115	LD	49	0.0143	LD
19	0.0108	LD	50	0.0154	CD
20	0.0102	LD	51	0.0164	CD
21	0.0096	LD	52	0.0174	CD
22	0.0091	LD	53	0.0185	CD
23	0.0086	LD	54	0.0194	CD
24	0.0082	LD	55	0.0204	CD
25	0.0078	LD	56	0.0212	CD
26	0.0074	LD	57	0.0220	CD
27	0.0071	LD	58	0.0226	CD
28	0.0068	LD	59	0.0231	CD
29	0.0066	LD	60	0.0236	CD
30	0.0065	LD	61	0.0240	CD
31	0.0065	LD	62	0.0242	CD

Table E.33 Mean strain values and performance level for left column bottom reinforcements of A1 Axis for O13 Bridge

Reinf. Fiber ID	**Mean**	**Performance Level**	**Reinf. Fiber ID**	**Mean**	**Performance Level**
1	0.0243	CD	32	0.0064	LD
2	0.0243	CD	33	0.0065	LD
3	0.0241	CD	34	0.0066	LD
4	0.0238	CD	35	0.0067	LD
5	0.0233	CD	36	0.0069	LD
6	0.0227	CD	37	0.0071	LD
7	0.0221	CD	38	0.0074	LD
8	0.0213	CD	39	0.0077	LD

9	0.0204	CD	40	0.0081	LD
10	0.0194	CD	41	0.0085	LD
11	0.0184	CD	42	0.0090	LD
12	0.0172	CD	43	0.0097	LD
13	0.0160	CD	44	0.0103	LD
14	0.0148	LD	45	0.0111	LD
15	0.0135	LD	46	0.0119	LD
16	0.0122	LD	47	0.0128	LD
17	0.0114	LD	48	0.0138	LD
18	0.0106	LD	49	0.0149	LD
19	0.0098	LD	50	0.0160	CD
20	0.0091	LD	51	0.0170	CD
21	0.0085	LD	52	0.0180	CD
22	0.0081	LD	53	0.0190	CD
23	0.0076	LD	54	0.0200	CD
24	0.0072	LD	55	0.0208	CD
25	0.0068	LD	56	0.0216	CD
26	0.0065	LD	57	0.0224	CD
27	0.0064	LD	58	0.0230	CD
28	0.0063	LD	59	0.0235	CD
29	0.0063	LD	60	0.0239	CD
30	0.0063	LD	61	0.0241	CD
31	0.0063	LD	62	0.0242	CD

Table E.34 Mean strain values and performance level for right column bottom reinforcements of P Axis for O13 Bridge

Reinf. Fiber ID	Mean	Performance Level	Reinf. Fiber ID	Mean	Performance Level
1	0.0290	CD	32	0.0246	CD
2	0.0291	CD	33	0.0246	CD
3	0.0291	CD	34	0.0246	CD
4	0.0290	CD	35	0.0246	CD
5	0.0287	CD	36	0.0244	CD
6	0.0283	CD	37	0.0241	CD
7	0.0278	CD	38	0.0238	CD
8	0.0271	CD	39	0.0234	CD
9	0.0265	CD	40	0.0229	CD
10	0.0259	CD	41	0.0224	CD
11	0.0253	CD	42	0.0219	CD
12	0.0246	CD	43	0.0214	CD
13	0.0241	CD	44	0.0208	CD
14	0.0235	CD	45	0.0203	CD
15	0.0234	CD	46	0.0199	CD
16	0.0233	CD	47	0.0195	CD
17	0.0233	CD	48	0.0192	CD
18	0.0232	CD	49	0.0192	CD
19	0.0231	CD	50	0.0198	CD
20	0.0231	CD	51	0.0205	CD
21	0.0231	CD	52	0.0212	CD
22	0.0232	CD	53	0.0221	CD
23	0.0234	CD	54	0.0231	CD
24	0.0236	CD	55	0.0240	CD

25	0.0237	CD	56	0.0248	CD
26	0.0239	CD	57	0.0257	CD
27	0.0241	CD	58	0.0266	CD
28	0.0242	CD	59	0.0273	CD
29	0.0243	CD	60	0.0279	CD
30	0.0245	CD	61	0.0283	CD
31	0.0246	CD	62	0.0287	CD

Table E.35 Mean strain values and performance level for middle column bottom reinforcements of P Axis for O13 Bridge

Reinf. Fiber ID	**Mean**	**Performance Level**	**Reinf. Fiber ID**	**Mean**	**Performance Level**
1	0.0288	CD	32	0.0248	CD
2	0.0288	CD	33	0.0250	CD
3	0.0286	CD	34	0.0252	CD
4	0.0284	CD	35	0.0252	CD
5	0.0280	CD	36	0.0251	CD
6	0.0276	CD	37	0.0250	CD
7	0.0270	CD	38	0.0249	CD
8	0.0263	CD	39	0.0247	CD
9	0.0255	CD	40	0.0245	CD
10	0.0246	CD	41	0.0243	CD
11	0.0238	CD	42	0.0239	CD
12	0.0230	CD	43	0.0235	CD
13	0.0222	CD	44	0.0230	CD
14	0.0214	CD	45	0.0225	CD
15	0.0210	CD	46	0.0221	CD
16	0.0209	CD	47	0.0218	CD

17	0.0209	CD	48	0.0215	CD
18	0.0208	CD	49	0.0215	CD
19	0.0208	CD	50	0.0221	CD
20	0.0210	CD	51	0.0227	CD
21	0.0211	CD	52	0.0234	CD
22	0.0214	CD	53	0.0240	CD
23	0.0218	CD	54	0.0246	CD
24	0.0222	CD	55	0.0253	CD
25	0.0225	CD	56	0.0261	CD
26	0.0228	CD	57	0.0267	CD
27	0.0232	CD	58	0.0273	CD
28	0.0235	CD	59	0.0278	CD
29	0.0238	CD	60	0.0281	CD
30	0.0242	CD	61	0.0284	CD
31	0.0246	CD	62	0.0286	CD

Table E.36 Mean strain values and performance level for left column bottom reinforcements of P Axis for O13 Bridge

Reinf. Fiber ID	**Mean**	**Performance Level**	**Reinf. Fiber ID**	**Mean**	**Performance Level**
1	0.0293	CD	32	0.0256	CD
2	0.0291	CD	33	0.0259	CD
3	0.0288	CD	34	0.0261	CD
4	0.0285	CD	35	0.0262	CD
5	0.0280	CD	36	0.0264	CD
6	0.0274	CD	37	0.0265	CD
7	0.0268	CD	38	0.0265	CD
8	0.0260	CD	39	0.0264	CD

9	0.0252	CD	40	0.0263	CD
10	0.0242	CD	41	0.0261	CD
11	0.0231	CD	42	0.0258	CD
12	0.0221	CD	43	0.0254	CD
13	0.0211	CD	44	0.0250	CD
14	0.0201	CD	45	0.0246	CD
15	0.0194	CD	46	0.0243	CD
16	0.0189	CD	47	0.0240	CD
17	0.0188	CD	48	0.0237	CD
18	0.0188	CD	49	0.0237	CD
19	0.0189	CD	50	0.0243	CD
20	0.0193	CD	51	0.0248	CD
21	0.0198	CD	52	0.0255	CD
22	0.0204	CD	53	0.0261	CD
23	0.0210	CD	54	0.0266	CD
24	0.0215	CD	55	0.0271	CD
25	0.0220	CD	56	0.0276	CD
26	0.0225	CD	57	0.0282	CD
27	0.0231	CD	58	0.0286	CD
28	0.0238	CD	59	0.0289	CD
29	0.0243	CD	60	0.0292	CD
30	0.0248	CD	61	0.0293	CD
31	0.0252	CD	62	0.0294	CD

Table E.37 Mean strain values and performance level for right column bottom reinforcements of A2 Axis for O13 Bridge

Reinf. Fiber ID	Mean	Performance Level	Reinf. Fiber ID	Mean	Performance Level
1	0.0069	LD	32	0.0204	CD
2	0.0071	LD	33	0.0203	CD
3	0.0073	LD	34	0.0200	CD
4	0.0075	LD	35	0.0198	CD
5	0.0078	LD	36	0.0194	CD
6	0.0080	LD	37	0.0189	CD
7	0.0082	LD	38	0.0184	CD
8	0.0085	LD	39	0.0177	CD
9	0.0087	LD	40	0.0170	CD
10	0.0090	LD	41	0.0162	CD
11	0.0094	LD	42	0.0153	CD
12	0.0099	LD	43	0.0145	LD
13	0.0104	LD	44	0.0136	LD
14	0.0109	LD	45	0.0126	LD
15	0.0116	LD	46	0.0116	LD
16	0.0123	LD	47	0.0108	LD
17	0.0130	LD	48	0.0100	LD
18	0.0137	LD	49	0.0093	LD
19	0.0145	LD	50	0.0087	LD
20	0.0152	CD	51	0.0082	LD
21	0.0159	CD	52	0.0077	LD
22	0.0166	CD	53	0.0075	LD
23	0.0172	CD	54	0.0073	LD
24	0.0178	CD	55	0.0071	LD

25	0.0184	CD	56	0.0069	LD
26	0.0189	CD	57	0.0068	LD
27	0.0194	CD	58	0.0066	LD
28	0.0198	CD	59	0.0065	LD
29	0.0200	CD	60	0.0065	LD
30	0.0202	CD	61	0.0066	LD
31	0.0203	CD	62	0.0068	LD

Table E.38 Mean strain values and performance level for middle column bottom reinforcements of A2 Axis for O13 Bridge

Reinf. Fiber ID	**Mean**	**Performance Level**	**Reinf. Fiber ID**	**Mean**	**Performance Level**
1	0.0066	LD	32	0.0204	CD
2	0.0068	LD	33	0.0204	CD
3	0.0069	LD	34	0.0202	CD
4	0.0071	LD	35	0.0200	CD
5	0.0073	LD	36	0.0196	CD
6	0.0075	LD	37	0.0192	CD
7	0.0077	LD	38	0.0186	CD
8	0.0080	LD	39	0.0180	CD
9	0.0082	LD	40	0.0173	CD
10	0.0084	LD	41	0.0166	CD
11	0.0087	LD	42	0.0158	CD
12	0.0092	LD	43	0.0149	LD
13	0.0098	LD	44	0.0141	LD
14	0.0104	LD	45	0.0132	LD
15	0.0110	LD	46	0.0124	LD
16	0.0117	LD	47	0.0116	LD

17	0.0125	LD	48	0.0109	LD
18	0.0133	LD	49	0.0102	LD
19	0.0140	LD	50	0.0095	LD
20	0.0148	LD	51	0.0089	LD
21	0.0155	CD	52	0.0084	LD
22	0.0163	CD	53	0.0081	LD
23	0.0169	CD	54	0.0079	LD
24	0.0176	CD	55	0.0076	LD
25	0.0183	CD	56	0.0074	LD
26	0.0188	CD	57	0.0072	LD
27	0.0193	CD	58	0.0071	LD
28	0.0197	CD	59	0.0069	LD
29	0.0200	CD	60	0.0068	LD
30	0.0202	CD	61	0.0067	LD
31	0.0204	CD	62	0.0065	LD

Table E.39 Mean strain values and performance level for left column bottom reinforcements of A2 Axis for O13 Bridge

Reinf. Fiber ID	**Mean**	**Performance Level**	**Reinf. Fiber ID**	**Mean**	**Performance Level**
1	0.0068	LD	32	0.0208	CD
2	0.0067	LD	33	0.0208	CD
3	0.0066	LD	34	0.0206	CD
4	0.0067	LD	35	0.0204	CD
5	0.0069	LD	36	0.0201	CD
6	0.0071	LD	37	0.0197	CD
7	0.0072	LD	38	0.0192	CD
8	0.0074	LD	39	0.0186	CD

9	0.0076	LD	40	0.0179	CD
10	0.0078	LD	41	0.0172	CD
11	0.0080	LD	42	0.0164	CD
12	0.0083	LD	43	0.0156	CD
13	0.0089	LD	44	0.0148	LD
14	0.0094	LD	45	0.0139	LD
15	0.0101	LD	46	0.0131	LD
16	0.0109	LD	47	0.0124	LD
17	0.0117	LD	48	0.0116	LD
18	0.0125	LD	49	0.0108	LD
19	0.0133	LD	50	0.0102	LD
20	0.0141	LD	51	0.0096	LD
21	0.0150	LD	52	0.0089	LD
22	0.0158	CD	53	0.0086	LD
23	0.0166	CD	54	0.0083	LD
24	0.0173	CD	55	0.0080	LD
25	0.0180	CD	56	0.0078	LD
26	0.0186	CD	57	0.0076	LD
27	0.0192	CD	58	0.0075	LD
28	0.0197	CD	59	0.0074	LD
29	0.0201	CD	60	0.0073	LD
30	0.0204	CD	61	0.0071	LD
31	0.0207	CD	62	0.0070	LD

Table E.40 Mean strain values and performance level for right column top reinforcements of A1 Axis for O13 Bridge

Reinf. Fiber ID	Mean	Performance Level	Reinf. Fiber ID	Mean	Performance Level
1	0.0018	Elastic	32	0.0018	Elastic
2	0.0015	Elastic	33	0.0021	Elastic
3	0.0014	Elastic	34	0.0024	Elastic
4	0.0014	Elastic	35	0.0026	LD
5	0.0015	Elastic	36	0.0029	LD
6	0.0016	Elastic	37	0.0032	LD
7	0.0018	Elastic	38	0.0034	LD
8	0.0019	Elastic	39	0.0036	LD
9	0.0020	Elastic	40	0.0038	LD
10	0.0021	Elastic	41	0.0040	LD
11	0.0022	Elastic	42	0.0042	LD
12	0.0023	Elastic	43	0.0043	LD
13	0.0024	Elastic	44	0.0044	LD
14	0.0025	Elastic	45	0.0045	LD
15	0.0025	Elastic	46	0.0046	LD
16	0.0026	LD	47	0.0046	LD
17	0.0025	LD	48	0.0046	LD
18	0.0025	Elastic	49	0.0045	LD
19	0.0025	Elastic	50	0.0045	LD
20	0.0024	Elastic	51	0.0044	LD
21	0.0024	Elastic	52	0.0043	LD
22	0.0026	LD	53	0.0041	LD
23	0.0024	Elastic	54	0.0040	LD
24	0.0023	Elastic	55	0.0038	LD

25	0.0022	Elastic	56	0.0036	LD
26	0.0019	Elastic	57	0.0033	LD
27	0.0017	Elastic	58	0.0031	LD
28	0.0016	Elastic	59	0.0028	LD
29	0.0015	Elastic	60	0.0026	LD
30	0.0015	Elastic	61	0.0023	Elastic
31	0.0016	Elastic	62	0.0020	Elastic

Table E.41 Mean strain values and performance level for middle column top reinforcements of A1 Axis for O13 Bridge

Reinf. Fiber ID	**Mean**	**Performance Level**	**Reinf. Fiber ID**	**Mean**	**Performance Level**
1	0.0024	Elastic	32	0.0024	Elastic
2	0.0024	Elastic	33	0.0026	LD
3	0.0026	LD	34	0.0028	LD
4	0.0029	LD	35	0.0032	LD
5	0.0032	LD	36	0.0035	LD
6	0.0034	LD	37	0.0038	LD
7	0.0037	LD	38	0.0041	LD
8	0.0039	LD	39	0.0044	LD
9	0.0041	LD	40	0.0047	LD
10	0.0043	LD	41	0.0049	LD
11	0.0045	LD	42	0.0051	LD
12	0.0047	LD	43	0.0053	LD
13	0.0048	LD	44	0.0054	LD
14	0.0049	LD	45	0.0055	LD
15	0.0049	LD	46	0.0056	LD
16	0.0050	LD	47	0.0056	LD

17	0.0050	LD	48	0.0056	LD
18	0.0049	LD	49	0.0056	LD
19	0.0049	LD	50	0.0055	LD
20	0.0048	LD	51	0.0054	LD
21	0.0047	LD	52	0.0053	LD
22	0.0045	LD	53	0.0051	LD
23	0.0044	LD	54	0.0049	LD
24	0.0042	LD	55	0.0046	LD
25	0.0040	LD	56	0.0044	LD
26	0.0037	LD	57	0.0041	LD
27	0.0035	LD	58	0.0038	LD
28	0.0032	LD	59	0.0035	LD
29	0.0029	LD	60	0.0031	LD
30	0.0026	LD	61	0.0028	LD
31	0.0024	Elastic	62	0.0025	LD

Table E.42 Mean strain values and performance level for left column top reinforcements of A1 Axis for O13 Bridge

Reinf. Fiber ID	**Mean**	**Performance Level**	**Reinf. Fiber ID**	**Mean**	**Performance Level**
1	0.0018	Elastic	32	0.0018	Elastic
2	0.0020	Elastic	33	0.0016	Elastic
3	0.0023	Elastic	34	0.0017	Elastic
4	0.0025	Elastic	35	0.0018	Elastic
5	0.0027	LD	36	0.0020	Elastic
6	0.0029	LD	37	0.0022	Elastic
7	0.0030	LD	38	0.0024	Elastic
8	0.0032	LD	39	0.0026	LD

9	0.0034	LD	40	0.0028	LD
10	0.0035	LD	41	0.0030	LD
11	0.0036	LD	42	0.0031	LD
12	0.0037	LD	43	0.0032	LD
13	0.0038	LD	44	0.0033	LD
14	0.0039	LD	45	0.0034	LD
15	0.0039	LD	46	0.0034	LD
16	0.0039	LD	47	0.0035	LD
17	0.0039	LD	48	0.0035	LD
18	0.0039	LD	49	0.0035	LD
19	0.0038	LD	50	0.0034	LD
20	0.0038	LD	51	0.0033	LD
21	0.0037	LD	52	0.0032	LD
22	0.0036	LD	53	0.0031	LD
23	0.0035	LD	54	0.0030	LD
24	0.0033	LD	55	0.0028	LD
25	0.0032	LD	56	0.0027	LD
26	0.0030	LD	57	0.0025	Elastic
27	0.0028	LD	58	0.0023	Elastic
28	0.0026	LD	59	0.0021	Elastic
29	0.0024	Elastic	60	0.0019	Elastic
30	0.0022	Elastic	61	0.0017	Elastic
31	0.0020	Elastic	62	0.0017	Elastic

Table E.43 Mean strain values and performance level for right column top reinforcements of P Axis for O13 Bridge

Reinf. Fiber ID	Mean	Performance Level	Reinf. Fiber ID	Mean	Performance Level
1	0.0061	LD	32	0.0063	LD
2	0.0058	LD	33	0.0069	LD
3	0.0061	LD	34	0.0082	LD
4	0.0067	LD	35	0.0083	LD
5	0.0073	LD	36	0.0090	LD
6	0.0080	LD	37	0.0096	LD
7	0.0086	LD	38	0.0109	LD
8	0.0092	LD	39	0.0108	LD
9	0.0097	LD	40	0.0114	LD
10	0.0102	LD	41	0.0118	LD
11	0.0106	LD	42	0.0122	LD
12	0.0110	LD	43	0.0126	LD
13	0.0113	LD	44	0.0129	LD
14	0.0115	LD	45	0.0131	LD
15	0.0117	LD	46	0.0132	LD
16	0.0118	LD	47	0.0133	LD
17	0.0118	LD	48	0.0133	LD
18	0.0117	LD	49	0.0132	LD
19	0.0116	LD	50	0.0131	LD
20	0.0113	LD	51	0.0128	LD
21	0.0111	LD	52	0.0125	LD
22	0.0111	LD	53	0.0122	LD
23	0.0103	LD	54	0.0117	LD
24	0.0099	LD	55	0.0113	LD

25	0.0094	LD	56	0.0107	LD
26	0.0088	LD	57	0.0101	LD
27	0.0081	LD	58	0.0093	LD
28	0.0074	LD	59	0.0089	LD
29	0.0068	LD	60	0.0082	LD
30	0.0062	LD	61	0.0075	LD
31	0.0059	LD	62	0.0067	LD

Table E.44 Mean strain values and performance level for middle column top reinforcements of P Axis for O13 Bridge

Reinf. Fiber ID	**Mean**	**Performance Level**	**Reinf. Fiber ID**	**Mean**	**Performance Level**
1	0.0061	LD	32	0.0061	LD
2	0.0065	LD	33	0.0063	LD
3	0.0072	LD	34	0.0070	LD
4	0.0081	LD	35	0.0077	LD
5	0.0088	LD	36	0.0084	LD
6	0.0095	LD	37	0.0091	LD
7	0.0101	LD	38	0.0098	LD
8	0.0107	LD	39	0.0104	LD
9	0.0113	LD	40	0.0110	LD
10	0.0118	LD	41	0.0115	LD
11	0.0123	LD	42	0.0119	LD
12	0.0127	LD	43	0.0123	LD
13	0.0130	LD	44	0.0126	LD
14	0.0132	LD	45	0.0128	LD
15	0.0134	LD	46	0.0129	LD
16	0.0134	LD	47	0.0130	LD

17	0.0135	LD	48	0.0130	LD
18	0.0134	LD	49	0.0129	LD
19	0.0132	LD	50	0.0128	LD
20	0.0130	LD	51	0.0125	LD
21	0.0127	LD	52	0.0122	LD
22	0.0123	LD	53	0.0116	LD
23	0.0119	LD	54	0.0114	LD
24	0.0114	LD	55	0.0109	LD
25	0.0108	LD	56	0.0104	LD
26	0.0102	LD	57	0.0097	LD
27	0.0095	LD	58	0.0091	LD
28	0.0088	LD	59	0.0084	LD
29	0.0081	LD	60	0.0077	LD
30	0.0073	LD	61	0.0069	LD
31	0.0066	LD	62	0.0063	LD

Table E.45 Mean strain values and performance level for left column top reinforcements of P Axis for O13 Bridge

Reinf. Fiber ID	**Mean**	**Performance Level**	**Reinf. Fiber ID**	**Mean**	**Performance Level**
1	0.0067	LD	32	0.0066	LD
2	0.0074	LD	33	0.0060	LD
3	0.0082	LD	34	0.0059	LD
4	0.0089	LD	35	0.0063	LD
5	0.0095	LD	36	0.0068	LD
6	0.0102	LD	37	0.0076	LD
7	0.0108	LD	38	0.0082	LD
8	0.0114	LD	39	0.0088	LD

9	0.0119	LD	40	0.0093	LD
10	0.0124	LD	41	0.0098	LD
11	0.0128	LD	42	0.0102	LD
12	0.0132	LD	43	0.0106	LD
13	0.0135	LD	44	0.0108	LD
14	0.0137	LD	45	0.0111	LD
15	0.0138	LD	46	0.0112	LD
16	0.0139	LD	47	0.0113	LD
17	0.0139	LD	48	0.0113	LD
18	0.0138	LD	49	0.0112	LD
19	0.0137	LD	50	0.0111	LD
20	0.0134	LD	51	0.0109	LD
21	0.0131	LD	52	0.0106	LD
22	0.0128	LD	53	0.0102	LD
23	0.0123	LD	54	0.0098	LD
24	0.0119	LD	55	0.0094	LD
25	0.0113	LD	56	0.0088	LD
26	0.0108	LD	57	0.0083	LD
27	0.0101	LD	58	0.0077	LD
28	0.0094	LD	59	0.0070	LD
29	0.0088	LD	60	0.0064	LD
30	0.0080	LD	61	0.0060	LD
31	0.0073	LD	62	0.0062	LD

Table E.46 Mean strain values and performance level for right column top reinforcements of A2 Axis for O13 Bridge

Reinf. Fiber ID	Mean	Performance Level	Reinf. Fiber ID	Mean	Performance Level
1	0.0017	Elastic	32	0.0018	Elastic
2	0.0015	Elastic	33	0.0020	Elastic
3	0.0014	Elastic	34	0.0023	Elastic
4	0.0014	Elastic	35	0.0025	LD
5	0.0015	Elastic	36	0.0028	LD
6	0.0016	Elastic	37	0.0030	LD
7	0.0017	Elastic	38	0.0032	LD
8	0.0018	Elastic	39	0.0035	LD
9	0.0019	Elastic	40	0.0036	LD
10	0.0020	Elastic	41	0.0038	LD
11	0.0021	Elastic	42	0.0040	LD
12	0.0022	Elastic	43	0.0041	LD
13	0.0022	Elastic	44	0.0042	LD
14	0.0023	Elastic	45	0.0043	LD
15	0.0023	Elastic	46	0.0043	LD
16	0.0023	Elastic	47	0.0043	LD
17	0.0023	Elastic	48	0.0043	LD
18	0.0023	Elastic	49	0.0043	LD
19	0.0023	Elastic	50	0.0042	LD
20	0.0023	Elastic	51	0.0042	LD
21	0.0022	Elastic	52	0.0040	LD
22	0.0021	Elastic	53	0.0039	LD
23	0.0021	Elastic	54	0.0038	LD
24	0.0020	Elastic	55	0.0036	LD

25	0.0019	Elastic	56	0.0034	LD
26	0.0018	Elastic	57	0.0032	LD
27	0.0016	Elastic	58	0.0029	LD
28	0.0015	Elastic	59	0.0027	LD
29	0.0014	Elastic	60	0.0025	Elastic
30	0.0015	Elastic	61	0.0022	Elastic
31	0.0016	Elastic	62	0.0019	Elastic

Table E.47 Mean strain values and performance level for middle column top reinforcements of A2 Axis for O13 Bridge

Reinf. Fiber ID	**Mean**	**Performance Level**	**Reinf. Fiber ID**	**Mean**	**Performance Level**
1	0.0022	Elastic	32	0.0022	Elastic
2	0.0023	Elastic	33	0.0024	Elastic
3	0.0025	LD	34	0.0027	LD
4	0.0028	LD	35	0.0030	LD
5	0.0031	LD	36	0.0033	LD
6	0.0033	LD	37	0.0036	LD
7	0.0035	LD	38	0.0039	LD
8	0.0037	LD	39	0.0042	LD
9	0.0039	LD	40	0.0044	LD
10	0.0041	LD	41	0.0046	LD
11	0.0043	LD	42	0.0048	LD
12	0.0044	LD	43	0.0050	LD
13	0.0045	LD	44	0.0051	LD
14	0.0046	LD	45	0.0052	LD
15	0.0046	LD	46	0.0053	LD
16	0.0047	LD	47	0.0053	LD

17	0.0047	LD	48	0.0053	LD
18	0.0046	LD	49	0.0053	LD
19	0.0046	LD	50	0.0052	LD
20	0.0045	LD	51	0.0051	LD
21	0.0044	LD	52	0.0050	LD
22	0.0043	LD	53	0.0048	LD
23	0.0041	LD	54	0.0046	LD
24	0.0039	LD	55	0.0044	LD
25	0.0037	LD	56	0.0042	LD
26	0.0035	LD	57	0.0039	LD
27	0.0033	LD	58	0.0036	LD
28	0.0031	LD	59	0.0033	LD
29	0.0028	LD	60	0.0030	LD
30	0.0025	LD	61	0.0027	LD
31	0.0023	Elastic	62	0.0024	Elastic

Table E.48 Mean strain values and performance level for left column top reinforcements of A2 Axis for O13 Bridge

Reinf. Fiber ID	**Mean**	**Performance Level**	**Reinf. Fiber ID**	**Mean**	**Performance Level**
1	0.0021	Elastic	32	0.0025	Elastic
2	0.0023	Elastic	33	0.0023	Elastic
3	0.0025	Elastic	34	0.0024	Elastic
4	0.0026	LD	35	0.0025	Elastic
5	0.0028	LD	36	0.0027	LD
6	0.0029	LD	37	0.0029	LD
7	0.0031	LD	38	0.0031	LD
8	0.0032	LD	39	0.0032	LD

9	0.0033	LD	40	0.0034	LD
10	0.0035	LD	41	0.0035	LD
11	0.0035	LD	42	0.0036	LD
12	0.0036	LD	43	0.0037	LD
13	0.0037	LD	44	0.0037	LD
14	0.0038	LD	45	0.0038	LD
15	0.0038	LD	46	0.0038	LD
16	0.0038	LD	47	0.0038	LD
17	0.0039	LD	48	0.0037	LD
18	0.0039	LD	49	0.0037	LD
19	0.0039	LD	50	0.0036	LD
20	0.0038	LD	51	0.0036	LD
21	0.0038	LD	52	0.0035	LD
22	0.0038	LD	53	0.0034	LD
23	0.0037	LD	54	0.0032	LD
24	0.0036	LD	55	0.0031	LD
25	0.0035	LD	56	0.0029	LD
26	0.0034	LD	57	0.0028	LD
27	0.0033	LD	58	0.0026	LD
28	0.0031	LD	59	0.0024	Elastic
29	0.0030	LD	60	0.0022	Elastic
30	0.0028	LD	61	0.0020	Elastic
31	0.0027	LD	62	0.0020	Elastic